Western University

Scholarship@Western

Digitized Theses

Digitized Special Collections

2010

Applications of Ultrafine Powder Coatings

A.S. Mohammad Sayem Mozumder
Western University

Follow this and additional works at: https://ir.lib.uwo.ca/digitizedtheses

Part of the Biomedical Engineering and Bioengineering Commons, Chemical Engineering Commons, and the Dentistry Commons

APPLICATIONS OF ULTRAFINE POWDER COATINGS

(Thesis format: Integrated-Article)

by

A. S. Mohammad Sayem Mozumder

Graduate Program in Engineering Science
Department of Chemical and Biochemical Engineering

A thesis submitted in partial fulfillment
of the requirements for the degree of
Doctor of Philosophy

The School of Graduate and Postdoctoral Studies
The University of Western Ontario
London, Ontario, Canada

Abstract

Powder coatings have emerged as an alternative to the conventional liquid coatings when environmental regulations become stricter every year. The advantage of powder coatings mainly renders to their solvent-free formulations, because solvent(s) used in liquid coatings are to be evaporated to environment contributing to the total volatile organic compounds (VOCs) emissions. Although advantageous, until recently, powder coating was not able to provide surface finishes comparable to the liquid coatings. However, when ultrafine powders (particularly, in the size range of 15~25 μm) becomes flowable with the aid of nano-additive(s), ultrafine powder coatings (UPCs) came into business with its thinner and smoother films well-comparable to the liquid coatings. Thus UPC offers environmentally friendly alternative to the coating industries having applied to develop many functional coatings.

Ultrafine powder coating (UPC) technology has been utilized to develop superhydrophobic powder coatings that mimic lotus leaf surfaces and exhibit water contact angles (CAs) of over 160° and sliding angle (SA) of less than 5° on the coated substrates. Water droplets tend to be very unstable on these surfaces so that they run away from the superhydrophobic surfaces even with the slightest inclination. This unique phenomenon is attributed to the double-scale micro-/nano hierarchical structures that have been successfully fabricated on such surfaces just by incorporating nano-sized hydrophobic additive(s) in the coating formulations. Thus the solvent-free UPC technique

has offered simple but environmentally friendly solution in developing superhydrophobic surfaces that could be used as self-cleaning surfaces.

Ultrafine powder coating (UPC) technique has been employed to develop polymeric biocompatible powder coatings enriched with nano-TiO_2 with varying degree of nanoroughness ranging from ~37 nm to ~260 nm. The developed coatings have been assessed for their biocompatibility when human mesenchymal cells were cultured on them. Cells attached spread and expressed Runx2 and Collagen Type I on these biocompatible coatings. Interestingly, they performed even better than commercially pure titanium (cpTi) when their nanoroughness could be maintained below ~50 nm. UPC has been able to tune up the nanoroughness of the developed coatings without changing anything in the existing processes, rather by changing amount of the constituents in the coating formulations. Thus UPC could possibly replace the traditional techniques (plasma treatment, sputter-coating or vapour deposition) to develop bioactive coatings for medical devices with offering simple and inexpensive coating method.

Ultrafine powder coating (UPC) technique has also been used to apply flow-modified glass ionomer cement (GIC) powders onto exposed dentine surfaces to occlude exposed dentinal tubules that could effectively treat dentine hypersensitivity. Proprietary ultrafine GIC powders, (Ketac-Cem® and Fuji I®) have been processed with appropriate amounts of nano-sized Al_2O_3 to improve their flowability before applying them to the dentine sections by using UPC process employing Corona spraying gun. With this powder spraying technique, dentinal tubules have been occluded as deep as ~1 mm μm, in some

instances. Such deeper dentinal tubule occlusion renders superiority over any other existing technique (i.e., highest penetration depth was revealed in the literatures is ~270 μm). Moreover, UPC technique showed a higher proportion of tubules filled. Thus, UPC could enter into the treatment of dentine hypersensitivity.

Key Words: Ultrafine Powder Coating, Powder characterization, Powders flowability, Nano-sized additives, Nano-sized Polytetrafluoroethylene (PTFE), Titanium Dioxide nanoparticles, Powder flow-modification, Lotus Leaf, Superhydrophobic surfaces, Water contact angle, Water sliding angle, Double-scale micro-/nano- hierarchical structures, Nanoroughness, Nanotopography, Mesenchymal cell attachment and spreading, Runx2 expression, Dentine hypersensitivity, Dentinal tubule occlusion, Tubule penetration depth, Glass ionomer cements (GICs).

Title: Mimicking *lotus leaf*: Development of Superhydrophobic Surfaces by Ultrafine Powder Coating Technology

Authors: Mozumder, Mohammad Sayem; Zhang, Hui and Zhu, Jesse

All the experimental works were conducted by Mohammad Sayem Mozumder under the supervision of Dr. Hui Zhang and Prof. Jesse Zhu. All drafts and modifications of this manuscript were done by Mohammad Sayem Mozumder under the supervision of Dr. Hui Zhang and Prof. Jesse Zhu. The final version of this manuscript will be submitted to *Advanced Materials* for future publication.

Title: Nano-TiO$_2$ Enriched Polymeric Powder Coatings Support Human Mesenchymal Cell Attachment and Growth

Authors: Mozumder, Mohammad Sayem; Zhu, Jesse and Perinpanayagam, Hiran

All the experimental works were conducted by Mohammad Sayem Mozumder with the help of Aruni Shamalee Perera under the close supervision of Dr. Hiran Perinpanayagam and Prof. Jesse Zhu. All drafts and modifications of this manuscript were done by Mohammad Sayem Mozumder under the supervision of Dr. Hiran Perinpanayagam and Prof. Jesse Zhu. The final version of this manuscript has been accepted for publication in *Journal of Biomaterials applications*.

Title: Micro-nano Topography of Polymeric Powder Coatings Promotes Runx2 Expression

Authors: Mozumder, Mohammad Sayem; Zhu, Jesse and Perinpanayagam, Hiran

All the experimental works were conducted by Mohammad Sayem Mozumder with the help of Aruni Shamalee Perera under the supervision of Dr. Hiran Perinpanayagam and Prof. Jesse Zhu. All drafts and modifications of this manuscript were done by Mohammad Sayem Mozumder under the supervision of Dr. Hiran Perinpanayagam and Prof. Jesse Zhu. The final version of this manuscript will be submitted to the *Journal of Biomedical Materials Research Part A*.

Title: Effect of nanoroughness and nano topographies of Polymeric Powder Coatings on Human Mesenchymal Cell Responses

Authors: Mozumder, Mohammad Sayem; Zhang, Hui; Zhu, Jesse and Perinpanayagam, Hiran

All the experimental works were conducted by Mohammad Sayem Mozumder with the help of Aruni Shamalee Perera under the close supervision of Dr. Hiran Perinpanayagam, Dr. Hui Zhang and Prof. Jesse Zhu. All drafts and modifications of this manuscript were done by Mohammad Sayem Mozumder under the supervision of Dr. Hiran Perinpanayagam and Prof. Jesse Zhu. The final version of this manuscript will be submitted to *Biomaterials* for future publication.

Title: Flow modification of ion-leachable glass powders for novel dental application

Authors: Mozumder, Mohammad Sayem; Zhu, Jesse; Zhang, Hui and Ferrier, Stephen,

All the Experimental works were conducted by Mohammad Sayem Mozumder under the supervision of Dr. Hui Zhang, Dr. Stephen Ferrier and Prof. Jesse Zhu. All drafts and modifications of this manuscript were done by Mohammad Sayem Mozumder under the supervision of Dr. Hui Zhang, Dr. Stephen Ferrier and Prof. Jesse Zhu. The final version of this manuscript will be submitted to The *Journal of Dental Research* for future publication.

Title: Initial investigation of a novel application of flow-modified ion-leachable glass ionomer as powders to occlude dentinal tubules for the treatment of dentine hypersensitivity

Authors: Mozumder, Mohammad Sayem; Zhu, Jesse and Ferrier, Stephen

All the research works were conducted by Mohammad Sayem Mozumder under the supervision of Dr. Stephen Ferrier and Prof. Jesse Zhu. All drafts and modifications of this manuscript were done by Mohammad Sayem Mozumder under the supervision of Dr. Stephen Ferrier and Prof. Jesse Zhu. The final version of this manuscript will be submitted to The *Journal of Dental Research* for future publication.

Title: Effect of working voltage of corona spray system on the penetration depth of ion-leachable glass ionomer powders into the dentinal tubules

Authors: Mozumder, Mohammad Sayem; Zhu, Jesse and Ferrier, Stephen

All the research works were conducted by Mohammad Sayem Mozumder under the supervision of Dr. Stephen Ferrier and Prof. Jesse Zhu. All drafts and modifications of this manuscript were done by Mohammad Sayem Mozumder under the supervision of Dr. Stephen Ferrier and Prof. Jesse Zhu. The final version of this manuscript will be submitted to The *Journal of Dental Research* for future publication.

Dedicated to

My father, *Mr. Aminul Islam Mozumder*

My mother, *Mrs. Ferdous Jahan*

My father-in-law, *Mr. Khairul Alam Chaklader*

My mother-in-law, *Mrs. Nilufar Chaklader*

My wife, *Khaleda Alam Chaklader*

&

My daughter, *Umamah Sayem Mozumder*

Acknowledgements

First, I would like to express my deepest gratitude and sincere appreciation to my supervisor Professor Jesse Zhu for his continuous support, inspiration and guidance throughout my doctoral program. I am grateful for the opportunity and experience, and the logistic supports that he has provided me to carry out this research in an uninterrupted manner. I deeply acknowledge Dr. Hui Zhang's sincere guidance to build up numerous skills that eventually made me confident to give this research a great shape. I would like to convey a special thank to Dr. Zhang for all the contribution he has made during the whole period.

I would be grateful to Dr. Hiran Perinpanayagam and Dr. Stephen Ferrier for their constant support and ideas that have helped me develop myself into completely new areas of research in Dentistry. Their continuous inspiration and guidance allowed me to make the bridge between Chemical & Biochemical Engineering and Dentistry. I also like to offer special thanks to Professor Jeff Dixon who connected us with Dentistry. His initial encouragement rendered the foundation of my today's success in dental materials research.

I would also like to thank the staff and other graduate students working in the powder coating group, particularly Mohamad Rahbari, Mr. Wen, Scott Zhang, Dr. Henry Meng and Wen Shi who were the catalysts for the success of this work through their thoughtful criticism and assistance in the laboratory. I also like to thank my friends Dr. Lucky, Mr. Khaled, Dr. Razzak, Dr. Shahed, Mr. Badrul, Mr. Ashraf, Mr. Iftekhar and their families

for their support. My heartfelt gratitude goes to Dr. Mozahar Hossain, Mr. Farid Ahmad and Mr. Anwar Pervez for their encouragement and contribution in my whole career/life.

I would like to express my thanks to Aruni Perera for helping me learn cell culture and other techniques used for biomaterial assessment. Dr. Perinpanayagam's summer students, particularly Miranda and Nelly also deserve my thanks.

Finally, I would like to express my heartfelt gratitude to my parents and parents-in-laws for their continuous prayer, unconditional support and sacrifices throughout my life. I also like to convey my earnest thanks to all of my grand parents, uncles, aunts, and all relatives and friends for having faith on me. With high appreciation, I want to mention my brothers and sister Jahirul, Asma and Mobasherul who are living here in Canada and have given me the enjoyment of little Bangladesh here in abroad. My very special thanks goes to my other brothers and sisters Nahid, Runu, Morshedul, Farzana and Moin for believing and praying for me from far away. This acknowledgement will not be fulfilled without mentioning the love of my life, my inspiration, my wife Khaleda's name, who has been with me in every step of my ups and downs. At the very end, the arrival of our little wonder Umamah has given me the boost to complete this work. It might seem this acknowledgment is never ending, but I do not want to miss the opportunity to thank everyone out there who helped me even for a single moment in my life. Above all, I am so grateful to the Almighty for everything.

A. S. Mohammad Sayem Mozumder
April 19, 2010.

Table of Contents

xiii

List of Tables

List of Figures

CHAPTER 1
Introduction and Project Overview

1.1. Powders

Particulate materials have attracted human attention since the early age of human civilization. From then on, food products (i.e., sugar, flour, salt, sand etc), detergents, fertilizers, cements, paints and pigments, cosmetics, medicines and chemicals have been manufactured and used in their powder forms. Indeed, powdered materials provide more surface area and chemical reactivity to the application site(s) compared to their bulk form. As far as surface area is concerned, the smaller the powders, the more are they advantageous. This is the reason why ultrafine or nano-sized particles are so popular in today's world. Therefore, significant efforts involved into manufacturing and dispensing powder products have been proven to be worthy.

1.2. Powder classification

Finer particles, which exhibit exceptionally high surface to volume ratio, provide excellent interaction in multiphase environment. This increased interaction in particulate level eventually ensures high mass and heat transfer. Hence, influenced by particle size and particle density, Geldart[1] classified powders into four different groups that are graphically depicted in figure 1.1. According to Geldart classification, the particles that fall in the size range of 40 μm to 200 μm are aerated particles (Group A) while bigger particles between 200 μm to 900 μm are bubbly-ready or sand-like powders (Group B).

Cohesive powders (Group C) are identified in the range from 1 μm to 40 μm and

spoutable powders (Group D) are larger than 900 μm.
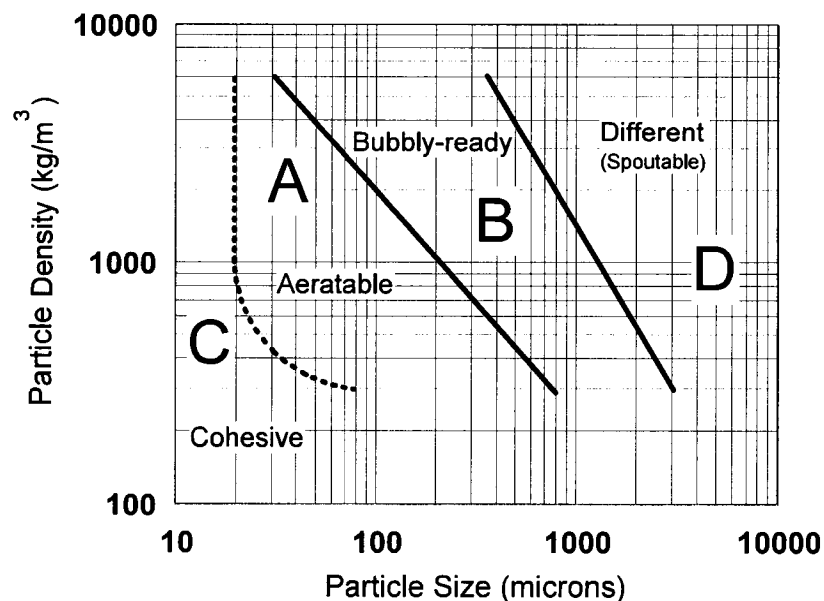
Figure 1.1: Geldart's classification of powders according to their fluidization properties[1]

1.3. Ultrafine Powders and their flowability

Geldart Group C powders, often termed as Ultrafine Powders (UFPs), are the smallest in

Geldart's classification. Although they offer enormously high surface area and excellent

surface finish while deposited onto the substrates, handling and processing of Group C

powders are extremely difficult as they are very cohesive in nature. It is well-established

that the cohesiveness of Group C particles is resulted from the stronger interparticle

forces (i.e., van der Waals forces and electrostatic forces, chemical bonds, interfacial

forces etc.).[2,3] When the particles become smaller and smaller, the separation distance

between the particles gets reduced so that the relative magnitude of the interparticle

forces, particularly the van der Waals forces, become predominant over the gravitational

force.[4] Such dominant interparticle forces insist individual particles to stick to each other

leading to the formation of agglomerates that diminishes the advantages associated with

the ultrafine powders by significantly decreasing their flowability. Therefore,

cohesiveness of UFPs limits their usefulness in many different applications.

As a consequence, cohesiveness of UFPs has to be reduced in order to improve their

flowability. Given numerous practical application of UFPs, extensive research has so far

been conducted to get rid of the agglomeration of the UFPs, which includes introducing

external energies in the form of mechanical vibration, acoustic vibration, mechanical

stirring and magnetic or electrical filed disturbance, or adding coarser or finer particles as

flow conditioners. However, Zhu and Zhang's breakthrough innovation outlined the

introduction of nano-sized additives with UFPs followed by high shear mixing.[5] This

way, nano-additive particles take place in between the UFPs leading to the increment of

their separation distance that eventually decreases the magnitude of interparticle forces

acting among themselves. Thus, upon reduced their cohesiveness, easily flowable UFPs

could be utilized in different practical applications in chemical, advanced materials, food,

pharmaceuticals and paint industries.

1.4. Ultrafine Powder Coatings

Due to the enforcement of the stringent environmental regulations associated with

volatile organic compounds (VOCs) emissions, powder coating has been emerged to be

an alternate to the conventional organic solvent-based liquid coatings which include

solvent evaporation step that is identified as one of the major sources of VOC emissions.

Whereas, powder coating is a dry finishing process that does not need to use any solvent. Indeed, paint ingredients (i.e., resins, pigments, fillers, curing agent, flow agent and degassing agent) are extruded to make solid composites of homogeneous chemical properties and sprayed onto the substrates followed by curing in the oven.

Although advantageous from the environmental perspective, conventional powder coatings, which use coarser powder particles of average particle size between 30 and 60 μm, can not compete with the liquid coatings when the aesthetic is concerned. Due to the usage of bigger particles, powder coatings can not create uniform finish; rather they result in orange-peel like textures. However, use of finer particles (10~20 μm) could solve this issue (Kenny et al., 1996).[6] But the problem is that such smaller particles do not flow well in the powder coating process due to their excessive cohesiveness.

Zhu and Zhang's innovative ultrafine powder coating (UPC) Technology[7] based on their earlier innovation[5] has offered the opportunity to use UFPs in the powder coating processes. Indeed, UPCs use dry-blended nano-additive(s) in the final coating formulations that provide desired flowability of UFPs in the coating process. Thus UPC is now able to utilize powder of particle sizes less than 20 μm. As a result, UPC can create thinner coating film with uniform finishes comparable to liquid coatings.

1.5. Applications of Ultrafine Powder Coating (UPC) technology

UPC is able to coat wide ranges of substrates including metallic, non-metallic, wooden or plastic surfaces. Besides coatings for regular interior or exterior uses, UPC has enormous

potential to develop a number a different functional coatings. Upon incorporating desired

functional fillers and/or additives by standard procedure[5], UPC could develop

superhydrophobic, superhydrophilic, anti-microbial, anti-scratch, conductive,

biocompatible and many other functional coatings. Moreover, by varying the constituents

of the coatings, it can create surface finishes with changeable surface roughness from

very rough to very smooth. In addition, UPC can also be used to apply finer powders to

coat human dentine surfaces to treat tooth hypersensitivity.

1.6. Overview of the projects

1.6.1. Development of Superhydrophobic Coatings

Natural *lotus leaf* (as shown in figure 1.2) is the best example of a superhydrophobic

surface. Water can not stay on the *lotus leaf* surfaces. Water droplets form spheres and

readily bead up with water contact angle of over $150°$ and water sliding angle of less than

$5°$. Indeed, this unique nature is not only attributed to its waxy cuticles, but also to the

existence of double-scale micro-/nano features on the *lotus leaf* surfaces.[8,9] On the leaf

surfaces, droplets roll off very quickly collecting the dirt, which is known as the self-

cleaning property of *lotus leaf*. Evidently, an enormous number of researchers all over the

world have been trying to mimic the unique nature of *lotus leaf* surface that may have

potential applications as self-cleaning glasses, car windshields, window frames, anti-icing

and anti-fogging coatings. However, the success is only limited until today, because it is

very difficult to fabricate the desired dual-scale textures on man-made surfaces.
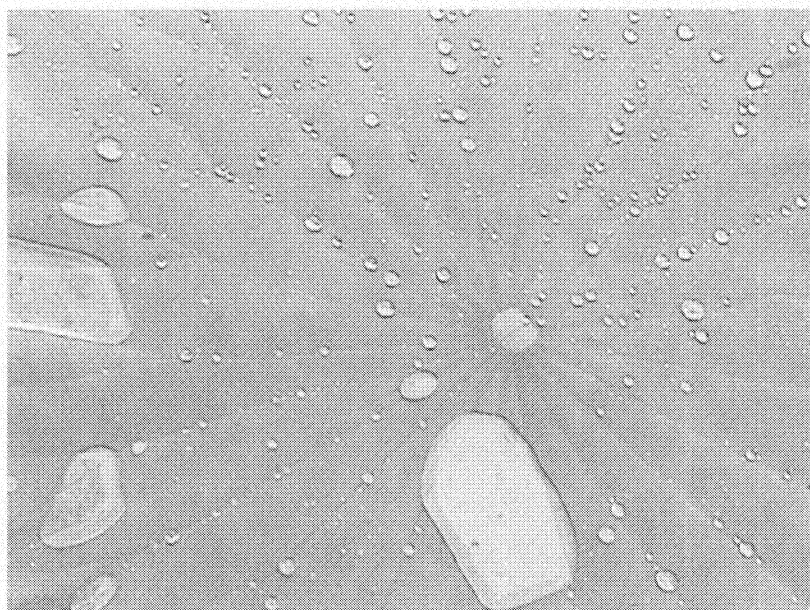
Figure 1.2: Water droplets on the lotus leaf. (Source: http://news.thomasnet.com/IMT/archives/lotus%20leaf,%20water%20droplets.jpg)

So far, many different techniques have been explored to develop superhydrophobic surfaces, which include micropatterning, nanoprinting, lithography, chemical vapour deposition, chemical etching, plasma treatment, surface-modification with sol-gel reactions etc. Almost all of these techniques use toxic solvent(s) to create the coatings. Subsequently, the solvent(s) have to be evaporated that may cause VOC emissions. Due to this environmental issue, the solvent-free coating procedures might be advantageous.

As mentioned earlier in this chapter, ultrafine powder coating (UPC) technique is a solvent-free dry finishing process that might be capable of developing several functional coatings by incorporating functional materials into the coating formulations. In this project, we aim to develop superhydrophobic powder coatings by adding nano-sized low-

energy fluoropolymeric additives into polymeric resin (i.e., preferably, polyester clearcoat) and by spraying them onto the substrates followed by curing process.

1.6.2. Development of Biocompatible Coatings

Implants are designed to replace missing teeth or damaged or broken bones. They are surgically placed into the human body. Hence, they have to be highly biocompatible; otherwise human body would eventually reject these artificial devices due to lack of desired osseointegration with the surrounding tissues. Thus, keeping the implants failure rate in consideration, they are carefully designed sto meet the requirements of both mechanical strength and bioactivity. Due to this reason, titanium and its alloys have been considered as the best candidates for implant materials for many years. However, the biocompatibility of titanium metal could be improved by modifying its surface topography, since the surface topography or roughness significantly influences biocompatibility.[10] As a result, in order to fabricate desired roughness on titanium or its alloys surfaces; they are modified using several techniques including machining, blasting, polishing and etching.

Recently polymeric materials or composites are also being explored to be used as implant materials, although in many instances, they have to be coated with tiny tatinum or titania particles to increase their biocompatibility.[11-13] Traditionally, sputter coating, plasma treatment, and physical and chemical vapour deposition are employed to achieve a thinner coating of titanium on the polymeric substrates.

Particularly, fabrication of nanoscale surface roughness on the implant surfaces may be exceptionally advantageous, because when they are placed into human body, they interact with the tissues, which themselves are nonostructured.[14] As a result, some efforts have been made to develop nano-scale rough surfaces whose biological activity seemed to be enhanced remarkably.[15,16] However, many of the fabrication methods are complicated and costly.

Therefore, it is necessary to develop a simple, but inexpensive technique of fabricating nano-scale structures on the surfaces that could show superior biocompatibility. In this project, we have focused on employing ultrafine powder coating technology to develop such a surface coating that is enriched with nano-TiO_2 exhibiting desired nanoscale topographies on the final coating. Moreover, surface roughness has also been varied by changing the coating formula that eventually showed significant variability in biocompatibility against human mesenchymal cells.

1.6.3. Dentinal Tubule Occlusion with GICs

Enamel, the hardest substance of the human body, covers dentine, which shields dental pulp (as shown in figure 1.3). Enamel is a non-vital cellular secretion, whereas dentine is bone-like and cellular with cell processes and nerve endings extending from the pulpal side towards the enamel dentine junction. Dentine may become exposed by erosion of enamel, which could be caused by overzealous brushing or regular ingestion of acidic substance, periodontal diseases or aging. As the dentine is softer, it may be more rapidly damaged due to these factors. Exposed dentinal tubules may be patent, allowing several

stimuli to cause tubular fluid flow inside the tubules. The fluid movement in turn stimulates the pulpal nerves, as depicted in figure 1.4, which eventually causes the sensation of pain.[17]
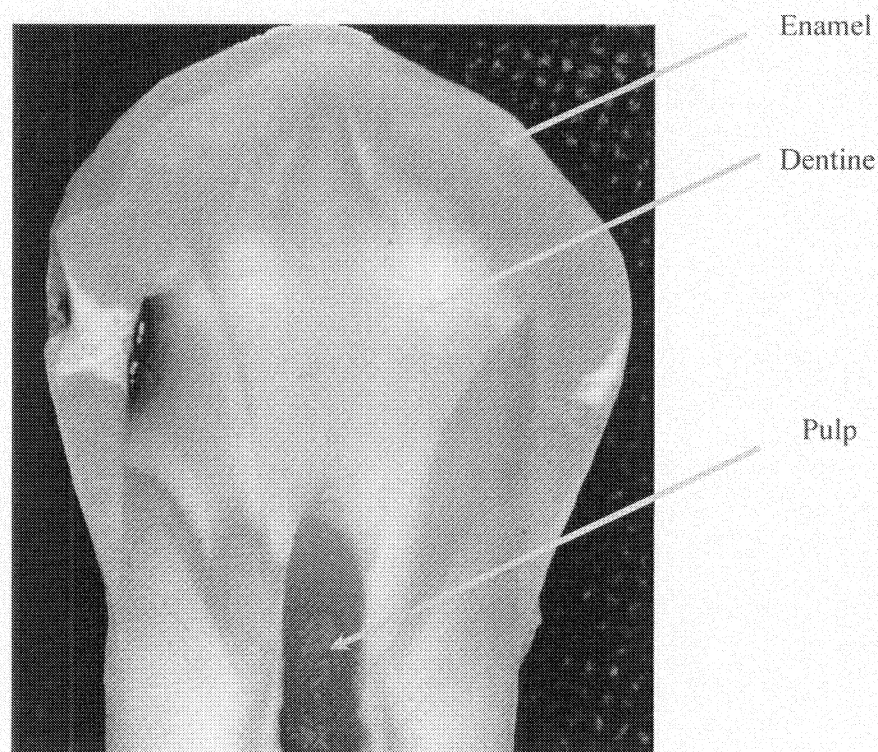
Figure 1.3: Tooth cross-section (Courtesy: Dr. S. Ferrier)

This short but sharp pain arising from exposed dentine, in response to hot or cold drinks or sweet or sour foods is termed as dentine hypersensitivity. It is such a common dental condition that the prevalence rate of dentine hypersensitivity is 30% among general Canadian population.[18] Since the exposed dentinal tubules are thought to be one of the main causes of dentine hypersensitivity, its treatments are generally aimed at occluding dentinal tubules and preventing fluid movement inside the tubules.
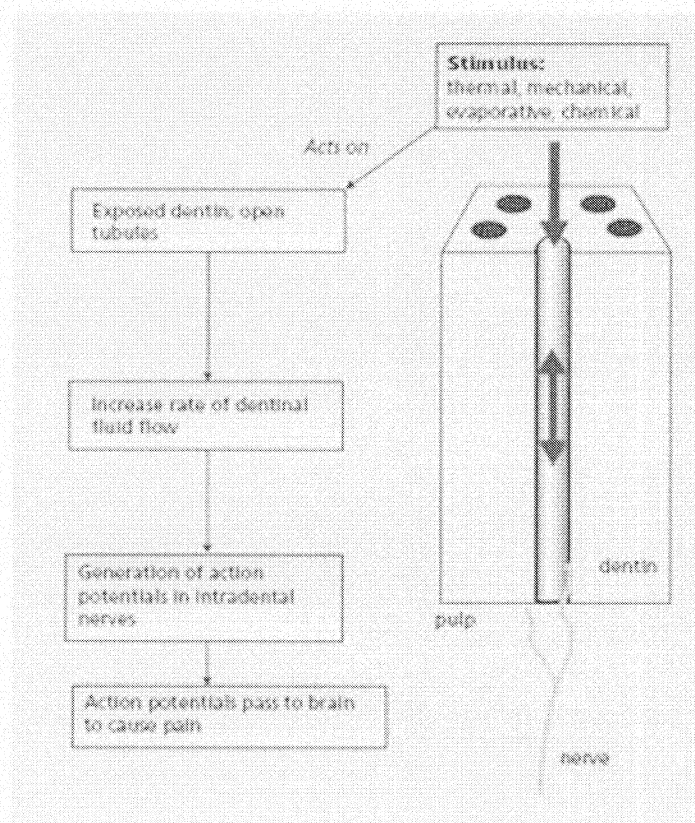
Figure 1.4: The hydrodynamic mechanism by which stimuli could initiate dental tubular fluid flow activating the sensory nerves to cause pain.17 (*Orchardson R, Gillam DG. Managing dentin hypersensitivity. JADA 2006;137(7):990-98. Copyright © 2006 American Dental Association. All rights reserved. Reproduced by permission.*)

Current treatments available fall into two broad categories: Self-applied and dentist-applied. In general the self-applied are dentifrices (toothpastes) and mouthwashes containing agents such as potassium salts and fluoride. The dentist-applied agents take the form of high fluoride gels and resins. Typically the penetration of these agents into dentine has been poor, in the order of 50 μm.[19-21] More recently, there has been a report of a sol-gel bioglass compound showing penetration into dentine of ~270 μm.[22] However, such a shallow penetration of these agents into dentinal tubules can not offer long-term

solution in the treatment of dentine hypersensitivity as these desensitizing agents could easily be brushed off.

Therefore, the development of novel treatment techniques, which could be able to send dental materials far deeper into the tubules, is necessary. In this project, we propose ultrafine powder spraying process to apply glass ionomer cement (GICs) powders into the exposed dentine surfaces. The advantage of these proposed GICs is that they have been used in dentistry for many years as cavity sealants. GICs are durable, having fluoride releasing and recharge capability, are well tolerated by the dental tissues, and form a chemical bond to dentine. Traditionally, GICs are applied as slurry by mixing them with water or polyacid solution. But the problem is that GIC slurry has a very short working time; within only 30 seconds it solidifes. Therefore, GIC slurry may not be an ideal choice. However, if the GIC powders could be applied into wet dentine, they may offer superior solution to dentine sensitivity. Hence, in order to apply GIC powders onto exposed dentine surfaces, powder spraying technique could be employed.

This method would not only be useful in the treatment of dentine hypersensitivity but also in caries prevention and treatment in vulnerable exposed root surfaces. As glass polyalkenoates may be formulated to bond well with dental composite resins, this technique may enhance the quality of bond as well as seal dentine under resin restorations.

1.7. Objectives

Given the immediate potential applications of the above mentioned projects, the overall objectives of this doctoral research are outlined as follows:

Development of superhydrophobic coatings:

➢ To apply ultrafine powder coating (UPC) technology to develop superhydrophobic coatings that resemble *lotus leaf*, exhibiting water contact angle of over $160°$ and water sliding angle of less than $5°$.

➢ To fabricate desired micro-/nanostructure in the powder coated surfaces by using an appropriate amount of nano-sized hydrophobic additive(s) to achieve superhydrophobicity on the created surfaces.

Development of biocompatible coatings:

➢ To develop a new series of biocompatible rougher polymeric coating that has been enriched with nano-TiO_2 and subsequently, to assess their biocompatibility by growing human mesenchymal cells on them.

➢ To develop another series of biocompatible polymeric coatings by varying their surface roughness from ~37 nm to ~260 nm that has been enriched with nano-TiO_2 and subsequently, to assess their biocompatibility by growing human mesenchymal cells on them.

➢ To culture human mesenchymal cells on the two series of biocompatible polymeric coatings and to assess (by SEM and Immunofluorescence imaging) and count the cell attachment on the coatings after some specified time periods.

➢ To assess the metabolic activity of the mesenchymal cells grown on the developed biocompatible polymeric coatings.

➤ To extract RNA from the cells grown on the surfaces and to run PCR to determine

whether GAPDH, RUNX2 and Collagen Type I are expressed within first seven

days.

➤ To run Real-Time PCR to determine the level of RUNX2 and Collagen Type I in

RNA extracted from the cells grown on the biocompatible coatings over a seven

days time period.

Dentinal tubule occlusion:

➤ To modify the flow behaviour of the proprietary Glass Ionomer Cements (GICs).

➤ To apply the flow-modified GICs in their powder form onto exposed dentine with

the aid of Corona spray gun with the aim of occluding the tubules that cause

hypersensitivity.

➤ To assess the GICs penetration depths into the dentinal tubules with the aid of

SEM-EDX analysis.

1.8. Thesis Structures

This thesis consists of eight chapters and follows the "Integrated-Article" format as

outlined in the *Thesis Regulation Guide* by the School of Graduate and Postdoctoral

Studies (SGPS) of the University of Western Ontario. At the beginning of this research,

three separate applied research projects were chosen to be undertaken in the course of this

doctoral program. As a result, this thesis is structured so that Chapter 2 presents the

research performed in 'Superhydrophobic Powder Coating' project, chapter 3 to 5

demonstrate the works done in 'Biocompatible Powder Coatings' project, while Chapter

6 to 7 illustrate the research conducted in 'Occlusion of Dentinal Tubule' project. The brief summary of the subsequent chapters included in this thesis is outlined as follows: Chapter 1 gives a brief introduction of powders, powder classification, ultrafine powder coatings and their application followed by a short overview of the three projects conducted in this doctoral program. In addition, research objectives, thesis structure and the major contributions are stated.

Chapter 2 reports the development of Superhydrophobic Powder Coatings by using ultrafine powder coating (UPC) technology. The characteristics of these unique coatings were compared with those of the natural *lotus leaf*. The morphology (micro-/nanostructure) of the cured coatings was also revealed with the aid of SEM and AFM images.

Chapter 3 discusses how biocompatible rougher (~ 260 nm) polymeric coatings have been developed with the enrichment of nano-TiO_2. The cellular responses of human mesenchymal cells to these developed coatings were also illustrated in a systematic manner. Cell culture, cell attachment assay and MTT assay's protocols were also reported.

Chapter 4 illustrates gene expression in mesenchymal cells grown on the coatings mentioned in chapter 3. Both conventional bench-top and Real-time PCR were used to detect the level of important transcription factors such as RUNX2 and collagen type I. GAPDH represents the positive control.

Chapter 5 outlines the development of biocompatible coatings with varying surface roughness from ~37 nm to ~260 nm and reports the effect of nanoroughness/topographies on the responses of mesenchymal cells cultured on the developed coatings. Cell morphology was also reported with the aid of SEM and immunofluorescence images.

Chapter 6 describes the flow modification of the proprietary glass ionomer cements (GICs), Fuji I®, by adding nano-Al_2O_3. Powder characterization techniques are also illustrated.

Chapter 7 reports the novel application of flow-modified GICs powders in occluding dentinal tubules through ultrafine powder spraying system. Results are reported for two different grades of GICs (Ketac–Cem® and Fuji I®). SEM images are analysed to report the penetration depths of GICs into the exposed tubules.

Chapter 8 summarizes the conclusions of this research, along with a set of recommendations for future studies.

1.9. Major Contributions

This doctoral research has aimed to utilize Ultrafine Powder Coating (UPC) technology in three practical applications leading to the following major contributions:

❖ Ultrafine powder coating (UPC) technology has been first time applied to develop superhydrophobic powder coatings to coat any metallic or non-metallic substrates that exhibit very high water contact angles (over 160°) and very low water sliding angle (less than 5°). This unique phenomenon has been achieved by mimicking *lotus leaf*, on which water droplets form beads and roll off easily to leave the leaf surface along with the dirt deposited on it. The developed superhydrophobic coatings exhibit the same effect as *lotus effect*. This effect has not only been attributed to the hydrophobic nature of the base materials, but also to the double-scale hierarchical micro-/nanostructures. Incorporation of an appropriate amount of nano-sized low-energy hydrophobic additive(s) and their processing with the base coating formulation has ensured the desired micro-/nanostructures on the cured coatings.

❖ Two new series biocompatible ultrafine powder coatings have been developed that could be used as implant coatings. In the first series, the regular UPC formula has been modified with the incorporation of TiO_2, which is well-known for its superior biocompatibility. Both TiO_2 nanoparticles and micron-sized pigment-grade TiO_2 have been added to the formula to make the coated surface bioactive. Since surface roughness influences the interaction of several cells to the biomaterial surfaces, the second series of biocompatible coatings were created that possess roughness between ~37 nm and ~260 nm with varying concentration of polytetrafluoroethylene (PTFE). Human mesenchymal cells have been attached to both series of bioactive coatings. Interestingly, the bioactive coatings, which

have ~37 nm roughness, performed as good as the commercially pure titanium substrates. A provisional patent has been submitted on these new biocompatible coatings.

❖ A novel approach of applying flow modified-Glass Ionomer Cements (GICs) to the exposed dentinal tubules has been developed by utilizing UPC technology with the aim of treating dental hypersensitivity. Spraying GICs in their powder form onto the wet dentine has helped bypass the handleability issue associated with GIC slurry, which is the conventional mode of applying GICs to patient's teeth. Moreover, this is the first instance that GICs have been used to occlude dentinal tubules in order to stop the fluid movement inside the dentinal tubules that causes dentine hypersensitivity. Given numerous advantageous properties of GICs as restorative material, which include fluoride ion-leachability, chemical bonding with dentine, biocompatibility etc., we sprayed them onto dentine with the aid of Corona spray gun. A clearly superior tubule penetration depth (~ 1 mm) has been reported in this thesis, which is about four-times more than that (~ 270 μm) reported in the best and most recent article (yet to be printed) on this topic of interest. A Report of Invention (ROI) has already been submitted to WorlDiscoveries™ on this novel invention.

❖ More importantly, through this research, an engineering coating technology has been successfully applied in Dentistry. Thus, an effective interdisciplinary collaboration has been initiated to carry out the challenging projects with clear success.

References

1. Geldart D., Types of Gas Fluidization. *Powder Technology* **1973**, 7 (5):285-297.

2. Visser J., An invited review- van der Waals and other cohesive forces affecting powder fluidization. *Powder Technology* **1989**, 58 (1):1-10.

3. Krupp, H. "particle adhesion theory and experiment", *Adv. Colloid Interface Science* **1967**, 1, 111-239.

4. Hamaker HC., The London-Van der Waals Attraction between Spherical Particles. *Physica (Utrecht)* **1937**, 4, 1058-1072.

5. Zhu J.; Zhang H., Fluidization Additives to Fine Powders, *US Patent 6,833,185.* **2004**.

6. Kenny, JC.; Ueno, T.; Tsutsui, K., Analytical approach for high quality appearance powder coatings. *J. Coat. Technol.* **1996**, 68, 35-43.

7. Zhu, J.; Zhang, H., Ultrafine powder coatings: An innovation. *Powder Coat.,* **2005**, 16 (7): 39-47.

8. Zhai, J.; Li, H.J.; Li, Y.S.; Li, S.H.; Jiang, L., *Physics* **2002**, 31, 483.

9. Herminghaus, S., *Europhys. Lett.,* **2000**, 52, 165.

10. Feinberg, A.W.; Wilkerson, W.R.; Seegert, C.A.; Gibson, A.L.; Hoipkemeier-Wilson, L.; Brennan, A.B., Systematic variation of microtopography, surface chemistry and elastic modulus and the state dependent effect on endothelial cell alignment, *J. Biomed. Mater. Res. A* **2008**, 86, 522-534.

11. Pareta, R.A.; Reising, A.B.; Miller, T.; Storey, D.; Webster, T.J., An understanding of enhanced osteoblast adhesion on various nanostructured

polymeric and metallic materials prepared by ionic plasma deposition, *J. Biomed. Mater. Res. A* **2010**, 92A (3), 1190–1201.

12. Reising, A.; Yao, C.; Storey, D.; Webster, T.J., Greater osteoblast long-term functions on ionic plasma deposited nanostructured orthopedic implant coatings, *J. Biomed. Mater. Res. A* **2008**, 87, 78-83.

13. Yao, C.; Storey, D.; Webster, T.J., Nanostructured metal coatings on polymers increase osteoblast attachment, *Int. J. Nanomedicine* **2007**, 2, 487-492.

14. Kaplan, F.S.; Hayes, W.C.; Keaveny, T.M.; Boskey, A.; Einhorn, T.A.; Iannotti, J.P., Form and function of bone. In Simon SR, editor. Orthopaedic Basic Science, Rosemont, IL: *American Academy of Orthopaedic Surgeons* **1994**, 127-185.

15. Ranjan, A.; Webster, T.J., Increased endothelial cell adhesion and elongation on micron-patterned nano-rough poly(dimethylsiloxane) films. *Nanotechnology* **2009**, 20, 305102.

16. Chun, Y.W.; Khang, D.; Haberstroh, K.M.; Webster, T.J., The role of polymer nanosurface roughness and submicron pores in improving bladder urothelial cell density and inhibiting calcium oxalate stone formation. *Nanotechnology* **2009**, 20, 85104.

17. Orchardson, R.; Gillam, D.G., Managing dentin hypersensitivity. *J Am Dent Assoc.* **2006**, 137 (7), 990-998.

18. Consensus-Based Recommendations for the Diagnosis and Management of Dentin Hypersensitivity. Canadian Advisory Board on Dentin Hypersensitivity. *J Can Dent Assoc* **2003**, 69 (4), 221-6.

19. Lee, B.S.; Chang, C.W.; Chen, W.P.; Lan, W.H.; Lin, C.P., In vitro study of dentin hypersensitivity treated by Nd:YAP laser and bioglass. *Dent Mater* **2005,** 21, 511-519.

20. Lee, B.S.; Tsai, H.Y.; Tsai, Y.L.; Lan, W.H.; Lin, C.P., In vitro study of DP-bioglass paste for treatment of dentin hypersensitivity. *Dent Mater J* **2005,** 24, 562-569.

21. Lee, B.S.; Kang, S.H.; Wang, Y.L.; Lin, F.H.; Lin, C.P., In vitro study of dentinal tubule occlusion with Sol-gel DP-bioglass for treatment of dentin hypersensitivity. *Dent Mater J* **2007,** 26 (1), 52-61.

22. Curtis, A.R.; West, N.X.; Su, B., Synthesis of nano-bioglass and formation of apatite-rods to occlude exposed dentine tubules and eliminate hypersensitivity. *Acta Biomater.* **2010** Mar 2. [Epub ahead of print]

CHAPTER 2
Development of Superhydrophobic Coatings

Chapter Summary

This study demonstrates the development of superhydrophobic surfaces by a solvent-free ultrafine powder coating technique that exhibit Lotus Effect with water contact angles (CAs) of over 160° and sliding angle (SA) of less than 5°. It is evident that the higher CA and lower SA of the low energy surfaces are attributed to the appropriate surface textures of micro- and/or nano-scales. AFM and SEM images revealed the unique double-scale hierarchical structures on the developed superhydrophobic surfaces. As an additional advantage, these superhydrophobic ultrafine powder coatings eliminate the use of toxic solvents that are responsible for the hazardous emissions of volatile organic compounds (VOCs) and hence make it less expensive than the conventional liquid-based coatings. Therefore, fabrication of superhydrophobic surfaces by solvent-free powder coating technology has enormous opportunities for a revolutionary expansion in coating industry to save the surfaces from the intervention of moisture.

2.1. Introduction

In recent years, fabrication of superhydrophobic surfaces by mimicking the unique nature of *lotus leaf* has been receiving growing interest among an enormous number of researchers all over the world. It is well-known that *lotus leaves* are the best example of a non-wetting, super water repellent and superhydrophobic surfaces. On *lotus leaf* surfaces water droplets form spheres with very little adhesion to the surfaces, bead up readily with a very high water contact angle (CA; >150°), roll off very quickly at the slightest inclination (<5°) and collect the dirt along the way. Hence *lotus leaf* acts as a self-

cleaning surface by removing dusts or pollutants by rolling water droplets (i.e., rain water); this phenomenon is often termed as *Lotus Effect*.[1-3] Thus, the man-made surfaces with such unique properties of *lotus leaf* can be potentially used as self-cleaning glasses, car windshields, traffic guidance and signs, window frames, solar cells, marine vessels and aircrafts, and in low-friction pipelines. Moreover, these superhydrophobic surfaces could possibly prevent or lessen fogging, icing, snow sticking and oxidation.[4]

However, the superhydrophobicity of the lotus leaves does not come only from the epicuticular waxes, but also from their micro- and nano-scale hierarchical structures on top of the micropapillae.[5] Indeed, the combination of micro- and nano-scale structures (i.e., micron-sized papillae apart from each other by a micrometer scale distance and nano-hair-like things on each micropapillae) give lotus leaves the very high water CA but very low sliding angle. Therefore, mimicking lotus leaves does not only require low energy hydrophobic materials, but also needs both micro- and nano-scale roughness on the top surfaces. Indeed, low energy fluoropolymers themselves cannot produce surfaces of more than 120° water CAs.[6] Hence, surface roughness, combination of micro-nano structures, plays the decisive role to further increase the water CA of the developed surfaces to the superhydrophobic range. Decisively, superhydrophobicity is attributed from both the surface chemical composition and the surface microstructure/roughness.[7]

Subsequently, an enormous effort has already been made to develop lotus leaf-like micro-nano structured superhydrophobic surfaces or coatings.[8-44] Low surface energy hydrophobic fluoropolymers such as polyethylene and polypropylene[8-10],

polytetrafluoroethylene (PTFE)[11,12], polydimethylsiloxane (PDMS)[13,14] and

fluoroalkylsilane (FAS)[15-20] were widely used in preparation of superhydrophobic

surfaces. Efforts have also been made to use carbon nano tubes (CNTs)[21-23] and

nanocomposites.[24-27]. Furthermore, many different techniques were also employed to

introduce desired micro-/nano-roughness on the substrates of desired chemical properties

including plasma treatment[23,28-30], chemical etching[31,32], chemical vapour deposition

(CVD)[4,15,33], micropatterning[11,14,34-38], nanoprinting[39], lithography[40-42], sol-gel reaction[43],

phase separation[8,44] and others. However, almost all of these techniques involved toxic

solvent(s) that might be responsible for hazardous volatile organic compound (VOC)

emissions. As VOCs pollute the environment, those toxic solvents are often considered as

environmental hazards. Therefore, the use of toxic solvents has to be reduced to comply

with the increasingly stringent environmental regulations. However, powder coatings

(PC) are considered as environmentally friendly as they eliminate use of any solvent.

Moreover, powder coatings have the provision of recycling the over-sprayed paint

powders. Hence, solvent-free powder coatings are also relatively cheaper than the

solvent-based competitors as they cut the costs of solvents and wasted powders.

In this chapter, we will describe a solvent-free ultrafine powder coating (UPC)

technology for creating superhydrophobic coating on metallic substrates. UPC is a dry

finishing process in which ultrafine polymeric resin along with pigment, filler, curing

agent and nano-sized additives are applied to the target metallic or non-metallic

substrates with the aid of electrostatic Corona charging spraying gun. To improve the

flowability of the ultrafine powders, they are processed with nano-additives according to

Zhu and Zhang's patented technology.[45] The well-fluidized powder particles are entrained to the tip of the corona gun. There the corona-discharge ionizes the air molecules that eventually charge the paint powders. As the target part remains electrostatically grounded, the charged particles are attracted to the target substrate and form a coating layer on its surface. The coated panel is then cured in an oven at 200° C for around 10 minutes. While curing, the powder coating is melted and fuses into a homogeneous film. When low surface energy nano-additive(s) are incorporated into the powder formulation, the cured films exhibit the unique double scale (micro- and nano-) structures that resemble those of *lotus leaf*. Interestingly, these developed coatings reveal water contact angle of over 160° and sliding angle of less than 5°. Thus they could be considered as superhydrophobic coatings. The developed coatings were characterized by using scanning electron microscope (SEM) and atomic force microscope (AFM).

2.2. Materials and Methods

Development of Superhydrophobic Powder Coatings

Superhydrophobic powder coatings were prepared by a solvent-free ultrafine powder coating technique using commonly available polymeric resins processed with nano-sized additives. Mixture of polyester clearcoat (UCB Chemicals Corp., GA, USA) and other minor compounds was extruded into a twin-screw extruder (Donghui Powder Processing Equipment Co., Yantai, China) that was preheated to 80°C and operated at screw rotation speed of 500 rpm. The extrudate was squeezed, flattened and cooled by the rotating rollers which were refrigerated with chilled water. The sheets of extrudate were further cooled down by the fans on top of the conveyor belt while the sheets were transported to

the chipper roller. This roller broke the sheets into chips that possessed homogeneous chemical composition. Those chips were then fine ground into ultrafine powder particles (15-20 μm). However, these ultrafine Geldart Group C particles did not flow well due to the dominant interparticle forces.[46] As a result, these ultrafine powders formed agglomerates when they were transported through a channel. To overcome this flowability issue, the ultrafine powders were processed with 0.5 wt.% nano-sized additive (TiO_2, Degussa, USA, ~40 nm average particle size) through high-shear mixing as described in elsewhere.[45] Due to the high shear mixing, the agglomerates of both the nano and micron-sized particles were broken up, and the nano particles took place in between the micron-sized particles. Thus they served to increase the separation distance between the micron-sized powder coating particles, and thereby ensured an adequate flow of the ultrafine mixture.[45]

Upon resolving the flowability problem, low-energy nano-addtives were added into the coating formulation to increase hydrophobicity of the coatings. At this stage, nano-sized hydrophobic additive(s) were dry-blended with the ultrafine mixtures that provided both the superhydrophobicity and the desired micro and nano-scale roughness as well as flow enhancement. Moreover, 1.0 wt.% of functional filler was added into the formulation to prevent the hydrophobic additives from being rubbed off easily since the fillers are hollow-structured (85% porous) as shown in figure 2.1.
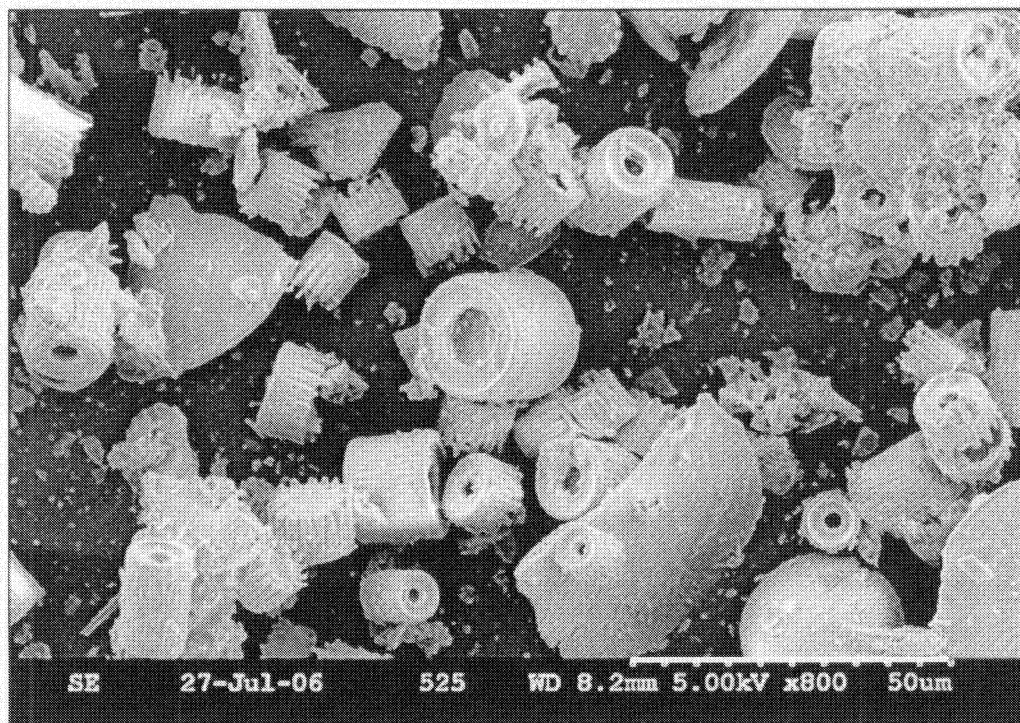
Figure 2.1: Scanning Electron Microscope (SEM) image of the hollow functional fillers revealing their morphologies. (Bar = 50 μm)

The final powder mixture of ultrafine polymeric resin, nano-sized TiO_2, nano-sized hydrophobic additive(s) and the functional fillers were passed through a 32-μm sieve to further homogenize the mixture. The powder processing and spraying process is illustrated in figure 2.2.
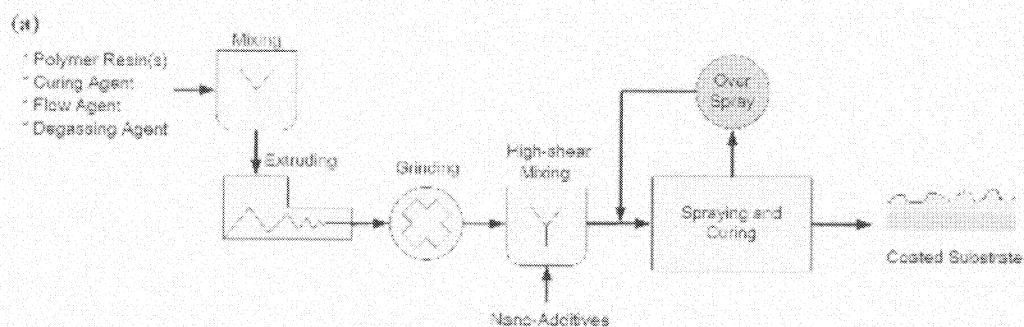
Figure 2.2 (a): Ultrafine powder coating process for preparation of superhydrophobic powder coatings. Polymeric resins and curing, degassing and flow agents were mixed and extruded to make homogeneous chips. The chips were then ground into ultrafine powders (15-20 µm) and dry blended with nano-sized hydrophobic and flow additive(s) (TiO$_2$). These ultrafine mixtures were electrostatically sprayed onto a grounded workpiece, and cured in a furnace (at 200°C, 10 min). Over-sprayed powders were recycled and reused.

As shown in Figure 2.2 (b), the powder mixture was then fed through a hopper and entrained to the tip of a Corona spray gun (Nordson Corporation). When the Corona spray gun was triggered, a set voltage of 20 kV was applied to charge the coating particles that were then electrostatically sprayed onto the grounded substrates. Subsequently, the powder-coated substrates were cured in a furnace at 200°C for 10 minutes. Upon curing, the melted powder particles formed a homogeneous surface finish. However, due to the incorporation of hydrophobic particles into the coating formulation, the final coatings became superhydrophobic with desired micro and nano-structures.
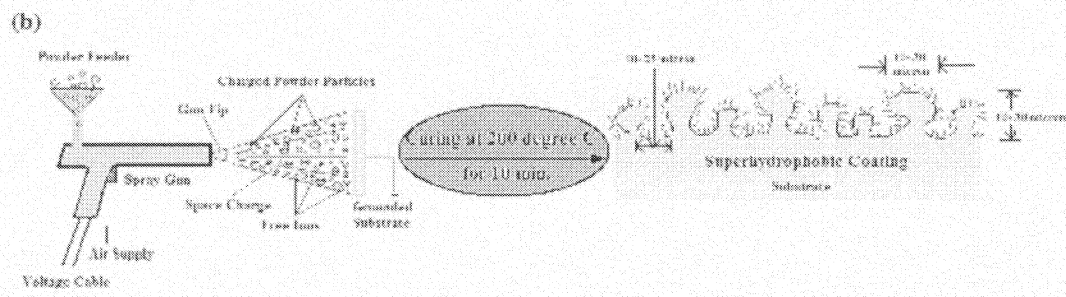
Figure 2.2 (b): Illustration of powder spraying and curing process. When the Corona Spray Gun was triggered, a set voltage of 20 kV was used to generate a corona discharge that made the powder particles negatively charged. Those negatively charged particles were easily attracted to the grounded substrate and eventually formed a uniform film. When the film was cured at 200°C for 10 minutes, the powder particles melted and spread out onto the substrate. In our study, the finished coating was textured with both micro- and nano-features which made the coated surface superhydrophobic.
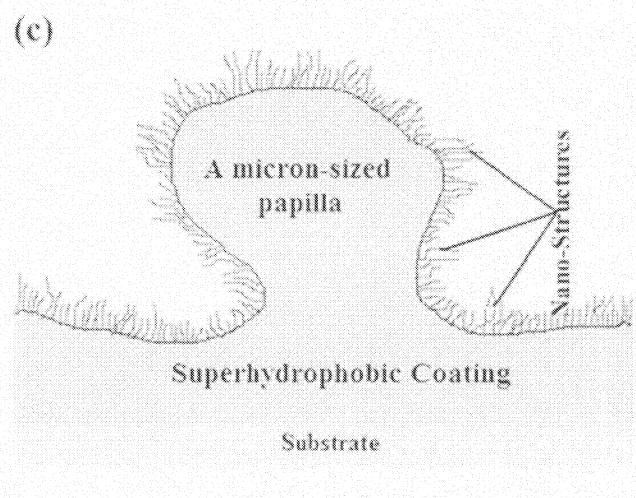
Figure 2.2 (c): Micro- and nano-structures in a micron-sized papilla

Adhesion of the Superhydrophobic Coatings

The adhesion of the superhydrophobic coatings to the underlying substrates was measured by using an Elcometer 107 Cross Hutch Cutter (Elcometer Ltd., Windsor, Canada). The Elcometer used a blade (11 mm by 1.5 mm) to cut the coatings down to the substrates. Several perpendicular cuts were made to create a grid of small squares, as specified in ASTM D3359. An ASTM standard adhesive tape was attached to the grid. The tape was then withdrawn by a single smooth pull so that some of the squares could be pulled off with the tape. Then the remaining grid squares were counted and compared for coatings retention. The lattice was then assessed for adhesion by using the ASTM D3359 standards.

SEM of the Superhydrophobic Surfaces

The developed superhydrophobic surfaces were examined by scanning electron microscopy (SEM) to verify their micro- and nano-structures. The prepared surfaces were cut into 10 mm by 10 mm square pieces which were mounted on metal stubs with the aid of adhesive carbon tape and were sputter coated with gold (15 nm thick layer). The gold-sputtered superhydrophobic surfaces were then carefully examined with a Hitachi S-2600 (Hitachi, Pleasonton, CA) SEM. The working voltage (5 kV), beam (30) and working distance (~5.2 mm) were set.

AFM of the Developed Coatings

To determine their surface features, superhydrophobic surfaces were analyzed with the dynamic force mode Atomic Force Microscopy (AFM) (Park Systems AFM XE-100). A

silicon cantilever with a spring constant of ~40 N/m and a nominal tip radius of 10 nm

was used. The length, width and thickness of the cantilever were 125 μm, 40 μm long and

4 μm, respectively. The cantilever was oscillated around its resonant frequency (~300

kHz) and its amplitude decreased when the tip interacted with the sample surface. Such

damped amplitude (set point) was used as the feedback parameter to probe the surface

features. The images of 256 x 256 pixels were collected in air at room temperature.

Surface Roughness Measurement

The surface roughness of the superhydrophobic coatings was measured with a Dektak 8

Stylus Surface Profiler (Veeco Metrology Group, Santa Barbara, CA). The samples were

loaded onto a high precision stage that moved beneath a diamond-tipped stylus according

to specified scan length (20 mm), scan resolution (1.111 μm) and stylus force (8 mg).

Each surface was scanned at 10 different locations to obtain consistent average readings.

The mean deviation of the vertical features from the centerline was then calculated as a

measure for surface roughness (R_a).

Contact Angle and Sliding Angle Measurement

Water contact angles (CAs) of the superhydrophobic surfaces were measured with a

Rame-Hart 100 Goniometer equipped with a horizontal microscope. A 10 μl droplet of

deionized water was gently dispensed on the coated surfaces using a micrometric syringe

(Gilmont Instrument). The static CA was measured by calculating the slope of the tangent

to the drop at the liquid-solid-vapor interface line. The CA was measured in at least five

different locations on the superhydrophobic panels. Statistical means and standard deviations of the readings were reported.

Sliding angle (SA) was also used to evaluate superhydrophobicity of the developed coatings. SA was measured as the tilt angle at which the water droplet became unstable and rolled off from the surface.

Durability Test

A 100% cotton cloth wrapped on a 1 cm × 1 cm ×1 cm cubic rubber head with 100 g normal force was exerted on the cured coating surfaces. The durability of superhydrophobicity was measured as the number of rubbing cycles performed before a significant change in water CA was observed.

2.3. Results and Discussion

A solvent-free ultrafine powder coating technique were been utilized to develop superhydrophobic powder coatings from commonly available polymeric resins incorporated with low energy hydrophobic additives. The created coatings revealed double-scale (both micro- and nano-) hierarchical structures that resembled those of natural *lotus leaf*. Subsequently they possessed famous *lotus effect* as the finished surfaces superbly repelled water exhibiting very high water contact angles. The droplet preferred more to be stick to the tip of the needle of the dispensing syringe while we tried to dispense them onto the coated surface to measure the water contact angle. In some cases, water droplets repelled the coated surface so intensely that it was very hard to

place them on the superhydrophobic coatings. More interestingly, the droplets became

unstable and ran away from the surface with an inclination of only 1 or 2 degrees.

Indeed, when the powder coating film was cured at 200°C, the powder mixtures melted,

homogenized and spread onto the underlying substrates. During melting and spreading,

the hydrophobic nanoparticles tended to move up to the top of the coatings and formed

the nano-structures as the top-most layer on the cured polymeric resin. Moreover, due to

the differences in surface energies among the nano-sized hydrophobic additive(s) and the

other hydrophilic constituents of the mixture, micron-sized porous polymeric surfaces

were developed upon melted and cured. Not only that, the developed superhydrophobic

coatings also exhibited ~250 nm surface roughness. Therefore, the micro-porous nano-

structured coatings resembled that of *lotus leaf*. Cross-sectional view of the finished

superhydrophobic coatings was conceptualized in figure 2 (b). Figure 2 (c) further

depicted a single micron-sized papilla that was covered with protruding nano-hairs.

Scanning electron microscope (SEM) images confirmed the similarity of micro- and

nanostructures present in the *lotus leaf* and in our superhydrophobic coatings. SEM

images of figures 2.3 (a-c) showed the double-scale hierarchical structures of *lotus leaf*

(*Nelumbo Nucifera*) in different magnifications[47] while figures 2.3 (d-i) showed the

micro-nano binary structures of the developed superhydrophobic powder coatings. It is

evident from these SEM images that the double-scale hierarchical structures of lotus leaf

and of our superhydrophobic surfaces were almost interchangeable. Therefore,

mimicking of lotus leaf was successfully accomplished by ultrafine powder coatings.
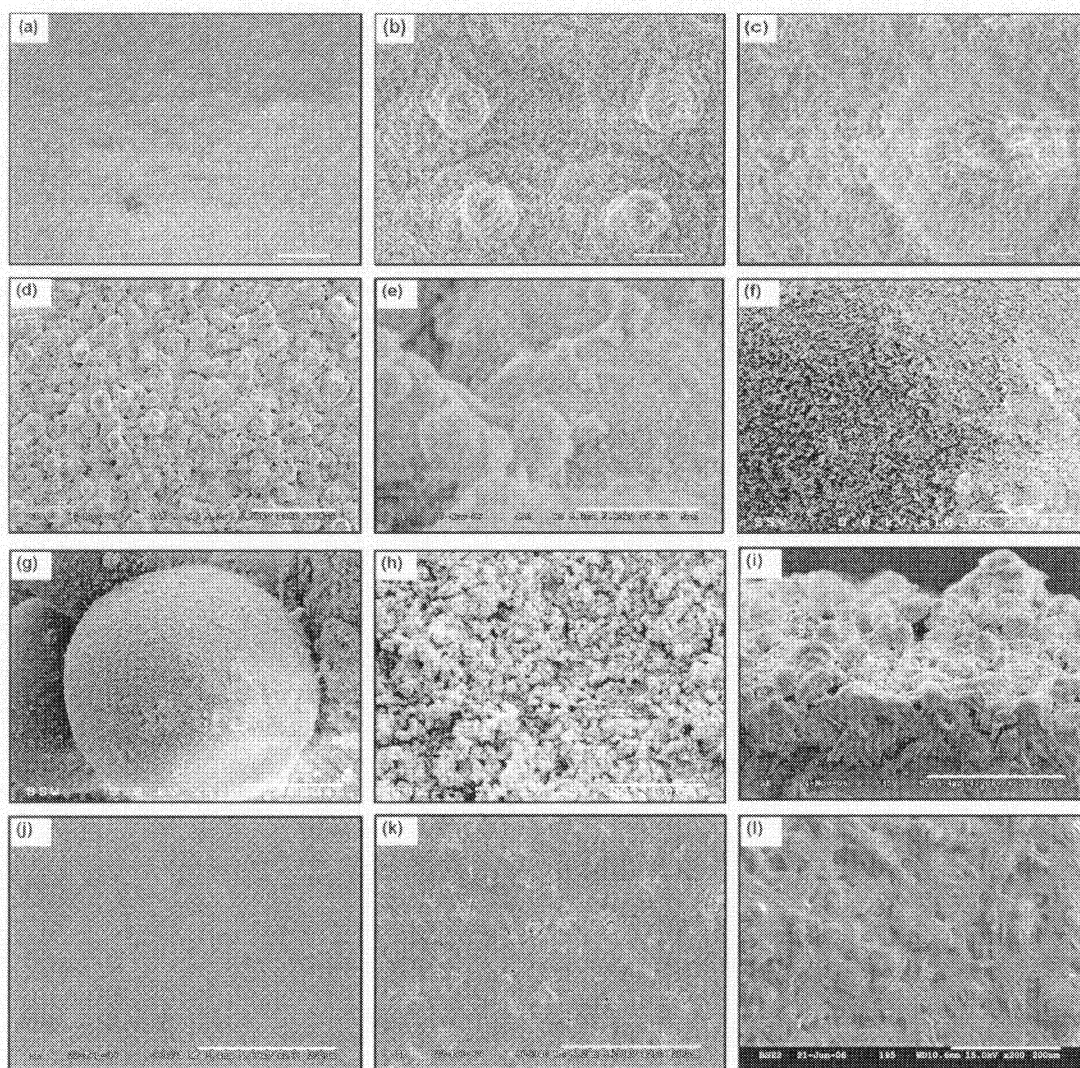
Figure 2.3: Micro- and nanostructures of lotus leaf (Nelumbo Nucifera) (a-c)[47] and that of superhydrophobic powder coatings (d-i) and regular hydrophobic coatings (j-l).

(a) Top view of lotus leaf (bar = 50 μm). (b) Magnified view of lotus leaf taken from (a) (bar = 5 μm). (c) Magnification of a papillae from (b) (bar = 1 μm). (d) Top view of our superhydrophobic coating (bar = 100 μm). (e) Magnified section of (d) (bar = 5 μm). (f) Magnification of (e) (bar = 3 μm). (g) A micro-papilla (bar = 7.5 μm). (h) Fabricated nanostructures on the micro-papillae (bar = 600 nm). (i) Cross-sectional view of (d) (bar = 100 μm). (j). Top view of a regular coating (without any hydrophobic additive) (bar =

200 µm) (k). Top view of coating containing 2 wt.% of hydrophobic additive A (bar =

200 µm) (l). Top view of coating containing hydrophobic additive B only (bar = 200 µm).

(a-c), Reproduced by permission of The Royal Society of Chemistry (http://dx.doi.org/10.1039/b110420a).

In particular, SEM image of figure 2.3 (g) depicted a single micro-papilla that is roofed

with an enormous amount of nano-structures that is shown in figure 2.3 (h). The nano

matters were 40~70 nm in diameter; however, they formed bundles and developed

submicron-sized (400~600 nm) valleys. Similar results were reported by other

researchers with different approaches.[48,49] In addition to the top views, figure 2.3 (i)

showed the cross-sectional view of the superhydrophobic coating (shown in figure 2.3

(d)). The cross-sectional SEM image further confirmed the presence of micro- and

nanostructures that made the developed coatings superhydrophobic in nature.

However, it is imperative to investigate what caused those desired micro-nanostructures

on the superhydrophobic surfaces. It is not surprising that the appropriate amount of low-

energy hydrophobic additive(s) incorporated into the polymeric resin was responsible for

those protruding micro-nano textures. This claim is confirmed by the SEM images of

another set of coatings (figure 2.3 (j-l) that either did not contain any of the hydrophobic

additives or did not possess optimum amount of these hydrophobic additive(s). Figure 2.3

(j) showed fairly smooth finish when no hydrophobic additive(s) was used in the coating

formulation and evidently did not exhibit superhydrophobicity. When 2 wt.% of

hydrophobic additive A was included into the formula, porous structure were formed

although they did not exhibit the desired combination of micron and nano-sized features

(figure 2.3 (k)). As a result, they did not achieve superhydrophobicity. Similarly, when

only additive B was incorporated into the powder coating formulation keeping other ingredients the same, protruding micro-nano structures were not formed as obviously.

Atomic Force Microscope (AFM) images shown in figure 2.4 also proved the same fact. AFM images revealed the importance of double-scale hierarchical structures to attain superhydrophobicity of the developed powder coatings. They also exemplified how the concentration of the hydrophobic additive(s) influenced on the overall micro- and nanostructures of the finished coatings. Figure 2.4 (a) showed the surface topography of the powder coating without any hydrophobic additive. Its top surface was wholly covered with nanostructures that came from the nano-sized flow additive (TiO_2) and evidently only nanostructures were not adequate enough to exhibit water CA of more than 90°. When 1 wt.% of hydrophobic additive A was included into the powder coating formula, the texture was changed a bit (figure 2.4 (b)), but still was not able to produce water CA much higher than 100°. Subsequently, powder coating with 2 wt.% of hydrophobic additive A revealed some micron-sized features (figure 2.4 (c)) although their dimensions were too small to create a superhydrophobic surface coating (water CAs ~110°).[48,50,51] However, when 3 wt.% of the same additive was incorporated in polymeric resin (figure 2.4 (d)), the cured coating exhibited both micro- and nanostructures that caused water CA over 160°.
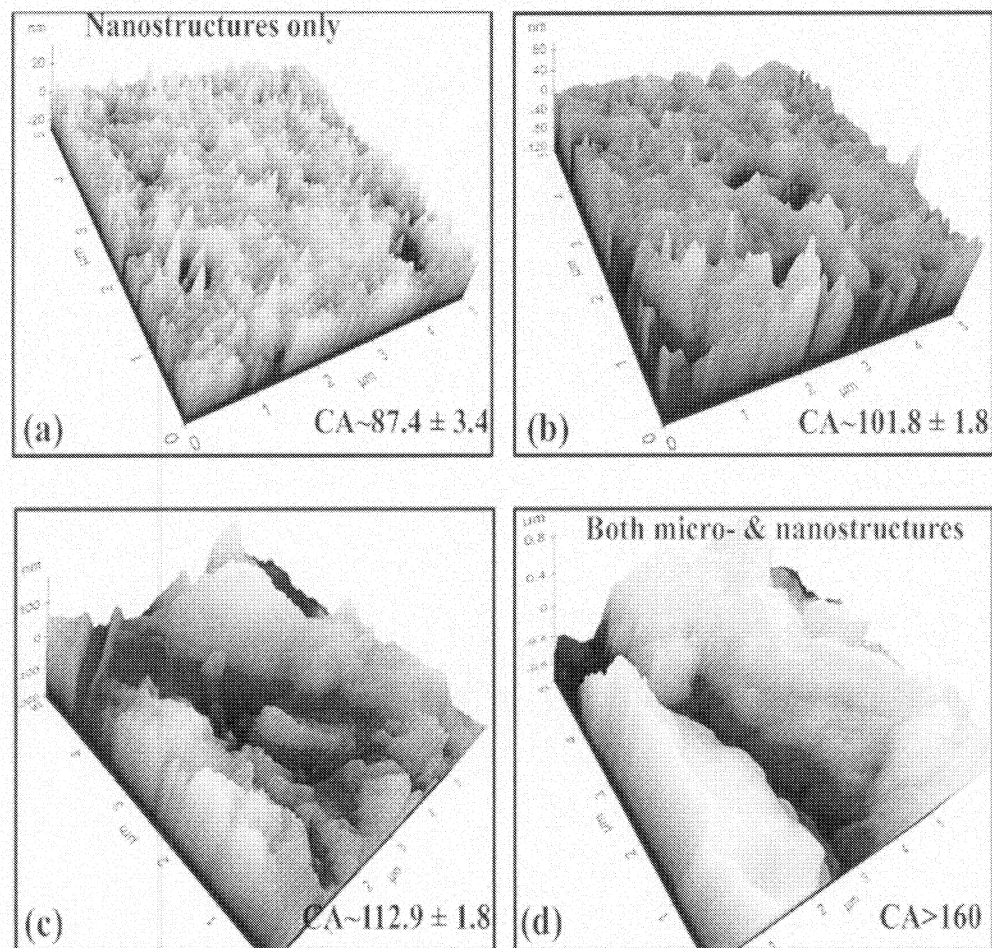
Figure 2.4: AFM images of the developed powder coatings with increasing hydrophobicity. (a) Powder coating without any hydrophobic additive; (b) Powder coating with 1 wt.% of hydrophobic additive A; (c) Powder coating with 2 wt.% of hydrophobic additive A; (d) Powder coating with 3 wt.% of the same additive (A)

Figure 2.5 shows how easily water droplets formed spheres and rolled off on the *lotus leaf* and the comparison with superhydrophobic coating developed by ultrafine powder coating technology. On both surfaces, water droplets formed very high contact angles. The measured CA confirmed that the developed coating was as hydrophobic as the

natural *lotus leaf*. Our superhydrophobic coatings exhibited water CA of more than 160°.

Not only that, the water droplets were so unstable on the coated surfaces that they rolled

off and ran away from the surfaces even when they were tilted only 1 or 2 degrees. That

gave the water sliding angles as minimum as possible, which is another important criteria

for a surface to be superhydrophobic.[14,52]
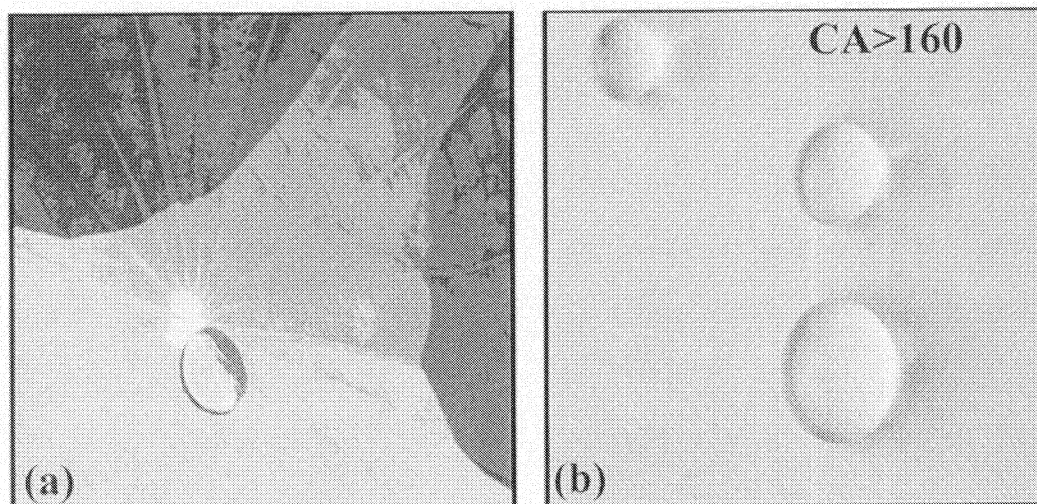
Figure 2.5: Water droplet formed sphere on lotus leaf (a) and on the superhydrophobic powder coating (b).

The reason behind the very high water CA was the enclosed air (shown in figure 2.6) in

between the water droplets and superhydrophobic surface. Indeed, ideal

superhydrophobic surfaces usually possess an enormous number of this type of air

pockets. Due to these air pockets, the contact line or the interface between the water

droplet and the surface became very small, while the water/air interface was enlarged. As

a result, water droplets did not spread on such superhydrophobic surfaces because of

gaining only very little energy through adsorption since the water/solid interface

remained minimum.[2] In fact, the fraction of water/solid interface significantly influenced

the water CA on these micro-nano textured surface[18,34,51] as illustrated by the Cassie-Baxter equation:[53]

$$\cos\theta^* = -1 + \phi_s(\cos\theta + 1) \qquad \text{------------(1)}$$

where θ represents the contact angle of a flat surface and θ^* is that of a textured surface while ϕ_s is the fraction of solid/water interface. According to Cassie-Baxter equation, the smaller the value of ϕ_s the higher would be the hydrophobicity.
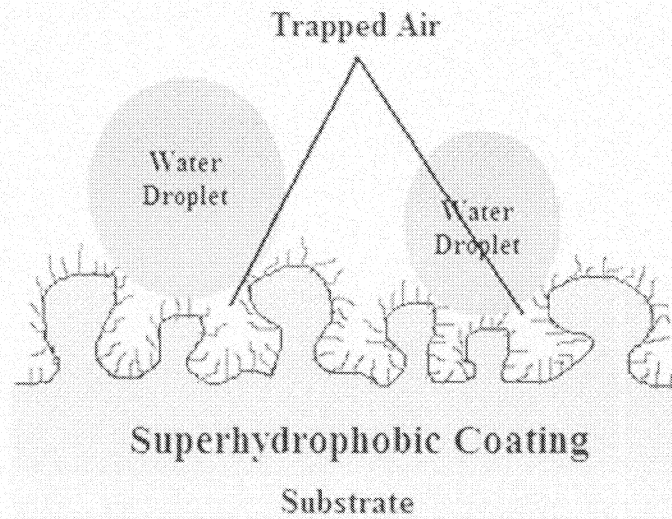
Figure 2.6: Trapped air caused the high water contact angle produced on the superhydrophobic coating

In fact, the trapped air exerted an upward pressure on the water droplet so that the air could be released. Due to this fact, whenever the superhydrophobic surfaces were trembled or inclined to only few degrees, the trapped air came out from the air pockets while they displaced the water droplets. That caused water droplets to become unstable and to roll off on the superhydrophobic surfaces. In other words, discontinuous or discrete three-phase (solid-liquid-air) contact line (TCL) was developed that potentially

drove the droplets off the superhydrophobic surfaces.[54] As a result, this type of unique surface exhibited very low sliding angles.

Due to the incorporation of nano-sized low-energy hydrophobic additives into the coating formula, micro- and nanostructured surfaces were created. Indeed, these unique dual-size features caused surface energy minimization in the superhydrophobic surfaces. In fact, when the nano-hairs of each papilla came together and formed submicron bundles of nanostructures, the overall surface energy of the created superhydrophobic surfaces was minimized.[55] It is well established that the surfaces with minimum surface energies would give the highest water CA possible.

The developed superhydrophobic coatings were highly adherent to their underlying substrates. When subject to the standard test for coating adhesion, they were found to have excellent adhesion (5B, according to ASTM D3359) to their substrate. Indeed, none of the lattice squares were dislodged by the removal of the tape during the testing. In addition to the superior coating adhesion, the developed surfaces also showed higher degree of durability in terms of their hydrophobicity. The wet cloth rubbing test revealed that the superhydrophobic coatings, which, were made of polymeric clearcoat resin incorporated with hollow fillers, nano-sized hydrophobic additive(s) and flow additive (TiO$_2$), passed 2500 rubs with a change of water CA less than 10°. In many cases, the coatings regained superhydrophobicity when they were dried up at ambient air.

Essentially, since no solvent was used in this unique superhydrophobic coating

fabrication process, the reported ultrafine powder coating technique did not contribute to

hazardous VOC emissions to the environment. Furthermore, this method cut the cost of

solvent(s). Moreover, solvent evaporation step (that consumes a significant amount of

energy) was not needed to be included in our simple powder coating process. This further

reduced the manufacturing costs of superhydrophobic surfaces.

2.4. Conclusions

The environmentally friendly and cost-effective superhydrophobic powder coatings

exhibited water CA of above 160° and sliding angle of less than 5° that made them

comparable to the natural *lotus leaf.* The higher CA and lower sliding angle were

supposedly attributed to their unique dual-size (micro and nano-scale) roughness leading

to the minimization of surface energy. Due to the presence of micron-sized peaks and

valleys, the superhydrophobic surfaces could trap air in between the water droplet and the

surface (i.e., air pockets), which determined the minimal contact of water droplet with the

superhydrophobic surface. Trapped air also caused the droplets to be unstable and to roll

away from the surface with slightest inclination.

References

1. Sun, T.; Feng, L.; Gao, X.; Jiang L., *Acc. Chem. Res.* **2005**, *38*, 644.

2. Barthlott, W.; Neinhuis, C., *Planta* **1997**, *202*, 1.

3. Neinhuis, C.; Barthlott, W., *Ann. Bot.* **1997**, *79*, 667.

4. Nakajima, A.; Fujishima, A.; Hashimoto, K.; Watanabe, T., *Adv. Mater.* **1999**, 11, 1365.

5. Zhai, J.; Li, H.J.; Li, Y.S.; Li, S.H.; Jiang, L., *Physics* **2002**, 31, 483.

6. Shafrin, E.G.; Zisman, W.A., In contact angle, wettibility and adhesion. *Adv. Chem. Ser. 43; Fowkes, F.M., Ed.; American Chemical Society*: Washington, DC, **1964**, 145-167.

7. Herminghaus, S., *Europhys. Lett.*, **2000**, 52, 165.

8. Erbil, H.Y.; Demirel, A.L.; Avci, Y.; Mert, O., *Science* **2003**, 299, 1377.

9. Lu, X.Y.; Zhang, C.C., Han, Y.C., *Macromol. Rapid Commun.* **2004**, 25, 1606.

10. Lu, X.Y.; Zhang, C.C.; Han, Y.C., *Macromol. Rapid Commun.* **2005**, 26, 637.

11. Feng, L.; Li, S.H.; Li, H.J.; Zhai, J.; Song, Y.L.; Jiang, L.; Zhu, D.B., *Angew. Chem. Int. Ed.* **2002**, 41, 1221.

12. Wal, P.V.; Steiner, U., Superhydrophobic surfaces made from Teflon. *Soft Matter* **2007**, 3, 426-429.

13. Dou, Q.; Wang, C.; Cheng, C.; Han, W.; Thune, P.C.; Ming, W., PDMS-modified polyurethane films with low water contact angle hysteresis. *Macromolecular chemistry and Physics* **2006**, 207, 2170-2179.

14. Jin, M.; Feng, X.; Xi, J.; Jin, Z.; Cho, K.; Feng, L.; Jiang, L., Super-hydrophobic PDMS surface with ultra-low adhesive force. *Macromol. Rapid. Commun.* **2005**, 26, 1805-1809.

15. Hozumi, A.; Takai, O., Preparation of ultra water-repellent films by microwave plasma-enhanced CVD. *Thin Solid Films* **1997**, 303, 222-225.

16. Hong, B.S.; Han, J.H.; Kim, S.T.; Cho, Y.J.; Park, M.S.; Dolukhanyan, T.; Sung, C., Endurable water-repellent glass for automobiles. *Thin Solid Films* **1999**, 351, 274-278.

17. Nakajima, A.; Fujishima, A.; Hashimoto, K.; Watanbe, T., *Adv. Mater.* **1999**, 11, 1365.

18. Bico, J.; Marzolin, C.; Quéré, D., Pearl drops. *Europhysics Letters* **1999**, 47, 220.

19. Akamatsu, Y.; Makita, K.; Inaba, H.; Minami, T., Water-repellent coating silms on glass prepared from hydrolysis and polycondensation reactions of fluoroalkyltrialkoxysilane. *Thin Solid Films* **2001**, 389, 138-145.

20. Zhang, H.; Lamb, R.; Lewis, J., Engineering nanoscale roughness on hydrophobic surface-preliminary assessment of fouling behaviour. *Sci. and Tech. of Adv. Mater.* **2005**, 6, 236-239.

21. Li, H. J.; Wang, X. B; Song, Y. L.; Liu, Y. Q.; Li, Q. S.; Jiang, L.; Zhu, D. B., *Angew. Chem. Int. Ed.* **2001**, 40, 1743.

22. Li, S.; Li, H.; Wang, X.; Song, Y.; Liu, Y.; Jiang, L.; and Zhu, D., Superhydrophobicity of large-area honeycomb-like aligned carbon nanotubes. *J. Phys. Chem. B* **2002**, 106, 9274-9276.

23. Cho, S.C.; Hong, Y.C.; Uhm, H.S., Hydrophobic coating of carbon nanotubes by CH₄ glow plasma at low pressure and their resulting wettability, *J. Mater. Chem.* **2007**, 17, 232-237.

24. Yan, L.; Wang, K.; Ye, L., Superhydrophobic property of PVDF/CaCO3 nanocomposite coatings. *J. of Mat. Sci. Lett.* **2003**, 22, 1713-1717.

25. Jiang, L.; Zhao, Y.; Zhai, J., *Angew. Chem. Int. Ed.* **2004**, 43, 4338;

26. Li, Y.; Cai, W. P.; Duan, G. T.; Cao, B. Q.; Sun, F. Q.; Lu, F., J., *Colloid. Interf. Sci.* **2005**, 248, 634.

27. Hsiang, H.-I.; Liang, M.-T.; Huang, H.-C.; Yen, F.-S., Preparation of superhydrophobic boehmite and anatase nanocomposite coating films. *Materials Research Bulletin* **2007**, 42, 420-427.

28. Woodward, I.; Schofield, W.C.E.; Roucoules, V.; Badyal, J.P.S., *Langmuir* **2003**, 19, 3432.

29. Fresnais, J.; Benyaha, L.; Chapel, J.P.; Poncin-Epaillard, F., *Eur. Phys. J. Appl. Phys.* **2004**, 26, 209.

30. Kim, S.H.; Kim, J.-H.; Kang, B.-K.; Uhm, H.S., Superhydrophobic CFx coating via in-line atmospheric RF plasma of He-CF₄-H₂ *Langmuir* **2005**, 21, 12213-12217.

31. Krupenkin, T.N.; Taylor, J.A.; Schneider, T.M.; Yang, S., *Langmuir* **2004**, 20, 3824.

32. Qian, B.T.; Shen, Z.Q., *Langmuir* **2005**, 21, 9007.

33. Ma, M.; Mao, Y.; Gupta, M.; Gleason, K.K.; Rutledge, G.C., *Macromolecules* **2005**, 38, 9742.

34. Oner, D.; McCarthy, T.J., *Langmuir* **2000**, 16, 7777.

35. Bico, J.; Tordeux, C.; Quere, D., Rough wetting, *Europhys. Lett,* **2001**, 55(2), 214-220

36. He, B.; Lee, J.; Patanker, N.A., Contact angle hysteresis on rough hydrophobic surfaces. *Colloids and Surfaces A: Physicochemical and Engineering Aspects* **2004**, 248, 101-104.

37. Shirtcliffe, N.J.; McHale, G.; Newton, M.I.; Chabrol, G.; Perry, C.C., *Adv. Mater.* **2004**, 16, 1929.

38. Furstner, R.; Barthlott, W.; Neinhuis, C.; Walzel, P., Wetting and self-cleaning properties of artificial superhydrophobic surfaces. *Langmuir* **2005**, 21, 956-961.

39. Pozzato, A.; Zilio, S. D.; Fois, G.; Vendramin, D.; Mistura, G.; Belotti, M.; Chen, Y.; Natali, M., *Microelectron. Eng.* **2006**, 83, 884.

40. Lee, S. M.; Kwon, T. H., *Nanotechnology* **2006**, 17, 3189.

41. Liu, B.; He, Y.; Fan, Y.; Wang, X., *Macromol. Rapid Commun.* **2006**, 27, 1859–1864

42. Lee, Y.; Park, S-H.; Kim, K-B.; Lee, J-K., *Adv. Mater.* **2007**, 19, 2330.

43. Tadanaga, K.; Morinaga, J.; Matsuda, A.; Minami, T., *Chem. Mater.* **2000**, 12, 590.

44. Xie, Q.; Xu, J.; Feng, L.; Jiang, L.; Tang, W.; Luo, X.; Han, C., *Adv. Mater.* **2004**, 16(4), 302.

45. Zhu, J.; Zhang, H., Fluidization Additives to Fine Powders. *U.S. Patent 6,833,185,* **2004**.

46. Geldart, D., Types of gas fluidization. *Powder Technol.* **1973**, 7 (5), 285-292.

47. Liu, Y.; Tang, J.; Wang, R.; Lu, H.; Li, L.; Kong, Y.; Qi, K.; Xin, J.H., Artificial lotus leaf structures from assembling carbon nanotubes and their applications in hydrophobic textiles. *Journal of Materials Chemistry* **2007**, 17 (11), 1071-1078.

48. He, B.; Patanker, N.A.; Lee, J., Multiple equilibrium droplet shapes and design criterion for rough hydrophobic surfaces, *Langmuir* **2003**, 19, 4999-5003.

49. Lee, W.; Jin, M.-K.; Y, W.-C.; Lee, J.-K., Langmuir **2004**, 20, 7665-7669.

50. Patanker, N.A., On the modeling of hydrophobic contact angles on rough surfaces. *Langmuir* **2003**, 19, 1249-1253.

51. Bico, J.; Thiele, U.; Quere, D., Wetting of textured surfaces. *Colloids and Surfaces A: Physicochemical and Engineering Aspects* **2002**, 206, 41-46.

52. Marmur, A., Wetting on hydrophobic rough surfaces: To be heterogeneous or not to be? *Langmuir* **2003**, 19, 8343-8348.

53. Cassie, A.B.D.; Baxter, S., *Trans. Faraday Soc.* **1944**, 40, 546.

54. Feng, L.; Li, S.; Li, H.; Zhang, L.; Zhai, J.; Song, Y.; Liu, B.; Jiang, L.; Zhu, D., Superhyfrophobic Surfaces: From Natural to Artificial. *Adv. Mater.* **2002**, 14 (24), 1857-1860.

55. Xie, Q.; Fan, G.; Zhao, N.; Guo, X.; Xu, J.; Dong, J.; Zhang, L.; Zhang, Y.; Han, C.C. *Adv. Mater.* **2004**, 16 (20), 1830-1833.

CHAPTER 3
Nano-TiO₂ Enriched Polymeric Biocompatible Powder Coatings[1]

Chapter Summary

The objective of this study was to utilize ultrafine powder coating technology to prepare

polymeric powder coatings that can support human mesenchymal cell attachment and growth.

Resins were modified with titanium dioxide and polytetrafluoroethylene (PTFE), and enriched

with either SiO₂ or TiO₂ nanoparticles (nSiO₂ or nTiO₂) to create continuous polymeric powder

coatings (PPC). Scanning electron microscopy (SEM) revealed complex surface topographies

with nano features, and energy dispersive x-ray (EDX) analysis with Ti mapping confirmed a

homogenous dispersion of the material. SEM and inverted fluorescence microscopy showed that

human embryonic palatal mesenchymal (HEPM) cells attached and spread out on the PPC

surfaces, particularly those enriched with nTiO₂. Cell counts were higher, and the MTT assay

measured more metabolic activity from the nTiO₂ enriched PPCs. Furthermore, these cellular

responses were enhanced on PPC surfaces that were enriched with a higher concentration of

nTiO₂ (2% versus 0.5%), and appeared comparable to that seen on commercially pure titanium

(cpTi). Therefore the nTiO₂ enrichment of polymeric powder coatings was shown to favor human

mesenchymal cell attachment and growth. Indeed, this modification of the materials created

continuous surface coatings that sustained a favorable cellular response.

---

[1] A version of this chapter has been accepted in the *Journal of Biomaterials Applications* for publication (Mohammad Sayem Mozumder, Jesse Zhu, Hiran Perinpanayagam. "Nano-TiO2 Enriched Polymeric Powder Coatings Support Human Mesenchymal Cell Attachment and Growth" *Journal of Biomaterials Application 2010*, In Press.) *Copyright is owned by both the authors and the SAGE publication Ltd.*

3.1. Introduction

The long-term success of orthopedic and dental implants is dependent on their

osseointegration with the surrounding bone. This integration is dependent on the

biocompatibility of the materials, and therefore highly biocompatible titanium and

titanium alloys have become widely used as implant materials. In addition, since surface

topography and biochemistry affect their interaction with the surrounding tissues,[1] the

titanium surfaces have been modified by various polishing, grit blasting, machining,

microfabrication, and acid and chemical etching techniques, to optimize the cellular

response.[2-7]

Now, recent studies have reported on the use of polymeric materials and composites for

orthopedic implants[8-11] and for vascular grafts.[12, 13] Furthermore, these polymeric

substrates have been modified and coated with titanium or titania to enhance their

cytocompatibility. The different polymers have had sputter-coating, vapor and plasma

deposition for the application of titanium and other metals, to enhance the cellular

response.

An earlier study by Lehle et al.[13] used a plasma-assisted chemical vapor deposition

process to apply a titanium-carboxonitride layer onto polyethylene terephthalate (PET),

polypropylene (PP), polytetrafluoroethylene (PTFE), polyurethane, and silicone. They

found that endothelial cell adhesion was enhanced on the titanium-coated surfaces.

Likewise, Jain et al.[14] sputter-coated titanium onto smooth and micro-textured

polyethylene terephthalate (PET) surfaces, and found that fibroblasts preferentially

attached to the textured surfaces that had been coated with titanium. Later, Webster et al.[15] studied the incorporation of both conventional and nano TiO_2 ($nTiO_2$) into poly-lactic-co-glycolic acid (PLGA) and reported superior Osteoblast-like cell attachment to $nTiO_2$ enriched PLGA than the conventional ones when they maintained PLGA to TiO_2 (70:30) ratio.

Therefore, the recent trend is to apply titanium or titania nanoparticles or to fabricate titanium nano features onto polymeric surfaces to further improve the cellular responses. As an example, Yao et al.[10] used a novel ionic plasma deposition (IPD) process to apply titanium or gold, and also to create nano-sized features of titanium on polyetheretherketone, ultra-high molecular weight polyethylene (UHMWPE) and PTFE. They found that osteoblast adhesion and spreading were better on the coated polymers than on the uncoated surfaces. Similarly, Reising et al.[9] used the IPD process to apply titanium and to add nano-features on UHMWPE and PTFE. They found that osteoblast proliferation and mineral deposition were enhanced on the coated polymers compared to the uncoated material and titanium controls. Recently, Ozkucur et al.[16] used a physical vapor deposition technique to deposit a thin film (<100 nm) of titanium or zirconium onto polyurethane surfaces and reported enhanced endothelial cell adhesion and proliferation. Most recently, Pareta et al.[8] used IPD and nitrogen ion immersion plasma deposition to apply nano-particulate titanium onto metallic implant materials such as titanium and titanium alloy (Ti6Al4V), and onto polymers such as PET, polyvinyl chloride, polyurethane, PTFE, UHMWPE and nylon. They found an increase in osteoblast adhesion on the modified surfaces compared to the untreated controls. However, despite

of being able to retain original particle size, chemistry and crystallinity in the coated surfaces,[8-10,12] IPD process involves a much higher installation and operating costs. Therefore, it is necessary to inquire into simple and inexpensive coating process to fabricate nano features onto target substrates.

Now, in this study we have utilized an entirely novel but simple and inexpensive approach for applying nano-sized metal oxides in combination with polymeric resins to create nano-featured cytocompatible coatings. We used a patented ultrafine powder coating technique[17,18] to disperse nano-sized metal oxides and polymeric resins. By using this advanced powder coating technology, we combined ultrafine resin powders containing polyester or epoxy with nano-sized silica or titanium dioxide and dispersed them homogenously. This novel powder coating technology enabled the utilization of ultrafine particles (15-20 μm) and nano-sized particles, whereas conventional powder coating can only use larger particles that ensure adequate fluidization. In addition, the ultrafine powder coating technology is environmentally friendly since it does not use any toxic solvent in the whole process that may emit volatile organic compounds (VOCs).

Furthermore, we have now studied the cellular response to these powder coatings and herein report on their capacity to support human mesenchymal cell attachment and spreading, and to sustain metabolic activity. We will also report on the variation in cytocompatibility of alternative formulations of these coatings, and described a markedly enhanced cellular response to nano-titania enriched polymeric coatings.

3.2. Materials and Methods

<u>Preparation of Polymeric Powder Coatings (PPC)</u>

Polymeric powder coatings (PPC) were prepared by the modification of commercially

available resins (table 3.1), and the application of Zhu and Zhang's patented powder

coating technology,[17,18] to ensure adequate flow of the ultrafine resins and additives

mixtures (Figure 3.1). Either Avalanche white polyester (PE embedded with 25 wt.%

micron-sized TiO_2) (Links Coating, London, Canada) (PPC-2, -3 and -4), or epoxy resins

(Links Coating, London, Canada) (PPC-1) were combined with filler, and flow,

degassing and curing agents. These mixtures were processed through a twin-screw

extruder (Donghui Powder Processing Equipment Co., Yantai, China) to create chips that

were then ground into powder particles (15-20 μm). The fine powders were then mixed

with nano-sized polytetrafluoroethylene (PTFE, 3%), which served to increase the

surface roughness of the final coatings. Then, either titanium dioxide (TiO_2; Degussa,

USA; PPC-3 and -4), or silica (SiO_2; Degussa, USA; PPC-1 and -2) nano-particles were

added through high-shear mixing. Due to the high shear mixing, the agglomerates of

both the nano and micron-sized particles were broken up, and the nano particles took

place in between the micron-sized particles. Thus they served to increase the separation

distance between the micron-sized powder coating particles, and thereby ensured an

adequate flow of the ultrafine mixture.[17] Without these nano-additives, the ultrafine

powder particles (15-20 μm) would agglomerate significantly and hinder flow.[19]
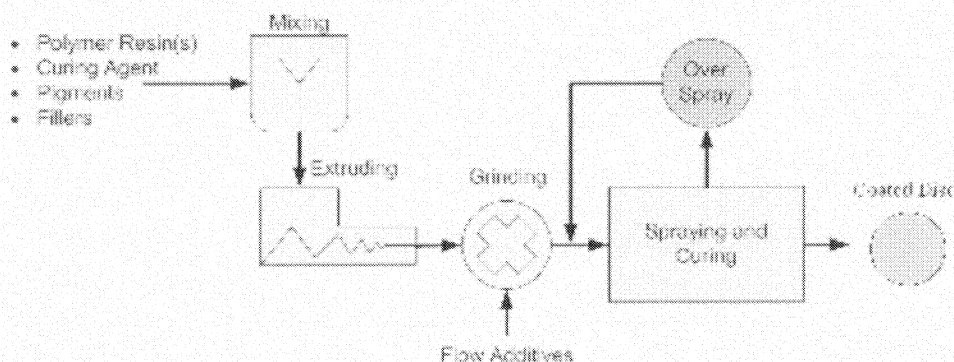
Figure 3.1: Ultrafine powder coating process. Polymeric Powder Coatings (PPC) were prepared through an advanced ultrafine powder coating process. Polymeric resins, pigments, fillers and curing agent were mixed and then extruded as homogeneous chips. The chips were then ground into ultrafine powders (15-20 µm), dry blended and mixed with nano-sized flow additives (nTiO2 and nSiO2). These ultrafine mixtures were electrostatically sprayed onto a grounded workpiece, and cured in a furnace (200°C, 10 min). Oversprayed powders were recycled and reused.

Table 3.1: PPC formulations

No.	Base Coating	Additive	Embedded [TiO$_2$] (%)[3]	Added [nTiO$_2$] (%)[3]
PPC-1	Polymeric Resin[1] + PTFE	nSiO$_2$	0	0
PPC-2	Polymeric Resin[2] + PTFE	nSiO$_2$	25.0	0
PPC-3	Polymeric Resin[2] + PTFE	nTiO$_2$	25.0	0.5
PPC-4	Polymeric Resin[2] + PTFE	nTiO$_2$	25.0	2.0

[1] Epoxy

[2] Avalanche White Polyester

[3] Weight Percent

Finally, the powder mixtures (Table 3.1) were passed through a sieve (32 μm) to remove oversized particles, and then fed through a hopper to the tip of a spray gun. As the spray gun was activated, a voltage was applied to ionize the particles that were then sprayed onto sheets of aluminum that were grounded. Subsequently, the powder-coated sheets were cured (at 200° C for 10 min). Upon curing, the PPC coatings could become porous and nano topographic.

Adhesion to Substrate

The adhesion of the PPC to the underlying substrate was confirmed with an Elcometer 107 Cross Hutch Cutter (Elcometer Ltd., Windsor, Canada). The coatings were cut down to the substrate with a blade (11x1.5 mm), as recommended by ASTM D3359, and several perpendicular cuts were made to create a grid of small squares. This lattice was brushed to remove debris, covered with adhesive tape (ASTM standard), and firmed with a pencil eraser. The tape was then withdrawn by a single smooth pull, and the remaining grid squares compared for retention. The lattice was then assessed for adhesion by using the ASTM D3359 standards.

Surface Topography

The surface topography of the PPC was assessed by scanning electron microscopy (SEM). The PPC surfaces were mounted on metal stubs with the aid of adhesive carbon tape and were sputter coated with gold (10 nm), and then carefully examined with a Hitachi S-2600 (Hitachi, Pleasonton, CA) SEM. The working voltage (15 kV), beam (60) and working distance (5.2 mm) were set.

Elemental Analysis and Ti Mapping

The elemental composition of the PPC surfaces was analyzed by energy dispersive X-ray

spectroscopy (EDX) using a suitably equipped Hitachi S-2600 SEM. The PPC surfaces

were mounted on metal stubs and sputter coated with gold (10 nm) as detailed above.

The working voltage (15 kV), beam (60) and working distance (15 mm) were set. The

EDX analyses quantified nearly all the elements with a minimum detection limit of 0.0

wt%. These analyses were repeated at three separate locations on each surface and mean

surface concentrations of carbon and titanium were reported. In addition, mapping of

elemental Ti on PPC-4 was performed by EDX to visualize the actual distribution of Ti

over the entire surface. While doing Ti mapping, samples were loaded as same as they

were loaded for SEM and elemental EDX, only different mode of operation (back-

scattered electron at higher working distance (~15 mm)) was selected to get the elemental

mapping.

Surface Roughness

The surface roughness of the PPC was measured with a Dektak 8 Stylus Surface Profiler

(Veeco Metrology Group, Santa Barbara, CA). The PPC were loaded onto a high

precision stage that moved beneath a diamond-tipped stylus according to specified scan

length (20 mm), scan resolution (1.111 μm/sample) and stylus force (8 mg). Each PPC

surface was scanned at 10 different locations to measure vertical features. The mean

deviation of the vertical features from the centerline was then calculated as a measure for

surface roughness (R_a).

Disinfection and Sterilization

The PPC surfaces and cpTi were disinfected and sterilized in preparation for tissue culture. The PPC and cpTi disks were rinsed twice with ethanol (70%), washed thrice with phosphate-buffered saline (PBS) and then placed into individual wells of a 24-well tissue culture plate. The entire plate of disks were then placed in a tissue culture hood and exposed to UV light for 30 minutes to ensure sterility.

Cell Culture

Human embryonic palatal mesenchymal cells (HEPM, ATCC CRL-1486) were seeded onto cpTi and PPC in multiple 24-well tissue culture plates (50,000 cells/well). The cultures were maintained in Dulbecco's modified eagles medium (DMEM) supplemented with fetal bovine serum (FBS, 10%), L-glutamine (2 µmol/ml), penicillin G (100 U/ml), streptomycin sulfate (100 µg/ml) and amphotericin B (0.25 µg/ml)). Replicate cultures were incubated at 37°C for 24 and 72 hours and then harvested for analysis. Additional cultures were seeded at a higher cell density (100,000 cells/well) to identify extracellular matrix formation over 72 hours.

Cell Surface Interactions

After each incubation period, the replicate PPC disks were collected, washed three times with PBS, fixed with glutaraldehyde (2.5%) in cacodylate buffer (100 mM) for 20 minutes, dehydrated in ascending grades of ethanol (25, 50, 75, 95 and 100%) and immersed in hexamethyldisilazane. Then the surfaces were air dried, mounted on metal

stubs, sputtered with gold (20 nm) and examined with a Hitachi S-2600 SEM as detailed

above. The working voltage (5-12 kV), beam (60) and working distance (5.3 mm) were

set.

Cell Morphology and Cytoskeletal Organization

After 72 hours of growth on titanium and PPC surfaces, the cultures were harvested and

washed thrice with PBS. The cells that were attached to the surfaces were fixed with

paraformaldehyde (4% for 10 min) and permeabilized with Triton X-100 (0.1% for 5

min). The actin filaments of the cytoskeleton were labeled with rhodamine phalloidin

(Cytoskeleton, Denver, CO) for 2 hours at room temperature. The surfaces were then

mounted using Vectashield with DAPI (Vector Laboratories, Burlingame, CA) and

examined by an inverted fluorescence microscope (Axiovert 40 CFL, Carl Zeiss Canada

Ltd., Toronto, Canada) with the magnification of 20X.

Cell Attachment Assay

HEPM cells were seeded onto titanium disks and PPC surfaces in multiple 24-well tissue

culture plates (20,000 cells/well). After 24 and 72 hours of cell attachment and growth,

triplicate cultures were harvested from each surface, and carefully rinsed with PBS to

remove unattached cells. Then, trypsin (150 µl) was added to each well and the culture

plates were incubated (37°C for 5 minutes) to release the attached cells. These cells were

collected and counted in a hemocytometer.

Cell Viability and Metabolic Activity

The same numbers of HEPM cells (20,000 cells/well) were seeded onto titanium and PPC

surfaces in multiple 24-well tissue culture plates using the same protocol as in the cell

attachment assay. After 24 and 72 hours, the cpTi and the PPC surfaces were rinsed with

trypsin to release attached cells that were collected and reseeded into multiple 48-well

tissue culture plates. After 24 hours, MTT reagent (tetrazolium (3-(4, 5-

dimethylthiazolyl-2)-2, 5-diphenyltetrazolium bromide) was added and the cultures were

incubated (37°C) for an hour in the dark. The reagents were then carefully replaced with

MTT solubilizing solution (acid-isopropanol), and the absorbance (570 nm) measured in

a Safire Multi-Detection Microplate Reader (Tecan, Austria).

Statistical Analysis

In the cell attachment assay and the MTT assay, the differences between the replicate

cultures grown on different surfaces, and at different time points, were analyzed

statistically by a two-way analysis of variance (ANOVA) with a Bonferroni post-hoc test,

to a significance level of $P < 0.05$.

3.3. Results

Polymeric powder coatings (PPC) were created

When polymeric resins were combined with fillers and additives, and processed and

applied by advanced powder coating technology, polymeric powder coatings (PPC) were

created (Figure 3.1). The first coating, PPC-1, contained epoxy resin and PTFE, as well

as $nSiO_2$ (~25 nm average diameter) additive to ensure powder flow (Table 3.1). The

second coating, PPC-2, contained titanium-embedded polyester and PTFE, and again nSiO$_2$ as the additive. Then the third coating, PPC-3, contained titanium-embedded polyester resin and PTFE, but nTiO$_2$ (~40 nm average diameter) was the additive. Similarly the fourth coating, PPC-4, contained titanium-embedded polyester resin and PTFE, and nTiO$_2$ additive at a higher concentration.

All of these coatings had high levels of nano-scale surface roughness (Table 3.2). The mean roughness of the developed surfaces ranged from 250 to 280 nm, well within the nano-scale. The morphology of the coatings was shown in figure 3.2A. Moreover, the PPCs were highly adherent to their underlying substrate (Table 3.2). When subject to the standard test for adhesion, all of the PPC were found to have excellent adhesion to their substrate. Indeed, none of the lattice squares were dislodged by the tape removal during testing.

In addition, all of the coating surfaces had fairly similar elemental compositions, with the exception that PPC-1 lacked titanium (Figure 3.2B). The titanium was readily detected in PPC-2, -3 and -4 due to its incorporation in their formula; whereas titanium was undetected in PPC-1 due to its absence in its formulation. Furthermore, the concentration of titanium was progressively higher in PPC-3 and PPC-4, compared to PPC-2 (0% nTiO$_2$), due to the use of progressively higher concentrations of nTiO$_2$ as the nano-additive in PPC-3 (0.5% nTiO$_2$) and PPC-4 (2% nTiO$_2$).

Table 3.2: Coating Characterization

Coatings	Surface Roughness (nm)	Adhesion[1]
PPC-1	251.3 ± 22.3	5B
PPC-2	268.3 ± 26.9	5B
PPC-3	262.8 ± 18.1	5B
PPC-4	281.9 ± 13.8	5B

[1] Adhesion was assessed by comparing the lattice of cuts with ASTM D3359 standards from 5B to 0B. 5B corresponds to completely smooth edges of the cuts (i.e., none of the lattice squares were detached)

On those coatings that contained titanium (PPC-2, -3 and -4), it appeared to be evenly dispersed across their surfaces. The EDX analyses measured a similar concentration of titanium at each of the three measurement sites for each coating. Furthermore, surface mapping of PPC-4 showed that the titanium was evenly distributed across the surface (Figure 3.2C).

The PPC had complex surface topography

The PPC surfaces had complex micro-topographies (Figure 3.2A). When the PPC surfaces were prepared, SEM examination showed complicated and elaborate surface topographies. There were numerous surface projections of nanometer scale and an underlying labyrinth of concavities that created intricate and elaborate surface topography. There were shallow and deep pits and cavities of micron dimension that

contributed to surface roughness and porosity. The average porosity and the pore

diameter of the PPC surfaces were 25% and ~20 µm, respectively.
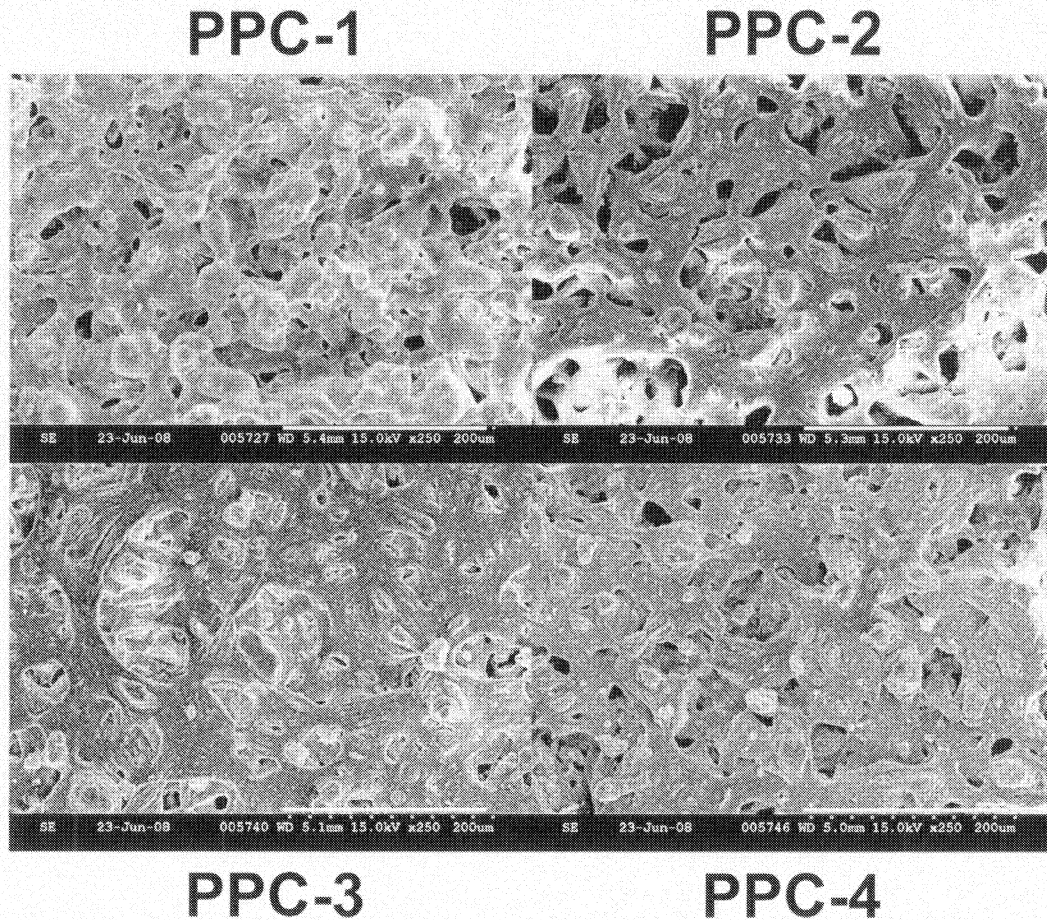
Figure 3.2A: Polymeric powder coatings (PPC-1, -2, -3 and -4) were prepared and
examined by scanning electron microscopy (SEM). All of the coatings were
characterized by outward projections and inward concavities that created rough surface
topographies. (Scale bar = 200 µm).

PPC-1

PPC-2

C: 81.2% ± 0.07%
Ti: 0.0% ± 0.0%

C: 55.6% ± 0.69%
Ti: 10.8% ± 0.49%

C: 53.4% ± 0.51%
Ti: 12.9% ± 0.28%

C: 49.5% ± 0.61%
Ti: 15.5% ± 0.27%

PPC-3

PPC-4
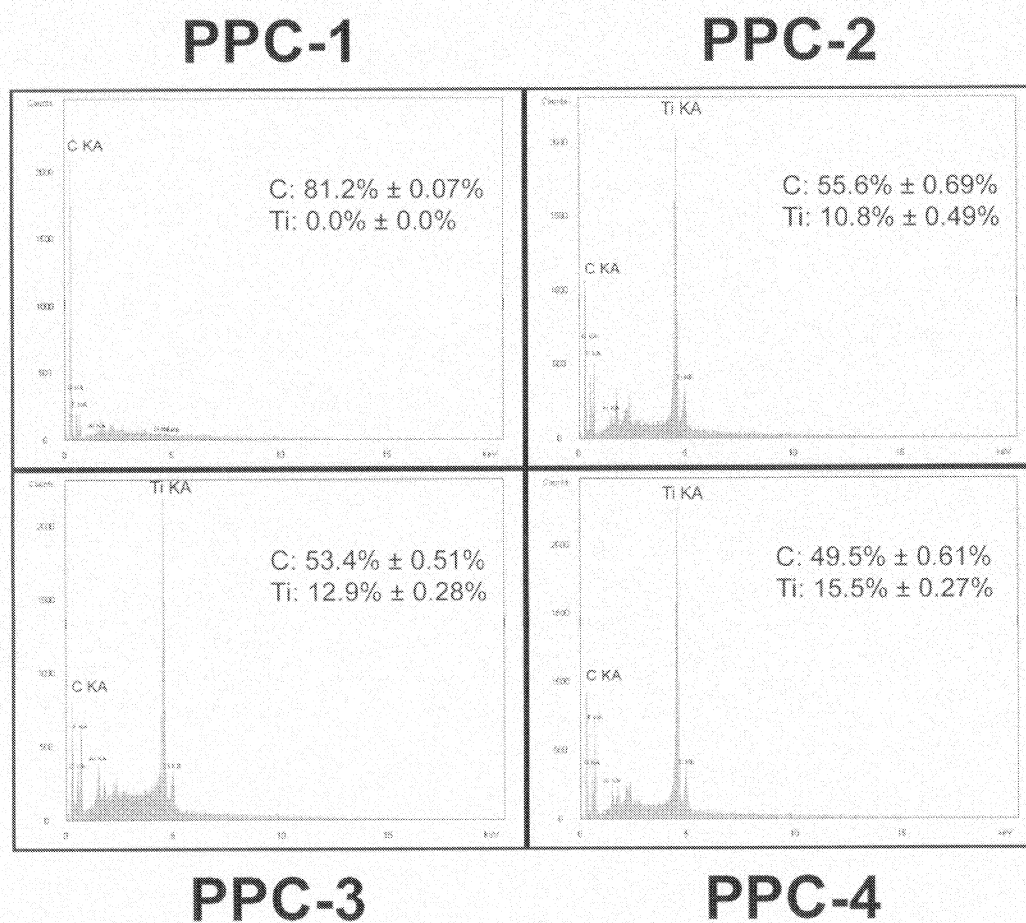
Figure 3.2B: Polymeric powder coatings (PPC-1, -2, -3 and -4) were prepared and their surfaces analyzed by energy dispersive X-ray (EDX) spectroscopy. The mean surface concentration of elemental carbon (C) and titanium (Ti) were reported with their standard deviations. Ti was undetected in PPC-1, and was detected at progressively higher levels in PPC-2, -3 and -4.
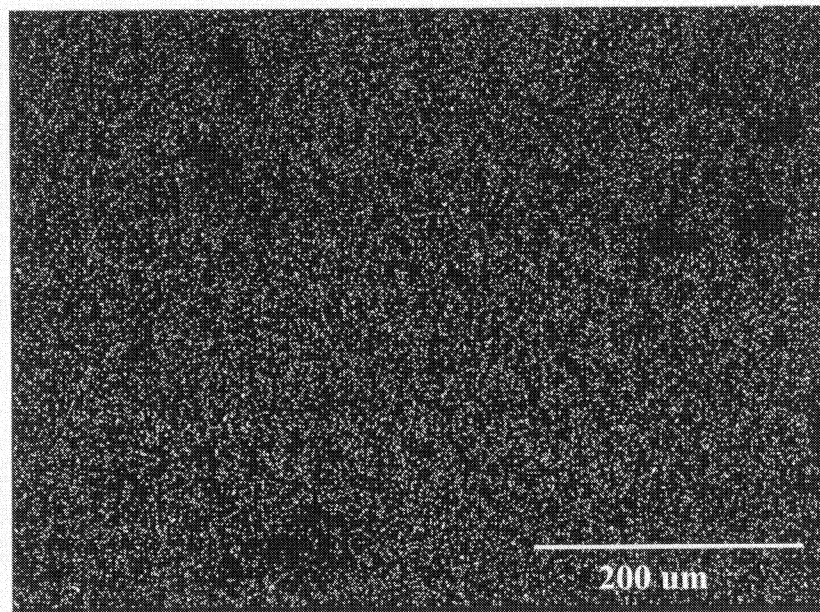
Figure 3.2C: During the EDX analysis of the PPC, the surface distribution of elemental titanium was mapped concurrently. An even dispersion of titanium was seen on PPC-2, -3 and -4. Shown here is a representative mapping of the surface titanium on PPC-4.

Cells attached to the PPC

The HEPM cells attached and spread out onto all of the PPC surfaces (Figures 3.3A, 3.3B, 3.4 and 3.5). When the cells (50,000 cells/well) were incubated in 24-well tissue culture plates for 24 hours, SEM showed that there were attached cells on all of the PPC surfaces (Figure 3.3A). There were numerous attached cells and they were well spread on PPC-4, and there were somewhat fewer attached cells and good spreading on PPC-3; but there were few attached cells and little spreading on PPC-1 and -2.
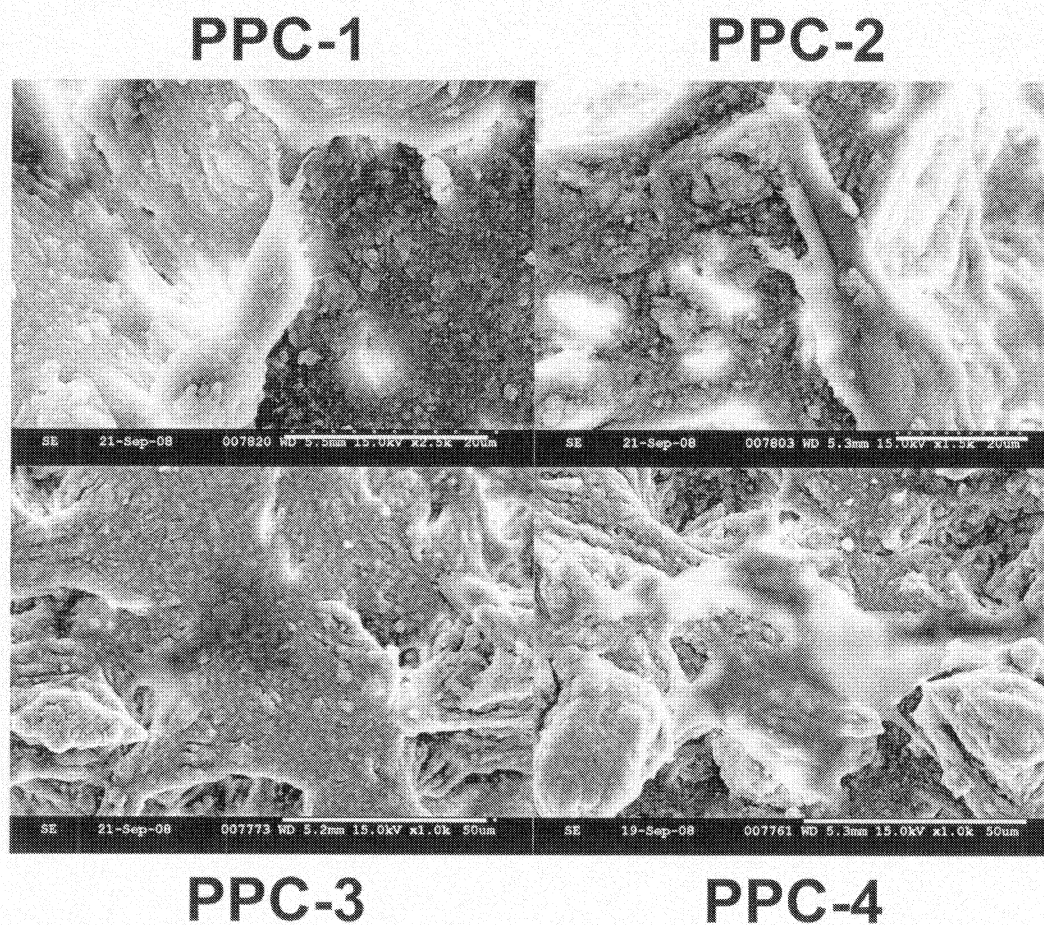
Figure 3.3A: Human mesenchymal cells (HEPM) were seeded onto polymeric powder coatings (PPC-1, -2, -3 and -4). After 24 hours, scanning electron microscopy (SEM) showed that there were few cells on PPC-1 and -2, but more cell attachment and spreading on PPC-3 and -4. (Scale bar = 20 μm for PPC-1 and PPC-2; Scale bar = 50 μm for PPC-3 and PPC-4).
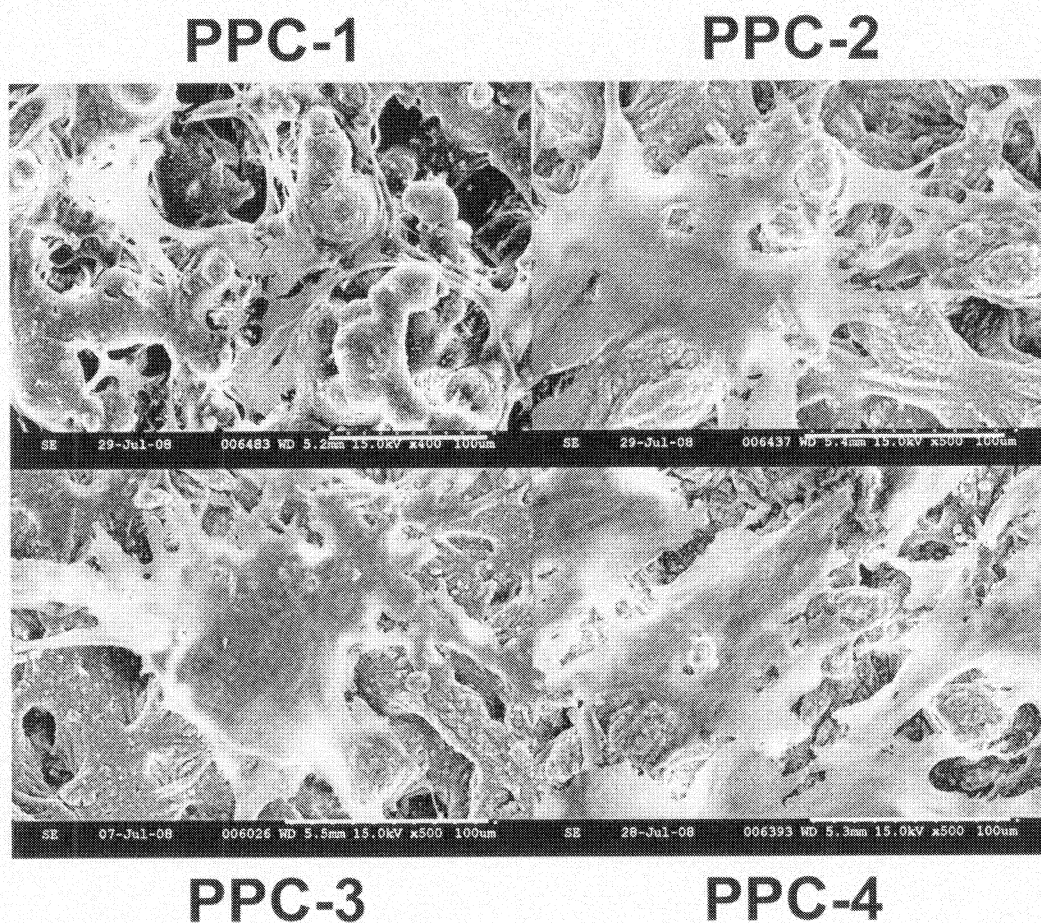
Figure 3.3B: Human mesenchymal cells (HEPM) were seeded onto polymeric powder coatings (PPC-1, -2, -3 and -4). After 72 hours, scanning electron microscopy (SEM) showed a few cells and cellular extensions on PPC-1; several cells spread out onto PPC-2 and -3; and numerous attached and well spread out cells on PPC-4. (Scale bar = 100 µm).

When these cells (50,000 cells/well) were incubated for 72 hours, SEM showed that the cells had attached and spread out on all of the PPC surfaces (Figure 3.3B). There were numerous cells that had attached and spread out on PPC-4 and -3, but fewer cells on PPC-2 and -1.

An extracellular matrix formed on some PPC

The HEPM cell cultures formed an extracellular matrix-like layer on some PPC surfaces (Figure 3.4). When a larger number of cells (100,000 cells/well) were grown for 72 hours, SEM showed that there were numerous attached cells on all of the PPC surfaces; and that a matrix-like layer had formed on some of the PPC surfaces. SEM showed that there was a matrix-like layer that covered most of PPC-4; smaller areas of matrix and cells that covered some of PPC-3; and clusters of cells on PPC-2 and -1.

Cells spread out on some PPC

The HEPM cells spread out on some of the PPC surfaces (Figure 3.5). When the cells (50,000 cells/well) were incubated in 24-well tissue culture plates for 72 hours, inverted fluorescence microscopy showed that there were attached cells on PPC-2, -3 and -4, and on the commercially pure titanium surfaces (cpTi, control samples). Numerous cell nuclei were detected on PPC-3 and -4, and on cpTi; several nuclei were detected on PPC-2; and very few were visible on PPC-1 (not shown). The cells were well spread out on the PPC-4 and titanium surfaces, whereas they were less spread on PPC-2 and -3. Fewer actin filaments were visible on PPC-3 and -4, than on titanium that supported more clearly defined stress fibers.
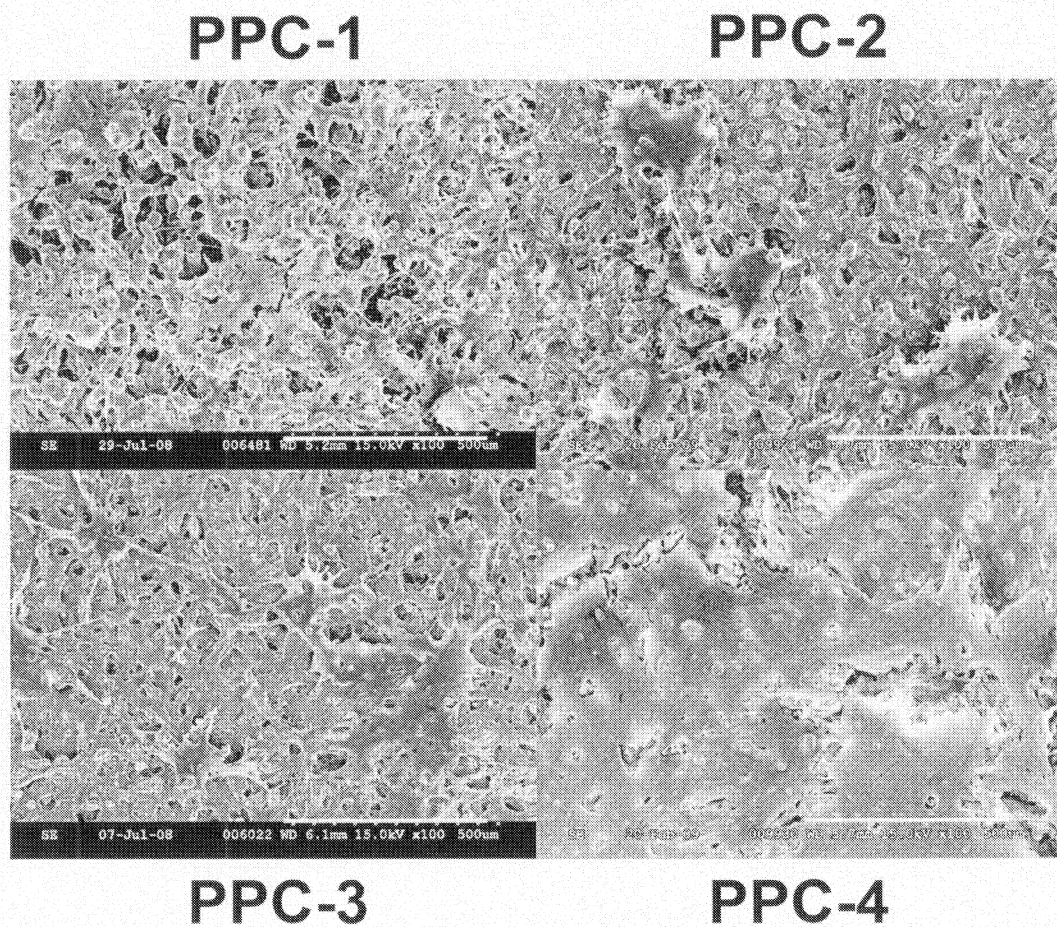
Figure 3.4: Human mesenchymal cells (HEPM) were seeded onto polymeric powder coatings (PPC-1, -2, -3 and -4). After 72 hours, scanning electron microscopy (SEM) showed that cells had attached and spread out onto PPC-1, -2 and -3, and had formed an extensive matrix-like layer on PPC-4. (Scale bar = 500 μm).
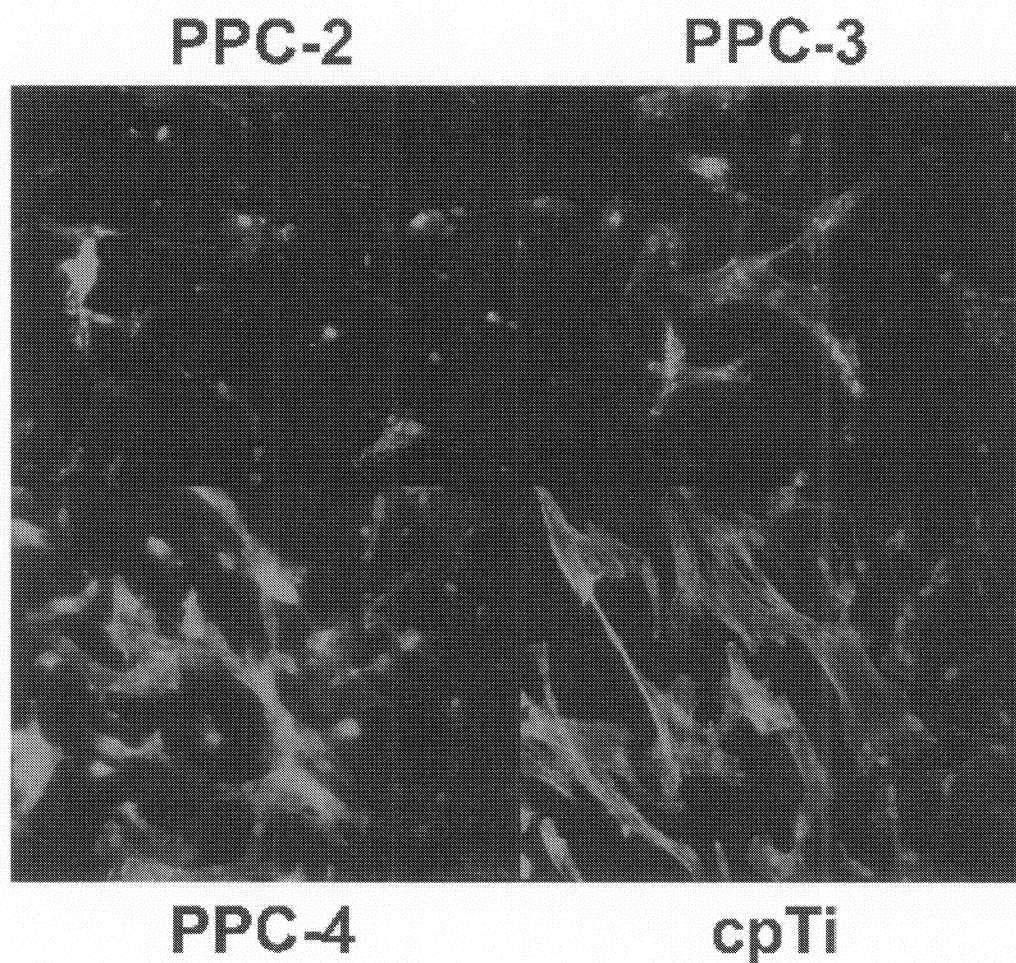
Figure 3.5: Human mesenchymal cells (HEPM) were seeded onto polymeric powder coatings (PPC-1, -2, -3 and -4) and titanium (cpTi) surfaces. After 72 hours, inverted fluorescence microscopy (20X) revealed cell nuclei (blue) and actin filaments (red) on PPC-2, -3 and -4, and on the titanium surfaces. There were numerous cells that had attached and were well spread out onto titanium and PPC-4. There were also several cells that had attached to PPC-2 and -3, but with less cell spreading. But there were hardly any cells that were visible on PPC-1 (not shown).

Cells attached and proliferated on PPC

The HEPM cells attached and proliferated on all of the PPC and titanium surfaces (Figure

3.6). Within 24 hours of seeding, the cell attachment assay counted a good number of

cells that had attached to all of the surfaces. The counts increased progressively from

PPC-1 through to PPC-4. The highest counts were on titanium, which were significantly

higher than that on PPC-1 (P<0.01), PPC-2 (P<0.01) and PPC-3 (P<0.05). Additionally,
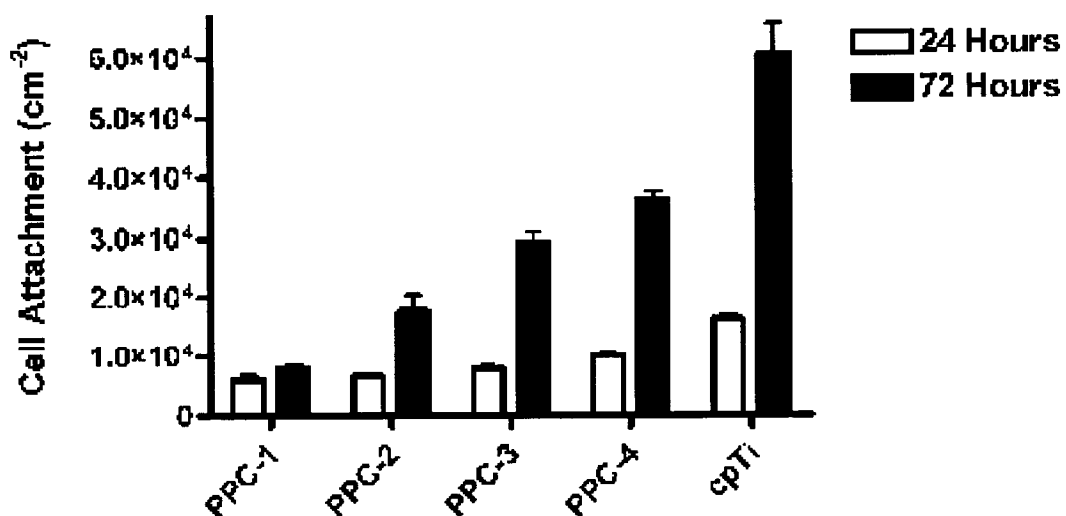
Figure 3.6: Human mesenchymal cells (HEPM) were seeded onto polymeric powder coatings (PPC-1, -2, -3 and -4) and titanium (cpTi) surfaces. At 24 hours there were attached cells on all of the surfaces. The highest counts were on titanium, which were significantly higher than on PPC-1, -2 and -3 (P<0.05), but were not significantly higher than on PPC-4 (P>0.05). After 72 hours the counts on titanium were significantly higher than on all of the coatings (P<0.001), and the counts on PPC-4 were significantly higher than on the other three coatings (P<0.05).

the cell counts on titanium were higher than on PPC-4, although statistical analysis

(ANOVA followed by Bonferroni) did not find a significant difference. Then, after 72

hours of growth, the cell counts increased markedly on PPC-3 and -4, and on titanium;

increased moderately on PPC-2; and increased slightly on PPC-1. After 72 hours, the

counts on titanium were significantly higher than that on PPC-1 ($P<0.001$), -2 ($P<0.001$),

-3 ($P<0.01$) and -4 ($P<0.05$); and the counts on PPC-4 were also significantly higher than

that on PPC-1 ($P<0.001$), -2 ($P<0.001$) and -3 ($P<0.05$).

Cells remained viable and were metabolic active on PPC

The HEPM cells maintained viability and metabolic activity on all of the PPC and

titanium surfaces (Figure 3.7). Within 24 hours of attachment, the MTT assay measured

high levels of mitochondrial enzyme activity in the cells that were collected from all of

the surfaces. The levels increased progressively from PPC-1 through to PPC-4. The

highest levels were measured in the cells from cpTi, which were significantly higher than

on PPC-1 and -2 ($P<0.05$), but not significantly higher than PPC-3 and -4 ($P>0.05$).

Then, after 72 hours of growth, the levels increased markedly on titanium, and were

significantly higher ($P<0.001$) than all of the PPC surfaces. The differences between

PPC-1, -2, -3 and -4 were not significant ($P>0.05$), with the exception that the levels on

PPC-4 were significantly higher ($P<0.01$) than on PPC-1 in both the 24 and 72 hour

cultures.
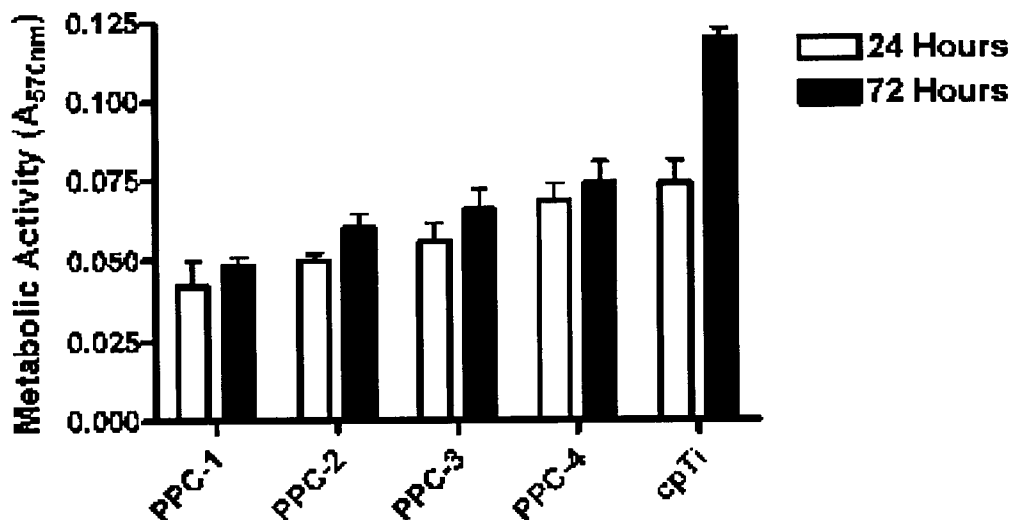
Figure 3.7: Human mesenchymal cells (HEPM) were seeded onto polymeric powder coatings (PPC-1, -2, -3 and -4) and titanium (cpTi) surfaces. After 24 hours of attachment, the MTT assay measured metabolically active cells that were collected from all of the surfaces. The highest measurements were from titanium, that were significantly higher than PPC-1 and -2 ($P<0.05$), but not significantly higher than PPC-3 and -4 ($P>0.05$). After 72 hours the levels from cpTi were significantly higher than from all of the coatings ($P<0.001$).

3.4. Discussion

This study has shown that polymeric powder coatings (PPC) can be successfully created from polymeric resins and nano-sized metal oxides, through the application of advanced ultrafine powder coating technology. These PPC coatings were created from either polyester or epoxy resins that were combined with fillers and additives, and applied with a solvent-free dry coating technique. This patented technology utilized nano-sized flow additives to prevent the aggregation of ultrafine powders, and thereby ensure adequate

flow.[17,18] Here we used 0.5% of $nSiO_2$ with epoxy resin to create PPC-1, and also with polyester to create PPC-2. Then, we used 0.5 and 2.0% of $nTiO_2$ with polyester to create PPC-3 and -4 respectively.

This advanced ultrafine powder coating technique ensured that there was an even dispersal of the materials to create a very homogenous and uniformly distributed surface coating. When each PPC was subjected to EDX, elemental analysis showed that there was little variation at the multiple sites, and the mapping of surface titanium showed an even distribution. Similarly, the SEM examination of PPC revealed topographical features that remained consistent across each surface.

Given the similarity of their constituents and their mode of preparation, it was not surprising to find that all of the PPC coatings had a similar composition. Furthermore, PPC-2, -3 and -4 were made from the same polyester resins, and were almost identical in their makeup. The elemental analyses by EDX confirmed these similarities, and detected an incremental increase in titanium concentration from PPC-2 through -3 and -4. Most of this titanium came from micron sized-titanium dioxide fillers that were added equally to PPC-2, -3 and -4. Therefore, the incremental increase in titanium from PPC-2 to -3 to -4 was entirely due to the $nTiO_2$ flow additive. Since $nSiO_2$ alone served as the flow additive in PPC-2; PPC-2, -3 and -4 had $nTiO_2$ concentrations of 0.0, 0.5 and 2.0% respectively.

These similarities in their chemical composition were accompanied by a likeness in physical properties. All of the PPC coatings had similarly complex micro-topographies and high levels of surface roughness. The SEM examination revealed a labyrinth of pits and concavities that created intricate nano-sized topographies across all of the surfaces. Likewise, the measurement of surface roughness recorded similarly high levels on all of the coatings. Both of these characteristics can be attributed to the use of PTFE. The equal amounts of PTFE in each PPC formulation accounted for the similarities in their surfaces.

However, despite the similarities in these PPC coatings, markedly different cellular responses were observed. We found that they differed widely in their capacity to support human mesenchymal cell attachment, spreading, proliferation and metabolic activity over three days of culture. While PPC-3 and especially -4, supported favorable cellular responses, PPC-1 and -2 displayed diminished effects. This was because of the use of more biocompatible $nTiO_2$ as the flow additive in PPC-3 and -4, while PPC-1 and -2 used $nSiO_2$ additive in their formula. Furthermore, PPC-4 prepared with 2% $nTiO_2$ had better cellular responses than the PPC-3 prepared with 0.5% of the nano-titanium additive.

Similarly, other studies have reported that nano-sized titanium can enhance the cellular response. Kay et al.[20] in 2002, and then Webster et al.[15] in 2005 reported that the incorporation of $nTiO_2$ into polymeric composites yielded better osteoblast cells adhesion and proliferation than when the materials were modified with micron-sized titanium. Jain et al. reported that cells responded better to polymeric substrates that had

been sputter-coated with a nano-sized thickness of titanium.[14] Then, Yao et al.[10], Reising et al.[9] and Pareta et al.[8] showed that the addition of titanium nano-features to UHMWPE and PTFE, enhanced osteoblast cells attachment and growth. Now, Ozkucur et al. have reported that a very thin nano-rough film (<100 nm) of titanium or zirconium on polyurethane, enhances human umbilical vein endothelial cells attachment and proliferation.[16]

In our study, all of the PPC surfaces supported cell attachment, although PPC-4 appeared to outperform the other coatings. SEM showed that within 24 hours of seeding, there were a few cells on PPC-1, some attachment and spreading on PPC-2 and -3, and even more on PPC-4. Then, after 72 hours of growth there were several cells on PPC-1 and -2, numerous cells on PPC-3 and a large number of cells that covered PPC-4. Similarly, Webster et al. and then Ozkucur et al. showed that nano titania and nano-titanium enriched surfaces had more attached cells under SEM, respectively.[15,16] The common factor in these studies has been the presence of nano features that contributed to the cell adhesion and proliferation. Our PPC surfaces also demonstrated significant nano features.

These SEM observations were confirmed by our quantitative analyses. The cell attachment assay counted adherent cells on all of the PPC surfaces within 24 hours of seeding and their numbers increased during three days of growth. Their numbers increased steadily from PPC-1 through to -4, with the highest counts on pure titanium. Indeed, the numbers of cells on the titanium controls were significantly higher than on PPC-1, -2 or -3, but were not significantly higher than on PPC-4 ($P>0.05$). Similarly,

Webster et al. reported that twice as many cells attached to $nTiO_2$ enriched poly-lactic-co-glycolic acid (PLGA) surfaces[15], and Pareta et al.[8] reported higher cell adhesion to nano-titanium enriched polymeric surfaces.

Following their adhesion, the human mesenchymal cells were able to proliferate on all of the coatings. SEM showed that there were many more cells on the PPC surfaces after 72 hours of growth, than there were those that adhered within 24 hours; and while their presence increased on all of the coatings, they had grown to create an extensive matrix-like layer that nearly covered the whole PPC-4. Furthermore, these observations were verified by the cell attachment assay, with cell counts that increased slightly on PPC-1, modestly on PPC-2 and markedly on PPC-3 and -4 after 72 hours of growth. Likewise, Reising et al. reported an increase in cell proliferation over 72 hours, when UHMWPE and PTFE were coated with titanium or gold nano-features.[9] Also, Ozkucur et al. (2009) reported an increase in proliferation over five days when polyurethane was coated with nano-titanium or zirconium.[16] In fact, when surfaces had nano features or nano roughness, seeded cells were exposed to a huge amount of surface defects for interaction that eventually translated into superior cellular responses.

These attached and proliferating cells displayed distinct morphologies and ultra-structural features. SEM showed that the cells that were attached to the coatings had cytoplasmic projections and numerous extensions onto the underlying surfaces. Also, inverted fluorescence microscopy showed that they had organized actin filaments within the cytoskeleton. Consistently, these cells on PPC had a narrower and extended morphology,

with less defined stress fibers, than the flattened cells that were seen on the cpTi controls. Indeed, other studies found similar morphologies and cytoskeletal features when cells attached to rough surfaces, as compared to smooth and flattened substrates. When Schuler et al. grew cells on adjacent smooth and rough surfaces; they found flattened cells on the smooth surfaces and narrow extended morphologies on the rough substrate.[11] Also, Al-Rabeah et al.[21] and then Deller-Quinn and Perinpanayagam[22] demonstrated these same characteristics in cells grown on rough mineral trioxide surfaces.

In addition to cell attachment, proliferation and cytoskeletal organization, metabolic activity was sustained on all of the surfaces. The MTT assay measured mitochondrial enzyme activity in the cells that were harvested from all of the coatings, with a gradual increase from PPC-1 through to -4, and the insignificant increment from 24 to 72 hours of growth indicated that the cells viability actually did not increase at the same rate as the cells proliferated. Furthermore, after 24 hours of attachment, the cells from PPC-3 and -4 had metabolic activities that were not significantly different from those on pure titanium. Therefore these findings further attest to the low cytotoxicity of these coatings, particularly those enriched with $nTiO_2$.

Collectively, these findings attest to the cytocompatibility of these polymeric coatings, and to effectiveness of their preparation. Through this study we have shown that advanced ultrafine powder coating techniques can be utilized to prepare homogenous polymeric coatings, and that these surfaces that can support a favorable cellular response. Furthermore, we have shown that the incorporation of very small amounts of nano-titania

can markedly enhance the biocompatibility of the coating. Their enrichment with as little as 2% of $nTiO_2$ created polymeric substrates that supported enhanced cellular responses. Moreover, the response of human mesenchymal cells to these $nTiO_2$-enriched coatings approached pure titanium in their performance. However, ultimately the value of these nano-titanium enriched polymeric coatings will need to be verified by in vivo studies.

3.5. Conclusions

Ultrafine powder coating technology was successfully utilized to create polymeric powder coatings (PPC). These coatings were continuous, evenly dispersed and highly adherent to their substrate. Furthermore, the PPC surfaces could support human mesenchymal cell attachment and growth. However, PPC-1 that contained neither micron-sized nor $nTiO_2$, had the least favorable response. PPC-2 contained only the micron-sized titania, and exhibited modest cell responses. In contrast, PPC-3 and -4 that were enriched with 0.5 and 2% $nTiO_2$ respectively, showed enhanced cell attachment, spreading and metabolic activity. Moreover, PPC-4 that was enriched with the higher concentration of $nTiO_2$ (2%) exhibited the most favorable cellular responses that were comparable to those seen on commercially pure titanium. Therefore the $nTiO_2$ enrichment of the polymeric powder coatings was shown to enhance their cytocompatibility.

References

1. Feinberg, A.W.; Wilkerson, W.R.; Seegert, C.A.; Gibson, A.L.; Hoipkemeier-Wilson, L.; Brennan, A.B., Systematic variation of microtopography, surface chemistry and elastic modulus and the state dependent effect on endothelial cell alignment. *J. Biomed. Mater. Res. A* **2008**, 86, 522-534.

2. Lincks, J.; Boyan, B.D.; Blanchard, C.R.; Lohmann, C.H.; Liu, Y.; Cochran, D.L.; Dean, D.D.; Schwartz, Z., Response of MG63 osteoblast-like cells to titanium and titanium alloy is dependent on surface roughness and composition. *Biomaterials* **1998**, 19, 2219-2232.

3. Howlett, C.R.; Zreiqat, H.; Wu, Y.; McFall, D.W.; McKenzie, D.R., Effect of ion modification of commonly used orthopedic materials on the attachment of human bone-derived cells. *J. Biomed. Mater. Res.* **1999**, 45, 345-354.

4. Wieland, M.; Chehroudi, B.; Textor, M.; Brunette, D.M., Use of Ti-coated replicas to investigate the effects on fibroblast shape of surfaces with varying roughness and constant chemical composition. *J. Biomed. Mater. Res.* **2002**, 60, 434-444.

5. Masaki, C.; Schneider, G.B.; Zaharias, R.; Seabold, D.; Stanford, C., Effects of implant surface microtopography on osteoblast gene expression. *Clin. Oral Implants Res.* **2005**, 16, 650-656.

6. Isa, Z.M.; Schneider, G.B.; Zaharias, R.; Seabold, D.; Stanford, C.M., Effects of fluoride-modified titanium surfaces on osteoblast proliferation and gene expression. *Int. J. Oral Maxillofac. Implants* **2006**, 21, 203-211.

7. Protivinsky, J.; Appleford, M.; Strnad, J.; Helebrant, A.; Ong, J.L., Effect of

   chemically modified titanium surfaces on protein adsorption and osteoblast precursor

   cell behaviour. *Int. J. Oral Maxillofac. Implants* **2007**, 22, 542-550.

8. Pareta, R.A.; Reising, A.B.; Miller, T.; Storey, D.; Webster, T.J., An understanding of

   enhanced osteoblast adhesion on various nanostructured polymeric and metallic

   materials prepared by ionic plasma deposition. *J. Biomed. Mater. Res. A* **2010**, 92A

   (3), 1190–1201.

9. Reising, A.; Yao, C.; Storey, D.; Webster, T.J., Greater osteoblast long-term functions

   on ionic plasma deposited nanostructured orthopedic implant coatings. *J. Biomed.*

   Mater. Res. A **2008**, 87, 78-83.

10. Yao, C.; Storey, D.; Webster, T.J., Nanostructured metal coatings on polymers

    increase osteoblast attachment. *Int. J. Nanomedicine* **2007**, 2, 487-492.

11. Schuler, M.; Kunzler, T.P.; de Wild, M.; Sprecher, C.M.; Trentin, D.; Brunette,

    D.M.; Textor, M.; Tosatti, S.G., Fabrication of TiO2-coated epoxy replicas with

    identical dual-type surface topographies used in cell culture assays. *J. Biomed.*

    Mater. Res. A **2009**, 88, 12-22.

12. Pareta, R.A.; Reising, A.B.; Miller, T.; Storey, D.; Webster, T.J., Increased

    endothelial cell adhesion on plasma modified nanostructured polymeric and metallic

    surfaces for vascular stent applications. *Biotechnol. Bioeng.* **2009**, 103, 459-471.

13. Lehle, K.; Buttstaedt, J.; Birnbaum, D.E., Expression of adhesion molecules and

    cytokines in vitro by endothelial cells seeded on various polymer surfaces coated

    with titaniumcarboxonitride. *J. Biomed. Mater. Res. A* **2003**, 65, 393-401.

14. Jain, R.; Von Recum, A.F., Fibroblast attachment to smooth and microtextured PET and thin cp-Ti films. *J. Biomed. Mater. Res. A* **2004**, 68, 296-304.

15. Webster, T.J.; Smith, T.A., Increased osteoblast function on PLGA composites containing nanophase titania. *J. Biomed. Mater. Res. A* **2005**, 74, 677-686.

16. Ozkucur, N.; Wetzel, C.; Hollstein, F.; Richter, E.; Funk, R.H.; Monsees, T.K., Physical vapor deposition of zirconium or titanium thin films on flexible polyurethane highly support adhesion and physiology of human endothelial cells. *J. Biomed. Mater. Res. A* **2009**, 89, 57-67.

17. Zhu, J.; Zhang, H., Fluidization additives to fine powders, *U.S. Patent 6,833,185*, **2004**.

18. Zhu, J.; Zhang, H., Ultrafine powder coatings: An innovation. *Powder Coat.* **2005**, 16 (7), 39-47.

19. Geldart, D., Types of gas fluidization. *Powder Technol.* **1973**, 7, 285-292.

20. Kay, S.; Thapa, A.; Haberstroh, K.M.; Webster, T.J., Nanostructured polymer/nanophase ceramic composites enhance osteoblast and chondrocyte adhesion. *Tissue Eng.* **2002**, 8, 753-761.

21. Al-Rabeah, E.; Perinpanayagam, H.; MacFarland, D., Human alveolar bone cells interact with ProRoot and tooth-colored MTA. *J. Endod.* **2006**, 32, 872-875.

22. Deller-Quinn, M.; Perinpanayagam, H., Osteoblast expression of cytokines is altered on MTA surfaces. *Oral Surg. Oral Med. Oral Pathol. Oral Radiol. Endod.* **2009**, 108, 302-307.

CHAPTER 4
Nano-TiO₂ Enriched Polymeric Coatings: Expression of Runx2 and Collagen(I)

Chapter Summary

The objective of this study was to prepare micro-nano rough polymeric powder coatings (PPC) by utilizing

ultrafine powder coating technology and to verify whether they can support human mesenchymal cell

attachment, spreading as well as Runx2 and Collagen(I) expression. Resins were modified with pigment

grade micron-sized titanium dioxide and nano-sized polytetrafluoroethylene (PTFE), and enriched with

either SiO₂ or TiO₂ nanoparticles (nSiO₂ or nTiO₂) to create the PPC. Atomic Force Microscopy (AFM)

revealed complex surface topographies with nano features consisting of micron-sized cavities. Scanning

electron microscopy (SEM) showed that human embryonic palatal mesenchymal (HEPM) cells attached

and spread out on the PPC surfaces, particularly on those enriched with nTiO₂. Image J analysis of

Immunofluorescence images quantified HEPM cell spreading on PPC surfaces. PCR analyses showed that

they expressed Type I Collagen and Runx2, which meant that they might be undergoing osteogenic

differentiation. Furthermore, we found that although Runx2 and Collagen(I) were expressed on all of the

PPC surfaces, higher levels were found on the surfaces that had been enriched with titanium (either nano-

or micron sized material). Indeed, when nTiO₂-enriched material was used, cell attachment and gene

expression appeared to approach the levels that were seen on the commercially pure titanium (cpTi)

control surfaces. This suggests that small amounts (as low as 2.0 wt.%) of nano-titanium enrichment may

be sufficient to obtain a beneficial cellular response seen at the molecular level of gene expression and cell

differentiation.

4.1. Introduction

Human embryonic palatal mesenchymal (HEPM) cells can migrate and home to implant surfaces leading to the differentiation into bone forming osteoblast-like cells. Therefore, bone-contacting devices such as orthopedic and dental implants should possess the desired chemical and topographical properties that enhance the differentiation of HEPM cells and eventually osseointegrate with the prosthesis. As a consequence, current research focuses on designing new synthetic implant materials that mimic the properties of natural tissues.

Since the interactions of implant surfaces with bone tissues are primarily dependent on the biocompatibility of the materials, titanium and its alloys have become widely used implant materials due to their superior biocompatibility and mechanical properties. However, in addition to biocompatibility, surface topography and biochemistry also affect their interaction with the surrounding tissues.[1-6] Due to this, the titanium surfaces have been modified by various polishing, grit blasting, machining, microfabrication, and acid and chemical etching techniques, to optimize the cellular response.[6-11]

Other than titanium and its alloys, recently polymeric materials and composites have been reportedly used for orthopedic implants[12-15] and for vascular grafts[16-18]. However, these polymeric substrates have been modified and coated with titanium or titania particles to enhance their cytocompatibility. A number of different techniques including sputter-

coating, vapor and plasma deposition, have been employed to make a titanium layer on the polymeric substrates to enhance their cellular responses.

An earlier study by Lehle et al.[18] applied a titanium-carboxonitride layer onto polyethylene terephthalate (PET), polypropylene (PP), polytetrafluoroethylene (PTFE), polyurethane, and silicone by using a plasma-assisted chemical vapor deposition process to determine the effect of titanium on human saphenous vein endothelial cells. They found that endothelial cell adhesion was enhanced on the titanium coated surfaces. Likewise, Jain et al.[19] sputter-coated titanium onto smooth and micro-textured polyethylene terephthalate (PET) surfaces, and found that within three days fibroblasts preferentially attached to the textured surfaces that had been coated with titanium. Later, Webster et al.[20] studied the incorporation of both conventional and nano-TiO_2 (nTiO_2) into poly-lactic-co-glycolic acid (PLGA) and reported superior osteoblast like cell attachment and Ca-containing mineral deposition onto nTiO_2 enriched PLGA than the conventional ones when they maintained PLGA to nTiO_2 (70:30) ratio.

Since human mesenchymal cells favor nanocues through filopodial production and subsequent differentiation[21], the recent trend is to apply titanium or titania nanoparticles or to fabricate titanium nano features onto polymeric surfaces to further improve the cellular responses. Subsequently, Yao et al.[14] used a novel ionic plasma deposition (IPD) process to apply titanium or gold, and also to create nanometer features of titanium on polyetheretherketone, ultra-high molecular weight polyethylene (UHMWPE) and PTFE and found that osteoblast cell adhesion and spreading were better on the coated polymers

than on the uncoated surfaces. Similarly, Reising et al.[13] studied the IPD process to add

titanium nano-features on UHMWPE and PTFE, and reported enhanced osteoblast

proliferation and mineral deposition on the coated polymers compared to the uncoated

material and titanium controls. Pareta et al.[12] used IPD and nitrogen ion immersion

plasma deposition to apply nano-particulate titanium onto metallic implant materials such

as titanium and titanium alloy (Ti6Al4V), and onto polymers such as PET, polyvinyl

chloride, polyurethane, PTFE, UHMWPE and nylon. They found an increase in

osteoblast adhesion on the modified surfaces compared to the untreated controls.

Recently, Ozkucur et al.[22] used a physical vapor deposition technique to deposit a thin

film (<100 nm) of titanium or zirconium onto polyurethane surfaces and reported

enhanced endothelial cell adhesion and proliferation.

More recently, some other studies reported on the bioactivity of micron-patterned nano

rough polymeric surfaces. Chun et al. etched poly(ether) urethane (PU) and PLGA

surfaces with HNO_3 and NaOH, respectively, to make them submicron and nanorough,

and observed greater urothelial cell density on the etched nano-rough surfaces.[23]

Similarly, Ranjan et al. fabricated the arrays of nano-grooves and alternating micro-nano

roughness on poly(dimethylsiloxane) (PDMS) films to enhance endothelial cell adhesion

and elongation.[17]

In addition to cell attachment, spreading and proliferation, it is imperative to study such

polymeric surfaces to verify whether the HEPM cells differentiate into bone-forming

osteoblasts. Particularly, the expression of Runx2 transcription factor primarily

determines subsequent osteoblasts differentiation on biomaterial surfaces,[24,25] while expression of collagen type I influences potential mineralization[8]. However, the expression of both Runx2 and collagen type I genes depends largely on the biomaterial surfaces microtopography and micro/nano roughness.[8,10,11,26-31] However, unfortunately there were only few references available that reported Runx2 expression on micro-/nano-rough polymeric surfaces. Having created rough topographic polymeric surfaces by using ultrafine powder coating technology as described elsewhere,[32] it is essential to explore whether HEPM cells grown on PPC surfaces express important regulatory genes that determined osteoblasts differentiation.

Therefore, in this study we have created nano-featured cytocompatible polymeric coatings by using a simple, environmentally friendly (i.e., no toxic solvents, no VOC emissions) and inexpensive approach. A patented ultrafine powder coating technique[33,34] was employed to disperse nano-sized metal oxides onto polymeric resins. By using this advanced powder coating technology we combined ultrafine resin powders containing polyester or epoxy with PTFE and nano-sized titanium dioxide or silica and dispersed them homogenously.

Moreover, we have studied these polymeric powder coatings for their capacity to support human mesenchymal cell attachment, spreading and differentiation. We will report on the variation in cytocompatibility of alternative formulations of these coatings, and will describe a markedly enhanced cellular response (particularly, Runx2 expression) on the micro-nano rough nano-titania enriched polymeric coatings.

4.2. Materials and Methods

PPCs formulations and preparation

Polymeric powder coatings (PPC) (Table 4.1) were prepared by the modification of commercially available resins by using Zhu and Zhang's patented ultrafine powder coating technology.[33,34] Coating compositions (table 4.1) and the coating preparation procedures were published elsewhere.[32] The powder coating particles of each formulations were sprayed onto the target substrates with the aid of corona powder spray gun and cured at 200° C for 10 min.

The adhesion of the coatings to the underlying substrate was confirmed with an Elcometer 107 Cross Hutch Cutter (Elcometer Ltd., Windsor, Canada). As recommended by ASTM D3359, several perpendicular cuts were made to the substrates to create a grid of small squares that was then covered with adhesive tape (ASTM standard). The tape was then withdrawn by a single smooth pull, and the number of remaining grid squares was compared for retention.

Atomic Force Microscopy (AFM)

To determine their surface features, PPC surfaces were examined with the dynamic force mode AFM (Park Systems AFM XE-100). A silicon cantilever was used to detect the surface features. The spring constant and the nominal tip radius of the silicon cantilever were ~40 N/m and 10 nm, respectively. The length, width and thickness of the cantilever were 125 μm, 40 μm long and 4 μm, respectively. The cantilever was oscillated around

its resonant frequency (~300 kHz) and its amplitude decreased when the tip interacted

with the sample surface. Such damped amplitude (set point) was used as the feedback

parameter to probe the surface features. The resolutions of the generated images were 256

x 256 pixels and the examination was performed at room temperature.

Table 4.1: Coating formulations and their characterizations

No.	Coating Formula	Surface Roughness (nm)	Porosity[3] (%)
PPC-1	Polymeric Resin[1] +3% PTFE+0.5% SiO_2	251.3 ± 22.3	24.7
PPC-2	Polymeric Resin[2] +3% PTFE+0.5% SiO_2	268.3 ± 26.9	24.5
PPC-3	Polymeric Resin[2]+3% PTFE+0.5% TiO_2	262.8 ± 18.1	22.3
PPC-4	Polymeric Resin[2]+3% PTFE+2.0% TiO_2	281.9 ± 13.8	26.2

[1] Epoxy

[2] Avalanche White Polyester

[3] Percentage of fraction of area covered by pores to the total area

Surface Roughness

The surface roughness of the PPC was measured with a Dektak 8 Stylus Surface Profiler

(Veeco Metrology Group, Santa Barbara, CA). The PPC were loaded onto a high

precision stage. The stage moved beneath a diamond-tipped stylus. The scan length, scan

resolution and stylus force used were 20 mm, 1.111 μm/sample and 8 mg, respectively.

Each PPC surface was scanned at ten different locations to measure the vertical features.

The mean deviation of the vertical features from the centerline was then calculated as a measure for surface roughness (R_a).

Porosity Measurement

SEM images of the PPC surfaces were analyzed by using Image J software. Individual pores/cavities were marked and outlined by using the drawing tool. The software then measured the area of each cavity. Fraction of the total area covered by the pores to the total area of the sample specimen revealed as the percentage porosity of each surface.

Sterilization

The PPC surfaces and cpTi were disinfected and sterilized to be used for tissue culture. The PPC and cpTi disks were rinsed twice with ethanol (70%) followed by three times washing with phosphate buffered saline (PBS) and then were placed into individual wells of a 24-well tissue culture plate. The entire plate were then placed in a tissue culture hood and exposed to UV light for 30 minutes on each side of the disks to ensure sterility.

HEPM Cell Culture

Human embryonic palatal mesenchymal cells (HEPM, ATCC CRL-1486) were seeded onto cpTi and PPC surfaces in multiple 24-well tissue culture plates (50,000 cells/well). The cultures were maintained in Dulbecco's modified eagles medium (DMEM) supplemented with fetal bovine serum (FBS, 10%), L-glutamine (2 μmol/ml), penicillin G (100 U/ml), streptomycin sulfate (100 μg/ml) and amphotericin B (0.25 μg/ml)).

Replicate cultures were incubated at 37°C for 6, 24 and 72 hours and then harvested for

examination under SEM.

SEM of the Cells

After 72 hours of incubation, the replicate PPC disks were collected, washed three times

with PBS, fixed with glutaraldehyde (2.5%) in cacodylate buffer (100mM) for 20

minutes. After fixing, the surfaces (including the grown cells) were dehydrated in

ascending grades of ethanol (25, 50, 75, 95 and 100%) and immersed in

hexamethyldisilazane. Then the surfaces were air dried, mounted on metal stubs, sputter

coated with gold (20 nm) and examined with a Hitachi S-2600 SEM (Hitachi, Pleasonton,

CA). The working voltage (5-12 kV), beam (60) and working distance (5.3 mm) were set.

Cell spreading

After 6 and 24 hours of growth on titanium and PPC surfaces the cultures were harvested

and washed three times with PBS. The cells that were attached to the surfaces were fixed

with paraformaldehyde (4% for 10 min) and permeabilized with Triton X-100 (0.1% for

5 min). The actin filaments of the cytoskeleton were labeled with rhodamine phalloidin

(Cytoskeleton, Denver, CO) for 2 hours at dark and at room temperature. The surfaces

were then mounted using Vectashield with DAPI (Vector Laboratories, Burlingame, CA).

The images of the cells were then taken by an inverted fluorescence microscope

(Axiovert 40 CFL, Carl Zeiss Canada Ltd., Toronto, Canada) with the magnification of

20X. Then Image J software's drawing tool was used to identify and outline discrete cells

on each test surfaces. The software then measured the area covered by individual cells

attached onto cpTi and PPC surfaces. The average areas of cells indicated the degree of

their spreading onto the biomaterial substrates used in this study. The differences in

average cell spreading on different surfaces/replicates, and at different time points, were

analyzed statistically by a two-way analysis of variance (ANOVA) followed by a

Bonferroni post-hoc test, to a significance level of P<0.05.

RNA extraction

Replicate cultures (200,000 HEPM cells/well in multiple 6-well plates) grown on cpTi,

PPC-1, PPC-2, PPC-3 and PPC-4 were gently taken out of the incubator, rinsed three

times with PBS so that unattached cells were washed off. The total cell RNA was

extracted with the RNeasy Mini Kit (Qiagen, Valencia, CA) according to the

manufacturer's instructions. The cells were resuspended in lysis buffer and homogenized

by passing through a QIAshredder column (Qiagen). The homogenized lysate was then

applied to the RNeasy column, rinsed repeatedly with a series of buffers (RLT), and

eluted into RNase-free deionized water. These RNA extracts were stored at -70°C.

Aliquots of the RNA extracts were diluted in deionized water and run into bioanalyser to

determine the concentration of RNA extracted from the cells grown on each biomaterial

surface. The RNA purity was determined from the A260/A280 ratio.

Conventional RT-PCR analysis

The RNA extracts were analyzed by conventional RT-PCR according to the following

protocol. The RNA was reverse transcribed into cDNA with Oligo(DT) primer and

SuperScript II RNase H Reverse Transcriptase at 42°C for 50 minutes. The specific

transcripts were then amplified in separate tubes by PCR with gene-specific primers

(Table 4.2) and Platinum Taq DNA Polymerase. The thermal cycling parameters were

Table 4.2: Primers for Reverse Transcription-Polymerase Chain Reaction (RT-PCR)

Gene	Primer	DNA Sequence	Product
GAPDH	Forward	5'-ATGCTTCATTCGCCTCACAAAC-3'	345 bp
	Reverse	5'-CCAAAAGAAGTTTTGCTGACATGG-3'	
Collagen Type I	Forward	5'-GCAAGAACCCCAAGGACAAGAG-3'	306 bp
	Reverse	5'-TCGTGCAGCCATCGACAGTGAC-3'	
Runx2	Forward	5'-TCCTGCACCACCAACTGCTTAGC-3'	261 bp
	Reverse	5'-CGCCTGCTTCACCACCTTCTTG-3'	

Runx2, Runt-related transcription factor 2; GAPDH, glyceraldehyde-3-phosphate dehydrogenase.

94°C for 2 minutes to activate the polymerase, followed by 40 cycles of 94°C for 30

seconds, 50°C for 30 seconds, and 72°C for 1 minute. The RT and PCR reactions were

performed in an Amplitron II thermocycler (Barnstead Thermolyne, Dubuque, IA). The

expression of glyceraldehyde 3-phosphate dehydrogenase (GAPDH) was used to check

RNA integrity.

The PCR products were separated on an agarose gel (1%) containing ethidium bromide

(0.05 μg/mL), visualized on a Transilluminator (Fisher, Pittsburgh, PA), and

photographed with a digital camera (Panasonic, Kadoma, Japan). Cells grown on PPC

substrates were compared with commercially pure Titanium (cpTi). The levels of all

genes were normalized to the respective levels of GADPH.

Real Time RT-PCR

HEPM cells cultured for 7 days were washed, and RNA was extracted for real-time
reverse-transcription polymerase chain-reaction analysis. Primers and probes were
designed for type I collagen, Runx2 and 18s with Primer Express software (Perkin Elmer,
Boston, MA, USA) from the known human sequences reported in Table 4.2. Indeed, the
probe was designed to partly cover the exon junction so that it would unlikely to
hybridize into genomic DNA that might have been present. Due to this, their PCR
amplification did not contribute to the Real Time analysis if genomic DNA contaminants
were present.

Triplicates of RNA extracts were analyzed by quantitative real-time multiplex RT-PCR,
with the aid of TaqMan Gold RT-PCR Kit (Perkin Elmer, Foster City, CA, USA).
TaqMan Ribosomal RNA Control Reagents kit (Perkin Elmer) was used in this study to
detect 18s ribosomal RNA (Applied Biosystems Kit 4310893E) as an endogenous
control. The Real Time PCR reactions were conducted in 96-well Optical Reaction plates
(Applied Biosystems) in an ABI Prism 7700 Sequence Detection System. The Type 1
Collagen and Runx2 and an endogenous 18S control were amplified by multiplex PCR
with thermal cycling parameters of 50°C for 2 min, 95°C for 10 min, 40 cycles of 95°C
for 15 sec and 60°C for 1 min, using TaqMan Universal PCR Master Mix (Applied
Biosystems). Steady-state mRNA levels were normalized to 18s mRNA. The mRNA
levels on different substrates were further normalized to that on cpTi. Statistical analysis
of the Ct value, the threshold cycle value of the multiplex reaction of the control *vs.*

experimental target gene ($\Delta\Delta$Ct), was performed by a two-way analysis of variance

(ANOVA) with Bonferroni post-hoc test to a significance level of $P < 0.05$.

4.3. Results

Preparation of PPC

Polymeric powder coatings (PPC) were prepared when polymeric resins were combined

and processed with fillers and additives and applied by using ultrafine powder coating

technology. PPC compositions are outlined in table 4.1. PPC-1 was composed of epoxy

resin and PTFE, as well as $nSiO_2$ (~25 nm average diameter) additive to ensure powder

flow, while PPC-2 was made from polyester (with embedded pigment-grade micron-sized

titanium) and PTFE, and again $nSiO_2$ was the additive. PPC-3 contained micron-sized

titanium embedded polyester resin and PTFE, but $nTiO_2$ (~40 nm average diameter) was

the additive. PPC-4 composition was very similar to that of PPC-3 except the $nTiO_2$

additives at a higher concentration. While 0.5 wt.% $nTiO_2$ was added into PPC-3, 2.0

wt.% $nTiO_2$ was used in PPC-4.

All of these PPC coatings were highly adherent (5B according to ASTM D3359) to their

underlying substrates. Following the standard test for adhesion, all of the PPC were found

to have an excellent adhesion to their substrates. Moreover, PPC surfaces had high levels

of nano-scale surface roughness (Table 4.1). The mean roughness of the PPC surfaces

ranged from 250 to 280 nm and was within the nano-scale. This similar degree of

nanoroughnesses was achieved by using same amount of nano-sized PTFE in all of the

formulations. However, the surface nanoroughness of the developed surfaces might also

be attributed to the $nSiO_2$ and $nTiO_2$ nano-additives that were used in the preparation of PPC-1 and -2, and PPC-3 and -4 respectively.

In addition, EDX detected similar elemental compositions in the PPC surfaces, with the only exception that PPC-1 lacked titanium. While PPC-1 did not contain either micron- or nano-sized TiO_2, all other coatings had 25% micron-sized TiO_2 embedded in their formula. On top of that PPC-3 and -4 contained 0.5 and 2.0 wt.% nTiO2 additive, respectively; but PPC-2 had 0.5 wt.% of nSiO2 additive.

Complex micro-nano topography of PPC

The PPC surfaces were characterized with complex micro-nano topographies (Figure 4.1). AFM examination of the as-prepared PPC surfaces showed complicated and elaborate surface topographies in both micro and nanometer-scale. There were numerous nano-sized projections and an underlying labyrinth of concavities that created intricate, elaborate, but discontinuous surface topographies. There were shallow and deep pits and cavities that were of micron dimension and contributed to the over all surface roughness of the PPC surfaces. Those cavities eventually made the PPC surfaces porous. The average porosity of the PPC surfaces was ~25% (Table 4.1).

Cells attachment to the PPC

The HEPM cells attached onto all of the PPC surfaces (Figures 4.2). When the 50,000 cells per well were incubated in 24-well tissue culture plates for 72 hours, SEM images showed that the cells had attached and spread out on all of the PPC surfaces (Figure 4.2).

There were numerous cells attached and spread out on PPC-4; somewhat less cells on

PPC-2 and -3; but only few cells were on PPC-1.

Cells spreading on some PPC

Image J analyses revealed that the HEPM cells spread out on the PPC surfaces (Figure

4.3). When the cells (50,000 cells/well) were incubated in 24-well tissue culture plates

for 6 and 24 hours, Image J analyses of cells showed that they spread well progressively

from PPC-1 through to PPC-4 in both time points as the average area of the attached cells

increased steadily. However, after 6 hours of seeding, cells spread significantly more on

cpTi than that on PPC-1 ($P<0.001$), -2 ($P<0.001$) and -3 ($P<0.05$), but not significantly

higher than that on PPC-4 ($P>0.05$). It is also evident that when incubation time increased

from 6 to 24 hours, cells stretched more on all of the surfaces with numerous narrower

and less defined stress fibers. However, after 24 hours of growth, cells spreading on CpTi

was significantly higher than that on all of PPC surfaces ($P<0.001$).
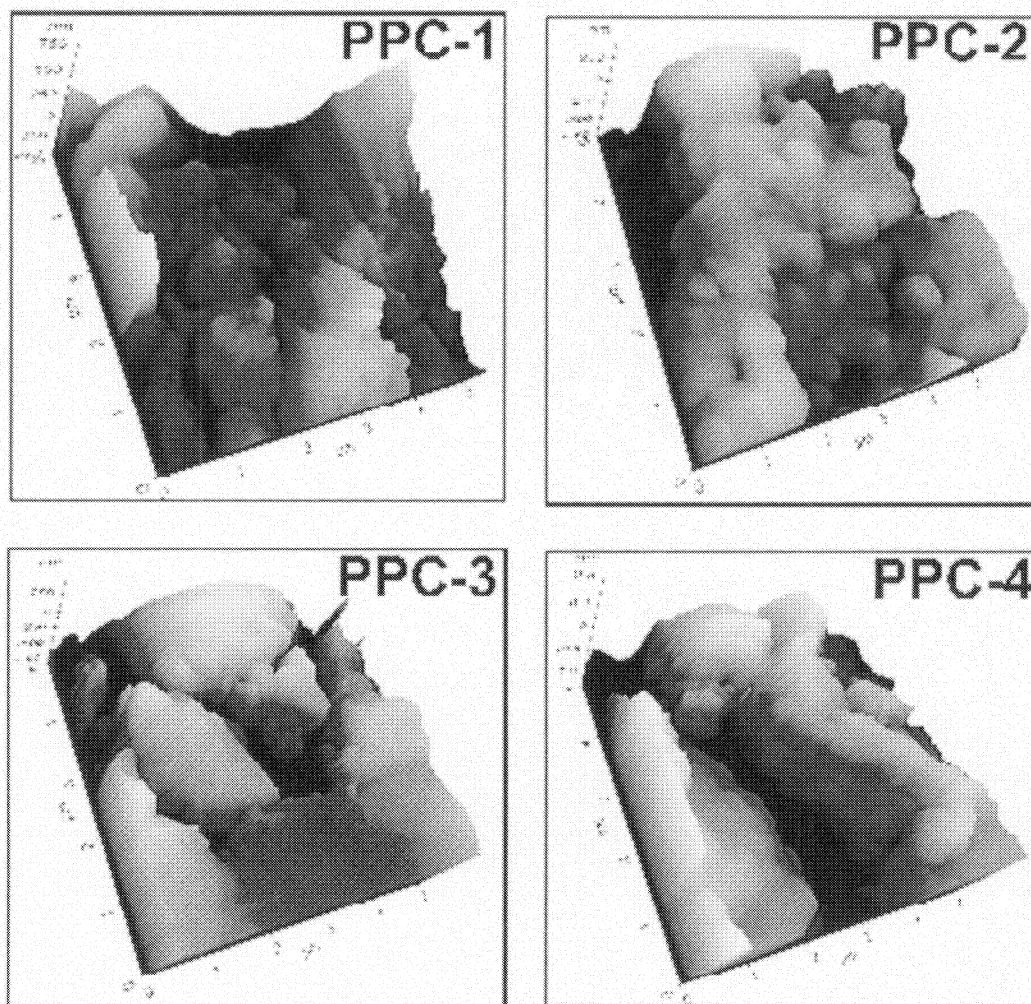
Figure 4.1: Polymeric powder coatings (PPC-1, PPC-2, PPC-3 and PPC-4) were prepared and examined by atomic force microscopy (AFM). The horizontal axis of the AFM images represented the x and y axes (in μm) and the vertical axis represented the z-axis (in nm). Scan size: 5 × 5 μm.
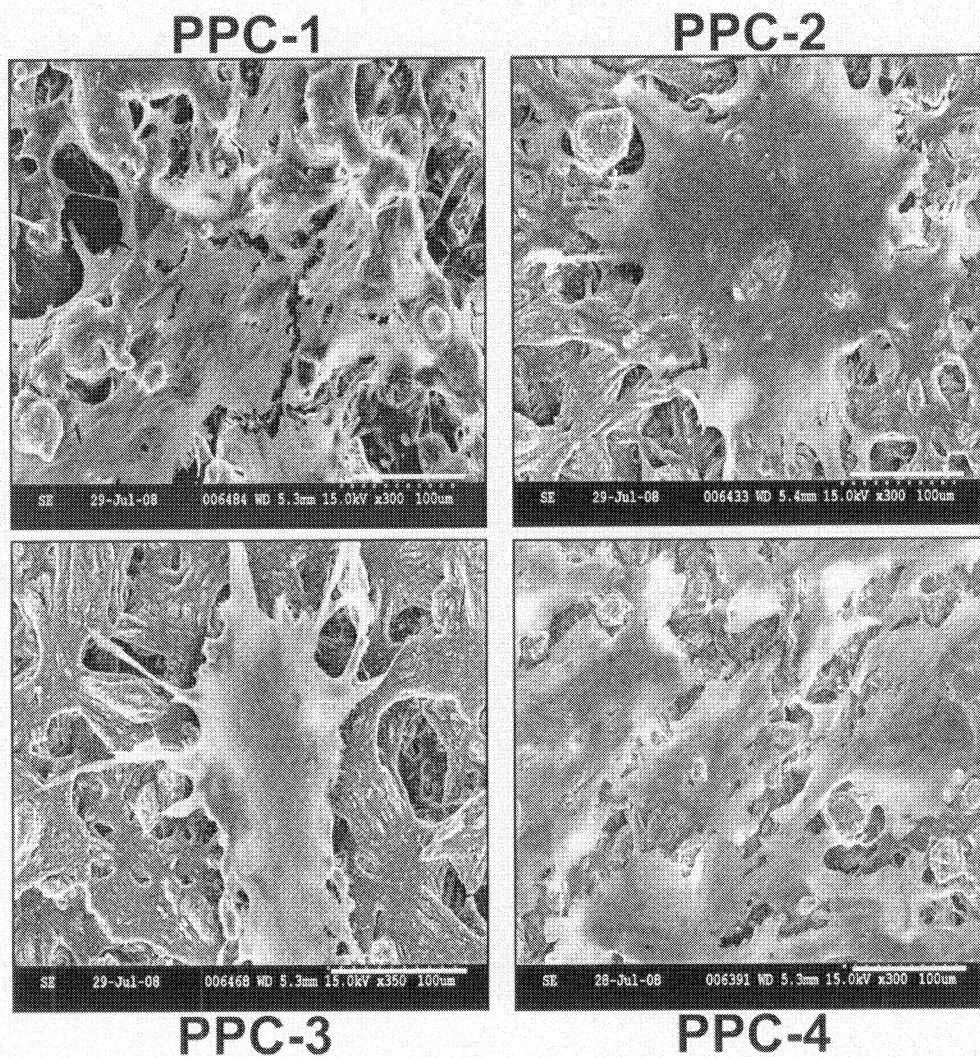
Figure 4.2: Human embryonic palatal mesenchymal (HEPM) cells were seeded onto polymeric powder coatings (PPC-1, PPC-2, PPC-3 and PPC-4) surfaces. After 72 hours of seeding, Scanning Electron Microscope (SEM) images showed several cells and cellular extensions on PPC-1; cells attached and spread onto PPC-2 and PPC-3; but PPC-4 became almost confluent with HEPM cells. (Scale bar = 100 μm).
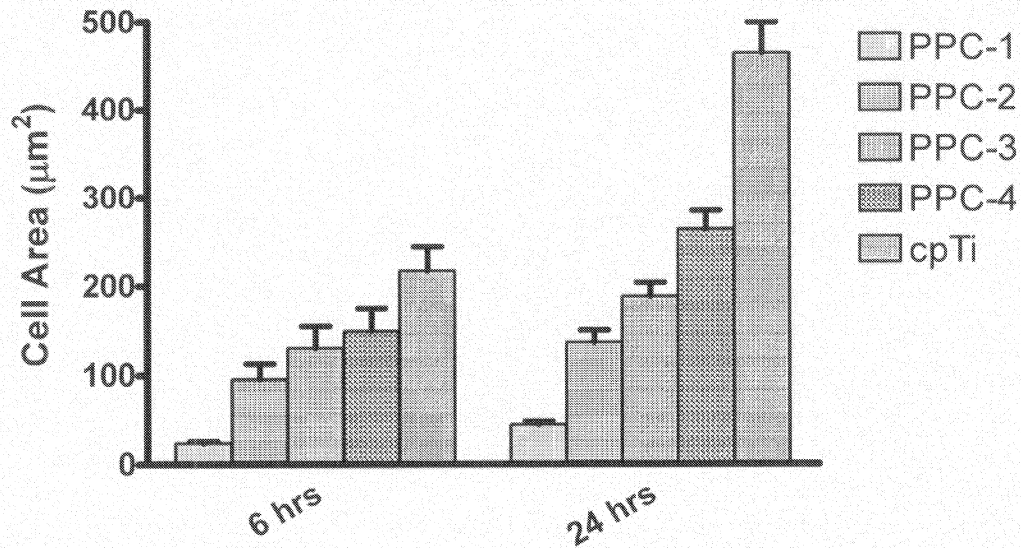
Figure 4.3: HEPM cells (100,000 cells/well) were seeded onto polymeric powder coatings (PPC-1, PPC-2, PPC-3 and PPC-4) and commercially pure Titanium (cpTi) surfaces. After 6 and 24 hours, the celled were harvested, fixed with 4% PFA and stained with Rhodamine Phalloidin. The images of the stained cells were taken by inverted fluorescence microscopy (20X). The images were analyzed by using Image J Software. 10-15 discrete cells were identified and outlined by using drawing tool. Then the software measured the total area covered by each cells. The average area of the cells grown on test surfaces indicated the degree of cell spreading. In both time points, cell spreading increased progressively from PPC-1 through to PPC-4 to cpTi.

Osteogenic differentiation and Runx2 expression on PPC

The human embryonic palatal mesenchymal (HEPM) cells appeared to express collagen type I and Runx2 transcription factor over 7 days of cultures (Figure 4.4A and 4.4B).

A
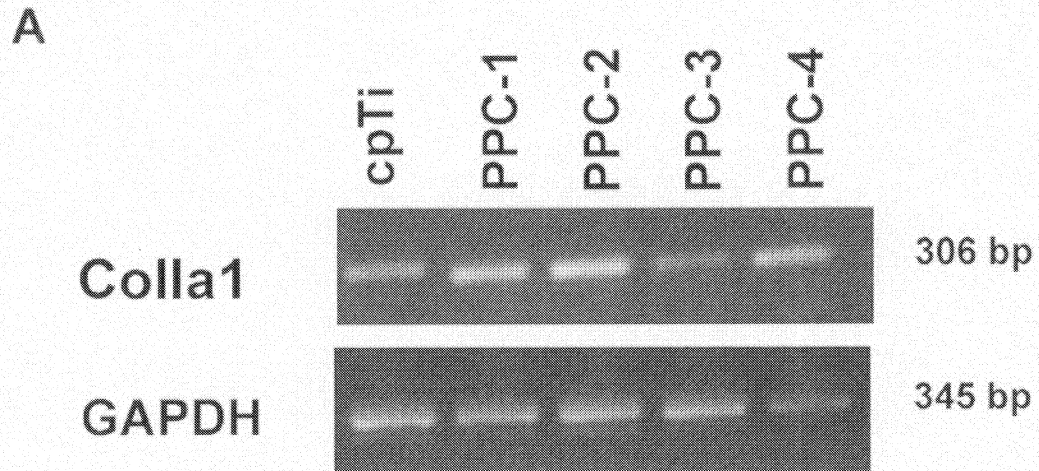
Figure 4.4A: Reverse-transcription polymerase chain reaction (RT-PCR) analysis was performed on RNA extracts from HEPM cells after 1 day of growth on PPC-1, PPC-2, PPC-3, PPC-4 and cpTi. A representative PCR analysis from the PCR amplification visualized with ethidium bromide staining is shown here. The RT-PCR analysis detected expression of type I collagen (Col1a1) at 306 bp on all of the PPC surfaces and on cpTi, but very little or no Runx2 expressed (not shown in the figure) on any of the test surfaces after 1 day of seeding. Glyceraldehyde-3-phosphate dehydrogenase (GAPDH) served as the control.

B
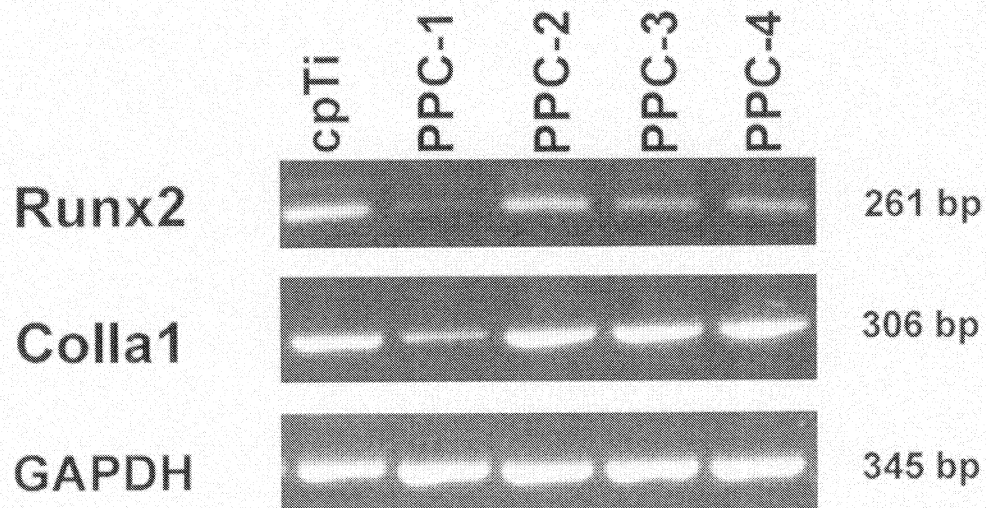
Figure 4.4B: RT-PCR analysis was performed on RNA extracts from HEPM cells after 7 days of growth. The RT-PCR analysis readily detected expression of the Runt-related transcription factor 2 (Runx2) at 261 bp and type I collagen (Colla1) at 306 bp on PPC-1, -2, -3, -4 and on cpTi. GAPDH served as the control.

Conventional RT-PCR analysis detected type I collagen from the RNA extracted after 1 day of growth on the control cpTi and PPC surfaces (Figure 4.4A), however, there was very little or no Runx2 expressed in the initial 24-hour cultures even on the control cpTi surfaces. Subsequently, Runx2 levels increased such that considerable Runx2 mRNA was detected after 7 days growth on all of the surfaces except PPC-1 (Figure 4.4B). RT-PCR detected ample Runx2 expression in the cells grown on cpTi control surfaces and on PPC-2, PPC-3 and PPC-4. And the Runx2 levels appeared to be similar in the cells that grew on PPC-2,

PPC-3, PPC-4, but the level was found to be the lowest on the PPC-1. Like 1 day culture, type I collagen expression was detected in all of the PPC surfaces after 7 days of cell cultures.

Gene expression and differentiation on PPC

Real Time RT-PCR analysis was performed to quantify the levels of Collagen type I and Runx2 gene expressed when the HEPM cells (200,000/well in multiple 6-well plates) were cultured on commercially pure titanium (cpTi) and PPC surfaces. Quantitative Real Time PCR studies detected Runx2 and Collagen type I in the mineralizing HEPM cultures grown on all test surfaces. Although, the steady state mRNA levels of both genes were found to be the highest on cpTi control surfaces, PPC-4 expressed higher level of Runx2 and Collagen type I than other PPC surfaces.

Figure 4.5 showed that the level of Runx2 expressed over 7 days on PPC-4 was significantly higher than that on PPC-1 (P<0.01), but not significantly higher than that on PPC-2 and PPC-3 (P>0.05), while cpTi maintained statistically significant superiority in Runx2 expression (P<0.001) over the same time point. Similarly, after 7 days of seeding, cpTi showed superior Collagen type I expression (P<0.001); however, the level of Collagen type I expressed on PPC-4 was significantly higher than that on PPC-1 (P<0.001), but not significantly higher than that on PPC-2 and PPC-3 (P>0.05) when RNA was extracted from the HEPM cells cultured for 7 days. This indicated that TiO_2 enriched PPC surfaces expressed similar levels of Collagen type I.
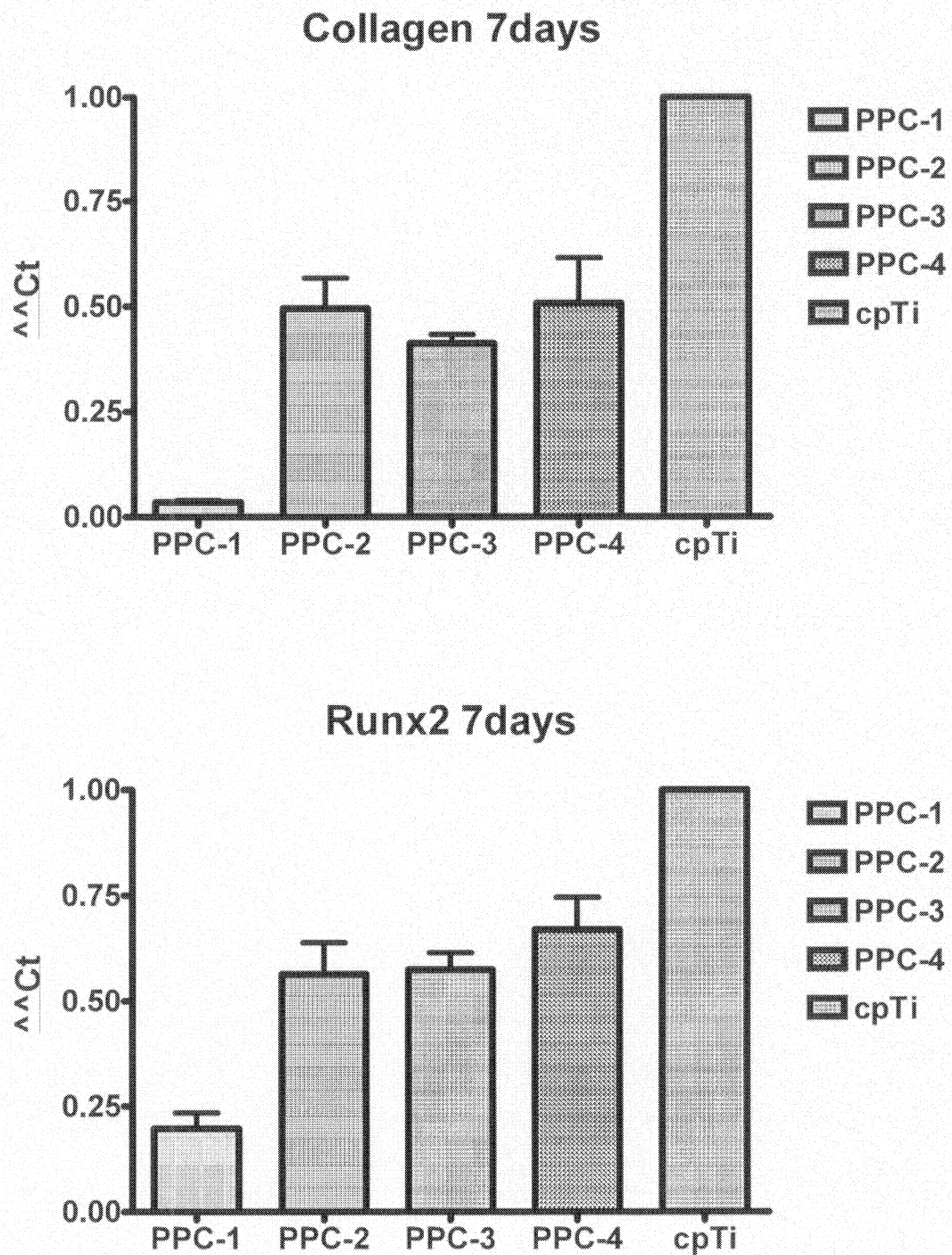
Figure 4.5: Real Time PCR analysis was performed on triplicate RNA extracts from
HEPM cells after 7 days of growth on PPC-1, PPC-2, PPC-3, PPC-4 and cpTi. Gene

expression (Collagen type I and Runx2) levels were normalized and presented as mean ± SD. After 7 days of growth, both Collagen and Runx2 levels on cpTi were significantly higher than on PPC surfaces ($P<0.05$); however, PPC-4 showed the highest levels of gene expression compared to other PPCs.

4.4. Discussion

In this study, polymeric powder coatings (PPC) were successfully created through the application of ultrafine powder coating technology from the polymeric resins and nano-sized metal oxides. This patented technology utilized nano-sized flow additives to prevent the aggregation of ultrafine powders, and thereby ensure adequate flow.[33,34] Here we used 0.5% of nSiO$_2$ with epoxy resin to create PPC-1, and same amount of nSiO$_2$ with polyester resin to create PPC-2. Then, we used 0.5 and 2.0% of nTiO$_2$ with polyester to create PPC-3 and PPC-4 respectively. Same amount (3.0 wt.%) of PTFE has been added to all four PPC surfaces.

Our earlier study showed[32] that this advanced ultrafine powder coating technique ensured an even dispersal of the materials to create a very homogenous and uniformly distributed surface coating. Moreover, PPC surfaces were found to be porous with nano topographical features that remained consistent across each surface.[32] In this study we analyzed PPC surface with the aid of AFM. AFM images again confirmed similar nano-scale surface features with pits/cavities.

These similarities in their surface features and chemical compositions were translated into a likeness in physical properties. AFM images showed the all of the PPC coatings had

similarly complex micro-topographies and high levels of surface nanoroughness. The images also revealed a labyrinth of pits and concavities that created intricate micro-nano sized topographies across all of the surfaces. Similarly, the surface roughness measurement recorded high levels on all of the coatings. Both of these characteristics can be attributed to the use of PTFE. The equal amounts of PTFE in each PPC formulation accounted for the similarities in their surface topographies.[32] Indeed, when the powder coatings cured at 200°C, the powder mixtures melted, homogenized and spread onto the substrates. During melting and spreading, the nanoparticles tended to move up to the top of the coatings and formed nano structures on top of the cured polymeric resin. Moreover, due to the differences in surface energies among the nano-sized PTFE (i.e., low surface energy) and the resin, micron-sized porous polymeric surfaces were developed upon melted and cured. Therefore, the porous discontinuous topographies were attributed to the presence of PTFE, while nano additives provided additional nano scale roughness to the PPC surfaces.

PPC surfaces exhibited markedly different cellular responses towards HEPM cells, despite having the similarities in their composition except the nano-TiO_2 enrichment. We found that PPC surfaces differed widely in their capacity to support human mesenchymal cell attachment, spreading, proliferation, metabolic activity and differentiation. While PPC-3 and particularly PPC-4, supported favorable cellular responses, PPC-1 and -2 displayed declined effects. Whereas PPC-3 and -4 had $nTiO_2$ as a flow additive, PPC-1 and -2 used $nSiO_2$ for their preparation. Furthermore, PPC-4 prepared with 2% $nTiO_2$

had better cellular responses than the PPC-3 that was prepared with 0.5% of the nano-titania additive.[32]

Similarly, it is well reported that the presence of nano-sized titania can enhance the cellular response. Kay et al.[35] and then Webster et al.[20] reported that the incorporation of nTiO$_2$ into polymeric composites yielded better osteoblast cells adhesion and proliferation. Jain et al. reported that cells responded better to polymeric substrates that had been sputter-coated with a nano-sized thickness of titanium.[19] Then, Yao et al.[14], Reising et al.[13] and Pareta et al.[12] showed that the addition of titanium nano-features to UHMWPE and PTFE, enhanced osteoblast cells attachment and growth. Recently, Ozkucur et al. have reported that a very thin nano-rough film (<100 nm) of titanium or zirconium on polyurethane, enhanced human umbilical vein endothelial cells attachment and proliferation.[22]

More recently, some other studies focused on incorporating micron-patterned nano roughness into polymeric surfaces since micro-nano features were proved to promote bioactivity of the respective biomaterials. Chun et al. in 2009 etched poly(ether) urethane (PU) and PLGA surfaces chemically with HNO$_3$ and NaOH, respectively, to create nano-scale surface features and observed greater bladder urothelial cell density on the etched surfaces.[23] Similarly, Ranjan et al. reported enhancement of endothelial cell adhesion and elongation on poly(dimethylsiloxane) (PDMS) films consisting of arrays of nano-grooves and alternating micro-nano roughness.[17] The mechanism of better cell attachment to the nano featured polymeric surfaces might be translated into increased adsorption of

vitronectin, which eventually attributed to the higher surface area of the nanorough

implant surfaces.[36]

In this current study, all of the PPC surfaces revealed attached HEPM cells, although

PPC-4 appeared to outperform the other PPC coatings. Alike our earlier study[32], SEM

showed that within 72 hours of seeding, there were some smaller cells on PPC-1 with

fewer extensions, some attachment and spreading on PPC-2 and -3, and even more

attached on PPC-4. Similarly, Webster et al. and then Ozkucur et al. showed that nano

titania and nano-titanium/zirconium (<100 nm then layer) enriched surfaces had more

attached cells under SEM, respectively.[20,22] Moreover, Webster et al. reported that twice

as many cells attached to poly-lactic-co-glycolic acid (PLGA) and nTiO$_2$ composite

surfaces,[20] and Pareta et al.[12] reported higher cell adhesion to nano-titanium enriched

polymeric surfaces. The common matter in these studies has been the presence of nano

features that contributed to the cell adhesion and proliferation. Our PPC surfaces also

demonstrated significant nano features. In fact, when surfaces had nano features or nano

roughness, seeded cells were exposed to huge amount of surface defects to interact with

that eventually translated to superior cellular responses.

Furthermore, we observed HEPM cells spreading onto the PPC surfaces. The attached

HEPM cells displayed distinct morphologies and ultra-structural features with

cytoplasmic projections and numerous extensions onto the underlying surfaces. Image J

analysis showed that these cells on PPC had a narrower and extended morphology, with

less defined stress fibers, than the flattened cells that were attached on the cpTi controls.

Largely, seeded cells exhibited significantly more spreading than the PPC surfaces; however, the $nTiO_2$ enriched surfaces showed steady increment in cell spreading. Indeed, other studies found similar morphologies and cytoskeletal features when cells attached to rough surfaces, as compared to smooth and flattened substrates. When Schuler et al. grew cells on adjacent smooth and rough surfaces; they found more spread and flattened cells on the smooth surfaces and narrower extended morphologies on the rough substrates.[15] Also, Al-Rabeah et al.[37] and then Deller-Quinn and Perinpanayagam[38] demonstrated the narrower spreading in cells grown rough mineral trioxide surfaces.

In addition to cell attachment and spreading, the seeded HEPM cells have to form extracellular matrix followed by differentiation into bone-forming osteoblasts to ensure osteogenesis and hence osseointegration. In particular, expression of Runx2 transcription factor regulates bone formation on biomaterial surfaces that is the important precondition for the success of dental and orthopedic implants.[25] Hence, Runx2 is considered as an essential transcription factor for osteoblast development and maturation,[24] while expression of collagen type I influences potential mineralization.[8] However, the expression of both Runx2 and collagen type I genes depends largely on the biomaterial surface topography. Having created nanorough topographic polymeric surfaces by using ultrafine powder coating technology, it is necessary to explore whether HEPM cells grown on PPC surfaces expressed important regulatory genes that determined the key pathway to bone formation.

Unfortunately, there are not many references found in the literature that reported on the

HEPM cells expression of Runx2 onto polymeric surfaces consisting of micro or micro-

nano features. Although Thomas J. Webster group published pioneering works of

endothelial or osteoblast cells adhesion, proliferation and growth on a number of

polymeric substrates modified by either chemical etching or ionic plasma deposition of

nano titanium onto PLGA composites,[12-14,16,17,20,23,39-41] they did not report Runx2

expression on any of those nano titanium enriched surfaces. Even in our earlier work[32],

we did not study gene expression on the epoxy and polyester-based micro-nano rough

polymeric coatings. However, Hamilton et al. replicated micrometer-sized tapered pits,

gap-cornered box and grooved topographical cues onto epoxy resin and reported

significant level of Runx2 in all these microfabricated epoxy surfaces.[42]

However, a number of previous studies reported modification of titanium implants

surfaces to incorporate rougher (micro/nano) topographies that promoted osteoblast

differentiation on the underlying biomaterial surfaces. While compared with smooth

titanium surfaces, grooved and roughened titanium surfaces yielded higher levels of

Runx2 and collagen type I expression.[8,28,30] Sometimes, titanium surfaces were

chemically modified to create nano pores onto the substrates that eventually showed

increased differentiation of osteoblast-like cells.[10,11,26,27,29,31] Masaki et al. used grooved

and roughened titanium to compare osteoblast differentiation with cpTi and found that

cell grown on roughened titanium expressed enhanced levels of Runx2, collagen type I,

ALP, BSP and osteocalcin.[8]

Subsequently, we created polymeric resin-based nanoscale rougher coatings that appeared to express Runx2 over 7 days of HEPM cell cultures. The average dimensions of the developed coatings were: nanoscale roughness ~280 nm, pore diameter ~20 μm and depth ~600 nm. We observed HEPM cells initiated to express Runx2 on all of the PPCs surfaces and off course, on the cpTi control surfaces in only 7 days. Although conventional RT-PCR analysis detected very little or no Runx2 expressed in the initial 24-hour cultures even on the control cpTi surfaces, a considerable level of Runx2 was detected from the RNA extracted from all of the test surfaces after 7 days of seeding. However, Hamilton et al. identified significant Runx2 expression at 4 weeks, when they seeded osteoblast cells on micron-sized (30 to 175 μm) tapered pits, grooves and gap-cornered boxes on epoxy-resin.[42] Similarly, enhanced Runx2 expression was reported on microtopographic (grooved and roughened) titanium surfaces at 3 weeks while compared to their smooth counterparts.[8,28,30] More importantly, we also observed that the level of Runx2 on PPC-1 was significantly lower than that of PPC-2, -3 and -4. This result must be correlated to the lower HEPM cell density found on PPC-1, which was again due to the absence of any form (either micro or nano-sized) of TiO_2 in PPC-1 formulation. Since PPC-2, -3 and -4 had same amount of μm-sized TiO_2 and PPC-3 and -4 had $nTiO_2$ in their formula, the nano features of these coatings might come from the added TiO_2 in the respective formulation. Due to this, cells grown on these surfaces exhibited similar degree of Runx2 expression at 1 week time point.

Moreover, conventional RT-PCR analysis detected the expression of type I collagen just after 1 day of growth on the control cpTi and PPC surfaces. Subsequently, HEPM cells

grown on the PPC surfaces for 7 days expressed a significant level of collagen type I after 7 days. This can be explained as collagen type I is highly expressed at the early stage of bone maturation.[11]

Largely, these findings of HEPM cell adhesion, spreading and Runx2 expression demonstrated the cytocompatibility of these polymeric coatings. Through this study we have shown that advanced ultrafine powder coating techniques can be utilized to prepare homogenous micro-nano featured polymeric coatings, and that these surfaces can support a favorable cellular response. Furthermore, we have shown that the incorporation of very small amounts of nano-titania can markedly enhance HEPM cell attachment and spreading on the PPC surfaces, although the levels of gene expression may not seem to be significantly different when the amount of $nTiO_2$ has been changed in the coating formulations from PPC-2 to PPC-4. However, the presence of TiO_2 into the coating formula provided clear superiority to some PPC surfaces in terms of Runx2 and Collagen(I) expression, although all of the PPC surfaces were made of similar degree of nano surface roughness. More importantly, the levels of expression of key genes expression (collagen(I) and Runx2) observed on nano featured PPC surfaces were approaching to that of commercially pure titanium (cpTi). However, ultimately the value of these nano-titanium enriched polymeric coatings will need to be verified by in vivo studies.

4.5 Conclusions

Nano rough polymeric powder coatings (PPC) were successfully developed by using ultrafine powder coating technology. These PPC surfaces could support human mesenchymal cell attachment, spreading and Runx2 expression. However, PPC-1 that contained neither micron-sized nor $nTiO_2$, had the least favorable response in terms of both cell adhesion and gene expression. PPC-2 contained only the micron-sized titania, and exhibited modest cell attachment in 72 hours, but greater levels of Runx2 expression in 7 days. In contrast, PPC-3 and -4 that were enriched with 0.5 and 2% $nTiO_2$ respectively, showed enhanced cell attachment, spreading, and Runx2 and Collagen(I) expression. Although PPC-2 exhibited less cell attachment in 72 hours than PPC-3 and PPC-4, all three of them (PPC-2, PPC-3 and PPC-4) showed similar levels of collagen type I and Runx2 expression over the extended period of cell growth. More importantly, the levels of gene expression detected on the PPC surfaces were as similar as that of cpTi, as their band intensity seemed to be the same. Therefore these nano rough polymeric powder coatings were shown to enhance their cytocompatibility. Thus this current research has provided novel information on newer biocompatible polymeric coatings that could mimic the desired nanoscale structure of dental and orthopedic implant surfaces.

References

1. Feinberg, A.W.; Wilkerson, W.R.; Seegert, C.A.; Gibson, A.L.; Hoipkemeier-Wilson, L.; Brennan, A.B., Systematic variation of microtopography, surface chemistry and elastic modulus and the state dependent effect on endothelial cell alignment. *J. Biomed. Mater. Res. A* **2008**, 86, 522-534.

2. Hallgren, C.; Reimers, H.; Chakarov, D.; Gold, J.; Wennerberg, A., An in vivo study of bone response to implants topographically modified by laser micromachining. *Biomaterials* **2003**, 24, 701-710.

3. Anselme, K.; Bigerelle, M.; Noel, B.; Iost, A., Hardouin, P. Effect of grooved titanium substratum on human osteoblastic cell growth. *J Biomed Mater Res* **2002**, 60, 529-540.

4. Sykaras, N.; Iacopino, A.M.; Marker, V.A.; Triplett, R.G.; Woody, R.D., Implant materials, designs, and surface topographies: their effect on osseointegration. A literature review. *Int J Oral Maxillofac Implants* **2000**, 15, 675-690.

5. Flemming, R.G.; Murphy, C.J.; Abrams, G.A.; Goodman, S.L.; Nealey, P.F., Effects of synthetic micro- and nano-structured surfaces on cell behavior. *Biomaterials* **1999**, 20, 573-588.

6. Lincks, J.; Boyan, B.D.; Blanchard, C.R.; Lohmann, C.H.; Liu, Y.; Cochran, D.L.; Dean, D.D.; Schwartz, Z., Response of MG63 osteoblast-like cells to titanium and titanium alloy is dependent on surface roughness and composition. *Biomaterials* **1998**, 19, 2219-2232.

7. Howlett, C.R.; Zreiqat, H.; Wu, Y.; McFall, D.W.; McKenzie, D.R., Effect of ion modification of commonly used orthopedic materials on the attachment of human bone-derived cells. *J. Biomed. Mater. Res.* **1999**, 45, 345-354.

8. Masaki, C.; Schneider, G.B.; Zaharias, R.; Seabold, D.; Stanford, C., Effects of implant surface microtopography on osteoblast gene expression. *Clin. Oral Implants Res.* **2005**, 16, 650-656.

9. Wieland, M.; Chehroudi, B.; Textor, M.; Brunette, D.M., Use of Ti-coated replicas to investigate the effects on fibroblast shape of surfaces with varying roughness and constant chemical composition. *J Biomed Mater Res* **2002**, 60, 434-444.

10. Protivinsky, J.; Appleford, M.; Strnad, J.; Helebrant, A.; Ong, J.L., Effect of chemically modified titanium surfaces on protein adsorption and osteoblast precursor cell behaviour. *Int. J. Oral Maxillofac. Implants* **2007**, 22, 542-550.

11. Isa, Z.M.; Schneider, G.B.; Zaharias, R.; Seabold, D.; Stanford, C.M., Effects of fluoride-modified titanium surfaces on osteoblast proliferation and gene expression. *Int. J. Oral Maxillofac. Implants* **2006**, 21, 203-211.

12. Pareta, R.A.; Reising, A.B.; Miller, T.; Storey, D.; Webster, T.J., An understanding of enhanced osteoblast adhesion on various nanostructured polymeric and metallic materials prepared by ionic plasma deposition. *J. Biomed. Mater. Res. A* **2010**, 92A (3), 1190-1201.

13. Reising, A.; Yao, C.; Storey, D.; Webster, T.J., Greater osteoblast long-term functions on ionic plasma deposited nanostructured orthopedic implant coatings. *J. Biomed. Mater. Res. A* **2008**, 87, 78-83.

14. Yao, C.; Storey, D.; Webster, T.J., Nanostructured metal coatings on polymers increase osteoblast attachment. *Int. J. Nanomedicine* **2007**, 2, 487-492.

15. Schuler, M.; Kunzler, T.P.; de Wild, M.; Sprecher, C.M.; Trentin, D.; Brunette, D.M.; Textor, M.; Tosatti, S.G., Fabrication of TiO2-coated epoxy replicas with identical dual-type surface topographies used in cell culture assays. *J. Biomed. Mater. Res. A* **2009**, 88, 12-22.

16. Pareta, R.A.; Reising, A.B.; Miller, T.; Storey, D.; Webster, T.J., Increased endothelial cell adhesion on plasma modified nanostructured polymeric and metallic surfaces for vascular stent applications. *Biotechnol. Bioeng.* **2009**, 103, 459-471.

17. Ranjan, A.; Webster, T.J., Increased endothelial cell adhesion and elongation on micron-patterned nano-rough poly(dimethylsiloxane) films. *Nanotechnology* **2009**, 20, 305102.

18. Lehle, K.; Buttstaedt, J.; Birnbaum, D.E., Expression of adhesion molecules and cytokines in vitro by endothelial cells seeded on various polymer surfaces coated with titaniumcarboxonitride. *J. Biomed. Mater. Res. A* **2003**, 65, 393-401.

19. Jain, R.; Von Recum, A.F., Fibroblast attachment to smooth and microtextured PET and thin cp-Ti films. *J. Biomed. Mater. Res. A* **2004**, 68, 296-304.

15. Webster, T.J.; Smith, T.A., Increased osteoblast function on PLGA composites containing nanophase titania. *J. Biomed. Mater. Res. A* **2005**, 74, 677-686.

21. Dalby, M.J.; McCloy, D.; Robertson, M.; Agheli, H.; Sutherland, D.; Affrossman, S.; Oreffo, R.O., Osteoprogenitor response to semi-ordered and random nanotopographies. *Biomaterials* **2006**, 27, 2980-2987.

22. Ozkucur, N.; Wetzel, C.; Hollstein, F.; Richter, E.; Funk, R.H.; Monsees, T.K., Physical vapor deposition of zirconium or titanium thin films on flexible polyurethane highly support adhesion and physiology of human endothelial cells. *J. Biomed. Mater. Res. A* **2009**, 89, 57-67.

23. Chun, Y.W.; Khang, D.; Haberstroh, K.M.; Webster, T.J., The role of polymer nanosurface roughness and submicron pores in improving bladder urothelial cell density and inhibiting calcium oxalate stone formation. *Nanotechnology* **2009**, 20, 85104.

24. Schroeder, T.M.; Jensen, E.D., Westendorf, JJ. Runx2: a master organizer of gene transcription in developing and maturing osteoblasts. *Birth Defects Res C Embryo Today* **2005**, 75, 213-225.

25. Ducy, P.; Zhang, R.; Geoffroy, V.; Ridall, A.L.; Karsenty, G., Osf2/Cbfa1: a transcriptional activator of osteoblast differentiation. *Cell* **1997**, 89, 747-754.

26. Maekawa, K.; Yoshida, Y.; Mine, A.; van Meerbeek, B.; Suzuki, K.; Kuboki, T., Effect of polyphosphoric acid pre-treatment of titanium on attachment, proliferation, and differentiation of osteoblast-like cells (MC3T3-E1). *Clin Oral Implants Res* **2008**, 9, 320-325.

27. Att, W.; Tsukimura, N.; Suzuki, T.; Ogawa, T., Effect of supramicron roughness characteristics produced by 1- and 2-step acid etching on the osseointegration capability of titanium. *Int J Oral Maxillofac Implants* **2007**, 22, 719-728.

28. Schneider, G.B.; Zaharias, R.; Seabold, D.; Keller, J.; Stanford, C., Differentiation of preosteoblasts is affected by implant surface microtopographies. *J Biomed Mater Res A* **2004**, 69, 462-468.

29. Guizzardi, S.; Galli, C.; Martini, D.; Belletti, S.; Tinti, A.; Raspanti, M.; Taddei, P.; Ruggeri, A.; Scandroglio, R., Different titanium surface treatment influences human mandibular osteoblast response. *J Periodontol* **2004**, 75, 273-282.

30. Schneider, G.B.; Perinpanayagam, H.; Clegg, M.; Zaharias, R.; Seabold, D.; Keller, J.; Stanford, C., Implant surface roughness affects osteoblast gene expression. *J Dent Res* **2003**, 82, 372-376.

31. Viornery, C.; Guenther, H.L.; Aronsson, B.O.; Pechy, P.; Descouts, P.; Gratzel, M., Osteoblast culture on polished titanium disks modified with phosphonic acids. *J Biomed Mater Res* **2002**,62, 149-155.

32. Mozumder M.S.; Zhu J.; Perinpanayagam H., Nano TiO_2 Enriched Polymeric Powder Coatings Support Human Mesenchymal Cell Attachment and Growth. *Journal of Biomaterials Applications* In Press, **2010**.

33. Zhu, J.; Zhang, H., Fluidization additives to fine powders, *U.S. Patent 6,833,185*, **2004**.

34. Zhu, J.; Zhang, H., Ultrafine powder coatings: An innovation. *Powder Coat.* **2005**, 16 (7), 39-47.

35. Kay, S.; Thapa, A.; Haberstroh, K.M.; Webster, T.J., Nanostructured polymer/nanophase ceramic composites enhance osteoblast and chondrocyte adhesion. *Tissue Eng.* **2002**, 8, 753-761.

36. Webster, T.J.; Schadler, L.S.; Siegel, R.W.; Bizios, R., Mechanisms of enhanced osteoblast adhesion on nanophase alumina involve vitronectin. *Tissue Eng* **2001**, 7, 291-301.

37. Al-Rabeah, E.; Perinpanayagam, H.; MacFarland, D., Human alveolar bone cells interact with ProRoot and tooth-colored MTA. *J. Endod.* **2006**, 32, 872-875.

38. Deller-Quinn, M.; Perinpanayagam, H., Osteoblast expression of cytokines is altered on MTA surfaces. *Oral Surg. Oral Med. Oral Pathol. Oral Radiol. Endod.* **2009**, 108, 302-307.

39. Sato, M.; Slamovich, E.B.; Webster, T.J., Enhanced osteoblast adhesion on hydrothermally treated hydroxyapatite/titania/poly(lactide-co-glycolide) sol-gel titanium coatings. *Biomaterials* **2005**, 26, 1349-1357.

40. Savaiano, J.K.; Webster, T.J., Altered responses of chondrocytes to nanophase PLGA/nanophase titania composites. *Biomaterials* **2004**, 25, 1205-1213.

41. Smith, L.J.; Swaim, J.S.; Yao, C.; Haberstroh, K.M.; Nauman, E.A.; Webster, T.J., Increased osteoblast cell density on nanostructured PLGA-coated nanostructured titanium for orthopedic applications. *Int J Nanomedicine* **2007**, 2, 493-499.

42. Hamilton, D.W.; Brunette, D.M., The effect of substratum topography on osteoblast adhesion mediated signal transduction and phosphorylation. *Biomaterials* **2007**, 28, 1806-1819.

CHAPTER 5
Nanotopographic Biocompatible Polymeric Powder Coatings

Chapter Summary

Recent studies reported that nano-scale roughness and topography of implant surfaces demonstrated superior cellular responses. As a result, several efforts have so far been made to incorporate nano roughness to the biomaterial surfaces although many of them are complicated and expensive processes. Therefore, the objective of this study was to utilize simple and inexpensive ultrafine powder coating technology to prepare nano-TiO_2 ($nTiO_2$)-enriched polymeric powder coatings (PPC) of different degree of nanoroughness and wettability to verify whether they could support human mesenchymal cell attachment and growth. In this study, it was observed that the nanoroughness decreased, but the wettability increased with the reduction of PTFE concentration into the coating formula keeping the other ingredients (avalanche white polyester and 0.5 % $nTiO_2$) same. Scanning electron microscopy (SEM) revealed from complex surface topographies composed of pits/cavities to flatter topographies with nano features only, and energy dispersive x-ray (EDX) analysis with titanium mapping confirmed a homogenous dispersion of the material. SEM and inverted fluorescence microscopy showed that human embryonic palatal mesenchymal (HEPM) cells attached and spread out on the $nTiO_2$-enriched PPC surfaces, particularly those that had surface roughness less than ~50 nm and were of relatively higher wettability. Cell counts were higher, and the MTT assay measured more metabolic activity from the cells seeded on nanotopographic $nTiO_2$ enriched PPC surfaces. Most importantly, the PPC surfaces that were very close to commercially pure titanium (cpTi) in nanoroughness appeared to perform as good as cpTi. Therefore the level of nanoroughness of $nTiO_2$-enriched PPCs proved to be the key to exhibit changes in human mesenchymal cell attachment and growth.

5.1. Introduction

It is well established that the interaction of host tissues with the underlying implant surfaces is the key to their long-term success when they are placed into human body. This desired bone-biomaterials interactions depends not only on the chemistry of the implant surfaces, but also on their surface roughness[1-3] and topography[4-6]. Recent studies showed nano-scale surface roughness and topography enhanced cellular responses to implant materials,[7-15] because these nanorough implant surfaces were exposed to the tissues of the body that possessed nano-scale surface roughness due to the presence of the nano-structured proteins such as collagen 1, hydroxiapatite crystals and other extracellular matrix molecules.[16] Therefore, it is imperative to incorporate these important properties (i.e., nanoroughness) of host tissues into the new biomaterials to facilitate efficient tissue generation that obviously ensures the long term success of the orthopedic and dental implants.

In order to obtain desired topography on metallic substrates, surfaces of titanium and titanium alloys surfaces have been modified by various polishing, grit blasting, machining, microfabrication, and acid and chemical etching techniques, to enhance their cytocompatibility.[3,17-21]

Recently reports have been published on the use of polymeric materials and composites for orthopedic implants[13-15,22] and for vascular grafts[23-25]. Subsequently, these polymeric substrates have been modified and coated with nano-sized titanium or titania particles to enhance their bioactivity, because clearly titanium and its alloys have been widely used

as implant materials due to their superior biocompatibility and mechanical properties. Therefore, the different polymers have had sputter-coating, vapor and plasma deposition for the application of nano titanium and other metals, to incorporate desired nano features to the implant surfaces.

In 2003, Lehle et al.[25] used a plasma-assisted chemical vapor deposition process to apply a thin titanium-carboxonitride layer onto polyethylene terephthalate (PET), polypropylene (PP), polytetrafluoroethylene (PTFE), polyurethane, and silicone. They found that endothelial cell adhesion was enhanced on the titanium coated surfaces. Later in 2005, Webster et al.[11] studied the incorporation of both conventional (i.e., greater than 100 nm grain size) and $nTiO_2$ into poly-lactic-co-glycolic acid (PLGA) and reported more favorable osteoblast like cell attachment to $n-TiO_2$ enriched PLGA than the conventional ones when they maintained PLGA to $nTiO_2$ (70:30) ratio.

Therefore, the current focus of the area is to apply titanium or titania nanoparticles to fabricate nano roughness and topography onto polymeric surfaces to further improve their cellular responses. As a consequence, Yao et al.[13] employed a novel ionic plasma deposition (IPD) process to apply titanium or gold, and also to create nano-sized features (less than 100 nm) of titanium on polyetheretherketone, ultra-high molecular weight polyethylene (UHMWPE) and PTFE. The osteoblast cell adhesion and spreading were found to be better on the coated polymers than on the uncoated surfaces[13]. Similarly, Reising et al.[14] investigated into used the IPD process to apply nanostructured titanium and to add less than 100 nm nano-features on UHMWPE and PTFE. They reported that

osteoblast proliferation was significantly enhanced on the coated polymers compared to the uncoated material and titanium controls. Recently, in 2009 Ozkucur et al.[26] deposited a thin film (<100 nm) of titanium or zirconium onto polyurethane surfaces by using a physical vapor deposition technique and reported enhanced endothelial cell adhesion and proliferation. Most recently, Pareta et al.[15] studied IPD and nitrogen ion immersion plasma deposition to apply titanium nano-particles titanium onto metallic implant materials such as titanium and titanium alloy (Ti6Al4V), and onto polymers such as PET, polyvinyl chloride, polyurethane, PTFE, UHMWPE and nylon. They obtained an increase in osteoblast adhesion on the modified surfaces compared to the untreated controls.

More recently, some other studies reported on the cellular responses to the micron-patterned nano rough polymeric surfaces. Ranjan et al. fabricated the arrays of nano-grooves and alternating micro-nano roughness on poly(dimethylsiloxane) (PDMS) films to enhance endothelial cell adhesion and elongation for cardiovascular use.[24] Similarly, Chun et al. etched poly(ether) urethane (PU) and PLGA surfaces with HNO_3 and NaOH, respectively, to make them submicron and nanorough, and observed greater urothelial cell density on the etched PLGA surfaces that exhibited nano roughness.[27]

In our previous study, we have utilized an entirely novel but simple, environmentally friendly (i.e., no toxic solvents, no VOC emissions) and inexpensive approach for applying nano-sized metal oxides in combination with polymeric resins to create nano-featured (200~300 nm) biocompatible coatings.[28] We used a patented ultrafine powder

coating technique[29,30] to homogeneously disperse nano-sized metal oxides, PTFE and

polymeric resins. By using this ultrafine powder coating technology we combined

ultrafine resin powders, which include polyester or epoxy resins, with nano-sized silica or

titanium dioxide and dispersed them homogenously. Due to the addition of same amount

of PTFE (3.0 wt.%), all of the polymeric powder coating (PPC) surfaces used in our

earlier study had same degree of surface roughness (200~300 nm) and identical

topographies composed of a number of pits and cavities.[28] Having this intricate nano

topography, PPC surfaces showed cytocompatibility towards human embryonic palatal

mesenchymal (HEPM) cells, although none of them exhibited cytocompatibility closer to

that of commercially pure titanium (cpTi; ~ 20 nm rough).[28] While nanostructured cells

(~50 nm) found cpTi rough enough to attach, spread and proliferate well, higher nano

(200~300 nm) featured PPC surfaces seemed no more rough to the seeded cells to be

attached as good as cpTi.

Now, in this study, we used the same ultrafine powder coating technology to create PPC

surfaces of varying nano-scale roughness and topography. The rationale was to develop

the coatings of surface roughness closer to that of cpTi (~20 nm) since cpTi exhibited

significantly higher cytocompatibility than the PPC surfaces (200~300 nm rough) studied

in our previous work.[28] To accomplish that, we kept all other ingredients (avalanche

white polyester resin incorporated with 25% pigment grade TiO_2 and 0.5 wt. % $nTiO_2$)

same except changing the amount of PTFE. In this current study, PTFE concentration

was reduced from 3.0 wt.% to 0 wt.% that decreased the nano-scale surface roughness to

~37 nm which was closer to that of cpTi. With decreasing nanoroughness, water contact

angles also reduced to make the newly developed PPC surfaces relatively hydrophilic. This change in wettability was also believed to be beneficial to cell attachment and growth.[11,26,31-33]

Moreover, we have studied these PPC coatings of varying nanoroughness and topography to verify their cellular responses to HEPM cells in terms of cell attachment, spreading and viability. We will also report on the variation in cytocompatibility of alternative coating formulations that provided a wider range of nano roughness starting from 37 nm to 262.8 nm, and will describe a markedly enhanced cellular response to the PPC surfaces having nano features of less than ~50 nm.

5.2. Materials and Methods

<u>PPC Preparation Procedure</u>

Polymeric powder coatings (PPC) were prepared by using Zhu and Zhang's patented powder coating technology.[29,30] Commercially available resins (table 5.1) were modified with nano-sized additives to ensure adequate flow of the ultrafine resins and additives mixtures. Avalanche white polyester (PE) resins (Links Coating, London, Canada) were combined with filler, and flow, degassing and curing agents (Figure 5.1). These mixtures were processed through a twin-screw extruder (Donghui Powder Processing Equipment Co., Yantai, China) to create chips that were then ground into powder particles (15-20 μm). The fine powders were then mixed with different percentages (0%, 1%, 2% and 3%) of nano-sized polytetrafluoroethylene (PTFE; Dupont, Canada), which served to alter the surface roughness of the final coatings. Then, 0.5 wt.% titanium dioxide (TiO_2;

Degussa, USA) nano-particles (~40 nm average particle size) were added to the

formulations through high-shear mixing in order to increase the flowability of the powder

mixtures. Without these nano-additives, the coating film would become non-

homogeneous, because the ultrafine powder particles (15-20 μm) would agglomerate

significantly due to their inherent cohesiveness and hinder flow leading to non-uniform

coating finish.[34]

Table 5.1: Coating compositions

No.	Resin	Embedded [μ-TiO₂] (%)[1]	Additive	Additive [nTiO₂] (%)[1]	[PTFE] (%)[1]
PPC-3	Avalanche White Polyester	25	nTiO₂	0.5	3.0
PPC-7	Avalanche White Polyester	25	nTiO₂	0.5	2.0
PPC-6	Avalanche White Polyester	25	nTiO₂	0.5	1.0
PPC-5	Avalanche White Polyester	25	nTiO₂	0.5	0.0

[1]Weight Percentage

Finally, the powder mixtures were fed to the spray gun through a hopper. As the spray

gun was activated, a voltage was applied to ionize the particles that were then sprayed

onto sheets of aluminum that were grounded. Subsequently, the powder-coated sheets

were cured (200° C for 10 min). Upon cured, the PPC coatings could become porous

(depending on the amount of PTFE present in the formula) and nano topographic.
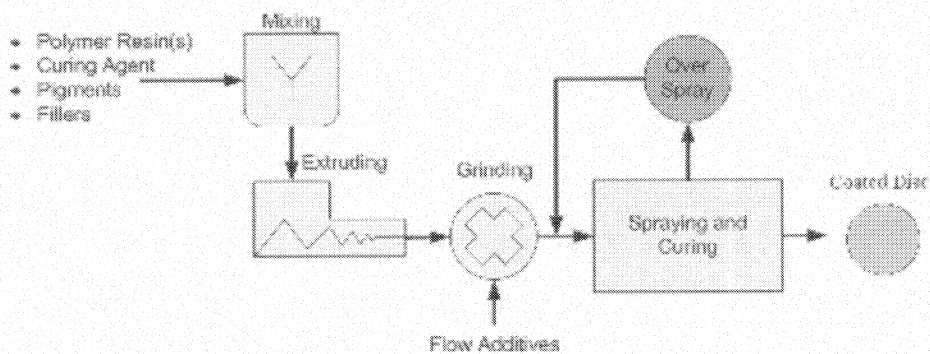
Figure 5.1: Polymeric Powder Coatings (PPC) were prepared through an advanced ultrafine powder coating process. Polymeric resins, pigments, fillers and curing agent were mixed and then extruded as homogeneous chips. The chips were then ground into ultrafine powders (15-20 μm), dry blended and mixed with nano-sized flow additives ($nTiO_2$). These ultrafine mixtures were electrostatically sprayed onto a grounded workpiece, and cured in a furnace ($200°C$, 10 min). Oversprayed powders were recycled and reused.

PPCs Adhesion Test

The adhesion of the PPC to the underlying substrate was measured with an Elcometer 107 Cross Hutch Cutter (Elcometer Ltd., Windsor, Canada). The coatings were cut down to the substrate with a blade (11x1.5 mm) to make several perpendicular cuts were made to create a grid of small squares, as recommended by ASTM D3359. This lattice was brushed to remove debris, covered with adhesive tape (ASTM standard). The tape was then withdrawn by a single smooth pull, and some of the squares could be pulled off with the tape. Then the remaining grid squares were compared for retention. The lattice was then assessed for adhesion by using the ASTM D3359 standards.

SEM of the PPC Surfaces

The surface topography of the PPC was assessed by scanning electron microscopy

(SEM). The PPC surfaces were mounted on metal stubs with the aid of adhesive carbon

tape and were sputter coated with gold (10 nm thick layer), and then carefully examined

with a Hitachi S-2600 (Hitachi, Pleasonton, CA) SEM. The working voltage (15 kV),

beam (60) and working distance (5.2 mm) were set.

AFM of the PPC Surfaces

To determine their surface features, PPC surfaces were analyzed with the dynamic force

mode Atomic Force Microscopy (AFM) (Park Systems AFM XE-100). A silicon

cantilever with a spring constant of ~40 N/m and a nominal tip radius of 10 nm was used.

The length, width and thickness of the cantilever were 125 μm, 40 μm long and 4 μm,

respectively. The cantilever was oscillated around its resonant frequency (~300 kHz) and

its amplitude decreased when the tip interacted with the sample surface. Such damped

amplitude (set point) was used as the feedback parameter to probe the surface features.

The images of 256 x 256 pixels were collected in air at room temperature.

EDX and Ti Mapping

The elemental composition of the PPC surfaces was analyzed by energy dispersive X-ray

spectroscopy (EDX) equipped with Hitachi S-2600 SEM. The PPC surfaces were

mounted on metal stubs and sputter coated with gold (10 nm thick) as detailed above.

The working voltage (15 kV), beam (60) and working distance (15 mm) were set. The

EDX analyses quantified nearly all the elements with a minimum detection limit of 0.0

wt%. These analyses were repeated at three separate locations on each surface and mean surface concentrations of carbon and titanium were reported. In addition, mapping of elemental Ti on the PPC surfaces was performed by EDX to visualize the actual distribution of Ti over the entire surface. While doing Ti mapping, sample was loaded as same as they were loaded for SEM and elemental EDX, only different mode of operation was selected to get the elemental mapping.

Surface Roughness Measurement

The surface roughness of the PPC was measured with a Dektak 8 Stylus Surface Profiler (Veeco Metrology Group, Santa Barbara, CA). The PPC were loaded onto a high precision stage that moved beneath a diamond-tipped stylus according to specified scan length (20 mm), scan resolution (1.111 μm/sample) and stylus force (8 mg). Each PPC surface was scanned at 10 different locations to measure vertical features. The mean deviation of the vertical features from the centerline was then calculated as a measure for surface roughness (R_a).

Contact Angle Measurement

Water contact angles (CAs) of the coated surfaces were measured with a horizontal microscope equipped with the Rame-Hart 100 Goniometer. A drop (10 μl in volume) of deionized water was placed on the coated surfaces using a micrometric syringe (Gilmont Instrument). Static CA was measured by calculating the slope of the tangent to the drop at the liquid-solid-vapor interface line. The mean value was calculated from at least five individual measurements.

Sterilization of PPC Surfaces

The PPC surfaces and cpTi were disinfected and sterilized in preparation for tissue culture. The PPC and cpTi disks were rinsed twice with ethanol (70%), washed thrice with phosphate-buffered saline (PBS) and then placed into individual wells of a 24-well tissue culture plate. The entire plate of disks were then placed in a tissue culture hood and exposed to UV light for 30 minutes to ensure sterility.

Cell Culture on PPC Surfaces

Human embryonic palatal mesenchymal cells (HEPM, ATCC CRL-1486) were seeded onto cpTi and PPC in multiple 24-well tissue culture plates (50,000 cells/well). The cultures were maintained in Dulbecco's modified eagles medium (DMEM) supplemented with fetal bovine serum (FBS, 10%), L-glutamine (2 μmol/ml), penicillin G (100 U/ml), streptomycin sulfate (100 μg/ml) and amphotericin B (0.25 μg/ml)). Replicate cultures were incubated at 37°C for 6, 24 and 72 hours and then harvested for analysis.

SEM of the HEPM Cells Grown on PPCs

After each incubation period the replicate PPC disks were collected, washed three times with PBS, fixed with glutaraldehyde (2.5%) in cacodylate buffer (100 mM) for 20 minutes, dehydrated in ascending grades of ethanol (25, 50, 75, 95 and 100%) and immersed in hexamethyldisilazane. Then the surfaces were air dried, mounted on metal stubs, sputtered with gold (20 nm thick) and examined with a Hitachi S-2600 SEM as

detailed above. The working voltage (5-12 kV), beam (60) and working distance (5.3 mm) were set.

Fluorescence Microscopy of the HEPM Cells

After 24 and 72 hours of growth on titanium disks and PPC surfaces the cultures were harvested and washed thrice with PBS. The cells that were attached to the surfaces were fixed with paraformaldehyde (4% for 10 min) and permeabilized with Triton X-100 (0.1% for 5 min). The actin filaments of the cytoskeleton were labeled with rhodamine phalloidin (Cytoskeleton, Denver, CO) for 2 hours at room temperature. The surfaces were then mounted using Vectashield with DAPI (Vector Laboratories, Burlingame, CA) and examined by an inverted fluorescence microscope (Axiovert 40 CFL, Carl Zeiss Canada Ltd., Toronto, Canada) with the magnification of 20X.

Cell Attachment Assay

HEPM cells were seeded onto titanium disks and PPC surfaces in multiple 24-well tissue culture plates (20,000 cells/well). After 24 and 72 hours of cell attachment and growth, triplicate cultures were harvested from each surface, and carefully rinsed with PBS to remove unattached cells. Then, 150 μL of trypsin was added to each well of the culture plates and the plates were then put into the incubator for 5 minutes so that the attached cells were released. The cells were then collected and counted by using hemocytometer.

128

MTT Assay

HEPM cells (20,000 cells/well) were seeded onto titanium and PPC surfaces in multiple

24-well tissue culture plates using the same protocol followed in the cell attachment

assay. After 24 and 72 hours, the cpTi and the PPC surfaces were rinsed with trypsin to

release attached cells that were collected and reseeded into multiple 48-well tissue culture

plates. After 24 hours, MTT reagent (tetrazolium (3-(4, 5- dimethylthiazolyl-2)-2, 5-

diphenyltetrazolium bromide) was added and the cultures were incubated (37°C) for an

hour in the dark. The reagents were then carefully replaced with MTT solubilizing

solution (acid-isopropanol), and the absorbance (570 nm) measured in a Safire Multi-

Detection Microplate Reader (Tecan, Austria).

Statistical Analysis

In the cell attachment assay and the MTT assay, the differences between the replicate

cultures grown on different surfaces, and at different time points, were analyzed

statistically by a two-way analysis of variance (ANOVA) with a Bonferroni post-hoc test,

to a significance level of $P<0.05$.

5.3. Results

Coating preparation and characterization

Polymeric resins were combined and processed with fillers and additives and applied by

ultrafine powder coating technology to create polymeric powder coatings (PPC) (Figure

5.1). As reported in table 5.1, all of the developed coatings (PPC-3, -5, -6 and -7) were

made of avalanche white polyester resins in which 25% pigment grade micron-sized TiO_2

was incorporated. Hence, PPCs had same amount of embedded TiO_2. They also had same

nano additive (nTiO2) in exact same amount (0.5 wt.%). The only difference among the

PPC formulations was the concentration of PTFE. PPC-5, -6. -7 and -3 had 0%, 1%, 2%

and 3% PTFE, respectively.

All of these coatings were highly adherent to their underlying substrate (Table 5.2).

When subject to the standard test for adhesion, all of the PPC were found to have

excellent adhesion to their substrate. Indeed, none of the lattice squares were dislodged

by the tape removal during testing.

The PPC surfaces revealed complex nanotopographies (Figure 5.2A and 5.2B). When the

PPC surfaces were prepared, SEM and AFM examination showed complicated and

elaborate surface topographies in PPC-3 that contained highest amount (3 wt.%) of

PTFE. PPC-3 had numerous surface projections of nanometer scale and an underlying

labyrinth of concavities that created intricate and elaborate surface topography. There

were shallow and deep pits and cavities of micron dimension that contributed to surface

roughness and porosity. With reduced amount (2 wt.%) of PTFE, PPC-7 had less number

of micron-sized cavities leading to the reduction in surface roughness. When PTFE

concentration was further decreased (1 wt.%), only few pits were seen on PPC-6. With no

PTFE at all, PPC-5 seemed to be a very flatter surface containing nano features only that

came from the added nano additive ($nTiO_2$).
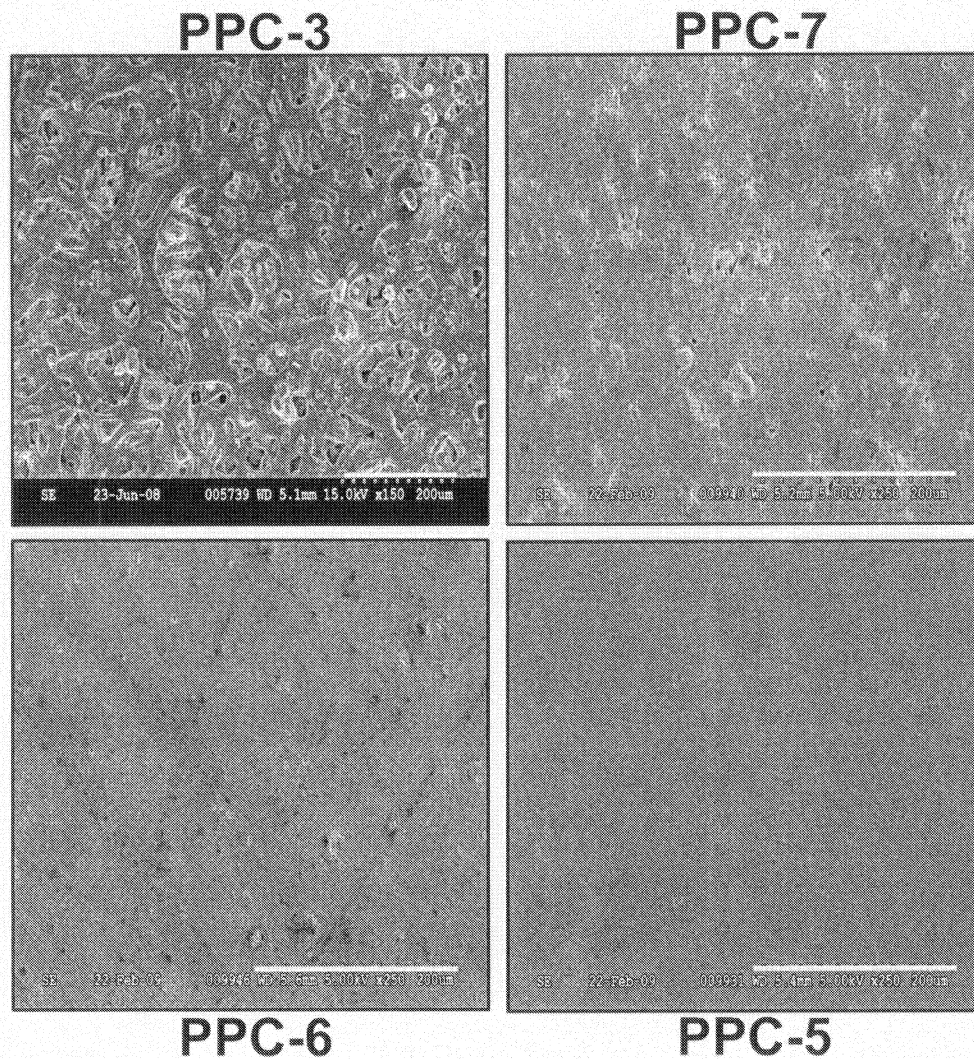
Figure 5.2A: Polymeric powder coatings (PPC-3, PPC-5, PPC-6 and PPC-7) were prepared and examined by scanning electron microscopy (SEM). PPC-3 and -7 were characterized by outward projections and inward concavities that created rough surface topographies whereas PPC-5 and -6 were created relatively flatter. (Scale bar = 200μm).
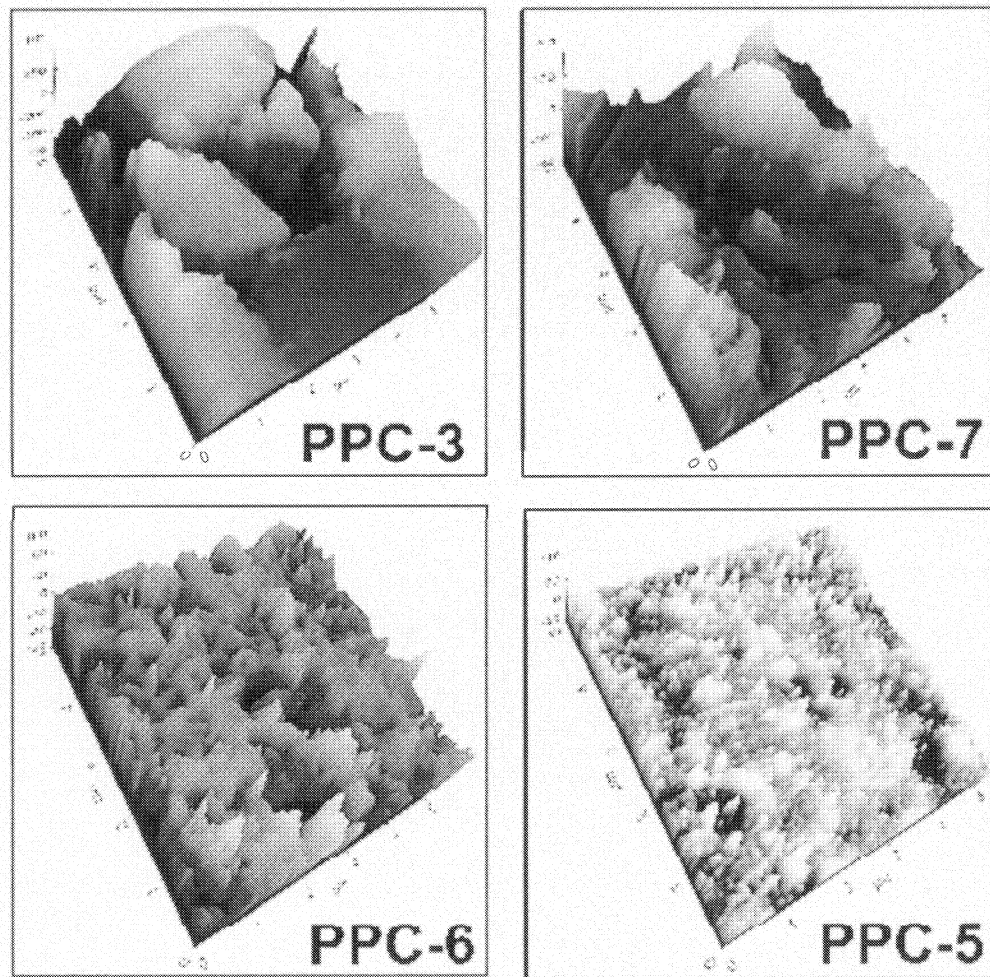
Figure 5.2B: Polymeric powder coatings (PPC-3, PPC-5, PPC-6 and PPC-7) were prepared and examined by atomic force microscopy (AFM). The horizontal axis of the AFM images represented the x and y axes (in µm) and the vertical axis represented the z-axis (in nm). Scan size: 5×5 µm.

All of these coatings had varying levels of nano-scale surface roughness (Table 5.2). The mean roughness of PPC-5, -6, -7 and -3 were 37.0, 50.9, 135.1 and 262.8 nm,

respectively (table 5.2). This variation in surface roughness was obtained when the

amount of PTFE added to the PPC formulations was changed. With increased

concentration of PTFE, roughness increased. However, the surface roughness of the

developed surfaces was within the nano-scale. These nanotopographies were also

attributed to the $nTiO_2$ nano-additives that were used in the preparation of PPCs.

Table 5.2: Coating Characterization

No.	Contact Angle (^{o})	Surface Roughness (nm)	Adhesion[1]
PPC-3	138.2 ± 6.0	262.8 ± 18	5B
PPC-7	112.9 ± 1.8	135.1 ± 18	5B
PPC-6	101.8 ± 1.8	50.9 ± 3.9	5B
PPC-5	87.4 ± 3.4	37.0 ± 2.8	5B

[1]Adhesion was assessed by comparing the lattice of cuts with ASTM D3359 standards

from 5B to 0B. 5B corresponds to completely smooth edges of the cuts (i.e., none of the

squares of the lattice is detached)

Alike surface roughness, PPCs showed the differences in water contact angles. Water

formed 87.4°, 101.8°, 112.9° and 138.4° contact angles on PPC-5, -6, -7 and -3,

respectively (table 5.2). That means, by analysing water contact angles, PPC-5 seemed to

be relatively hydrophilic, PPC-6 and -7 were hydrophobic, but PPC-3 exhibited the

nature of superhydrophobic surface. The degree of wettability again attributed to the

amount of PTFE added to the PPC formulations; because all other constituents remained

exact same among the developed coatings.

Furthermore, the titanium was readily detected in all PPC surfaces (Figure 5.3A) due to its incorporation in their formula. Furthermore, titanium appeared to be evenly dispersed across the PPC surfaces. The EDX analyses measured a similar concentration of titanium at each of the three measurement sites on each coating. Moreover, surface mapping of titanium on PPCs showed that the titanium was evenly distributed across the surface (Figure 5.3B).

HEPM cell study

The HEPM cells attached and spread out onto all of the developed PPC surfaces (Figures 5.4A, 5.4B, 5.4C and 5.4D). When the cells (50,000 cells/well) were incubated in 24-well tissue culture plates for 6 hours only, SEM showed that there were attached cells on all of the PPC surfaces (Figure 5.4A). Indeed, figure 4A has depicted an early attachment of HEPM cells on PPCs. There were numerous attached cells and they were well spread on PPC-5, and there were somewhat less attached cells, but good spreading on PPC-6; but there were few attached cells and little spreading on PPC-7 and almost no cells were visible on PPC-3.

PPC-3

PPC-7

C: 53.4% ± 0.51%
Ti: 12.9% ± 0.28%

C: 52.8% ± 0.74%
Ti: 15.6% ± 0.03%

C: 57.8% ± 0.16%
Ti: 15.5% ± 0.32%

C: 60.6% ± 0.16%
Ti: 16.4% ± 0.41%

PPC-6

PPC-5
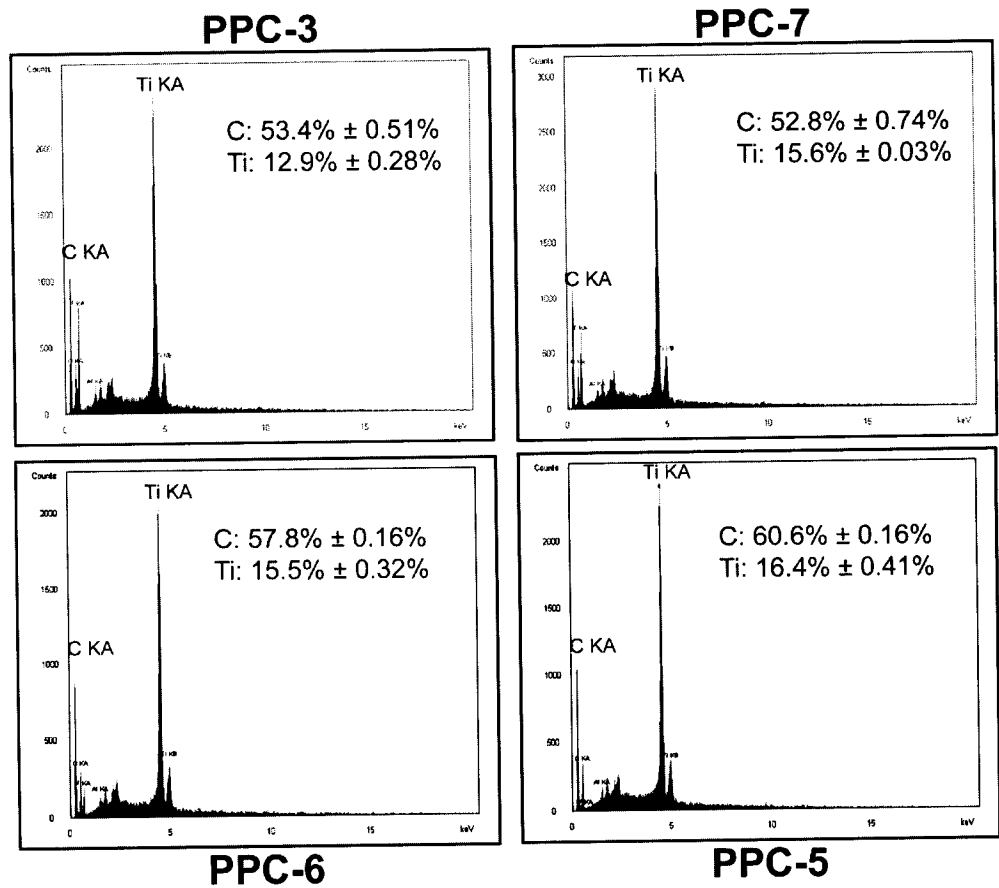
Figure 5.3A: Polymeric powder coatings (PPC-3, -5, -6 and -7) were prepared and their surfaces analyzed by energy dispersive X-ray (EDX) spectroscopy. The mean surface concentration of elemental carbon (C) and titanium (Ti) were reported with their standard deviations Ti peak is observed in all PPCs.
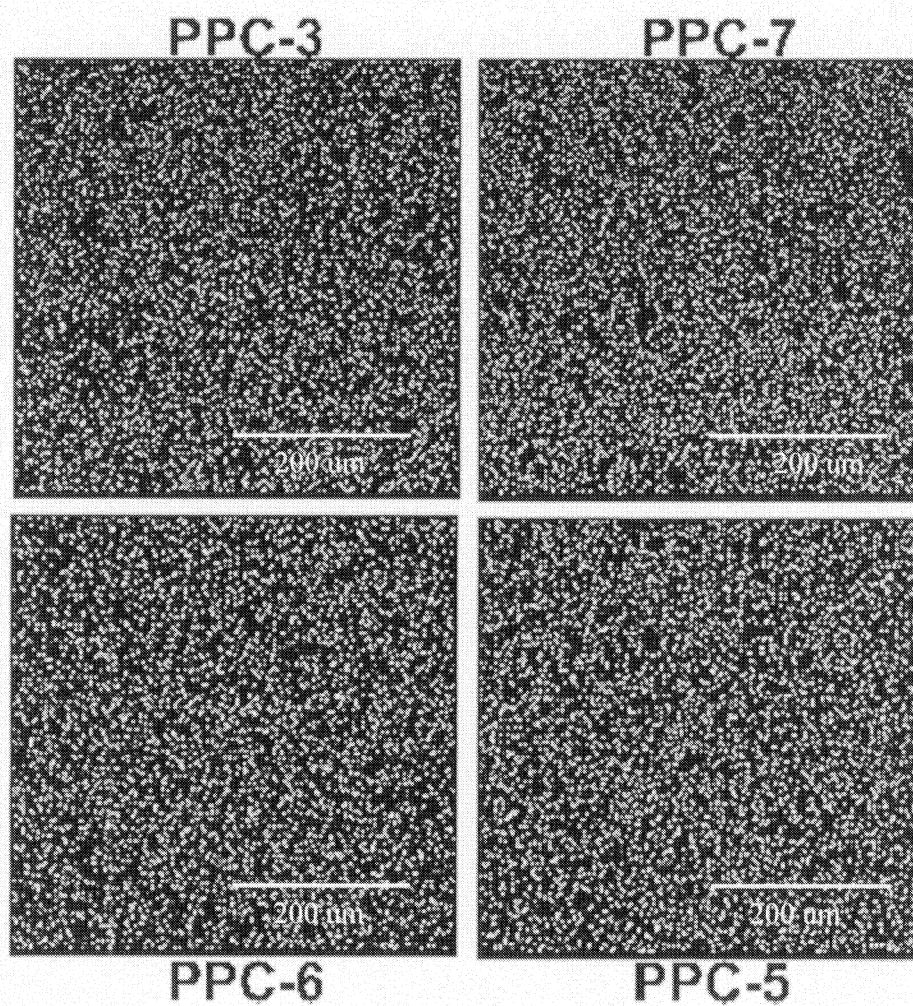
Figure 5.3B: During the EDX analysis of the PPCs, the surface distribution of elemental titanium was mapped concurrently. An even dispersion of titanium was seen on all the PPC surfaces used in this study. (Scale bar = 200 μm)

PPC-3   PPC-7

PPC-6   PPC-5
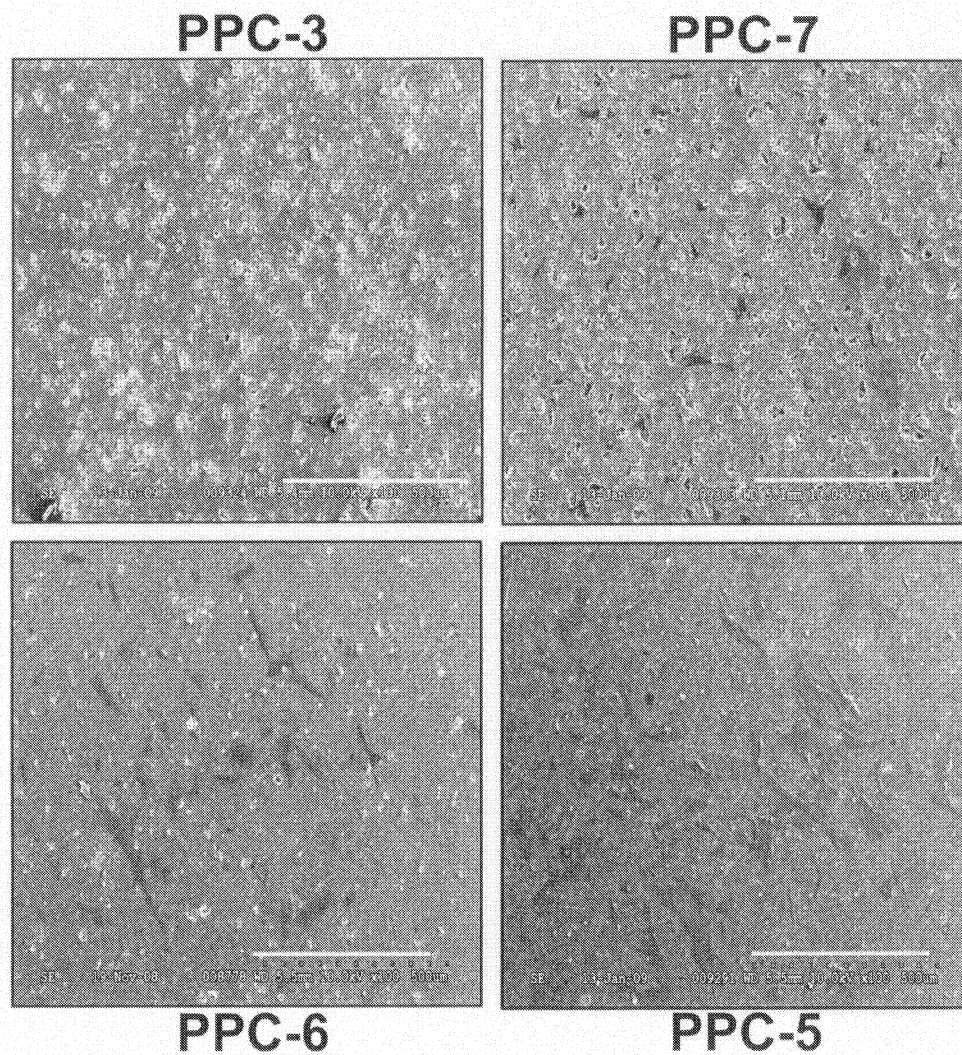
Figure 5.4A: Human mesenchymal cells (HEPM) were seeded onto polymeric powder coatings (PPC-3, PPC-5, PPC-6 and PPC-7) surfaces. After 6 hours, scanning electron microscopy (SEM) showed that there were only few cells on PPC-3 and PPC-7, but more cell attachment and spreading on PPC-5 and PPC-6. (Scale bar = 500 μm)

When these cells (50,000 cells/well) were incubated for 24 hours, SEM showed that the cells had attached and spread out on all of the PPC surfaces (Figure 5.4B). There were

numerous cells that had attached and spread out on PPC-5; a good number of HEPM cells

attached to PPC-6 and -7 and they were well spread too. However, although some cells

are attached on PPC-3, the seeded HEPM cells did not seem to be spread well onto PPC-

3.

When these cells (50,000 cells/well) were incubated for 72 hours, SEM showed that the

cells had attached and spread out on all of the PPC surfaces (Figure 5.4C and 5.4D). Low

magnification SEM images (Figure 5.4C) showed that PPC-5 was completely covered

with the HEPM cells; superb cell spreading was observed on PPC-6; although similar

number of HEPM cells was attached to PPC-3 and -7, cells spread better on PPC-7 than

on PPC-3. High magnification SEM images (Figure 5.4D) also revealed the similar

findings. There were numerous cells that had attached and spread out on all over PPC-5

and -6. Cells were found to be stretched into the cavities of PPC-3 and -7. It is also

evident that HEPM cells attached and spread so well onto PPC-5 that they seemed to

form a matrix-like layer on PPC-5.
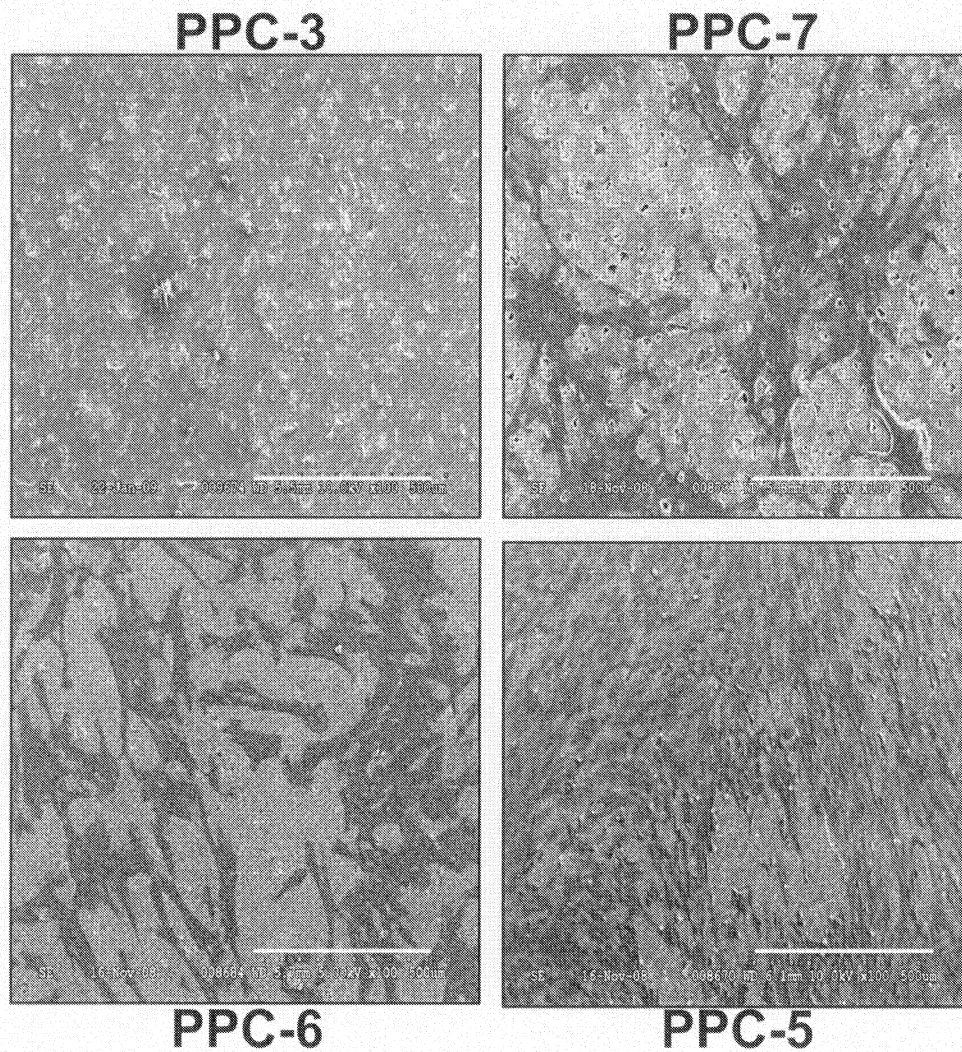
Figure 5.4B: Human mesenchymal cells (HEPM) were seeded onto polymeric powder coatings (PPC-3, PPC-5, PPC-6 and PPC-7) surfaces. After 24 hours, scanning electron microscopy (SEM) showed a few smaller cells on PPC-3, and few more cells attached with their cellular extensions on PPC-6 and -7; and numerous attached and well spread out cells on PPC-5. (Scale bar = 500 μm).
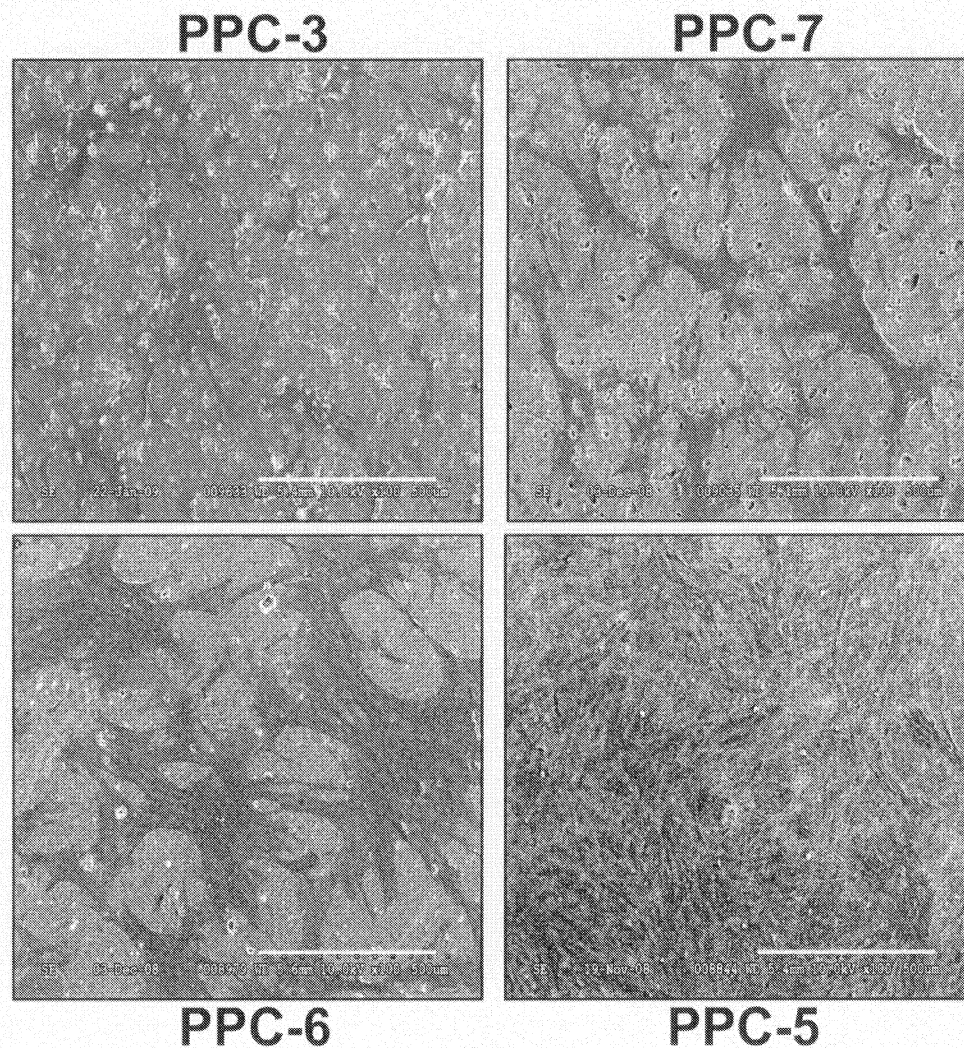
Figure 5.4C: Human mesenchymal cells (HEPM) were seeded onto polymeric powder coatings (PPC-3, PPC-5, PPC-6 and PPC-7) surfaces. After 72 hours, low magnification SEM images showed several cells and cellular extensions on PPC-3 and -7; numerous cells spread out onto PPC-6; but PPC-5 became almost confluent with HEPM cells. (Scale bar = 500 μm).
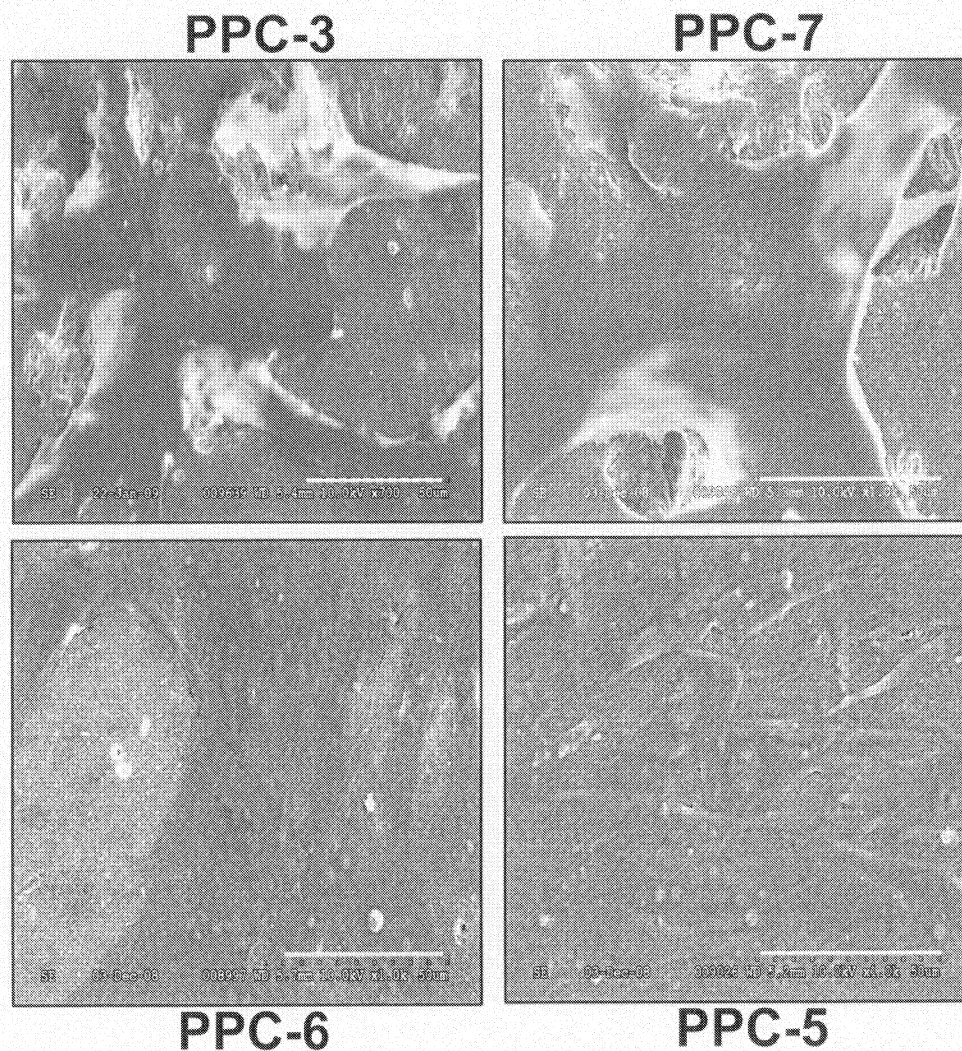
Figure 5.4D: Human mesenchymal cells (HEPM) were seeded onto polymeric powder coatings (PPC-3, PPC-5, PPC-6 and PPC-7) surfaces. After 72 hours, high magnification SEM images revealed that cells directed and migrated towards the cavities of underlying surfaces of PPC-3 and -7; whereas cells flattened onto PPC-5 and 6. However, PPC-5 was almost covered with the cells so that no empty space was seen on it after 72 hours of cell growth. (Scale bar = 50 μm).

The HEPM cells spread out on some of the PPC surfaces (Figure 5.5). When the cells (50,000 cells/well) were incubated in 24-well tissue culture plates for 24 and 72 hours,

inverted fluorescence microscopy showed that there were attached cells on all PPC

surfaces and on the commercially pure titanium surfaces (cpTi, control samples).

Numerous cell nuclei were detected on PPC-5 and -6, and on titanium in both 24 and 72

hours of incubations; several nuclei were also detected on PPC-3 and -7 although cells

were lean and rounded on these PPC surfaces. The cells were well spread out on the PPC-

5, -6 and titanium surfaces, whereas they were less spread on PPC-7 and -3. More actin

filaments were visible on PPC-5 and PPC-6 than on titanium; that meant PPC-5 and PPC-

6 supported more clearly defined stress fibers.
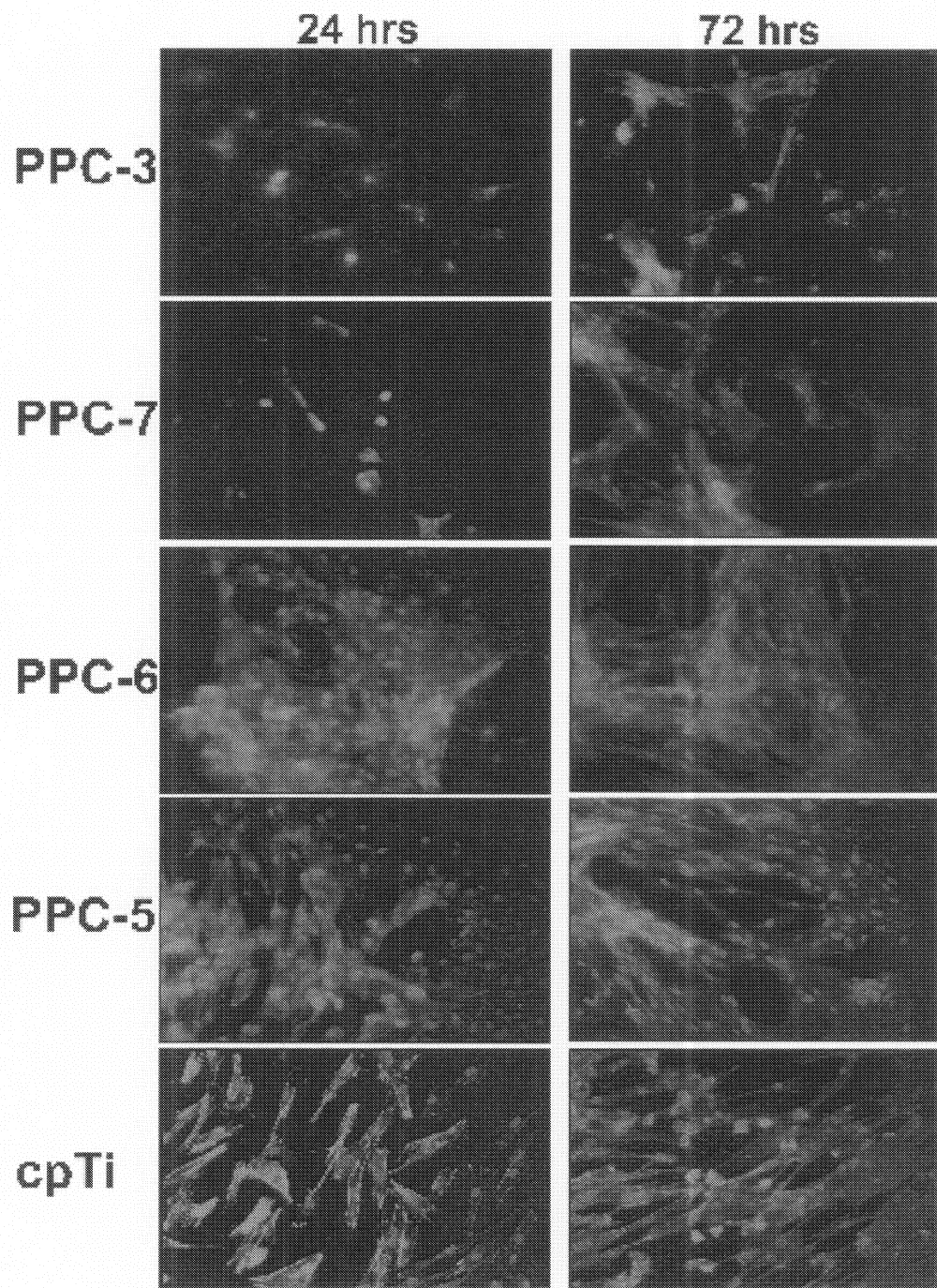
Figure 5.5: Human mesenchymal cells (HEPM) were seeded onto polymeric powder coatings (PPC-3, PPC-5, PPC-6 and PPC-7) and commercially pure Titanium (cpTi)

surfaces. After 24 and 72 hours, inverted fluorescence microscopy (20X) revealed cell nuclei (blue) and actin filaments (red) on all PPC surfaces and on cpTi disks. In both time points, there were fewer cells that had attached to PPC-3 and PPC-7, but with less cell spreading. However, there were numerous cells that had attached and were well spread out onto PPC-5, PPC-6 and onto Titanium disks.

Cell attachment assay revealed that the HEPM cells attached and proliferated on all of the PPC and titanium surfaces (Figure 5.6). Within 24 hours of seeding, the cell attachment assay counted a good number of cells that had attached to all of the surfaces. The counts increased progressively from PPC-3 to PPC-7 to PPC-6 to PPC-5. The highest counts were on titanium, which were significantly higher than that on PPC-3 (P<0.001), -7 (P<0.01) and -6 (P<0.01). However, at 24 hours, the cell counts on titanium were not significantly higher than that on PPC-5 (P>0.05), but the number of cells counted on PPC-5 were significantly higher than that on PPC-3 (P<0.01) and -7 (P<0.01). Then, after 72 hours of growth, the cell counts increased markedly on PPC-5 and -6, and on titanium; and increased moderately on PPC-3 and PPC-7. After 72 hours, the counts on titanium were significantly higher than that on PPC-3 (P<0.01) and -7 (P<0.01); but not significantly higher than that on PPC-6 (P>0.05) and PPC-5 (p>0.05). The counts on PPC-5 were also significantly higher than that on PPC-3 (P<0.05) and -7 (P<0.01) but not significantly higher than that on PPC-6 (P>0.05).
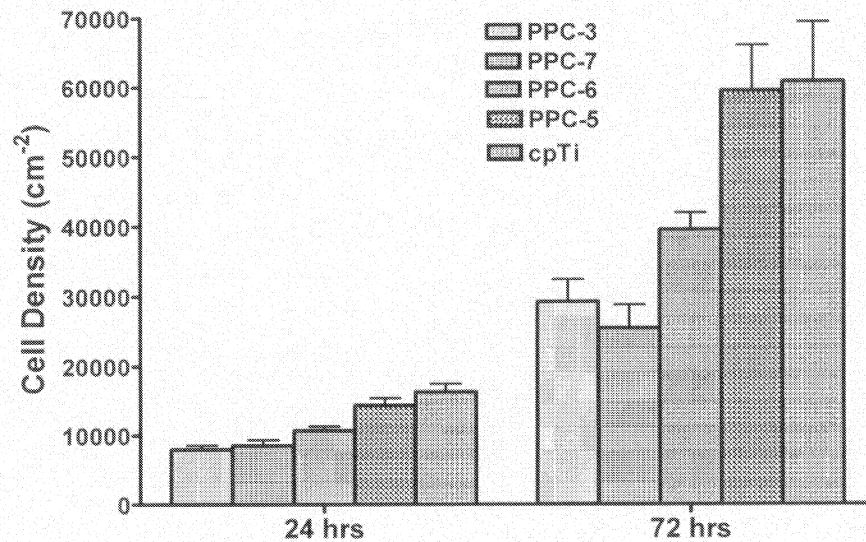
Figure 5.6: Human mesenchymal cells (HEPM) were seeded onto polymeric powder coatings (PPC-3, PPC-5, PPC-6 and PPC-7) and Titanium (cpTi) surfaces. At 24 hours there were attached cells on all of the surfaces. The highest counts were on Titanium, which were significantly higher than that on PPC-3 ($P<0.001$), PPC-6 ($P<0.01$) and PPC-7 ($P<0.01$), but were not significantly higher than that on PPC-5 ($P>0.05$). After 72 hours the counts on Titanium were significantly higher than that on PPC-3 ($P<0.01$) and PPC-7 ($P<0.01$), but were not significantly higher than that on PPC-5 and -6 ($P>0.05$). In both time points, the number of HEPM cells attached onto PPC-5 and -6 were significantly higher than that on PPC-3 and -7 ($P<0.01$).

MTT assay showed that the HEPM cells were found to be metabolically active (i.e., viable) on all of the PPC and titanium surfaces (Figure 5.7). Within 24 hours of attachment, the MTT assay measured high levels of mitochondrial enzyme activity in the cells that were collected from all of the surfaces. The highest level of metabolic activity of the cells grown on PPC surfaces was found in PPC-5 and the lowest was on PPC-7. However, the overall highest levels were measured in the cells from titanium, which were

significantly higher than that on PPC-3 ($P<0.05$), -7 ($P<0.001$) and -6 ($P<0.05$), but not than on PPC-5 ($P>0.05$). Then, after 72 hours of growth, the levels increased markedly on titanium, and were significantly higher than that on PPC-3 ($P<0.001$), -7 ($P<0.01$) and -6 ($P<0.01$), but not significantly higher than that on -5 ($P>0.05$). However, the differences between PPC-5 and -6 were not significant ($P>0.05$), but the metabolic activity of HEPM cells collected from PPC-5 was significantly higher that that on PPC-3 ($P<0.001$) and -7 ($P<0.001$) in both the 24 and 72 hour cultures.
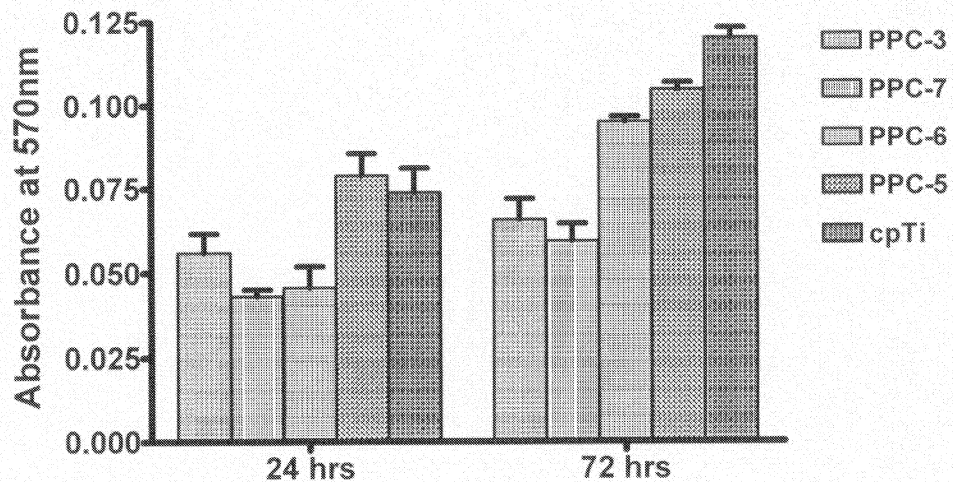
Figure 5.7: Human mesenchymal cells (HEPM) were seeded onto polymeric powder coatings (PPC-3, PPC-5, PPC-6 and PPC-7) and Titanium (cpTi) surfaces. After 24 hours of attachment, the MTT assay measured metabolically active cells that were collected from all of the surfaces. The highest measurements were from Titanium, which were not significantly higher than that on the PPC surfaces ($P>0.05$). But, after 72 hours the levels from cpTi were significantly higher than that on PPC-3 and -7 ($P<0.01$), but were not significantly higher than that on PPC-5 and -6 ($P>0.05$).

5.4. Discussion

This study has shown that polymeric powder coatings (PPC), of varying surface roughness and topography, can be successfully created from polymeric resins, nano-sized PTFE and nano-sized titanium dioxides by utilizing ultrafine powder coating technology. These PPC coatings were created from avalanche white polyester resins that were combined with fillers and additives, and applied with a solvent-free dry coating technique. This patented technology utilized nano-sized flow additives to prevent the aggregation of ultrafine powders, and thereby ensure adequate flow while spraying them onto target substrates.[29,30] Here we used 0.5% of $nTiO_2$ and several concentrations (0 to 3 wt.%) of nano-PTFE with polyester resins to create PPC surfaces that were $nTiO_2$-enriched and exhibited different degree of surface roughness in nano scale. Obviously, they all were $nTiO_2$-enriched.

This advanced ultrafine powder coating technique ensured that there was an even dispersal of the materials to create a very homogenous and uniformly distributed $nTiO_2$-enriched surface coating.[28] When each PPC was subjected to EDX, elemental analysis showed that there was only a little variation at the multiple sites, and the mapping of surface titanium showed an even distribution. Similarly, the SEM and AFM examination of PPC revealed topographical features that remained consistent across each surface.

Given the similarity of their constituents and their mode of preparation, it was not surprising to find that all of the PPC coatings had a similar composition except the changes in PTFE concentrations. Other than the PTFE amount, all other ingredients of

the PPC surfaces were exactly the same and their quantities were also equal. It is evident from SEM and AFM images and from our earlier work[28] that the presence of PTFE provided the desired roughness and topography to the PPC surfaces. Increment of PTFE concentration in the coating formula made the PPC surfaces (PPC-6, -7 and -3) rougher while PPC-5 had flatter finish due to the absence of PTFE in its formulation. Indeed, when the powder coatings cured at 200°C, the powder mixtures melted, homogenized and spread onto the substrates. During melting and spreading, the nanoparticles tended to move up to the top of the coatings and formed nano structures on top of the cured polymeric resin. Moreover, due to the differences in surface energies among the nano-sized PTFE and the resin, micron-sized porous polymeric surfaces were developed upon melted and cured. Therefore, the porous structure was attributed to the presence of PTFE, because when the amount of PTFE decreased the number and the size of pores also drastically decreased. And the PPC coating, which had no PTFE, had no such micron-sized pores. It is evident that PTFE containing surfaces had discontinuous porous topographies while $nTiO_2$ provided additional nano scale roughness to the PPC surfaces.

Indeed, the variations in surface roughness were accompanied by an alteration in surface properties such as topography. The PPC-3 surfaces had complex micro-topographies and high levels of surface nanoroughness. The SEM examination revealed a labyrinth of μm-sized pits and concavities that created intricate nano-sized topographies across the PPC-3 surfaces. AFM analysis showed that the cavities of PPC-3 were as deep as ~5μm. Likewise, the measurement of surface roughness recorded similarly high levels (~270 nm) on PPC-3. When the amount of PTFE decreased from 3 wt.% to 2 wt.% in PPC-7,

both the number of cavities and their depth reduced that made PPC-7 (~135 nm) less

rough than PPC-3 (~270 nm). Further reduction of PTFE amount (1 wt.%) drastically

decreased the roughness of PPC-6 to only ~50 nm. This change in roughness was

attributed to the drastic reduction of pits and cavities revealed in the SEM and AFM

images of PPC-6 surfaces. As a consequence, when no PTFE was added into PPC-5

formulations, nearly flatter (~37 nm) finish was achieved. This transition from rougher to

flatter surface finishes (only several nanometer roughnesses) was due to the change in

PTFE concentrations which was validated by our previous work when we created

surfaces of similar roughness by adding same amount of PTFE.[28]

Along with the surface roughness, water wettability of the PPC surfaces also altered with

the change of PTFE amount. Indeed, PTFE is a well known low surface energy material.

While 3 wt.% PTFE made PPC-3 superhydrophobic, 0 wt.% PTFE pushed PPC-5 into

hydrophilic range. Water contact angle data confirmed this dramatic shift of

hydrophobicity/hydrophilicity. In addition, current results showed that water contact

angles increased with the increase in surface roughness.[35] The shift in wettability was

also attributed to the reduction of surface energy of the PPC surfaces. Surface energy, in

turn the wettability, decreased from PPC-5 to PPC-6 to PPC-7 to PPC-3 with increasing

the amount of PTFE into the coating formula. However, the water contact angle on PPC-

5 was not much lower than 90 degree even though PPC-5 did not contain any PTFE. It

might be due to roughness induced hydrophobicity or because of adsorbed hydrocarbons

and carbonates from the ambient environment. Other efforts had also been made to

increase the wettability of the biomaterials by increasing their surface energies.[15,23,26]

As a consequence of variant surface roughness, topography and wettability among the

nTiO$_2$-enriched PPC surfaces, markedly different cellular responses were observed. We

found that they differed widely in their capacity to support human mesenchymal cell

attachment, spreading, proliferation and metabolic activity over three days of culture.

While PPC-5 and -6, supported favorable cellular responses, PPC-3 and -7 displayed

declining effects. By varying the PTFE concentrations, while PPC-5 and -6 were made

quite smoother (<~50 nm) and nearly hydrophilic in nature, PPC-7 and -3 remained

rougher (as high as ~ 270 nm) and hydrophobic.

Similarly, other studies including our previous work[28] have reported that nano-sized

titanium can enhance the cellular response of polymeric substrates. Kay et al.[36] in 2002,

and then Webster et al.[11] in 2005 reported that the incorporation of nTiO$_2$ into polymeric

composites gave better osteoblast cell attachment and proliferation than when the

materials were modified with micron-sized titanium. Jain et al. reported that cells

responded better to polymeric substrates that had been sputter-coated with a nano-sized

thickness of titanium.[37] Then, Yao et al.[13], Reising et al.[14] and Pareta et al.[15] showed that

due to the nano titania induced surface roughness (<~100 nm) and nano topographies,

UHMWPE and PTFE exhibited enhanced osteoblast cells attachment and growth. In

2009, Ozkucur et al. have reported that a very thin nano-rough film (<100nm) of titanium

or zirconium on polyurethane enhanced human umbilical vein endothelial cells

attachment and proliferation.[26] More recently, Chun et al.[27] etched poly(ether) urethane

(PU) and PLGA surfaces chemically with HNO$_3$ and NaOH, respectively, to create

submicron and nano-scale surface features and observed greater bladder urothelial cell density on the etched PLGA nano-rough surfaces. Similarly, Ranjan et al.[24] reported enhancement of endothelial cell adhesion and elongation on micron-patterned nano-rough poly(dimethylsiloxane) (PDMS) films.

In this current study, all of the PPC surfaces supported cell attachment, although PPC-5 appeared to outperform the other coatings. SEM showed that even within 6 hours of seeding, there were only a few cells on PPC-3, some attachment and spreading on PPC-7 and -6, and a lot more on PPC-5. Then, after 24 hours of growth there were several smaller cells on PPC-3 and few well spread cells on PPC-7, numerous flatten cells on PPC-6 and a large number of cells that covered PPC-5. When cells were incubated for 72 hours, HEPM cells spread and proliferated on all of the PPC surfaces although PPC-5 outnumbered other PPC surfaces used in this study. Indeed, nano roughness of less than 100 nm[13-15,38] and hydrophilicity[15,23,26,26] of PPC-5 surfaces made them so favorable to HEPM cell attachment and growth. While nano roughness increased the presence of higher surface area composed of surface defects (grooves/ridges)[11,14], hydrophilicity favored enhanced cell responses because increasing wettability ensured more interaction between the studied PPC surfaces and the biological environment (particularly, vitronectin).[31] Similarly, other studies also showed that nano-titania enriched hydrophilic nano rough surfaces had more attached cells under SEM.[11,26,32,33]

More importantly, quantitative analyses supported the above mentioned SEM observations. The cell attachment assay counted adherent cells on all of the PPC surfaces

within 24 hours of seeding and their numbers increased significantly on all of the PPC

surfaces during three days of growth. The number of cells attached increased steadily

from PPC-3 to PPC-7 to PPC-6 to PPC-5 to cpTi while both the surface roughness and

the water contact angles decreased in the same order. Indeed, the numbers of cells on the

commercially pure titanium controls were significantly higher than that on PPC-3 and -7,

but were not significantly higher than that on PPC-6 and PPC-5 ($P>0.05$). Again, close

enough surface roughness (<~50 nm) was the reason behind the similar degree of HEPM

cell attachment on PPC-5, -6 and cpTi. The reason behind the superior cell attachment to

these nano scale rough surfaces was that the cells were more prone to interact with the

nanostructure of the body.[11] Indeed, bone itself are composed of the nanostructured

proteins like collagen type 1 (300 nm long, 0.5 nm wide and 67 nm periodicity) and

hydroxyapatite crystals (50 nm long and 5 nm diameter).[16] Therefore, cells naturally liked

to be attached to the surfaces that had features of same size (~ 50 nm) as their biological

molecules.[11] Due to the same reason, less HEPM cells attached to PPC-7 and PPC-3

which had higher dimension of nano features (135.1 nm and 262.8 nm, respectively).

Moreover, compared to the PPC surfaces that had surface features of greater than 100

nm, that were of less than 100 nm rough possessed increased number of atoms at their

surfaces and higher surface area to adsorb more biological molecules.[39] Similarly,

Webster et al. reported that twice as many cells attached to nano featured (<100 nm)

poly-lactic-co-glycolic acid (PLGA) surfaces[11], and Pareta et al. reported higher cell

adhesion to nano-titania enriched nanotopographic (<100 nm) polymeric surfaces[15].

In addition to their adhesion, the human mesenchymal cells were able to proliferate on all of the coatings studied in this work. SEM showed that there were many more cells on the PPC surfaces after 72 hours of growth, than adhered within 24 hours; and while their presence increased on all of the coatings, they had grown to create an extensive matrix-like layer that nearly covered the whole surface of PPC-5. Furthermore, these observations were verified by the cell attachment assay, with cell counts that increased modestly on PPC-3 and -7, but markedly on PPC-5 and -6 after three days of growth. Within same period of seeding, the cell counts on cpTi increased 3.74 times, while 4.15 and 3.7 times on PPC-5 and PPC-3, respectively. The similar rate of HEPM cell proliferation resulted from the similar degree (20~50 nm) of surface roughness and topography. Largely, nano sized (~50 nm) extracellular matrix molecules found themselves onto rougher surfaces when they were exposed to 20-50 nm topographies and highly proliferated on those nano rough surfaces; but >100 nm topographies were no more biologically inspired nanometer dimensions to the biological molecules of the seeded cells and expressed less proliferation. Recently, Washburn et al. found that MC3T3-E1 proliferated more on the smoother regions (nano rough) of poly(L-lactic acid) when they were seeded onto the polymeric surfaces of 0.5 nm to 13 nm roughness.[9] Likewise, Reising et al. reported an increase in cell proliferation over three days, when UHMWPE and PTFE were coated with titanium or gold nano-features of less than 100 nm.[14] Also, Ozkucur et al. (2009) reported an increase in proliferation over five days when polyurethane was coated with nano-titanium or zirconium (<100 nm).[26]

These attached and proliferated HEPM cells displayed distinct morphologies and ultra-structural features on different PPC surfaces depending on their surface topography. SEM showed that the cells that were attached to the rougher coatings (PPC-3 and -7) had cytoplasmic projections and numerous extensions into the underlying cavities of those surfaces, but on PPC-5 and -6, cells spread widely. Inverted fluorescence microscopy also showed that they had organized actin filaments within the cytoskeleton. Consistently, these cells on PPC-3 and -7 had a narrower and extended morphology, with less defined stress fibers, than the flattened cells that were seen on the cpTi controls and PPC surfaces of flatter topographies (PPC-5 and -6). Indeed, other studies found similar morphologies and cytoskeletal features when cells attached to rough surfaces, as compared to smooth and flattened substrates.[33,40,41] More recently, when Schuler et al. grew cells on adjacent smooth and rough surfaces, they found flattened cells on the smooth surfaces and narrower extended morphologies on the rough substrate.[22]

In addition to cell attachment, proliferation and cytoskeletal organization, metabolic activity was sustained on all of the studied PPC surfaces. The MTT assay measured mitochondrial enzyme activity in the cells that were harvested from all of the coatings, with a gradual increase from rougher and hydrophobic (PPC-3 and -7) through to flatter (20-50 nm) and hydrophilic (PPC-5 and -6) surfaces, and from 24 to 72 hours of growth. Furthermore, after 24 hours of attachment, the cells from PPC-5 and -6 had metabolic activities that were not significantly different from those on pure titanium. Therefore these findings further attest to the low cytotoxicity of these coatings, particularly those had flatter topographies. Similar results were also found in our previous work in which

PTFE was used in all of the coating formula.[28] That indicated that incorporation of PTFE did not make PPC-3 and -7 less cytocompatible to HEPM cells, but 20~50 nm surface topographies and relative hydrophilicity made PPC-5, -6 and cpTi more cytocompatible. Likewise, Liu et al. found more HEPM cells attached and proliferated on hydrophilic nano-rod arrays.[33]

As a whole, these findings illustrate the cytocompatibility of these polymeric coatings, along with the effectiveness of their preparation with varying surface roughness and wettability. Through this study we have shown that advanced ultrafine powder coating techniques can be utilized to prepare homogenous $nTiO_2$-enriched polymeric coatings of different topographies, and that these surfaces can support a favorable cellular response. Furthermore, we have shown that the incorporation of PTFE into the coating formula made the PPC surfaces rougher and hydrophobic, while chopping of PTFE amounts led to the reduction of surface roughness to less than 50 nm and subsequently, enhanced the biocompatibility of the coatings markedly. In other words, PPC surfaces with flatter topographies were more favorable for the HEPM cells attachment, spreading and proliferation. The responses of human mesenchymal cells to the $nTiO_2$-enriched flatter and hydrophilic coatings were as good as (in some instances, even better than) that of commercially pure titanium (cpTi) in their performance. However, the effectiveness of these flatter biocompatible polymeric coatings composed of nano sized ridges will need to be verified by in vivo studies.

5.5. Conclusions

Ultrafine powder coating technology was successfully utilized to develop $nTiO_2$-enriched polymeric powder coatings (PPC) of varying nanoroughness and topography. Nanoroughness of the PPC surfaces decreased with reduction of PTFE amount in the formula keeping the polymeric resin and $nTiO_2$ exactly the same. Without PTFE, the PPC surface became flatter (i.e., no cavity) with 37 nm roughness whereas highest amount (3 wt.%) of PTFE provided the PPC the roughness close to 300 nm which was composed of pits and cavities. Existence of these pits/cavities contributed much to the surface nanoroughness. Wettability also changed with the change of nanotopography. Furthermore, the PPC surfaces could support human mesenchymal cell attachment and growth. However, PPC-3 and -7 that had 262.8 nm and 135.1 nm roughness, and hydrophobic in nature showed the least favorable response. PPC-5 and -6 that had surface roughness <~50 nm exhibited enhanced cell attachment, spreading and metabolic activity. In particular, PPC-5 performed even better than commercially pure Ti towards HEPM cells, although the performance difference between cpTi and PPC-5 was not significantly different. Therefore the $nTiO_2$-enriched polymeric powder coated flatter surfaces were shown to enhance their cytocompatibility significantly.

References

1. Sykaras, N.; Iacopino, A.M.; Marker, V.A.; Triplett, R.G.; Woody, R.D., Implant materials, designs, and surface topographies: their effect on osseointegration. A literature review. *Int J Oral Maxillofac Implants* **2000**, 15, 675-690.

2. Anselme, K.; Bigerelle, M.; Noel, B.; Iost, A., Hardouin, P. Effect of grooved titanium substratum on human osteoblastic cell growth. *J Biomed Mater Res* **2002**, 60, 529-540.

3. Lincks, J.; Boyan, B.D.; Blanchard, C.R.; Lohmann, C.H.; Liu, Y.; Cochran, D.L.; Dean, D.D.; Schwartz, Z., Response of MG63 osteoblast-like cells to titanium and titanium alloy is dependent on surface roughness and composition. *Biomaterials* **1998**, 19, 2219-2232.

4. Flemming, R.G.; Murphy, C.J.; Abrams, G.A.; Goodman, S.L.; Nealey, P.F., Effects of synthetic micro- and nano-structured surfaces on cell behavior. *Biomaterials* **1999**, 20, 573-588.

5. Hallgren, C.; Reimers, H.; Chakarov, D.; Gold, J.; Wennerberg, A., An in vivo study of bone response to implants topographically modified by laser micromachining. *Biomaterials* **2003**, 24, 701-710.

6. Feinberg, A.W.; Wilkerson, W.R.; Seegert, C.A.; Gibson, A.L.; Hoipkemeier-Wilson, L.; Brennan, A.B., Systematic variation of microtopography, surface chemistry and elastic modulus and the state dependent effect on endothelial cell alignment. *J. Biomed. Mater. Res. A* **2008**, 86, 522-534.

7. Dalby, M.J.; Giannaras, D.; Riehle, M.O.; Gadegaard, N.; Affrossman, S.; Curtis, A.S., Rapid fibroblast adhesion to 27nm high polymer demixed nano-topography. *Biomaterials* **2004**, 25, 77-83.

8. Savaiano, J.K.; Webster, T.J., Altered responses of chondrocytes to nanophase PLGA/nanophase titania composites. *Biomaterials* **2004**, 25, 1205-1213.

9. Washburn, N.R.; Yamada, K.M.; Simon, C.G.; Jr, Kennedy, S.B.; Amis, E.J., High-throughput investigation of osteoblast response to polymer crystallinity: influence of nanometer-scale roughness on proliferation. *Biomaterials* **2004**, 25, 1215-1224.

10. Sato, M.; Slamovich, E.B.; Webster, T.J., Enhanced osteoblast adhesion on hydrothermally treated hydroxyapatite/titania/poly(lactide-co-glycolide) sol-gel titanium coatings. *Biomaterials* **2005**, 26, 1349-1357.

11. Webster, T.J.; Smith, T.A., Increased osteoblast function on PLGA composites containing nanophase titania. *J. Biomed. Mater. Res. A* **2005**, 74, 677-686.

12. Dalby, M.J.; McCloy, D.; Robertson, M.; Agheli, H.; Sutherland, D.; Affrossman, S.; Oreffo, R.O., Osteoprogenitor response to semi-ordered and random nanotopographies. *Biomaterials* **2006**, 27, 2980-2987.

13. Yao, C.; Storey, D.; Webster, T.J., Nanostructured metal coatings on polymers increase osteoblast attachment. *Int. J. Nanomedicine* **2007**, 2, 487-492.

14. Reising, A.; Yao, C.; Storey, D.; Webster, T.J., Greater osteoblast long-term functions on ionic plasma deposited nanostructured orthopedic implant coatings. *J. Biomed. Mater. Res. A* **2008**, 87, 78-83.

15. Pareta, R.A.; Reising, A.B.; Miller, T.; Storey, D.; Webster, T.J., An understanding of enhanced osteoblast adhesion on various nanostructured polymeric and metallic

materials prepared by ionic plasma deposition. *J. Biomed. Mater. Res. A* **2010**, 92A

(3), 1190–1201.

16. Kaplan, F.S.; Hayes, W.C.; Keaveny, T.M.; Boskey, A.; Einhorn, T.A.; Iannotti, J.P.,

   Form and function of bone. In Simon SR, editor. Orthopaedic Basic Science,

   Rosemont, IL: *American Academy of Orthopaedic Surgeons* **1994**, 127-185.

17. Howlett, C.R.; Zreiqat, H.; Wu, Y.; McFall, D.W.; McKenzie, D.R., Effect of ion

   modification of commonly used orthopedic materials on the attachment of human

   bone-derived cells. *J. Biomed. Mater. Res.* **1999**, 45, 345-354.

18. Wieland, M.; Chehroudi, B.; Textor, M.; Brunette, D.M., Use of Ti-coated replicas to

   investigate the effects on fibroblast shape of surfaces with varying roughness and

   constant chemical composition. *J Biomed Mater Res* **2002**, 60, 434-444.

19. Masaki, C.; Schneider, G.B.; Zaharias, R.; Seabold, D.; Stanford, C., Effects of

   implant surface microtopography on osteoblast gene expression. *Clin. Oral Implants

   Res.* **2005**, 16, 650-656.

20. Isa, Z.M.; Schneider, G.B.; Zaharias, R.; Seabold, D.; Stanford, C.M., Effects of

   fluoride-modified titanium surfaces on osteoblast proliferation and gene expression.

   Int. J. Oral Maxillofac. Implants **2006**, 21, 203-211.

21. Protivinsky, J.; Appleford, M.; Strnad, J.; Helebrant, A.; Ong, J.L., Effect of

   chemically modified titanium surfaces on protein adsorption and osteoblast precursor

   cell behaviour. *Int. J. Oral Maxillofac. Implants* **2007**, 22, 542-550.

22. Schuler, M.; Kunzler, T.P.; de Wild, M.; Sprecher, C.M.; Trentin, D.; Brunette, D.M.;

   Textor, M.; Tosatti, S.G., Fabrication of TiO2-coated epoxy replicas with identical

dual-type surface topographies used in cell culture assays. *J. Biomed. Mater. Res. A* **2009**, 88, 12-22.

23. Pareta, R.A.; Reising, A.B.; Miller, T.; Storey, D.; Webster, T.J., Increased endothelial cell adhesion on plasma modified nanostructured polymeric and metallic surfaces for vascular stent applications. *Biotechnol. Bioeng.* **2009**, 103, 459-471.

24. Ranjan, A.; Webster, T.J., Increased endothelial cell adhesion and elongation on micron-patterned nano-rough poly(dimethylsiloxane) films. *Nanotechnology* **2009**, 20, 305102.

25. Lehle, K.; Buttstaedt, J.; Birnbaum, D.E., Expression of adhesion molecules and cytokines in vitro by endothelial cells seeded on various polymer surfaces coated with titaniumcarboxonitride. *J. Biomed. Mater. Res. A* **2003**, 65, 393-401.

26. Ozkucur, N.; Wetzel, C.; Hollstein, F.; Richter, E.; Funk, R.H.; Monsees, T.K., Physical vapor deposition of zirconium or titanium thin films on flexible polyurethane highly support adhesion and physiology of human endothelial cells. *J. Biomed. Mater. Res. A* **2009**, 89, 57-67.

27. Chun, Y.W.; Khang, D.; Haberstroh, K.M.; Webster, T.J., The role of polymer nanosurface roughness and submicron pores in improving bladder urothelial cell density and inhibiting calcium oxalate stone formation. *Nanotechnology* **2009**, 20, 85104.

28. Mozumder M.S.; Zhu J.; Perinpanayagam H., Nano TiO_2 Enriched Polymeric Powder Coatings Support Human Mesenchymal Cell Attachment and Growth. *Journal of Biomaterials Applications* In Press, **2010**.

29. Zhu, J.; Zhang, H., Fluidization additives to fine powders, *U.S. Patent 6,833,185*, **2004**.

30. Zhu, J.; Zhang, H., Ultrafine powder coatings: An innovation. *Powder Coat.* **2005**, 16 (7), 39-47.

31. Webster, T.J.; Schadler, L.S.; Siegel, R.W.; Bizios, R., Mechanisms of enhanced osteoblast adhesion on nanophase alumina involve vitronectin. *Tissue Eng* **2001**, 7, 291-301.

32. Zhao, G.; Schwartz, Z.; Wieland, M.; Rupp, F.; Geis-Gerstorfer, J.; Cochran, D.L.; Boyan, B.D., High surface energy enhances cell response to titanium substrate microstructure. *J Biomed Mater Res A* **2005**, 74, 49-58.

33. Liu, Y.; Chen, W.; Yang, Y.; Ong, J.L.; Tsuru, K.; Hayakawa, S.; Osaka, A., Novel fabrication of nano-rod array structures on titanium and in vitro cell responses. *J Mater Sci Mater Med* **2008**, 19, 2735-2741.

34. Geldart, D., Types of gas fluidization. *Powder Technol* **1973**, 7 (5), 285-292.

35. Lim, Y.J.; Oshida, Y.; Andres, C.J.; Barco, M.T., Surface characterizations of variously treated titanium materials. *Int J Oral Maxillofac Implants* **2001**, 16, 333-342.

36. Kay, S.; Thapa, A.; Haberstroh, K.M.; Webster, T.J., Nanostructured polymer/nanophase ceramic composites enhance osteoblast and chondrocyte adhesion. *Tissue Eng.* **2002**, 8, 753-761.

37. Jain, R.; Von Recum, A.F., Fibroblast attachment to smooth and microtextured PET and thin cp-Ti films. *J. Biomed. Mater. Res. A* **2004**, 68, 296-304.

38. Webster, T.J.; Siegel, R.W.; Bizios, R., Osteoblast adhesion on nanophase ceramics. *Biomaterials* **1999**, 20, 1221-1227.

39. Klabunde, K.J.; Strak, J.; Koper, O.; Mohs, C.; Park, D.; Decker, S.; Jiang, Y.; Lagadic, I.; Zhang, D., Nanocrystals as stoichiometric reagents with unique surface chemistry. *J Phys Chem* **1996**, 100, 12141.

40. Huang, H.H.; Ho, C.T.; Lee, T.H.; Lee, T.L.; Liao, K.K.; Chen, F.L., Effect of surface roughness of ground titanium on initial cell adhesion. *Biomol Eng* **2004**, 21, 93-97.

41. Schuler, M.; Kunzler, T.P.; de Wild, M.; Sprecher, C.M.; Trentin, D.; Brunette, D.M.; Textor, M.; Tosatti, S.G., Fabrication of TiO2-coated epoxy replicas with identical dual-type surface topographies used in cell culture assays. *J. Biomed. Mater. Res. A* **2009**, 88, 12-22.

CHAPTER 6
Flow modification of Ion-leachable glass ionomer powders for novel dental application

Chapter Summary

Ion-leachable glass powders may offer advantages over conventional aqueous cement slurries for treatment of dentine sensitivity. Many proprietary glass ionomer cement (GIC) powders have particle sizes in the range (10-20 μm), and are classified as ultrafine. Ultrafine powders do not flow easily due to cohesiveness inherent in small particles and tend to form agglomerates and clumps. This makes them difficult to handle and transport and, in particular, difficult to apply as a powder coating. One method of reducing this problem is to increase inter-particle separation distance by means of coating ultra-fine powder particles in nano-metre-sized flow-additives. The current study outlines the modification of a proprietary GIC powder (Fuji I) by incorporating and coating them by nano-Al_2O_3. The flowability of the resultant powder was measured by angle of repose and avalanche angle.

6.1. Introduction

<u>Why do powders agglomerate?</u>

As particles approach each other, inter-particle attraction forces dominate over gravitational and shear forces causing cohesion and clumping. Inter-particle attraction increases as separation distance decreases. There are three types of interparticle forces, the van der Waals force, the electrostatic force and the capillary force[1] - Van der Waals force usually being the largest. This force becomes dominant when the particles come sufficiently close, for example 0.2 to 1.0 nanometer.[2] Therefore, the smaller the particles are, the closer they can approach and the more cohesive they are. That is the reason why sub-micron or nanoparticles are always found as agglomerates instead of individual particles.

Classification of powder flowability

The most important theory with regard to the flowability of powders is the Geldart Powder Classification[3,4] where all powders are divided into four groups depending on the particle size and their density in relation to their flowability.

According to his classification (shown in figure 6.1), aeratable particles (Group A) comprise of powders in the range of 25-35 μm to 200 μm that can be well fluidized (i.e. one which will flow easily); bubbly-ready or sand-like powders (Group B) are in the size range of 200 μm to 900 μm; cohesive powders (Group C) are those smaller than about 25-30 μm and are very fine and difficult to fluidize due to their predominant interparticle forces; This causes uneven flow in the transport process, sticking and accumulating on the inside of the equipment. Spoutable powders (Group D) are larger than 900 μm that tend to be somewhat unstable when fluidized.[4]
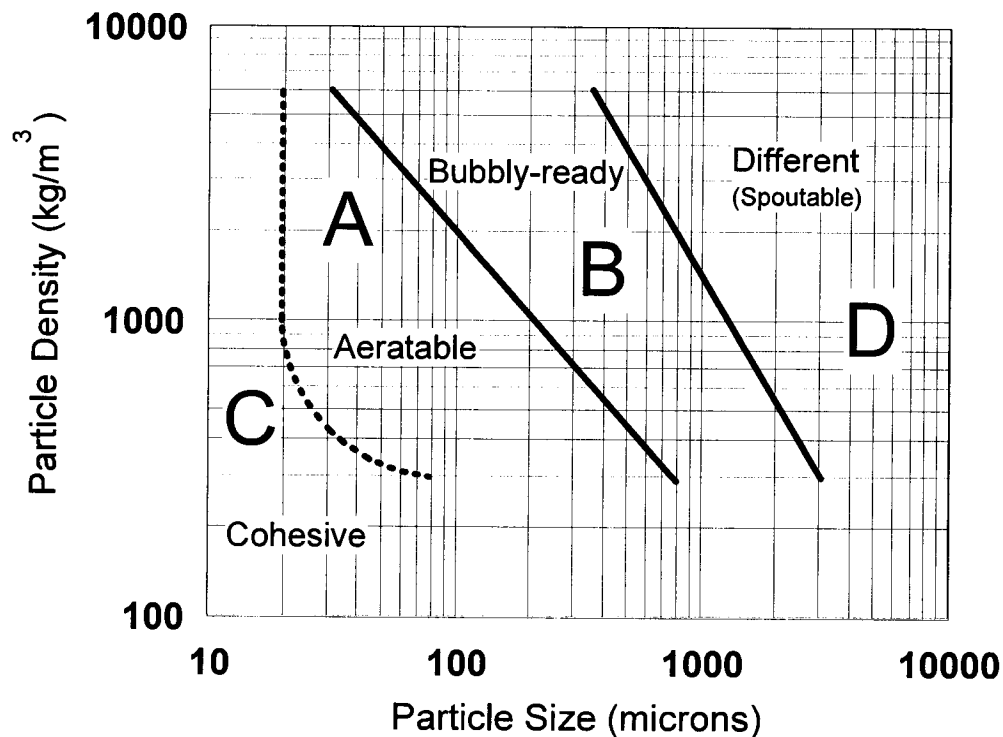
Figure 6.1: Geldart's classification of powders according to their fluidization properties.[4]

Alteration of powder flow characteristics

Many techniques have been proposed to assist the flowability of Group C powders. These methods, usually referred to as fluidization aids, include: introduction of external energies, i.e. mechanical vibration[5-7], acoustic vibration[8-13], mechanical stirring[14-16] and magnetic or electrical fied disturbance[17,18]. Particle surface properties can also be modified by gas adsorption to reduce interparticle forces.[19-21] Coarser or finer particles may be added to act as as flow conditioners/ modifiers[1,22-24]. Some of these measures are more effective than the others for a given Group C powder, but the effectiveness of almost all of these measures tend to diminish as the powder becomes smaller in size.

Adding much smaller particles of nanometre size range, such as fumed silica particles is another way to increase the flowability of ultrafine powders. Fumed alumina and silica are routinely added into the "regular" coarse powder coating products to enhance the flowability and reduce the risk of clumping. However, the use of the same technique for Geldart group C coating powders has had very limited success. Fumed alumina and silica, although extremely small by themselves, tend to form fairly strong and large agglomerates. A normal dry-blending process (even with high-shear mixers) would not assure a good dispersion of these flow agents among the base particles; on the other hand, addition of nano size additives to a coarse powder does not considerably increase the flowability of it due to the relatively insignificant separation of larger size particles of the powder; as a result, the effectiveness of the additive is significantly reduced and thus only limited flowability enhancement can be seen.

Novel flow-modification with nano-particles

The Particle Technology Research Centre at the University of Western Ontario has developed an ultra-fine powder technology[25-28] that can effectively eliminate the strong interparticle forces and significantly enhance the flow properties of Group C powders. These new technologies are based on gas-solid, two-phase flow and particulate theory.

The key of this new technology is to increase the separation distance between individual fine particles in order to increase their flowability (figure 6.2). Nano-sized additives such as Al_2O_3, SiO_2, TiO_2 etc. are mixed with the ultrafine particles through high shear mixing followed by sieving through an appropriate mesh, which assures a complete dispersion of

the nano-sized particles onto the surfaces of the base particles. Optimum additive

concentration and optimum mixing where high-shear mixing is coupled with a fine-mesh

screening are the key factors to be maintained to ensure increased flowability of the

ultrafine powders.
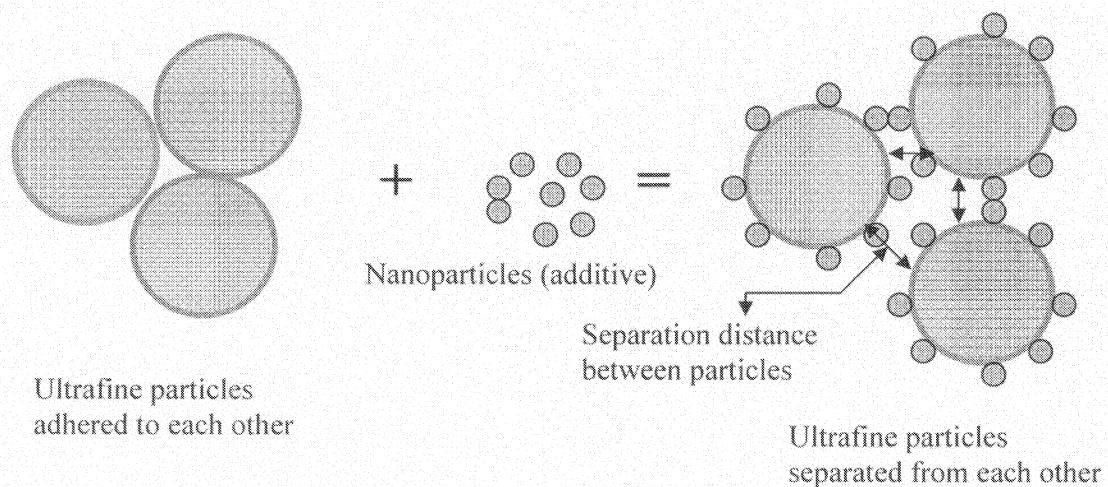
Figure 6.2: Mechanism of increasing separation distance between the particles

Characterisation of powder flowability

Flowability of powders is commonly characterized by angle of repose (AOR) and

Avalanche Angle (AA). AOR is the angle a powder pile forms with a horizontal surface.

The smaller the AOR of the powders the better is their flowability. An AOR of less than

40° normally indicates a well flowable powder. Avalanche angle (AA) is also used as a

measure of powder flowability. When powders are rotated in a drum at a certain rotation

speed (rpm), they form a maximum angle before collapsing. This maximum angle is

termed as AA. Like AOR, the lower the AA, the more flowable the powders. However,

while AOR is the dynamic method of testing powders, AA measurement technique lies closer to the static end, although both AOR and AA are performed under similar stress states.[29]

Dental applications of flowable powders

Flowable powders are found in dentistry, being used in sand-blasters, microetchers and the like. Typically these devices use alumina particles of varying sizes (mostly of Gelgart Group A particles) which are propelled in a pressurised air stream causing abrasion of dental tissues and materials.

Glass polyalkenoates, better known as glass ionomer cements (GICs), have been used in dentistry for many years and have the advantage of chemical bonding to enamel and dentine, and fluoride release and recharge. These are normally applied as aqueous slurries, however as such they usually require cavity preparation to allow placement in bulk. More recently, it has been shown that these materials applied as powders to prepared tooth surfaces exhibit enhanced penetration into dentine and therefore may provide more a more effective cavity seal and better treatment of dentine sensitivity. However, these GIC powders are much smaller in size and fall into Geldart Group C category which are known to be very cohesive in nature and form agglomerates readily. As a result of excessive cohesiveness, they are very difficult to apply in dry powder form. However, no report has been published in literature that describes the modification of these submicron-sized GICs to apply them to seal dental cavities or to treat dentine

hypersensitivity. Not only that, no other dental materials of submicron-size have ever been flow-modified.

Aims and Objectives

The objective of this study was to examine the effect of flow-modifiers on proprietary glass ionomer cement (GIC) powders and compare the flow properties with known flowable powders used in dentistry. The aim was to determine if it was possible to increase their flowability such that they could be manipulated and applied as a powder coating.

6.2. Materials and methods

A proprietary glass ionomer powder (GC Fuji I® Radiopaque Glass Ionomer Luting Cement Powder, GC America Inc., Alsip, Illinois, USA) was used as the 'base' powder in this study. The following processes were carried out:

Particle Size and Particle Size Distribution Tests

The particle size and distribution of the base powder were assessed using Mastersizer 2000 (Manufactured by Malvern Instruments Ltd, UK). Following the standard test procedures the field of particle technology, D10, D50 and D90 are the most popular parameters used to describe the particle size and size distribution of a powder. D50, often called the medium size of a powder, refers to the size that 50% by volume of the powder is smaller than the measured one. Similarly, D10 is the size that 10% by volume of the powder is smaller than that and likewise, with D90.

Flow additive and processing

The processed powder was made in the following manner: To the base powder was added different concentrations by weight of nano-Al_2O_3 (Degussa, USA) flow additive (~ 25 nm average diameter) and the mixtures were processed to ensure a homogeneous mixing of the base powder and the flow additive using a technique described previously by Zhu & Zhang.[26] This involves high-shear mixing and passing the powder mixture through a 32 μm sieve to ensure that the base powder particles are evenly coated with nano-sized Al_2O_3, thus ensuring greater separation distances.

Assessment of flow properties

a. Angle of repose tests

Angle of repose (AOR) is a commonly used parameter in determining the flowability of a powder. Powders form a pile when they were allowed to pour down onto a flat surface. Then the angle between the surface of the pile and the flat surface was defined as the angle of repose of the respective powders (Figure 6.3). A lower angle of repose indicates a better flowability. For powders used in the powder coating industry, an angle of repose smaller than 40 degrees is preferred, to assure good fluidization and defect-free finish. The angle of repose tests for each of the samples were conducted with a PT-N Powder Characteristic Tester (Manufactured by Hosokawa Micron Powder Systems Co.).

**Powders loading
through a funnel**

Powder pile

AOR

Flat base
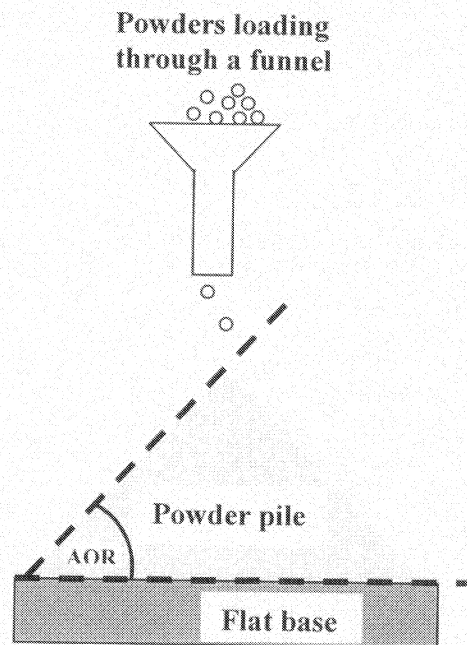
Figure 6.3: Angle of repose measurement

To ensure accuracy, the AOR tests were done at least three times for each sample and the mean and standard deviation were calculated.

b. Avalanche angle measurement

The avalanche angle was measured using a Revolution Powder Analyzer manufactured by Mercury Scientific Inc. The avalanche angle was determined by rotating 120 ml of powder (tapped volume) at 0.6 rpm and measuring the maximum angle that the powder achieves before it avalanches (collapses) to the bottom of the drum (figure 6.4). The angle is given for 200 avalanches. As with AOR, a lower avalanche angle indicates

increased powder flow. All measurements were performed three times; then mean and standard deviation were calculated.

| Powders in a rotating drum | Powders form avalanche before collapsing | After collapsing, powders rest |
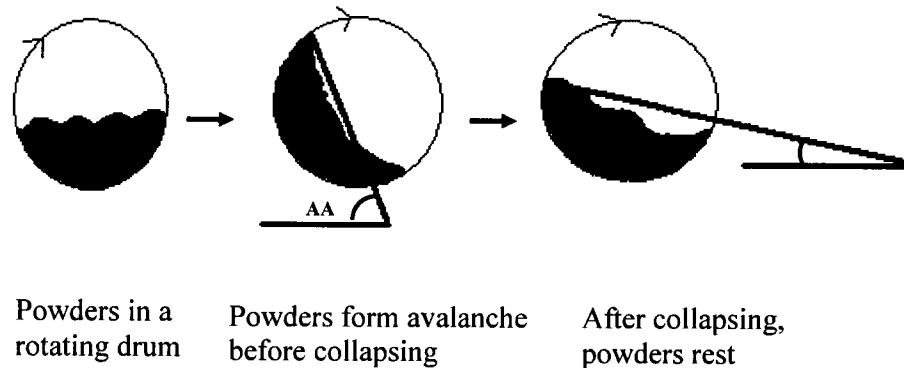
Figure 6.4: Avalanche angle measurement

Comparison to flowable dental powders

The particle size distribution, avalanche angle and AOR of the Fuji I® powder before and after processing with several concentration of nano-additive were compared to alumina powders of 27 and 50 micron average particle size. The alumina powders were designed for use in an intra-oral micro-etcher and known to be flowable.

Scanning Electron Microscope (SEM) imaging

The Fuji I® powders (both unprocessed and processed) were applied to a carbon tape that was affixed to a metal stub. The mounted samples were then sputtered with gold to put a thin gold layer (10-15 nm) on the powders to make them conductive under the exposure of ion beam. Images of the powders were taken using the Hitachi S-2600N (Hitachi, Pleasonton, CA) scanning electron microscope (SEM).

6.3. Results and Discussion

Particle size and distribution of base powder (Fuji I®) as received

The particle size distribution of the base powder was found to be: D90 = 15.9 µm; D50 =

4.1 µm; and D10 = 1.3 µm. This is shown in figure 6.5. According to Geldart's powder

classification, Fuji I fell into Group C category, very cohesive and not easy to apply or

handle.
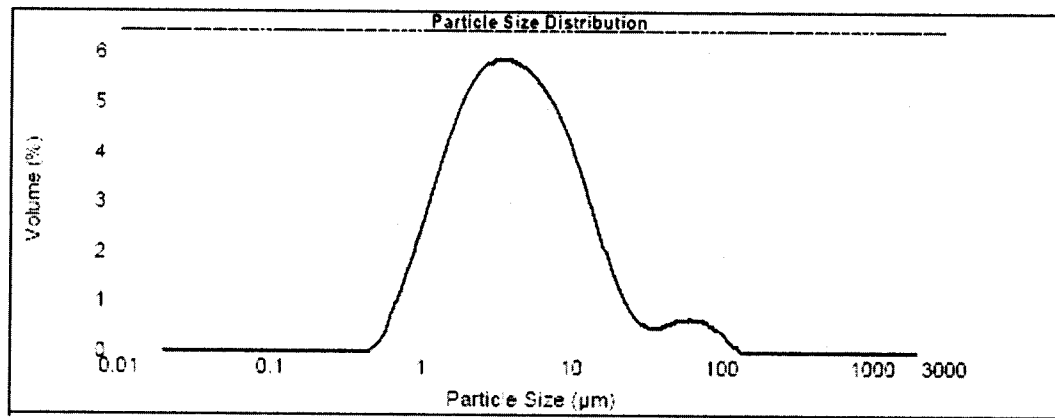
Figure 6.5: Particle size distribution of as received Fuji I®

Effect of the proportion of flow additive on flowability

a. Angle of repose

Angle of repose of Fuji I decreased with the amount of Al_2O_3, as shown in Figure 6.6.

The photographs in Figure 6.7 illustrate AOR measurement and the physical effect of
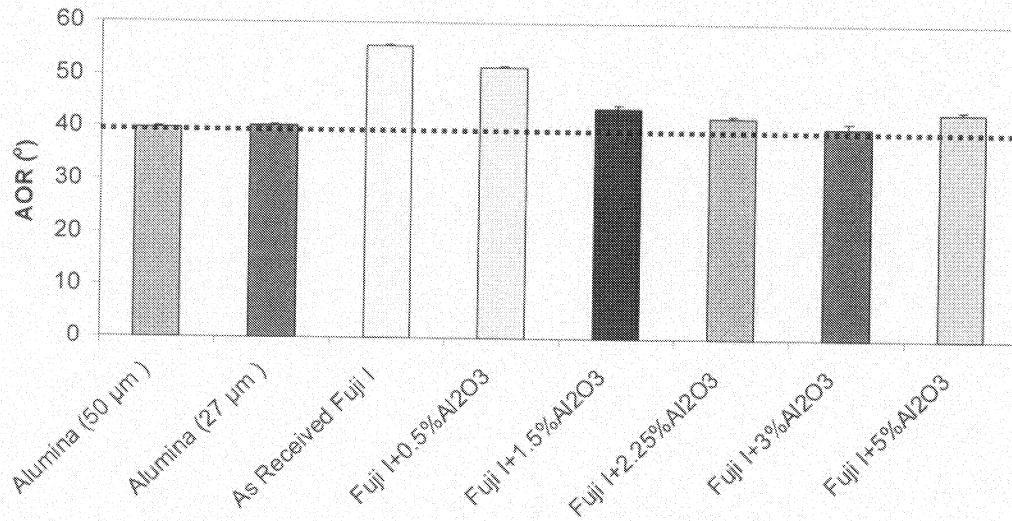
Figure 6.6: AOR of unprocessed and processed Fuji I and the reference powders
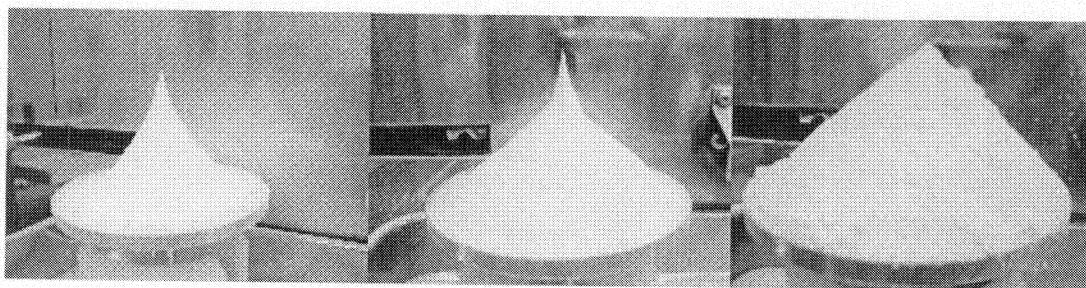
As Received Fuji I   Fuji I with 0.5 wt.% Al2O3   Fuji I with 3.0 wt.% Al2O3

Figure 6.7: Photograph of the effect of different concentrations of nano-Al_2O_3 on the shape of the powder pile from which AOR is measured.

adding nano- Al_2O_3 Fuji I[®] powder without additive formed a cone with the horizontal base giving an AOR of around 55°. Addition of 0.5, 1.5 & 3.0 wt.% nano-Al_2O_3 produced AOR values of 51°, 43° & 40° respectively. This effect was due to increasing

base powder particle separation with each increment of additive. At 3.0 wt% this mechanism reaches saturation with maximum achievable separation distances being reached. Further addition of flow additive (5.0 wt% Al_2O_3) increased the angle of repose to 43° as nano-particle agglomerates begin to have an effect. Although AOR of 43 degree is high, ultrafine powders remain almost unhandleable, but the flowability of the GIC powders was not noticeably bad and they were still handleable.

b. Avalanche angle

As expected, the avalanche angle decreased as the additive concentration was increased (figure 6.8). Although lower concentration of additive did not provide any significant change in avalanche angle, the angle decreased steadily until 3.0 wt.% of Al_2O_3 was processed with the ultrafine Fuji I®. However, unlike AOR, the avalanche angle did not reduce drastically with the addition of nano-additive. One explanation may be that this because the longer measurement time involved for AA allowed the powders to absorb moisture. However, moisture intervention might not be the reason for the discrepancy seen among AOR and AA. Instead these two characterization methods are different, so it is normal to see difference between the two, although they have certain extent of similarity in the mechanism.[29] Krantz et al.[29] also termed AOR as a dynamic method of testing powders' flowability, whereas AA is more-like static test method although it involves drum rotation. Despite this dissimilarity, the trend was similar to the AOR. AA decreased until 3.0 wt.% of Al_2O_3, increasing slightly with 5.0 wt.% additive. This pattern suggested the optimum quantity of additive might lie in between 2.25 wt% to 3.0 wt.%.
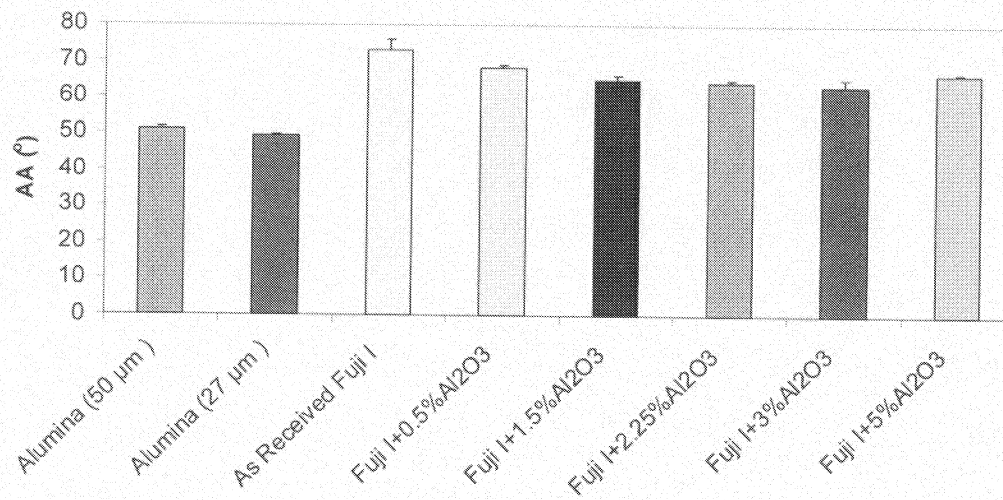
Figure 6.8: AA of unprocessed and processed Fuji I and the reference powders

Comparison with flowable alumina powders

AOR and AA measurements suggested that GIC powders could be modified by the addition of nano-Al_2O_3 to achieve similar flowability to alumina powders already used in microetchers, allowing GIC to be applied by such means.

SEM images

The SEM images in figures 6.9 and 6.10 showed the contrast between the unprocessed and processed powders. The Fuji I[®] powder as received comprised of enormous amount of smaller particles (2.0 µm) and a few of larger particles (10-20 µm). Particle separation is minimal and agglomerates can be seen of different size and shape. Figure 6.10 shows coated particles and increased particle separation and less clumping.
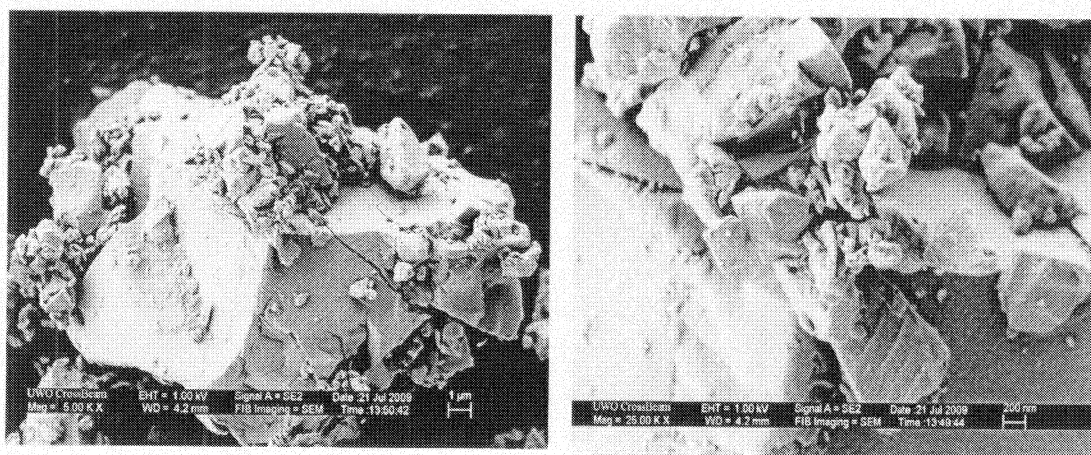
Figure 6.9: As received Fuji I®, showing agglomerations of the finer particles
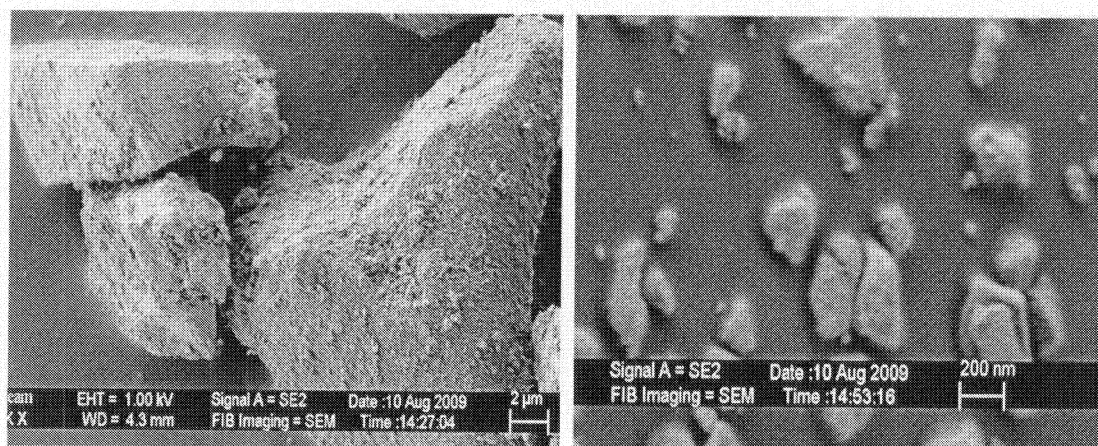
Figure 6.10: Fuji I® processed with 3% Al_2O_3

6.4. Conclusions

The flowability of the ultrafine Fuji I® powders was improved by processing with nano-Al_2O_3. Angle of repose and avalanche angle results confirmed the increased flowability of Fuji I® powders quantitatively, while SEM images showed the same qualitatively. With addition of 3.0 wt.% Al_2O_3, AOR reduced to 40° that was close to that of the

reference Alumina powders of bigger sizes. This improvement in flowability allowed GIC powders to be handled more easily and applied as powders to dental tissues.

References

1. Visser, J., An invited review- van der Waals and other cohesive forces affecting powder fluidization. *Powder Technology* **1989**, 58 (1), 1-10.

2. Hamaker, H.C., The London-Van der Waals Attraction between Spherical Particles. *Physica (Utrecht)* **1937**, 4, 1058-1072.

3. Geldart, D., The Effect of Particle Size and Size Distribution on the Behavior of Gas Fluidized Beds. *Powder Technology* **1972**, 6, 201-209.

4. Geldart, D., Types of Gas Fluidization. *Powder Technology* **1973**, 7 (5), 285-297.

5. Mori, S.; Yamamoto, A.; Iwata, S.; Haruta, T.; Yamada, I., Vibro-fluidization of group C particles and its industrial applications. *AICHE Symp Ser* **1990**, 86 (276), 88-94.

6. Dutta, A.; Dullea, L.V., Effects of external vibration and the addition of fibers on the fluidization of a fine powder. *AICHE Symp Ser* **1991**, 87 (281), 38-46.

7. Jaraiz, E.; Kimura, S.; Levenspiel, O., Vibrating beds of fine particles: estimation of interparticle forces from expansion and pressure drop experiments. *Powder Technology* **1992**, 72, 23-30.

8. Morse, R.D., Sonic energy in granular solid fluidization. *Ind & Eng Chem* **1955**, 47, 1170-1175.

9. Montz, K.W.; Beddow, J.K., Adhesion and removal particulate contaminants in a high-decibel acoustic field. *Powder Technology* **1988**, 55, 133-140.

10. Nowak, W.; Hasatani, M., Fluidization and heat transfer of fine particles in an acoustic field. *AICHE Symp Ser* **1993**, 89 (296), 137-149.

11. Chirone, R.; Massimilla, L.; Russo, S., Bubble-free fkuidization of a cohesive powder in an acoustic field. *Chem Eng Sci* **1993**, 48, 41-52.

12. Chirone, R.; Massimilla, L., Sound-assisted aeration of beds of cohesive solids. *Chem Eng Sci* **1994**, 49, 1185-1194.

13. Russo, P.; Chirone, R.; Massimilla, L.; Russo, S., The influence of frequency of acoustic waves on sound-assisted fluidization of fine particles. *Powder Technology* **1995**, 82, 219-230.

14. Reed, T.M. III.; Fenske, M.R., Effects of agitation on gas fluidization of solids. *Ind Eng Chem* **1955**, 47, 275-282.

15. Godard, K.; Richardson, J.F., Use of slow speed stirring to initiate particulate fluidization. *Chem Eng Sci* **1969**, 24, 194-195.

16. Nezzal, A.; Large, J.F.; Guigon, P., Fluidization behaviour of very cohesive powders under mechanical agitation. *Fluidization III, Proceedings of the Eng Foundation conference on Fluidization*, 8th, Tours, Fr. **1999**, May 14-19, 77-82.

17. Liu, Y.A.; Hamby, R.K.; Colberg, R.D., Fundamental and practical developments of magneto-fluidized beds: A review. *Powder Technology* **1991**, 64, 3-42.

18. Hristov, J.Y., The fluidization in a magnetic field is more than 40 years old. It is time to strike the balance in front of new century. *Recent Progress en Genie des Procedes* **2000**, 14, 251-260.

19. Geldart, D.; Abrahamsen, A.R., Homogeneous fluidization of fine powders using various gases and pressures. *Powder Technology* **1978**, 19, 133-136.

20. Piepers, H.W.; Cottaar, E.J.E.; Verkooijen, A.H.M.; Rietema, K., Effects of pressure and type of gas on particle-particle interaction and consequences for gas-solids fluidization behaviour. *Powder Technology* **1984**, 37, 55-70.

21. Xie, H.-Y., The role of interparticle force in the fluidization of fine particles. *Powder Technology* **1997**, 94, 99-108.

22. Lauga, C.; Chaouki, J.; Klvana, D.; Chavarie, C., Improvement of the fluidizability of Ni/SiO2 aerogels by reducing interparticle forces. *Powder Technology* **1991**, 65, 461-468.

23. Zhou, T.; Li, H., Effect of adding different size particles on fluidization of cohesive particles. *Powder Technology* **1999**, 102, 215-220.

24. Dutta, A.; Dullea, L.V., A comparative evaluation of negatively and positively charged submicron particles as flow conditioners for a cohesive powder. *AICHE Symp Ser* **1990**, 86 (276), 26-40.

25. Zhu, J.; Zhang, H., Fluidization Additives to Fine Powders, *US Patent 6,833,185*, **2004**.

26. Zhu, J.; Zhang, H., Powder Blending Methods for Uniformly Dispensing Additive Paticles to Fine Powders. *US Patent, filed,* **2006**.

27. Zhu, J.; Wen, J.; Ma, Y.; Zhang, H., Apparatus for Volumetric Metering of Small Quantity of Powder from Fluidized Beds. *U.S. Patent 6,684,917,* **2004**.

28. Zhu, J.; Luo, Y.; Ma, Y.; Zhang, H., Direct Coating Solid Dosage Forms Using Powdered Materials. *U.S. Patent, filed,* **2005**.

29. Krantz, M.; Zhang, H.; Zhu, J., Characterization of Powder Flow: Static and dynamic testing. *Powder technology* **2009**, 194, 239-245.

CHAPTER 7

Dentinal Tubule Occlusion by flow-modified ion-leachable glass ionomers as powders

Chapter Summary

Background: Dentine hypersensitivity is a painful dental condition that arises from pulpal stimulation via patent dentinal tubules that are exposed by gingival recession and a variety of other factors such as toothbrushing, diet, periodontal scaling and root planning, and parafunctional habits. Many treatments for hypersensitivity attempt to occlude the dentinal tubules. *Aim:* The aim of this initial investigation was to determine the advantage, if any, of applying ion-leachable glass as powders to dentine to occlude the exposed tubules. *Method: Sample preparation:* The roots of bovine incisor teeth were lapped to produce a flat surface, smoothed and treated with 35% ortho-phosphoric acid gel to remove the surface smear layer and cut into sections. *Powder preparation:* Proprietary glass ionomer (polyalkenoate) cements (GIC), (Ketac-Cem® and Fuji I®) were processed with appropriate amounts of nano-sized Al_2O_3 to improve their flowability and applied to the dentine sections. *Application:* The dentine surface was pretreated either with a 1:1 ratio of ortho-phosphoric acid to polyacid solution or with water. Powders were sprinkled, scrubbed in as slurry or applied using a corona spray gun as powders, with control samples left with pre-treatment only. The effect of varying the drive voltage of the corona gun was examined. *Analysis:* The samples were sectioned by splitting along their long axis and the fractured surfaces were examined using SEM and EDX. *Results:* Flow-modified powders applied with the corona gun showed tubular occlusion with deep penetration into dentine ~1 mm in some cases, whereas the pre-treatment only, sprinkled or scrubbed powders showed little or no occlusion. EDX analysis confirmed the presence of GIC elements within the dentinal tubules. Dehydration artifacts demonstrated a high proportion of tubules filled. *Conclusion:* Application of ion-leachable glass powders in this manner gives clearly superior tubular occlusion in terms of penetration depth. Although the precise mechanism is not yet clear, this technique has potential applications for the treatment of dentine hypersensitivity, as a cavity lining/ sealer or root canal sealer. In addition, due to the known properties of glass ionomer cements, this technique may be

useful in the prevention and treatment of root caries and offer improved dentine bonding of dental composites.

7.1. Introduction

Dentine hypersensitivity is a common dental condition. Reported prevalence rates vary widely, however one US study estimated that it affected 40 million people in the US year; in other words, one in every five people, with people aged between 30 and 40 being the most susceptible age group.[1] Dentine hypersensitivity is often identified as sudden and short-term acute pain when the exposed dentine comes in contact to thermal (hot or cold drinks), chemical, mechanical (touch) or osmotic (sweet or sour) stimuli[2-4]. Such stimuli are believed to cause the inwards or outwards movement of dentinal fluid within the tubule resulting in excitation of pulpal sensory nerves.[5] Indeed, dentine hypersensitivity is one of the consequences of gingival recession exposing root/dentine surfaces, particularly in combination with erosion[6] and periodontal therapy[7]. Since hypersensitivity is closely related to the dentinal tubule exposure, it can also be caused due to abrasion from toothbrushing, parafunctional habits, aging, root preparation and small cracks or notches in the teeth.[8] Therefore, treatment of dentine hypersensitivity requires the occlusion of the exposed dentinal tubules to prevent the undesired movement of tubular fluids.[9]

In the last several decades, a number of different desensitizing agents were evaluated for treating dentine hypersensitivity.[10-14] Fluoride gel dentifrices[15], unfilled resins[16], even glass containing dentifrices[17], gold and calcium hydroxyapatite nano-particles[18] and laser/ resin combinations[19] have also been evaluated for the same purpose. Moreover, Arrais et al. evaluated the efficacy of three commercially available desensitizing agents: 1)

potassium oxalate-based / Oxa-Gel (OX), 2) HEMA and glutaraldehyde-based / Gluma

Desensitizer (GD), and 3) acidulated phosphate fluoride-based / Nupro Gel (AF) in

occluding dentinal tubules.[20] Although they reported the ability of all three desensitizing

agents to block the tubules, none of them were able to be precipitated deeper than 15 μm

from the surface. Then in 2005, Lee et al. reported 10 μm of sealing depth when they

applied bioglass in combination with Nd:YAP laser treatment.[21] Later, the same group

synthesized DP-bioglass by melting related oxide precursors at 1410°C and mixing them

with 30% phosphoric acid before applying them over exposed dentine.[22] With this new

material, the penetration depth was increased to 60 μm, although they required three days

of reaction time, making them unfavourable for the clinical use. Subsequently, the same

group, working in the National Taiwan University, attempted to develop another similar

material of smaller particle size that could have shorter setting time (as low as 10

minutes) on dentine. They used sol-gel method in presence of acid catalysts to prepare the

DP-bioglass and found a similar degree of penetration (~62 μm) when applied to exposed

dentine as a paste.[23] Later, Lee et al. brushed nano-carbonate apatite and strontium

chloride containing dentifrice into one hundred human dentine specimens and reported

higher degree of tubule occlusion with nano-carbonate apatite containing dentifrice,

although the depth of dentifrice penetration into the tubules was not reported.[24] Recently,

Aranha et al. compared the use of five desensitizing agents (i.e., Gluma Desensitizer,

Seal&Protect, Oxa-gel, fluoride and Low Intensity Laser-LILT) on one hundred and one

non-carious teeth and assessed their efficiency in reducing hypersensitivity by exposing

them into cold air.[25] They reported similar degree of pain-level reduction efficiency with

all five desensitizing agents over six-month follow-up. More recently, Chiang et al.

reported dentinal tubule penetration of ~100 μm when they brushed highly supersaturated $Ca^{(2+)}$-and $HPO_{(4)}^{(2-)}$ion and nano-sized calcium oxide particles-containing novel mesoporous silica biomaterial (NCMS) paste into the exposed tubules.[26] Recently, there has been a report of slurry of novel sol-gel nano-bioglass and melt-derived bioglass compound showing penetration of 270 μm into dentine.[27]

Although there have been numerous efforts focusing on occluding dentinal tubules of exposed root surfaces in order to treat dentine hypersensitivity, none has been reported to successfully occlude the tubules deeper than ~270 μm. Therefore, the above mentioned efforts can only provide a short-term solution to this chronic problem. If the tubules are filled to as deep as only ~270 μm with the bioactive desensitizing agents or dentifrices, they could be brushed off fairly easily removing the so called tubular sealing. As a result, it is the utmost necessity to send the sealant materials far deeper into the tubules to achieve the long-term success in treating dentine hypersensitivity. To attain the goal, different dental materials could be explored and applied to the exposed root surfaces by using different application techniques.

In this study, we applied the most commonly used bioactive restorative dental materials (i.e., cavity sealant) named glass polyalkenoate or glass ionomer cement (GIC). GICs were derived from a family of such materials that include phosphate, silicate, and polycarboxylate cements. They set by acid/ base reaction and maintain the surface attachment of the cement via tooth calcium ions cross-linked with polyalkenoic acid chains. GICs consist of an acid soluble calcium fluoroaluminosilicate glass powder mixed with a polyacid solution (polyacrylic/ maleic/ tartaric/ itaconic/ others) to produce an

aqueous cement slurry. Cements are available in a variety of combinations: conventional

(glass powder with acid liquid); anhydrous (freeze dried polyacid/ glass powder); high-

viscosity (small particle size of 2-3 µm as opposed to 15-50 µm for all others); resin

modified (liquid consisting of a mixture of aqueous hydrophilic resin monomers

(HEMA), polyacrylic acid/ methacryloxy co-polymers); cermets (mixture of conventional

glass powder and sintered silver particles). When the slurry of GIC is applied to dentine,

it forms a chemical bond to dentine; leaches and absorbs (recharges) fluoride ion. The

mechanism of dentine bonding appears to be chelation of poly acid carboxyl groups with

dental apatite calcium.[28] Interestingly, this bond has been shown to be very durable;

indeed, GICs demonstrate superior clinical retention rates to any of the resin-based-

dentine bonding systems currently available.[29] However, GIC is very weak in thin section

and therefore can not be applied to an external tooth surface as a coating. Moreover, the

slurry of GIC is difficult to work with as it offers very short working time i.e., (i.e., they

solidify within only 30 seconds when mixed either with water or with the supplied

polyacid solution) but long setting times. Therefore, in order to bypass this problem,

GICs could be applied in their powder form; this has not yet been tried to the best of our

knowledge. Instead of applying as a slurry, the powdered GIC could be advantageously

applied to wet or pre-treated dentine surfaces to get the GICs reacted and leached into the

dentinal tubules. In fact, the GIC powders could make the slurry on the dentine surfaces

as they are already wet. Thus the handleability issue of GIC slurry, particularly the

slurry's quicker solidification problem could be resolved if we could make the slurry on

the target sites.

However, the problem associated with applying powdered GICs is their poor flowability as their average particle sizes are less than 10 μm. Such particles, which are less than 20 μm in diameter, are termed as cohesive particles by Geldart in 1973.[30] They pose enormous difficulties in handling and processing because of their inherent cohesiveness. The cohesive nature of ultrafine particles results from the fact that, as particle size decreases beyond a certain range, the separation distance between particles gets reduced so that the relative magnitude of interparticle forces becomes predominant compared to the gravitational force.[31] Such dominant interparticle forces cause individual particles to stick to each other leading to formation of channels and agglomerates. When the agglomerates of GICs are applied to dentine with the aid of sand blaster or micro-etcher, they can not make a continuous and homogeneous layer on the root surfaces. This results in only partial occlusion of dentinal tubules. Therefore, before moving forward with the GICs, their flowability issue has to be resolved first.

In this study, we have used Zhu and Zhang's patented technology to improve the flowability of GICs.[32] The key to this technology is to increase the separation distance between individual GIC particles in order to overcome their interparticle forces. This can be done by adding finer (preferably nano-sized metal-oxides) foreign particles (i.e., additives) into the ultrafine powder system of interest. In this current study, the ultrafine GIC powders were thoroughly mixed with the nano-sized Al_2O_3 additives with the aid of high shear mixer that resulted in significant improvement of the GIC powders. If these flow-modified GIC powders could be sprayed onto wet dentine, they could form homogeneous slurry on the dentine surfaces and within patient tubules. However, the

standard sandblaster or micro-etcher used in dentistry is unable to transport the flow-modified GIC powders, as they are designed to handle powders of particle size ~ 50 μm. Therefore, it is important to employ an appropriate powder delivery system gun to apply the GIC powders to the exposed root surfaces.

We have used ultrafine powder coating (UPC) system to apply the ultrafine flow-modified GIC powders onto dentine. UPC is a voltage-driven dry finishing process that enables powders to be deposited onto the grounded substrate(s) of interest. GIC powders are transported from the feed hopper to the tip of the Corona spray gun (Nordson Corporation) using compressed air (as shown in figure 7.1). On their way, powders pass through the corona-charging gun inside which has a special electrode that electrostatically charges the entrained powders. In the corona system, powders become negatively charged. Being like charges, powders electrically repel each other forming the cloud of finer particles.[33] Therefore, a cloud of finer particles leaves the spray gun with the aid of electrostatic and aerodynamic effect of outward airflow and the charged particles are easily attracted towards the wet or pre-treated dentines resulting in the formation of a continuous film of GIC powders.
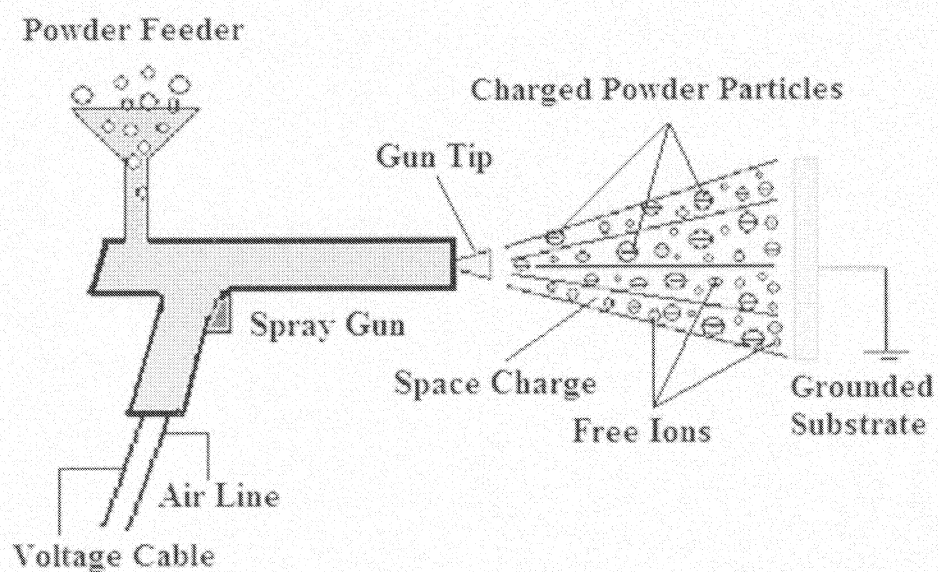
Figure 7.1: Corona-charging spray gun used in UPC system charges the powder particles and entrained them to the tip of the gun that delivers charged particles to the target substrates.

In this chapter, we report the novel approach of applying GICs in their powder forms, instead of slurry or paste, to occlude the exposed dentinal tubules The flow-modified GIC powders have exhibited superior penetration into dentinal tubules when they have been applied to the wet/acid pre-treated root surfaces by using the ultrafine powder coating system comprised of a corona spray gun. Interestingly, the GIC powders have reached as deep as ~ 1 mm into the tubules that is many-fold higher than that of any of the previously reported treatment methods or materials (i.e., dentifrice or desensitizing agent) to date. This novel approach involves applying the reactive glass/ polyacid particles onto the wet dentine surface or into the tubules, which would then undergo setting/ coalescence and chemical bonding to the tubule, creating a hermetic seal.

7.2. Materials and Methods

<u>Flow-modification of the glass ionomer powders:</u>

Proprietary glass ionomer powders (Ketac-Cem® radiopaque (Admixed glass/freeze-dried

acid powder) anhydrous powder (3M ESPE, St. Paul, MN, USA) and GC Fuji I® Glass

Ionomer Luting Cement Powder (GC America Inc., Alsip, Illinois, USA) were used as

the 'base' powder in this study. The following processing and characterization were

carried out:

Flow-modification: The base powders were mixed with different concentrations (by

weight) of Nano-Al_2O_3 (Degussa, USA) flow additive (~ 25 nm average diameter) and

the mixtures were processed to ensure a homogeneous mixing of the base powder and the

flow additive using a technique described previously by Zhu & Zhang in 2004.[32] This

involves high-shear mixing and passing the powders mixture through a 32 μm sieve to

ensure that the base powder particles were evenly coated with nano-sized Al_2O_3, thus

ensuring greater separation distances. During the high-shear mixing, agglomerates were

also broken into individual particles that also increased the flowability of the powder

mixtures.

<u>Powder Characterization:</u>

<u>Particle size measurement:</u>

The particle size of the base GIC powders was measured using Mastersizer 2000

(Manufactured by Malvern Instruments Ltd, UK). Following the standard test procedures

the field of particle technology, the average particle size (D50) was measured. D50 also refers that 50% by volume of the powder is smaller than the measured size.

Angle of repose (AOR) measurement:

The AOR measurement was used to characterize the flowability of the powder systems. When particles were allowed to fall onto a flat plate, the pile formed an angle with the horizontal plate. The flatter the powder pile, the higher is the flowability. Traditionally, powders exhibiting AOR of around $40°$ are believed to be flowable/fluidizable. Hokosawa Micron Corp. Powder Tester was used for the AOR measurements.

Preparation of bovine dentine blocks:

Bovine incisors had their crowns removed, then the root was polished using a Buelher Metaserve Grinder-Polisher (Buelher, USA) using 120 grit and smoothed with 320 grit silicon carbide grinding paper (Buelher-Met II, Buelher, USA). The root was then sectioned using a peripheral cutting diamond wheel (Buelher Isomet wafering blade, Buelher, USA) on a Struers Minitron cutting machine at 250 rpm. The flat and smoothed surface (as shown in figure 7.2) was then etched for 15 seconds with Ultra etch 35% orthophosphoric acid (OPA) gel (Ultradent Inc, USA) and rinsed for 30 s to open up the dentinal tubules by removing their smear-layers. The dentine samples were stored at all times in phosphate-buffered silane (PBS).
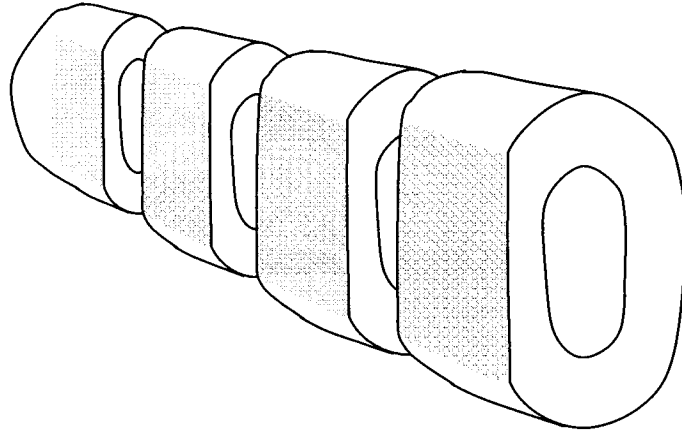
Figure 7.2: The flat and smoothed dentine blocks to be coated with the GIC powders.

Pre-treatment of the smear-layer removed dentine blocks:

Before being exposed to the GIC powder spray, the smear-layer removed dentine blocks

were pre-treated with 1:1 ratio of 35% orthophosphoric acid (OPA) gels and poly acrylic

(polyalkenoic) acid (PAA) (GC America Inc, Il, USA) solution or simply wet with

distilled water. Tthe excess water or the acid mixture was blotted with cotton wool. The

whole idea of this pretreatment was to make the dentine surfaces reactive before being

coated with GIC powders and to shorten the reaction time of GICs on the dentine

surfaces. Even stronger acid could be used for this purpose, as HNO_3 was used by Lee et

al.[23] to decrease the reaction time of DP-bioglasses.

Coating procedure:

Ultrafine powder coating (UPC) systems (shown in figure 3) typically include a feed

hopper (a fluidized bed), a powder spray gun, and an electrostatic power source

connected by hoses and cables, a spray booth, a over-sprayed powder collection system, a

powder recovery system and all the necessary regulators to activate the spray gun and

fittings to monitor and control the coating process parameters (working voltage, current

and aerodynamic settings). A UPC corona charging system is used to transfer the

electrostatic charge to the powders to be applied. A voltage source of 30 to 40 kV

generates current through a voltage cable that carries it to the powder gun tip, generating

an electrical field. With the aid of the generated electrical field in the UPC system,

actually an electrically charged cloud of fine particles is applied to the substrate.
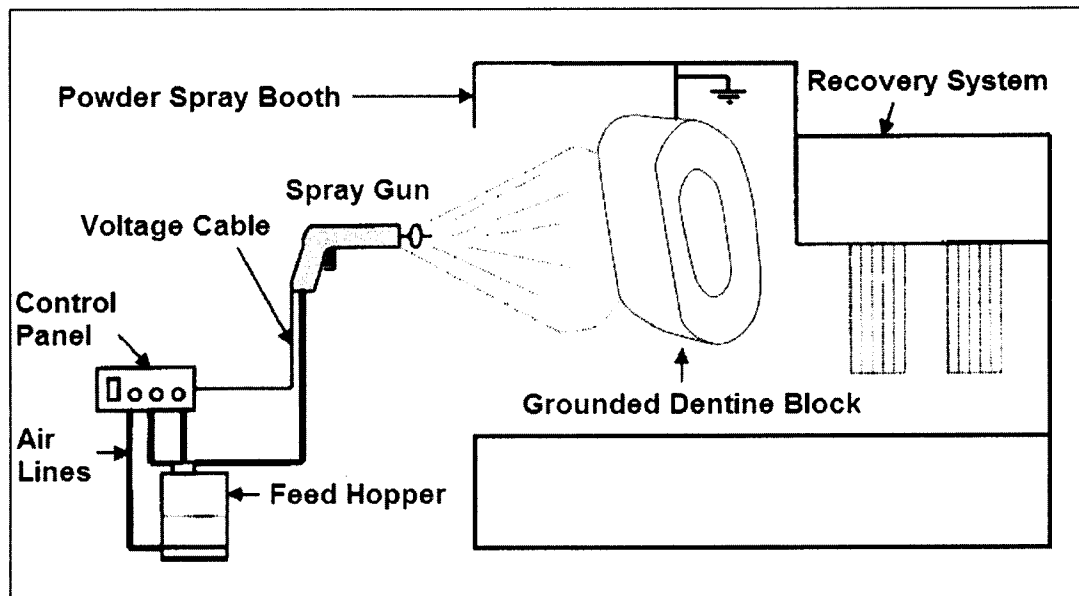
Figure 7.3: Ultrafine Powder Coating (UPC) System consisting of a feed hooper, air hose, electrostatic power supply, a control panel, a spray gun, a grounded hook to hold the dentine block, a powder spray booth and an over-sprayed powder recovery system.

The dentine blocks to be coated were hooked in the grounded holder and placed inside

the spray booth of the UPC system. A distance of 30~50 cm away was maintained

between the tip of the corona-charging gun and the dentine blocks. Operating parameters

were set in the PLC-based control system. The set parameters used in this study were: 0~

50 kV voltages, 1.5 bar feeding pressure (related to the amount of powder per unit of time

which passes through the tip of the gun), 1.0 bar auxiliary pressure (related to how spread

is the cloud of fine powders issuing from the tip of the gun) and 15 seconds exposure

time. GIC powder spraying was carried out at an ambient temperature of 20°C. After

depositing the powders on the dentine, a thin continuous and homogeneous film of GIC

powders was formed on the wet dentine surfaces. The dentine blocks were taken out of

the spray booth carefully and put into small sample containers in which moist

environment was maintained. The sample containers were then left at room temperature

to allow the applied GIC powders to be set in presence of either water or OPA/PAA

solution. The coated dentine blocks were then split into two parts to examine the cross-

section of the exposed (empty and filled) tubules.

Preparation of the control groups

Eight control groups were prepared for the purpose of comparing their tubule occlusion

depths with that achieved with the spraying technique used in this current study. The

control groups were: (1) Treatment of exposed dentine with 35% OPA gels (UltraEtch,

Ultradent Inc. USA) for 15 seconds followed by water rinsing; (2) Treatment of dentine

surfaces with a mixture PAA(GC America Inc, Il, USA) and OPA gels (with no rinse);

(3) Brushing or scrubbing of the slurry of Fuji I® (mixed with water) onto the dentine

surface; (4) Brushing or scrubbing of the slurry of Ketac-Cem® (mixed with water) onto

the dentine surface; (5) Brushing or scrubbing of the slurry of Fuji I® (mixed with

PAA/OPA) onto the dentine surface; (6) Sprinkling of the slurry of Fuji I® (mixed with

PAA/OPA) onto the dentine surface; (7) Brushing or scrubbing of the slurry of Ketac-

Cem® (mixed with PAA/OPA) onto the dentine surface; (8) Sprinkling of the slurry of

Ketac-Cem® (mixed with PAA/OPA) onto the dentine surface.

SEM-EDX of the dentine blocks:

Hitachi S-2600N (Hitachi, Pleasonton, CA) and LEO 1540XB (Carl Zeiss SMT Inc.)

Scanning Electron Microscopes (SEM) were employed to image both the opened and the

occluded dentinal tubules. A dentine block was mounted onto adhesive carbon tape that

was attached to a metal stub. The sample was then sputtered with gold (10 nm) to make

them conductive. The dentine sample had to be vacuum dried before gold-sputtering. In

addition to visual inspection, the SEM equipped with energy dispersive X-ray (EDX) was

used to perform elemental analysis and mapping of C, O, Na, Ca, Mg, P and Si on the

tubule cross-sections.

7.3. Results and Discussion

Brännström's hydrodynamic theory states that the dentinal tubular fluids move outward

or inward in the opened tubules causing sharp pain activating the pulpal nerves due to

change in pressure across the dentine when they are exposed to several stimuli.[5] Thus the

opened tubules are identified as the main cause of dentinal hypersensitivity. Evidently,

the treatment approaches are mostly concentrated on blocking the opened tubules that

could potentially desensitize the dentine. We, too, have focused on the same direction to solve the problem at its root.

While many approaches have been tried in recent years to fill the open tubules, none of them showed high penetration depth of the tubules sufficient to provide a long term solution to dentine hypersensitivity.[15,18-23] However, the higher level of penetration is necessary so that the tubule occluding materials could not be brushed off easily during daily toothbrushing.

In this study, we used dental restorative material, glass polyalkenoate (glass ionomer cement (GIC)) with the aim of penetrating far deeper into the opened tubules. Since the supplied poly acrylic (polyalkenoic) acid, which is usually used to make slurry of GICs, is highly viscous, it can wet the dentine surface, but it cannot fill the exposed tubules. Moreover, the GIC slurry solidifies very quickly making it difficult for the dentist to apply the slurry to the dentine surfaces. As a consequence, we focused our efforts on using these GICs in their powder form to seal and fill the exposed dentinal tubules.

Particle size measurement confirmed that the average size (D50) of Ketac-Cem® and Fuji I® were 3.22 μm and 4.14 μm respectively. Hence, according to Geldart classification[30], they both were Geldart Group C particles that were very difficult to flow. Rather than flowing as individual particles, they tended to form agglomerates causing puffing when they were applied on the dentine blocks. As received Ketac-Cem® and Fuji I® powders were further characterized for AOR, which was found to be 53.3 and 55.4 degree respectively (shown in table 7.1). The higher AOR also confirmed their poor flowability.

Therefore, these GIC powders were processed with several concentrations of nano-sized

Al_2O_3 additive by following Zhu & Zhang's technology.[32] Table 7.1 showed that after

adding 10% Al_2O_3, the AOR went down to 41.3 and 39.8 degree respectively. Therefore,

the GIC powders became flowable and no agglomerates were visible.

Table 7.1: AOR of Ketac-Cem® and Fuji I® in degree before and after the flow
modifications

	As received GICs	GICs+1% Al_2O_3	GICs+3% Al_2O_3	GICs+ 5% Al_2O_3	GICs+10% Al_2O_3
Ketac-Cem®	53.3 ± 1.2	47.8 ± 0.4	45.8 ± 0.3	44.2 ± 0.3	41.3 ± 0.7
Fuji I®	55.4 ± 0.5	43.9 ± 0.6	40.3 ± 1.0	43.3 ± 0.5	39.8 ± 0.6

The flow-modified GIC powders were sprayed onto the tubule-exposed dentine blocks

with the aid of ultrafine powder coating (UPC) technology. UPC employed corona spray

gun that charged the GIC powders electrostatically before they were being deposited on

the grounded dentine surfaces. In fact, a cloud of finer charged particles was delivered

onto the dentine surfaces. Since the GIC powders can not be cross-linked with tooth

calcium ions in absence of water or polyacid solution, the dentine surfaces were

pretreated with either water or with the diluted polyacid solution (PAA/OPA). The

approach was to form the desired slurry on the damaged dentine sites by spraying the

powders on the wet dentine blocks. However, the control groups used in this study were

prepared by brushing or sprinkling the GIC slurry onto the dentine surfaces.

Before spraying the GIC powders on the dentine surfaces, the smear layer of the dentine surfaces were removed by treating them with 35% OPA gel that eventually opened up the dentinal tubules. The opened tubules, shown in figure 7.4, more or less simulated the microstructure of hypersensitive dentine surfaces. Figure 7.4 showed both the top view and the cross-sectional view of the exposed tubules. The average diameters of the smear-layer removed tubules were ~1.5 μm. Absi et al. also reported the dimensions of the opened tubules and found that the diameter of the tubules of sensitive dentine was wider than that of non-sensitive dentine.[34]
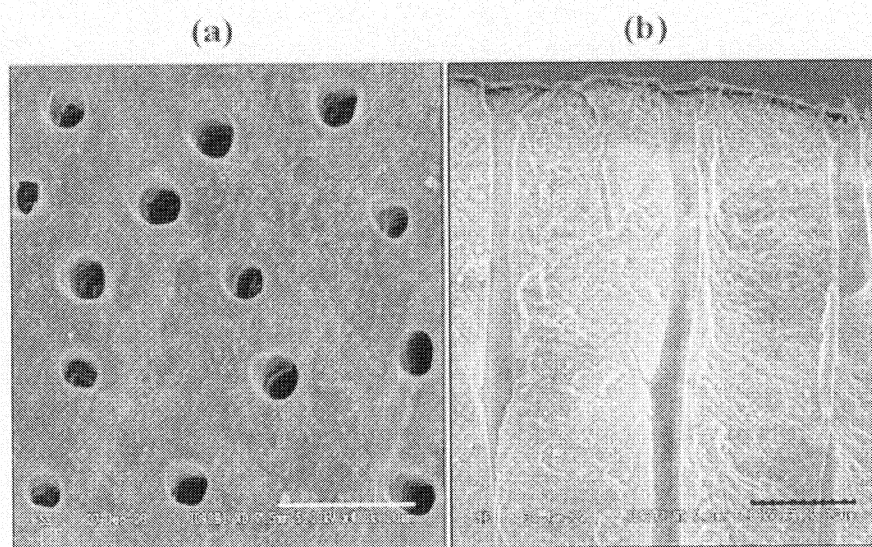
Figure 7.4: Exposed dentine surfaces before spraying the GIC powders. Smear-layer was removed by etching with 35% ortho-phosphoric acid for 15 seconds. The average opening or the diameter of the tubules were measured 1.5~ 2 μm while the bar = 10 μm. (a) Top view of the empty tubules; (b) Cross-sectional view of the empty tubules.

When the flow-modified Ketac-Cem® and Fuji I® slurry prepared with OPA/PAA solution were brushed onto exposed dentine surfaces, the dentinal tubule occlusion

seemed to insignificant (figure 7.5 (a) and (b)). However, figure 7.5 (c) and (d) showed that while sprinkled, the same powders exhibited some degree of tubule penetration, particularly the sprinkled Fuji I® penetrated in the tubules over 100 μm. These control group results would later be compared with those obtained by employing corona gun to apply the GIC powders onto the dentine surfaces.
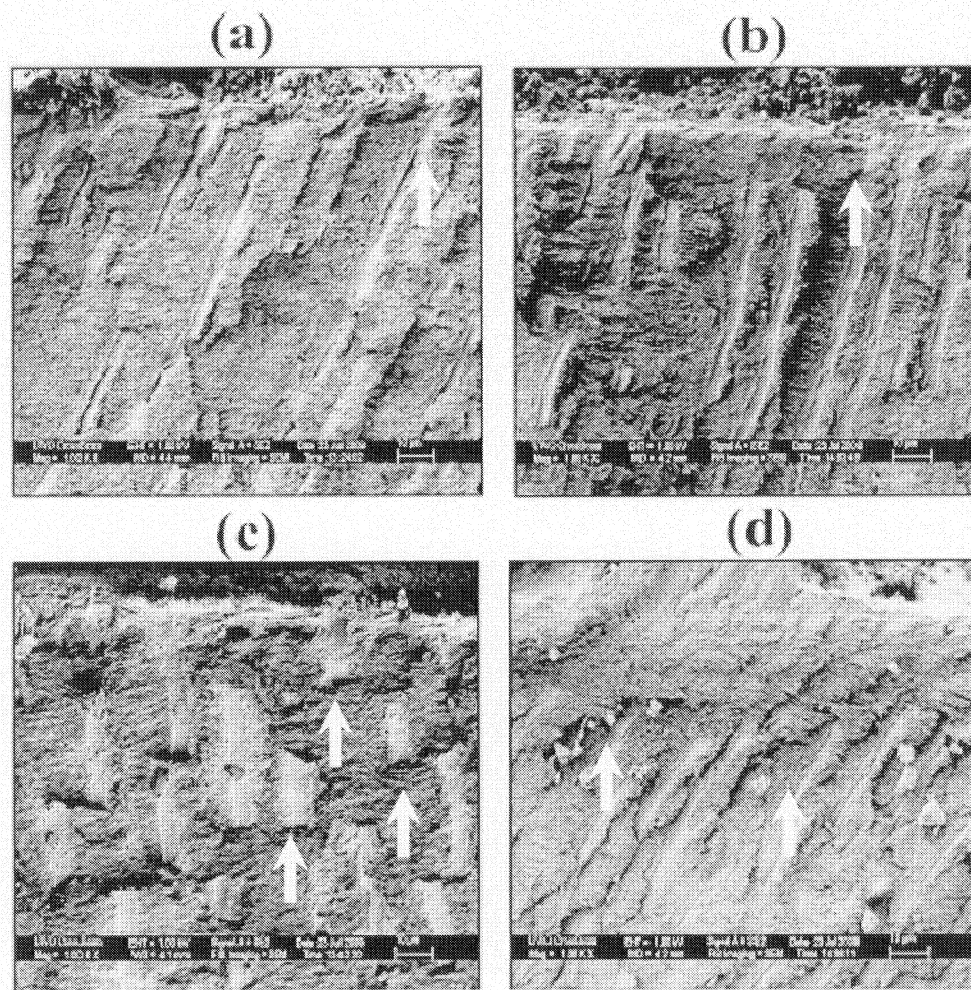
Figure 7.5: Cross-sectional views of the occluded tubules when Ketec-Cem® and Fuji I® slurry were brushed or sprinkled onto the dentine surface. (a) Fuji I® slurry brushed onto the dentine; (b) Ketec-Cem® slurry brushed onto the dentine; (c) Fuji I® slurry sprinkled

onto the dentine; (d) Ketec-Cem® slurry sprinkled onto the dentine. All slurries were prepared with OPA/PAA solutions. (Bar = 10 μm)

Figure 7.6 illustrates the cross-sectional views of the occluded tubules. When the flow-modified Ketac-Cem® powders (with 5 wt.% of Al_2O_3) were applied to the dentine that was pre-treated with 1:1 ratio of OPA and PAA, almost all of the visible tubules (through the crack) were filled with the applied materials. The crack shown in figure 7.6 (a) was formed due to excessive dehydration of dentine although in practical situation this type of crack would not form as the human mouth remains hydrated all the time. However, we have been fortunate to have this crack perpendicular to the tubules because it allowed us to visualize the filling that occurred in the inside of tubules. It was interesting to find almost all of tubules showed up in the crack were filled with the Ketac-Cem® material. The magnified views (figure 7.6 (b) and (c)) of the crack shown in figure 7.6 (a) gave even clearer view of the occluded tubules while figures 7.6 (d) and (e) magnified the portion above and below the crack, respectively. the total depth of penetration was found to be ~515 μm that was almost twice as much penetration depth as previously reported for other materials.[27] Figure 7.6 (f) hat showed outstanding filling of even the narrower branches of the tubules. The tubule occlusion seemed to be firm and confluent that could not be easily brushed off.
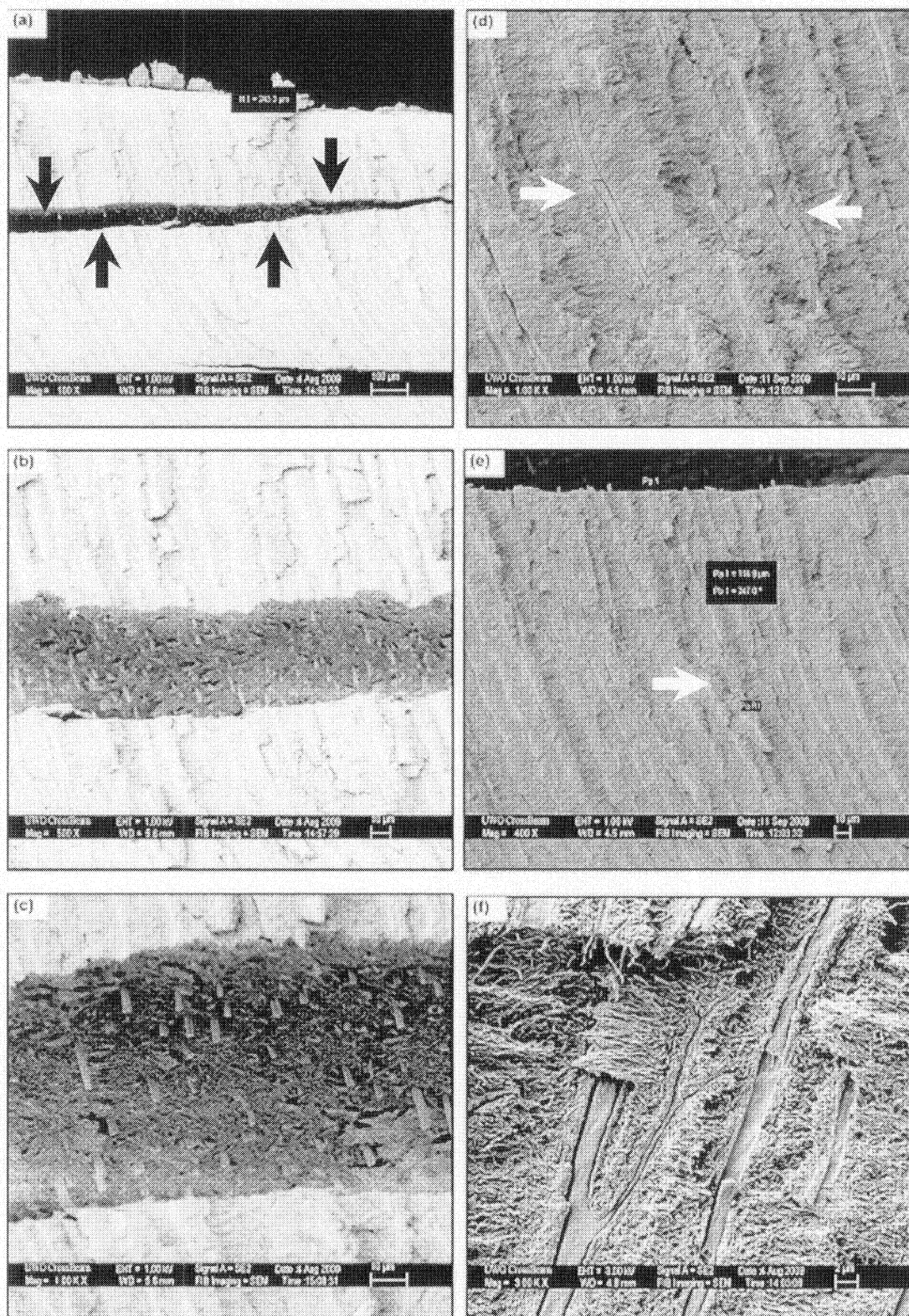
Figure 7.6: Cross-sectional views of the occluded tubules. Flow-modified Ketac-Cem® powders were applied to wet (with 1:1 ratio of OPA and PAA solution) dentine. (a) The crack perpendicular to the tubules was formed due to excessive dehydration of dentine; through the crack, it is visible that almost all of tubules showed up in the crack were filled with GIC materials; (b) and (c) Magnified view of the crack of (a) that further confirmed hermetic sealing of the tubules with the applied materials; (d) Magnified view of the portion above the crack; (e) The portion below the crack also showed the filling went further down till 115 μm depth; however (a) showed the portion above the crack is ~300 μm; therefore dentinal tubules showed in these figures were occluded as deep as ~415 μm; (f) The branches of the tubules were also nicely filled with the flow-modified Ketac-Cem® powders. Bar = 100 μm in (a), 10 μm in (b-e) and 2 μm in (f).

The occlusion of dentinal tubules was also achieved when flow-modified Fuji I® powders (with 3 wt.% of Al_2O_3) were applied to the smear-layer removed and pretreated dentine (with 1:1 ratio OPA and PAA solution). Figure 7.7 (a) showed the top view of the dentine surface that was completely covered with set Fuji I® materials, while figure 7.7 (b) and (c) presented the cross-sectional views of the filled tubules, where tighter sealing was visible. The solid filling was still visible where the current view was ended in the figure 7.7 (c) (shown with the arrow marks).

When the flow-modified Fuji I® powders were applied to the water-pretreated dentine, the tubule occlusion was visible on the crack which was found ~214 μm down from the origin of the tubules (figure 7.8 (a)). However, figure 7.8 (b) confirmed that the occlusion continued further down from the crack. Therefore, the penetration depth of the flow-modified Fuji I® powders was found be more than ~214 μm that was higher than that reported in literature.[21-23,26] Moreover, figure 7.8 (c) showed that all the tubules seen in

the crack were filled with the set materials. Figures 7.8 (c) and (d) also confirmed that tubules were occluded to the fullest as the diameters of the cylindrical plaques (~2 μm) were very close to that of the empty tubules shown in figure 7.4.
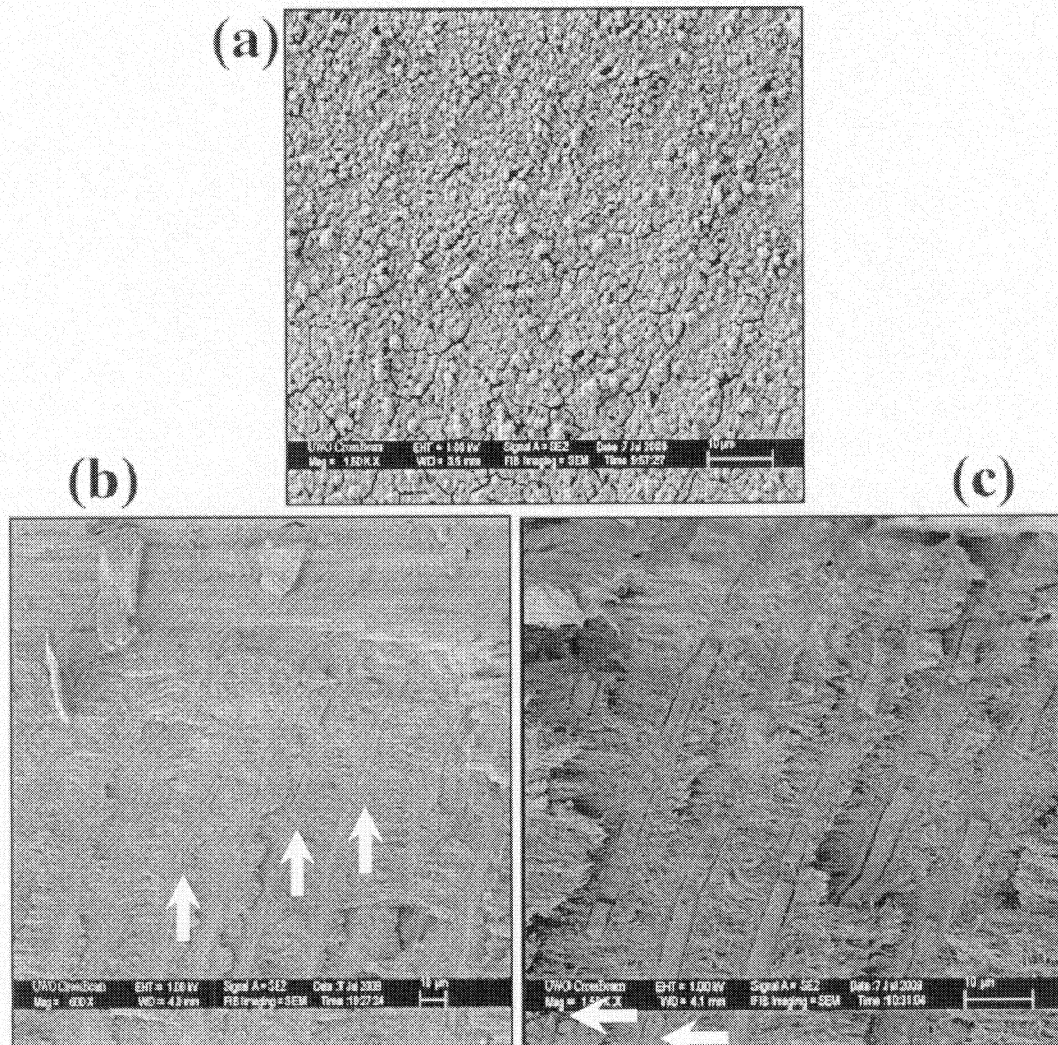
Figure 7.7: The smear-layer removed pretreated (with 1:1 ratio of orthophosphoric acid and polyacid solution) dentine was coated with the flow-modified Fuji I® powders. (a) The top view of the dentine surface; a confluent coating was achieved; (b) and (c) Cross-sectional views of the tubules. (Bar = 10 μm).
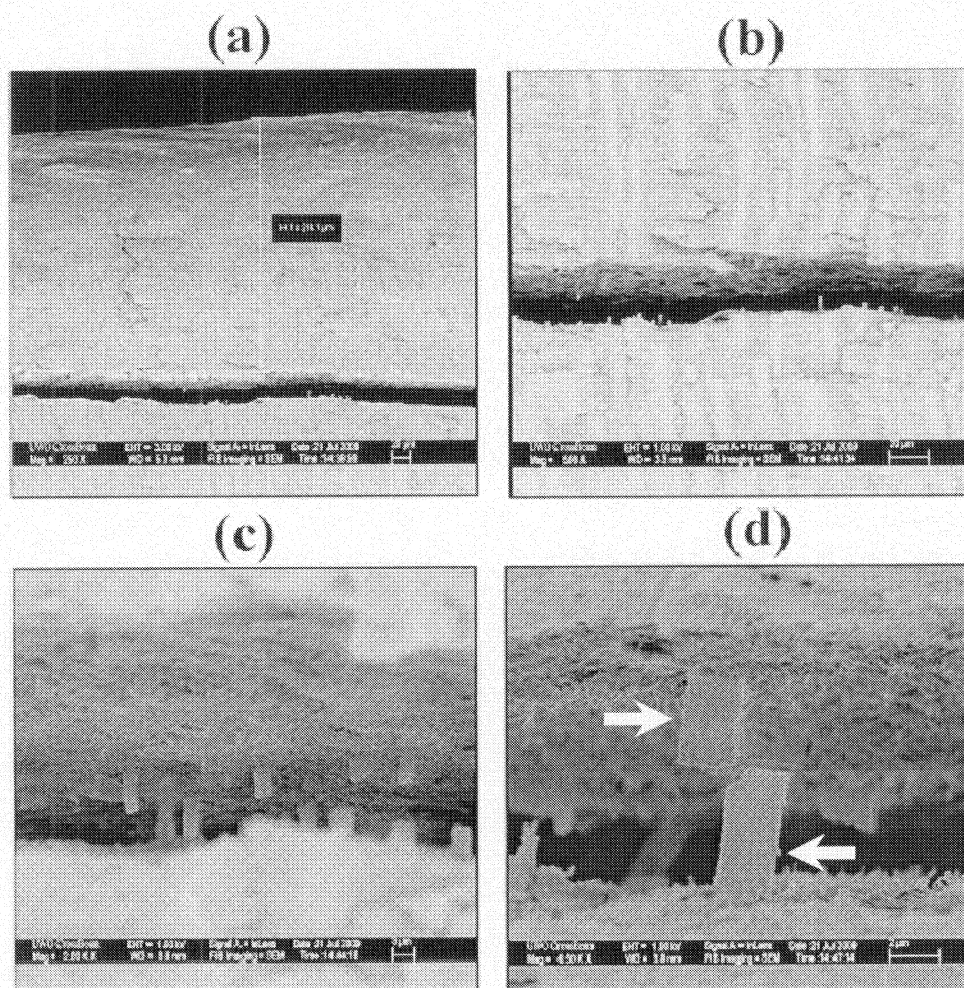
Figure 7.8: The water-pretreated dentine was coated with the flow-modified Fuji I® powders. (a) Tubule occlusion was visible on the crack which was found 214 μm down from the origin of the tubules. (b) Magnified view of the crack showed the occlusion continued further down from the crack. (c) Magnified view of the crack presented several filled tubules. (d) Filling of a tubule was broken when the dentine was split to form the crack. (Bar = 10 μm).
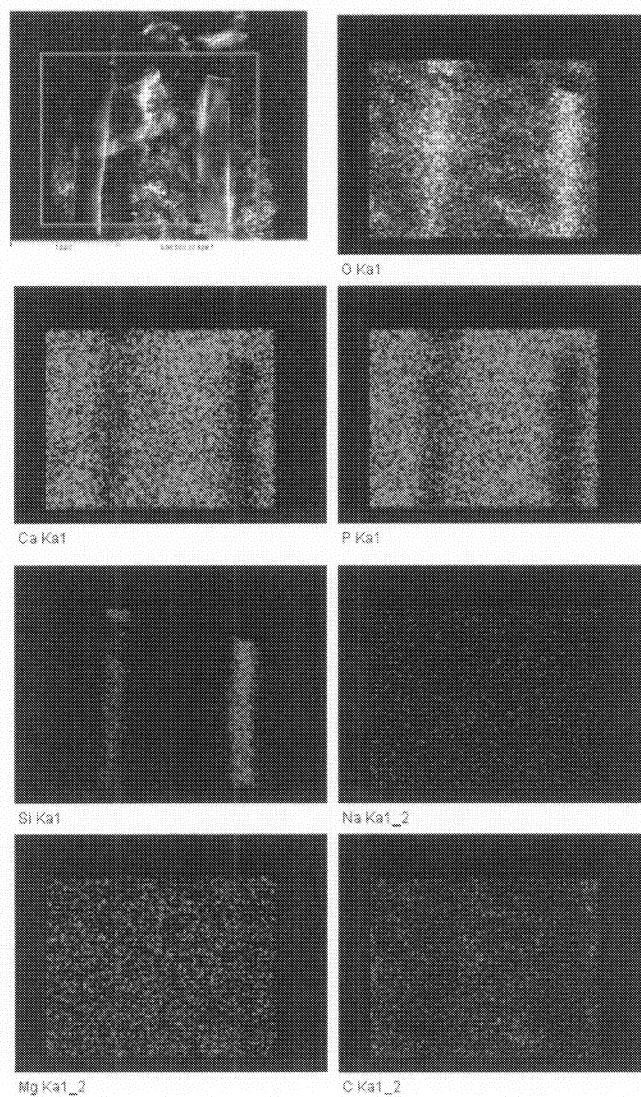
Figure 7.9 (a): Elemental mapping of filled tubules with flow-modified Fuji I®
powders. As expected Si was predominantly detected in the filled tubules as
Fuji I® composed of approximately 10 atomic% of Si.
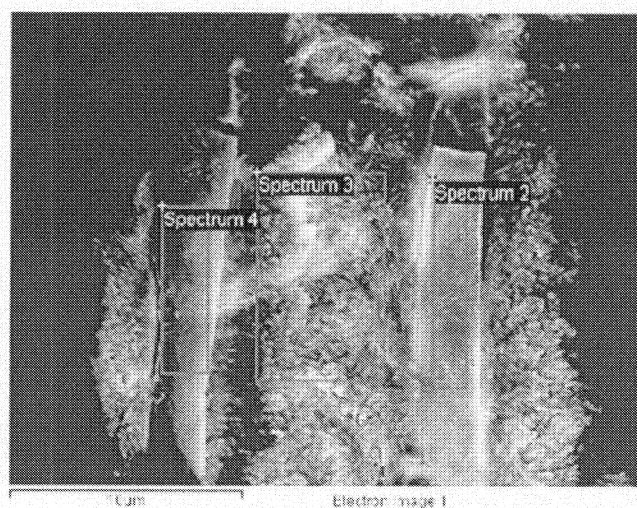
Figure 7.9 (b): Tubules filled with flow-modified Fuji I; filled dentinal tubules were chosen as spectrums 2 & 4 while spectrum 3 indicated the tooth dentine.

Table 7.2: Elemental analysis of the spectrums shown in figure 7.9 (b) [All results in atomic%].

Spectrum	C	O	Na	Mg	Si	P	Ca
Spectrum 2	4.92	67.96	0.54	0.50	10.08	7.75	8.25
Spectrum 3	10.56	62.71	0.87	0.70	0.22	11.01	13.93
Spectrum 4	7.59	67.73	0.79	0.49	6.29	7.90	9.23

Figure 7.9 (a) showed the EDX elemental mapping of C, O, Ca, Mg, Na, P and Si inside the occluded tubules when the flow-modified Fuji I® powders were applied to the water-pretreated dentine surface. Since, Ca, Mg and P were the common elements of the dentine and the Fuji I®, Si made the difference between the occluded tubules and the dentine surface. Evidently, distinct Si mapping was found inside the tubules that confirmed the existence of GIC powders into the tubules as the GICs contained approximately 10 atomic% of Si. For further quantification of several chemical species (table 7.2), three

spectrums were selected in figure 7.9 (b) where spectrums 2 and 4 were chosen into the

filled tubules, but spectrum 3 was the dentine surface. Table 7.2 presented significantly

high level of Si in spectrums 2 and 4 compared to spectrum 3 while Ca, Mg and P

remained closer.

Since, powders were being charged electrostatically in the UPC system, the working

voltage was varied from 0 kV to 50 kV as an observational study. When flow-modified

Ketac-Cem® powders were sprayed onto OPA/PAA-pretreated dentine surfaces, it was

interesting to observe that at lower working voltage Ketac-Cem® penetrated deeper into

the tubules compared to the higher working voltage (figure 7.10). At 0 kV working

voltage, powders penetrated into ~650 μm into the tubules (figures 7.10 (a) and (b)). At

10 kV, powders penetrated so deep (~915 μm) into the tubules that they hit the pulp

surface (figures 7.10 (c) and (d)). However, 20 kV sent the powders even further down

(~930 μm) to the tubules while fillings were observed even below the second crack from

the top (figures 7.10 (e) and (f)). Figure 9 (f) also showed the strength of the filling

plaque as it did not break even when the crack was formed into the dentine. Such a strong

and compact filling of dentinal tubules would likely stop the dentinal fluid flow.

Moreover, the penetration depths observed at 10 and 20 kV were almost four times more

than that reported by Curtis in 2010.[27] However, at higher voltages from 30 to 50 kV

(figures 7.10 (g-l)), although the magnitudes of penetration (~600 μm) were still higher

than any of such reports published in the literature, the quality of occlusion seemed to be

deteriorated. At higher voltages,
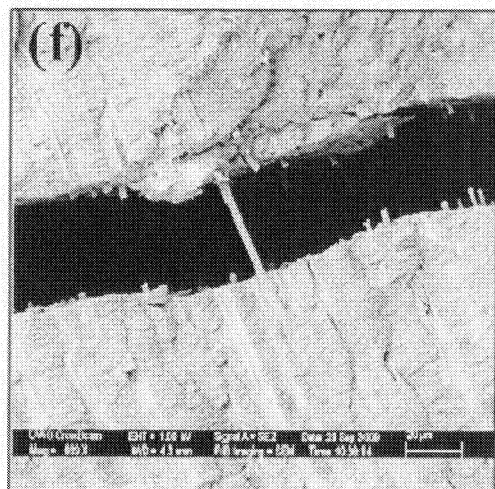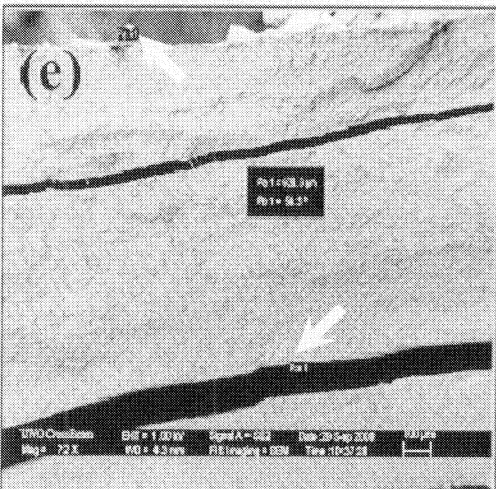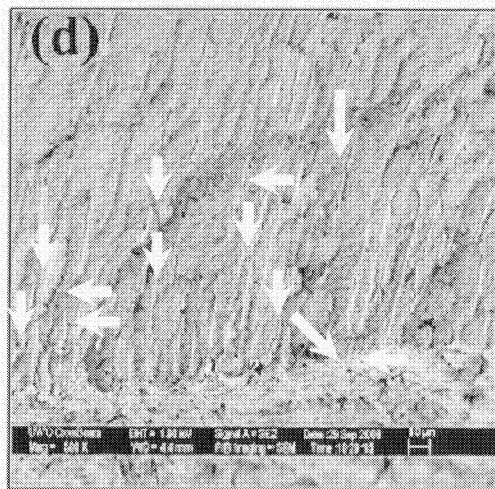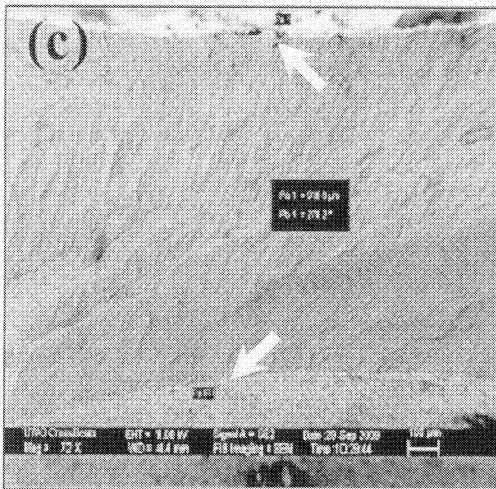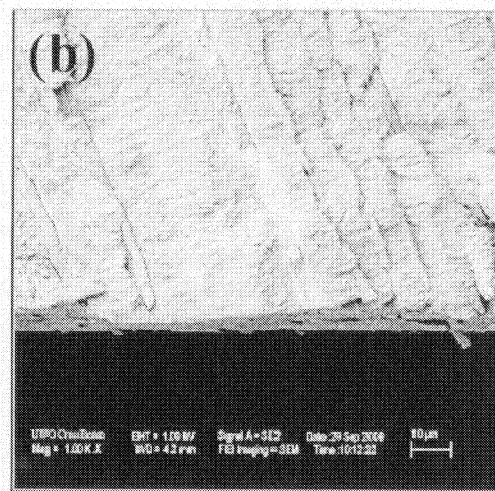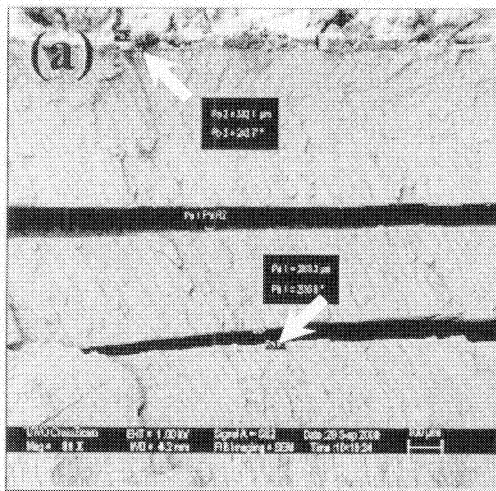
Figure 7.10: Flow-modified Ketac-Cem® powders were sprayed onto OPA/PAA pre-treated dentine surfaces. The working voltage of the powder spray system was varied from 0 to 20 kV. (a) and (b) showed tubule occlusion when 0 kV was the working voltage. (c) and (d) were captured from the sample that was sprayed at 10 kV while (e) and (f) were at 20 kV. Bar = 100 μm in (a), (c) and (e) and 10 μm in (b), (d) and (f).

powders were charged so much that they became fused up and created porous filling inside the tubules shown in figures 7.10 (h), (j) and (l). Due to the porous filling, the dentine surfaces were supposed to remain permeable to some extent. This would provide only partially efficacy in treating dentine hypersensitivity, because the fluid movement inside the tubules is proportional to the fourth power of their radius.[35]

As a whole, tighter and more compact dentinal tubule occlusion was obtained with lower working voltages. However, it is still tricky to conclude whether working voltage was the main factor that was responsible for the deeper tubule penetrations since 0 kV working voltage also produced ~650 μm deep occlusion (figure 7.10 (a)). Therefore, at this stage of the study, we are not going to speculate the mechanism of such a huge penetration of the GIC powders into the exposed dentinal tubules.

Moreover, we found that the penetration depth (figure 7.11) of the Ketac-Cem® powders was not very high when the powders were sprayed on the water-pretreated dentine surfaces compared to that pre-treated with OPA/PAA solutions; however, comparing with figure 7.10, figure 7.11 showed that the quality of occlusion was more compact into the water-pretreated dentine surfaces. Even at 50 kV working voltage, the occlusion was found to be very compact.

Although there were differences in the penetration depths and the quality of occlusion among the acid and water-treated dentine blocks, working voltage of 20 kV showed highest dentinal tubule penetration of GIC powders as shown in figures 7.10 and 7.11.

7.4. Conclusions

Although the mechanism of GICs' dentinal tubule occlusion has not yet been elucidated, it can be concluded that UPC technology has been successfully utilized to apply GIC as powders and subsequently, to occlude the exposed dentinal tubules as deep as ~ 1 mm from the dentine surface to the dentine-pulp interface. Novelty of this work has been rendered in applying GIC powders onto wet (either by water or by OPA/PAA solution) dentine surfaces onto which the applied powders eventually made the slurry. Moreover, it was interesting to find that GIC powders penetrated deeper into the acid-treated dentine surfaces compared to the water-treated ones at any given working voltage, while the opposite was found to be true while comparing the quality (compact vs. porous) of occlusion. However, working voltage of 20 kV offered the highest penetration depths of GIC powders to the dentinal tubules.
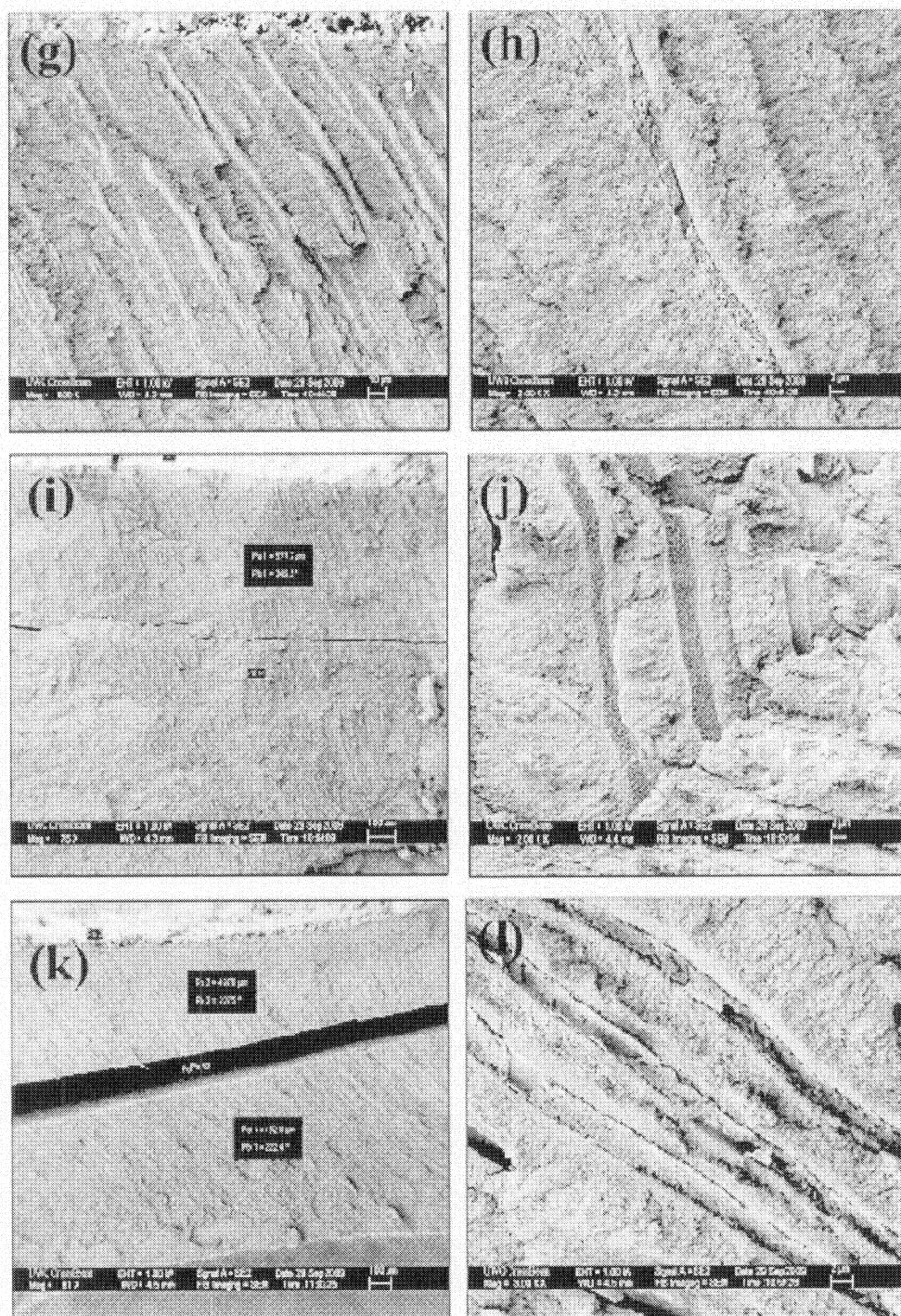
Figure 7.10 (continued): The depth and quality of penetration of Ketac-Cem® powders at 30 kV ((g) and (h)), 40 kV ((i) and (j)) and 50 kV ((k) and (l)) working voltages. Porous

occlusions were visible in (h), (j) and (l). Bar = 100 µm in (g), (i) and (k) and 10 µm in (h), (j) and (l).
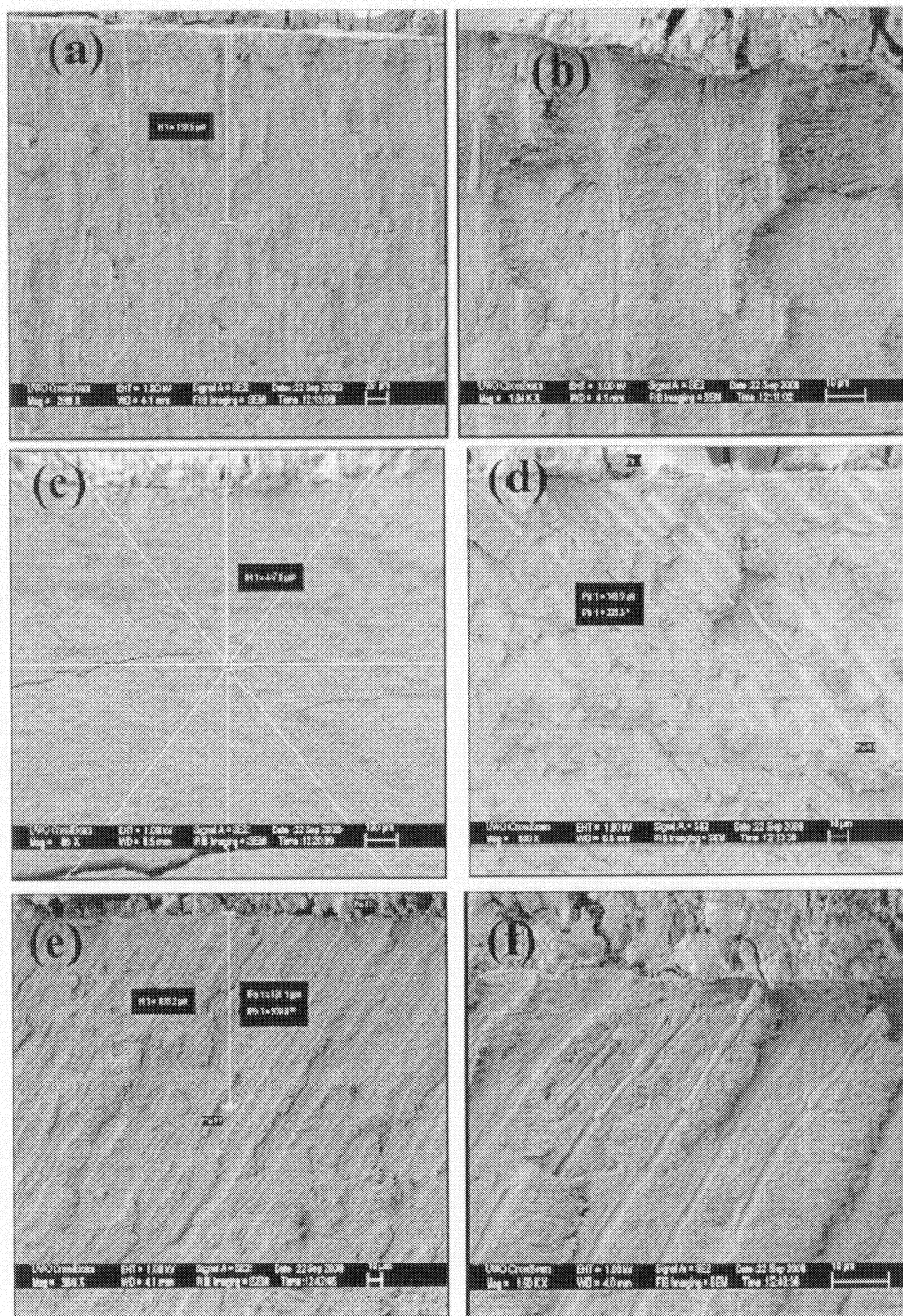
Figure 7.11: Working voltage of the UPC system was varied while Ketac-Cem® powders were sprayed on the water-pretreated dentine surfaces. (a) and (b): 10 kV; (c) and (d): 20 kV and (e) and (f): 40 kV. Bar = 20 µm in (a), 10 µm in (b) and (d-f) and 100 µm in (c).
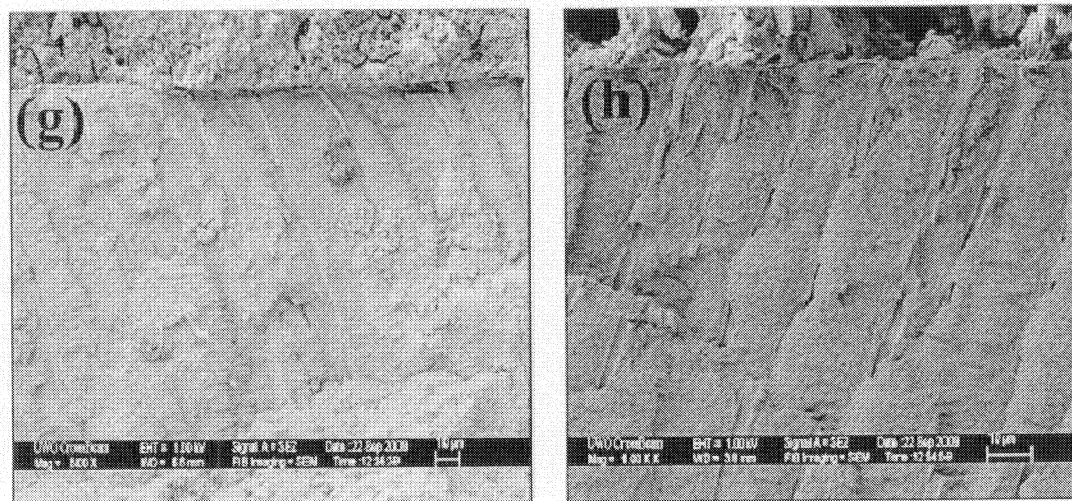
Figure 7.11 (continued): Working voltage of the UPC system was varied while Ketac-Cem® powders were sprayed on the water-pretreated dentine surfaces. (g): 30 kV and (h): 50 kV. Bar = 10 µm.

References

1. Kasper, D., Dentinal hypersensitivity: Assessing a chronic problem. *RDH Magazine* **2009**, 29 (9). <http://www.rdhmag.com/display_article/369655/56/none/none/Feat/Dentinal-hypersensitivity:-Assessing-a-chronic-problem>

2. Addy, M.; Urquhart, E., Dentine hypersensitivity: its prevalence, aetiology and clinical management. *Dent Update* **1992**, 19(10), 407-8,10-2.

3. Gaffar, A., Treating hypersensitivity with fluoride varnish. *Compend Contin Educ Dent* **1999**, 20(1 Spec No), 27-33.

4. Orchardson, R.; Gillam, D.G., Managing dentin hypersensitivity. *J Am Dent Assoc.* **2006**, 137(11), 990-8.

5. Brännström, M., Sensitivity of dentine. *Oral Surg Oral Med Oral Pathol.* **1966**, 21 (4), 517-527.

6. Bamise, C.T.; Olusile, A.O.; Oginni, A.O., An analysis of the etiological and predisposing factors related to dentin hypersensitivity. *The Journal of Contemporary Dental Practice* **2008**, 9 (5), 52-9.

7. Fiocchi, M.F.; Moretti, A.J.; Powers, J.M.; Rives, T., Treatment of root sensitivity after periodontal therapy. *American Journal of Dentistry* **2007**, 20 (4), 217-20.

8. Corona, S.A.; Nascimento, T.N.; Catirse, A.B.; Lizarelli, R.F.; Dinelli, W.; Palma-Dibb, R.G., Clinical evaluation of lower-level laser therapy and fluoride varnish for treating cervical dentinal hypersensitivity. *J. Oral Rehabil* **2003**, 30, 1183-1189.

9. Pashley, D.H., Dentin permeability, dentin sensitivity, and treatment through tubule occlusion. *J Endod* **1986,** 12, 465-74.

10. Pamir, T.; Dalgar, H.; Onal, B., Clinical evaluation of three desensitizing agents in relieving dentin hypersensitivity. *Operative Dentistry* **2007,** 32 (6), 544-8.

11. Chadwick, R.G.; Mason, A.G., An audit of dentine hypersensitivity treatments in six general dental practices in scotland. *Primary Dental Care : Journal of the Faculty of General Dental Practitioners (UK)* **2008,** 15 (4), 129-34.

12. Olusile, A.O.; Bamise, C.T.; Oginni, A.O.; Dosumu, O.O., Short-term clinical evaluation of four desensitizing agents. *The Journal of Contemporary Dental Practice* **2008,** 9(1), 22-9.

13. Chabansky, M.B.; Gillam, D.G., Etiology, prevalence and clinical features of cervical dentine densitivity. *J Oral Rehabil* **1997,** 24 (9), 15-19.

14. Kakaboura, A.; Rahiotis, C.; Thomaidis, S.; Doukoudakis, S., Clinical effectiveness of two agents on the treatment of tooth cervical hypersensitivity. *Am J Dent* **2005,** 18 (4), 291-295.

15. Docimo, R.; Montesani, L.; Maturo, P.; Costacurta, M.; Bartolino, M.; DeVizio, W.; Zhang, Y.P.; Dibart, S., Desensitizing efficacy of a new toothpaste containing 5.5% potassium citrate: A 4-week clinical study. *American Journal of Dentistry* **2007,** 20 (4), 209-11.

16. Fu, B.; Shen, Y.; Wang, H.; Hannig, M., Sealing ability of dentin adhesives/desensitizer. *Operative Dentistry* **2007,** 32 (5), 496-503.

17. Du Min, Q.; Bian, Z.; Jiang, H.; Greenspan, D.C.; Burwell, A.K.; Zhong, J.; Tai, B. J., Clinical evaluation of a dentifrice containing calcium sodium

phosphosilicate (novamin) for the treatment of dentin hypersensitivity. *American Journal of Dentistry* **2008**, 21 (4), 210-4.

18. Liu, M.-H.; Chan, C.-H.; Ling, J.-H.; Chris, W.C.R., Filling in dentinal tubules. *Nanotechnology* **2007**, 18 (47), 475104.

19. Tengrungsun, T.; Sangkla, W., Comparative study in desensitizing efficacy using the GaAlAs laser and dentin bonding agent. *Journal of Dentistry* **2008**, 36 (6), 392-5.

20. Arrais, C.A.G.; Chan, D.C.N.; Giannini, M., Effects of desensitizing agents on dentinal tubule occlusion. *J Appl Oral Sci* **2004**, 12(2), 144-8.

21. Lee, B.S.; Chang, C.W.; Chen, W.P.; Lan, W.H.; Lin, C.P., In vitro study of dentin hypersensitivity treated by Nd:YAP laser and bioglass. *Dent Mater* **2005**, 21, 511-519.

22. Lee, B.S.; Tsai, H.Y.; Tsai, Y.L.; Lan, W.H.; Lin, C.P., In vitro study of DP-bioglass paste for treatment of dentin hypersensitivity. *Dent Mater J* **2005**, 24, 562-569.

23. Lee, B.S.; Kang, S.H.; Wang, Y.L.; Lin, F.H.; Lin, C.P., In vitro study of dentinal tubule occlusion with Sol-gel DP-bioglass for treatment of dentin hypersensitivity. *Dent Mater J* **2007**, 26 (1), 52-61.

24. Lee, S.Y.; Kwon, H.K.; Kim, B.I., Effect of dentinal tubule occlusion by dentifrice containing nano-carbonate apatite. *Journal of Oral Rehabilitation* **2008**, 35, 847-853.

25. Aranha, A.C.C.; Pimenta, L.A.F.; Marchi, G.M., Clinical evaluation of desensitizing treatments for cervical dentin hypersensitivity. *Braz Oral Res* **2009**, 23(3), 333-339.

26. Chiang, Y.C.; Chen, H.J.; Liu, H.C.; Kang, S.H.; Lee, B.S.; Lin, F.H.; Lin, H.P.; Lin, C.P., A novel mesoporous biomaterial for treating dentin hypersensitivity. J Dent Res **2010**, 89 (3), 236-240.

27. Curtis, A.R.; West, N.X.; Su, B., Synthesis of nano-bioglass and formation of apatite-rods to occlude exposed dentine tubules and eliminate hypersensitivity. *Acta Biomater* **2010** Mar 2. [Epub ahead of print]

28. Anusavice, K.J., *Phillip's science of dental materials*. 11th ed. St. Louis: Saunders Elsevier, **2003**.

29. van Noort, R., Enamel and dentine bonding. In *An introduction to dental materials*. 3rd ed., 152. Edinburgh: Mosby Elsevier, **2007**.

30. Geldart, D., Types of gas fluidization. *Powder Technology* **1973**, 7 (5), 285-297.

31. Hamaker, H.C., The London-Van der Waals Attraction between Spherical Particles. *Physica (Utrecht)* **1937**, 4, 1058-1072.

32. Zhu, J.; Zhang, H., Fluidization Additives to Fine Powders. *US Patent 6,833,185*, **2004**.

33. Barletta, M.; Gisario, A.; Tagliaferri, V., Electrostatic spray deposition (ESD) of polymeric powders on thermoplastic (PA66) substrate. *Surface & Coatings Technology* **2006**, 201, 296–308.

34. Absi, E.G.; Addy, M.; Adams, D., Dentine hypersensitivity: a study of the patency of dentinal tubules in sensitive and non-sensitive cervical dentine. *J. Clin Periodontol* **1987**, 14, 280-284.

35. Wylie, S.G.; Wilson, P.R., An investigation into the pressure transmitted to the pulp chamber on crown cementation: a laboratory study. *J Dent Res* **1994**, 73, 1684-1689.

CHAPTER 8
Conclusions and Recommendations

8.1. Conclusions

This study investigated the utilization of ultrafine powder coating (UPC) technology in three different practical application projects, which included the development of superhydrophobic powder coatings, fabrication of nanoroughness to develop biocompatible polymeric coatings and occlusion of exposed dentinal tubules by applying glass ionomer cement (GIC) powders with the aid of corona spray gun. Ultrafine powders of 15~25 µm average particle sizes were used in superhydrophobic and biocompatible coatings preparation, while GICs involved in the dentinal tubules occlusion were only 3~5 µm in mean particle sizes. Same ultrafine powder coating process was employed in carrying out all three tasks that exhibited clear advantages over the traditional ones. However, successes of these ultrafine powder applications obviously depended on the success on modifying the ultrafine powders of interest so that they would flow well in the spraying system.

Superhydrophobic powder coatings were developed by using ultrafine powder coating (UPC) technology. The developed coating resembled natural *lotus leaf* in a way that water droplets formed very high water contact angles (CAs) (> 160°) and very low water sliding angle (SA) (<5°) on them. Like *lotus leaf*, the coated surfaces possessed unique micro-/nano-hierarchical structures that drastically reduced the fraction of water-solid interface, and increased that of air-water interface. Due to this fact, water droplets tended

to be very unstable on these surfaces and ran away from the superhydrophobic surfaces collecting dirt along its way. This gave the developed coatings self-cleaning properties.

Polymeric biocompatible powder coatings, enriched with nano-TiO_2, were created by using ultrafine powder coating (UPC) technique. On the developed coatings, human mesenchymal cells were grown. It was found that 2 wt.% nano-TiO_2 enriched coatings outperformed its other counterparts in terms of cell attachment, spreading and their metabolic activity, although they are only approaching the properties of commercially pure titanium (cpTi) disks. As these surfaces had micro-/nano- roughness, the cell morphology appeared to be narrower with elongated filaments, compared to the cells grown on cpTi. However, the cells seeded on these coatings started expressing Runx2 in seven days while Collagen Type 1 was detected after only one day of seeding.

Another set of polymeric biocompatible powder coating were developed that varied in their surface nanoroughness. Simple modification of the coating formula produced variable nanoroughness on the substrates in the range of ~37 nm to ~260 nm. As in the previous set, human mesenchymal cells were cultured on these surfaces. Although a good number of cells attached and spread on all the surfaces, it was surprisingly noticed that the coatings, whose nanoroughness was kept below ~ 50 nm, performed as good as the commercially pure titanium (cpTi). Cells grown on such coatings were also found be similar degree of metabolically active as grown on cpTi. Therefore, it can be concluded that nanoroughness played significant role in enhancing biocompatibility of the polymeric powder coatings, although hydrophobicity also mattered.

Applying the flow-modified glass ionomer cement (GIC) powders onto exposed dentine

surfaces to occlude exposed dentinal tubules was accomplished with using ultrafine

powder coating (UPC) technique. The average particle sizes of the proprietary Ketac-

Cem® and Fuji I® were only 3.22 μm and 4.14 μm, respectively and these powders

seemed to be unflowable as they exhibited AOR of 53.3 and 55.4 degree, respectively.

These powders were processed with nano-Al_2O_3 additive to improve their flow

properties. Upon modification with 10 wt. % Al_2O_3, their AOR went down to 41.3 and

39.8 degrees, respectively, and they became flowable in the powder spraying device. The

flow-modified GIC powders were applied onto smear-layer removed, wet dentine blocks

that were pre-treated with either water or 1:1 ratio of orthophosphoric acid (OPA) and

poly acrylic acid (PAA) solution. GICs appeared to penetrate deeper into the tubules of

the polyacid treated dentine blocks compared to that of water-treated ones. In some

instances, GICs were found ~1 mm down from the dentine surface, in the tubules

approaching the pulp area. These penetration depths were approximately four-times

higher than the best results (~270 μm) available in the literature. It was also observed that

lower working voltages (0-20 kV) yielded deeper and tighter filling of GICs into the

tubules, whereas higher voltages (30-50 kV) produced porous filling inside the tubules.

The tubule occlusion mechanism was not fully understood as even 0 kV working voltage

revealed penetration depth of about 650 μm.

Finally it can be concluded that ultrafine powder coating (UPC) technology has been

successfully utilized for the development of functional superhydrophobic and

biocompatible coatings with varying degree of micro-/nano- features. Moreover, UPC

showed superiority in applying GIC powders onto exposed dentine to occlude the open

tubules that may cause dentine hypersensitivity. Thus UPC has provided possible solution

to the as yet an resolved problem of hypersensitivity.

8.2. Recommendations

Although this study met the objectives of all three application projects that were set

before the actual work was started, there is still some theoretical and experimental works

that could definitely enrich the findings of this current study. Hence, to build on the

content of this doctoral thesis, the following recommendations should be considered as

future work:

- Although superhydrophobic powder coatings were developed in this work, the

  mechanism how exactly the special micro-/nano- texture was formed on the

  coated surfaces is still not clear. Theoretical and experimental studies can be

  designed to explore the curing process to investigate how the curing temperature

  and coating compositions affect the topography of the cured finishes. Moreover,

  the durability issue should be addressed further.

- Although the developed polymeric biocompatible coatings showed a good level of

  biocompatibility, still there is a room for the improvement. Incorporation of well-

  known bioactive mineral trioxide aggregates (MTAs) into the existing coating

formulations could further increase the biocompatibility of the powder coatings. In addition, only mesenchymal cells were cultured to assess the bioactivity of the developed coatings. Growing pre-osteoblast or osteoblast-like cells or endothelial cells on the coatings developed in this study would obviously strengthen the claim.

- Although the application of GIC powders on the exposed dentine with the aid of corona gun resulted clear superiority over conventional techniques in terms of dentinal tubule occlusion, what exactly causes such a deeper penetration of the tubules, is not fully understood. As the powders were charged while spraying in the powder coating system, the effect the applied working voltages could be further investigated. In addition, corona spraying gun may not be used in real life to apply GICs into patient's teeth as it involves high voltage in its functionality; hence, the patients could experience electrostatic shock. Therefore, internal charging gun could be explored to deliver the GIC powders. If the internal charging gun could produce similar results as the corona gun did, it could potentially solve the same problem without terrifying the patients with electrostatic shocks. Moreover, as in some instances GICs almost reached to the pulp area, it is also necessary to investigate whether the GICs could, damage the pulpal cells. Last, but not the least, instead of relying on the proprietary GICs, our own version of the glass ionomers could be developed.

Appendix A1

Flow improvement of ultrafine steel particles to be used in SLS Process

Rapid Prototyping (RP) technologies have emerged as the leading processes that reduce

the cost and time for the product development cycle. The term RP refers to all

manufacturing technologies that use Computer Aided Design (CAD) data to drive an

layer-by-layer additive process without any part specific tooling or human intervention.

The most widely used commercial RP systems are: Stereolithography (SL), Fused

Deposition Modelling (FDM), Laminated Object Manufacturing (LOM), Selective Laser

Sintering (SLS), and Three-Dimensional (3D) Printing. These systems utilize a variety of

different mechanisms to consolidate liquid, powder or sheet materials to form solid

parts.[1] Among these RP systems, the report will focus only on the SLS system.

Theoretically SLS systems can process any material that could be ground into powder,

such as, Castform™ PS (polystyrene powder), Duraform™ PA (polyamide (Nylon)

composite), Duraform™ GF (glass-filled polyamide (Nylon) composite), Laserform™

ST100 and ST200 (polymer coated stainless steel powder) etc. SLS system is able to

easily make complex, and finely detailed designs without the need for other supports.

This process can be used to build parts of almost any shape as shown in figure 1.

http://www.selecteng.com

http://www.laserproto.com/sls.pdf
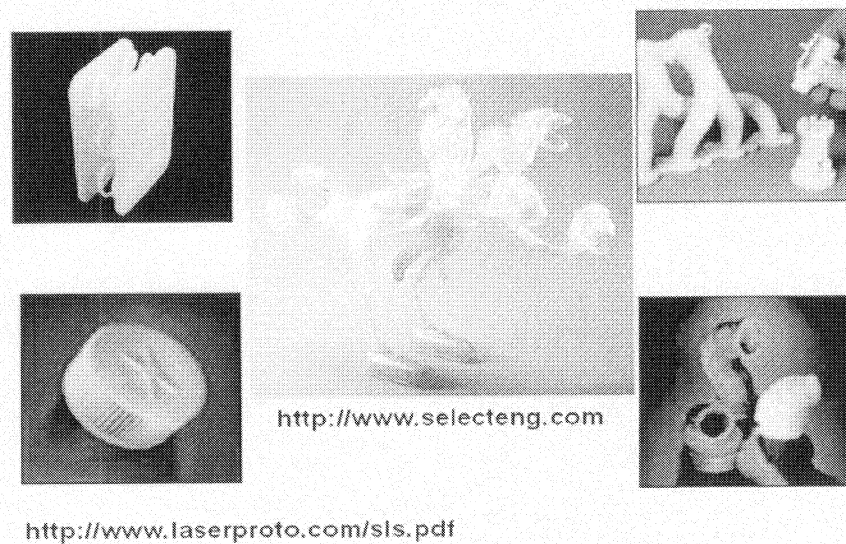
Figure 1: Different shapes of possible parts

Selective Laser Sintering (SLS):

Selective Laser Sintering (SLS) was developed by a group of researchers at the
University of Texas, Austin. The earliest published description of the technology
is available in a number of U.S patents, the first of which was Pat No. 4,863,538 issued
on September 5, 1989. The potential for commercialization of this new technology was
captured with the formation of DTM Corporation. DTM released its first version of the
SLS process in 1992, called the Sinterstation®. By the year 2000, DTM owned more than
80 patents worldwide covering different aspects of the SLS process, systems and
materials.[2] In August of 2001, the RP systems manufacturing giant 3D Systems acquired
DTM. With the acquisition 3D Systems, had its share of installed RP based machines
worldwide grow to a dominating 61.4%.[1]

The SLS Process:

The SLS system is shown in figure 2. The process uses solid powders as the starting

material and a CO_2 laser as the energy source for sintering the powder. During the build

process, a small quantity of powder is first moved upward by a piston in the feed

cartridge. A counter-rotating roller is then used to pick-up the raised powder from the

feed cartridge and deposits it over a work area called the "part bed". A computer

controlled 50-watt CO_2 laser beam is used to emit radiation directed by a pair of

orthogonal mirrors onto the surface of the part bed. Laser energy is applied selectively to

the part bed as defined by the cross-section of the object. The laser beam raises the

temperature of the powder exposed to just above the material melting point causing the

powder to sinter. Once the laser has completed tracing the object crosssection, the part

bed is lowered and another layer of powder is dispensed on top of the previous layer. The

laser traces over the new layer and sinter it to the previous layer. In this manner the object

is built layer-by-layer. Once the build is completed the green part is removed from the

chamber, and excess loose powder is brushed off the part.
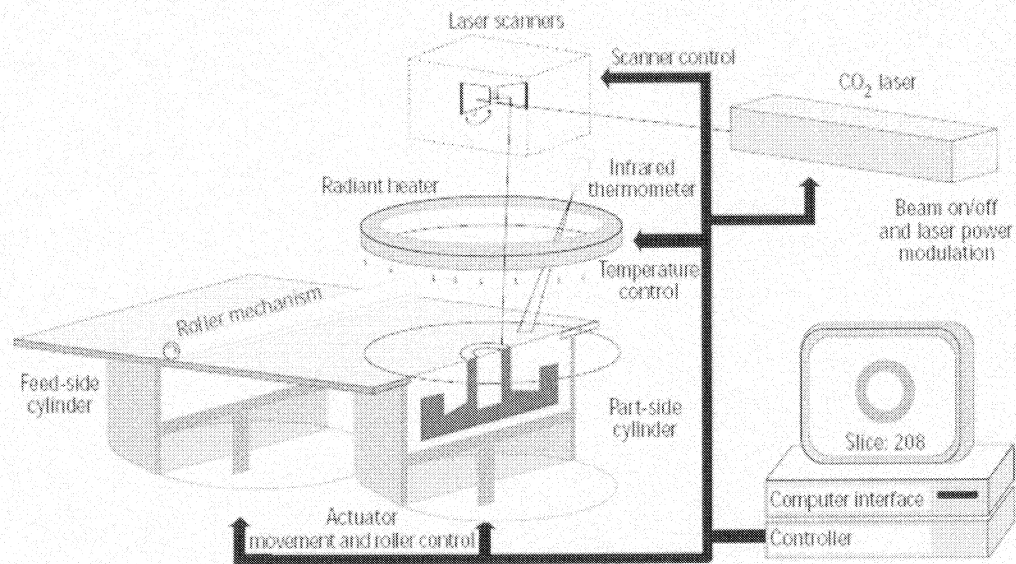
Figure 2: SLS system[3]

Furnace cycle and infiltration stage:

The process described in figure 2 is not able to produce fully-dense parts made from metallic powders. As the metallic parts produced through the SLS process are held together through low strength polymeric bonding, there are two post-process furnace heating cycles required to improve the strength of the parts.

The purpose of the first furnace cycle is to thermally decompose the polymer binder and to promote metal sintering by heating the powder to a much higher temperature (at the softening temperature of the metal). Nitrogen and hydrogen are supplied to the furnace to inhibit the undesired oxidation reactions. The brown part produced by this first furnace cycle contains approximately 40% porosity.

The second furnace cycle is used to infiltrate the porous metal part with bronze to achieve

full density. Brown part and the bronze tabs are placed on a plate. As DTM recommends, the furnace is being heated up to 1065°C and holds the temperature for two hours. This would allow the bronze to melt and infiltrate into the part through the tabs via capillary actions. Once the part is cooled down from this furnace cycle it would be composed of roughly 60% steel and 40% bronze. Other infiltrants such as copper, brass or any low melting metal with good wetting properties may be used.

Major drawbacks/challenges of SLS Process

The main challenge of SLS process lies in the surface roughness, and dimensional accuracy of SLS parts. It is well perceived that the improvements to surface roughness and dimensional accuracy are limited by the powder particle size. Using ultrafine powders is believed to be an effective, but also a challenging approach to improve this property.

Furthermore, there is an additional material costs associated with the existing metallic powder systems as a result of coating the metallic powder with the polymer binder. Using blended powder systems where the metal to polymer size ratio maximizes the powder packing would eliminate this costly step. It will also provide more control over part density and strength as well as improving the surface roughness of the parts produced.

Efforts to overcome the challenges to the SLS Process

A number of research groups have been investigating the above mentioned challenges. Ippolito et al.[4] reported that LOM and SLA produce the smoothest parts on average while SLS has the worst surface quality; however, the dimensional accuracies provided by the

five techniques are almost the same. Powder particle size, layer-wise building sequence, spreading of the powder and resolution of the scanning/deposition system are factors that directly affect the final surface roughness on SLS processed parts.[5] Ramos et al.[5] proposed laser polishing technique that can result in up to a three fold reduction in surface roughness. However, this expensive approach would require additional processing and add to the total part fabrication time and cost. As for the small scale features, the minimum-hole diameter possible with Duraform™ PA powder was 0.52 ± 0.02 mm, with up to 48% shrinkage in intended hole diameter of 1.0 mm.[6] As two furnace cycle result part shrinkage and increase production time and costs, Bourell and Boivie[7] in 2001 proposed a Fe-Cu-C system as a means for achieving more production-tool-like properties, without the requirement of infiltration. This and many other investigations have achieved limited success in producing fully dense parts without the need for an infiltration step.

Although it is easily understandable that powder particle size is one of the most significant factors effecting the surface roughness and accuracy of parts, only few researches have been done in this area. Subramanian et al investigated the effect of particle size on SLS and post processing of Alumina with polymer binder although they did not report any result for surface roughness and part shrinkage.[3] Aside from this study, very little work has been done that directly involves the effect of particle size. Furthermore, no work has been done in characterizing the improvement in surface roughness and part accuracy achieved by using finer powder before Rahbari[8] in 2005 has done some preliminary work to study the feasibility of using ultrafine powders in SLS process. This project is outlined to further improve the part quality by using the perfect

size ratio of base particle to the binder particle that is supposed to give maximum packing in the powder blends. Therefore, the new powder system to be proposed here is believed to reduce both shrinkage and surface roughness.

Effect of particle size reduction on SLS Process

Typical powders processed with SLS are in the size range of 30 μm – 100 μm (Geldart Group A particles[9]). As they are big enough, they have significant effects on the surface roughness and dimensional accuracy of the manufactured parts. Generally, materials with a smaller average particle size (like Geldart Group C particles[9]) are promising to achieve smoother surfaces, with better dimensional accuracy, higher part density, lower porosity, higher part strength, and an improved hardness. As finer particles are extremely cohesive in nature, they pose problems in poor flowability. It causes severe problem while roller dispenses and levels the powders on the bed. The cohesive nature of the powder also causes the formation of excessive natural agglomeration. Natural agglomerates are formed when cohesive. These aggregates would supposedly affect the quality of parts. Applying Zhu and Zhang's recent innovation[10,11] of successful handling of ultrafine powders (UFPs), the goal is to be able to use UFPs to sufficiently improve the flow quality of the powder, so that it can be easily dispensed and processed with the SLS system.

Binder characteristics

The lack of success with blending powders compared to coating them in the previous

investigations may be attributed to mainly to poor packing incorporated with inappropriate size ratios. When blending the powders it is imperative for the polymer binder to meet the 7:1 size ratio. Research into the packing of spherical powders conducted by McGeary in 1961[12] and German in 1994[13] concluded that to achieve maximum packing, the ideal size relationship between larger and smaller particles is at least 7:1. To exploit the advantages of blending the powders it is important to choose the appropriate binder of appropriate particle size. A number of different factors must be considered to select the right binder. Any thermoplastic or thermosetting material could be used as the binder. In this project, nano-sized polytetrafluoroethylene (PTFE) is chosen as the binder. PTFE serves in two ways: binding the steel particles and improving the flowability of the ultrafine steel particles (~ 16 μm). Indeed, nano-PTFE coats the outer layer of the spherical steel particles.

Objectives

The overall objective of this study is to investigate the coatings of steel particle with nano-PTFE and to determine whether their flowability is improved.

how much ultrafine

Experimental methods

Particle Size Analysis

The Better Particle Size Analyzer (BT-9300S) is used to analyze particle size of the UFP system. BT-9300S uses the technique of laser diffraction to determine the particle size of the submicron particles. The technique works by measuring the light scattered from particles as they pass through a laser beam.

Large particles scatter light at narrow angles with high intensity, whereas small particles scatter at wider angles with low intensity. The resulting scattering pattern is used to calculate the particle size distribution. To measure the powders used in this study, the powders are mixed with water and soap to produce a suspension.

Angle of Repose (AOR) measurement

Hokosawa Micron Corp. powder tester is used for measuring density and angle of repose (AOR) measurements of powders. Measurement technique is illustrated in chapter 6.

Scanning Electron Microscopy (SEM)

Hitachi S-2600 SEM (Hitachi, Pleasonton, CA) is employed to take analyze the uncoated and coated steel particles. The working voltage (5-12 kV), beam (60) and working distance (5.3 mm) were set. The particles are gold-sputter coated before inserting into the equipment for imaging.

Results and Discussion

Powder system: As our aim is to use ultrafine metal powders, we started with steel particles of 16 micron. Satisfying all the properties of a polymeric binder, we found a nano-sized thermoplastic (PTFE) as a binder. As the binder particles are nano-sized, they meet the criteria of the ratio of 7: 1 or higher. Figure 3 shows the effect of the size ratio of metal to polymer on overall packing of the material. It is evident from the figure 3 that metal to binder ratio of 7:1 or higher yields maximum packing as compared to 2:1. And it

is anticipated that the tightly packed metal-binder powder system will generate smoother

surface with high dimensional accuracy.
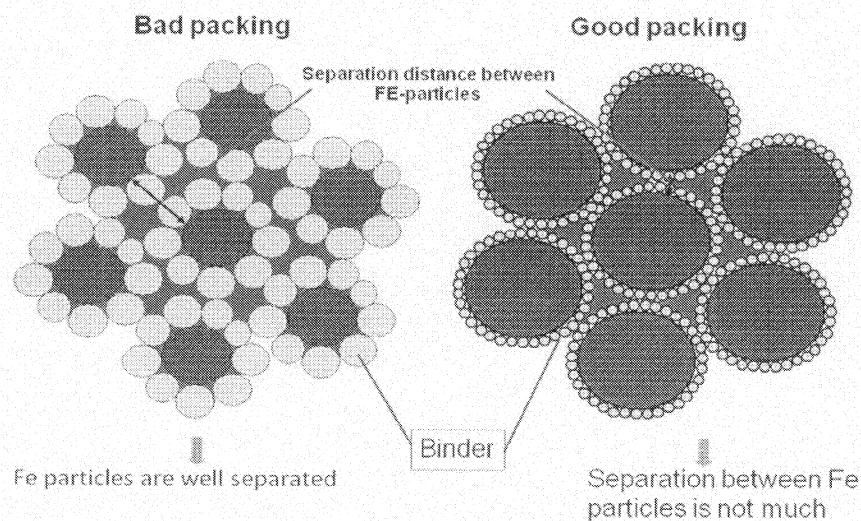
Figure 3: Packing comparison with different metal to binder ratios

Surface characterization of the powder blends:

The powder system is then well mixed and processed to achieve homogeneous mixture as

well as a thin layer of polymeric coating on the spherical Fe particle surfaces. Different

concentrations of binder starting from 1 vol% to 10 vol% are examined. The SEM images

of the bare Fe particle and Fe-binder mixtures are shown in figure 4. Comparing with

bare Fe-particle, even 1 vol% polymer coats a thin layer on the Fe particle. As the

concentration of polymer increases, the layer gets thicker, although the thickest layer is

no more than several hundred nanometers which well compares with the commercially

available polymer coated rapid steel particles.
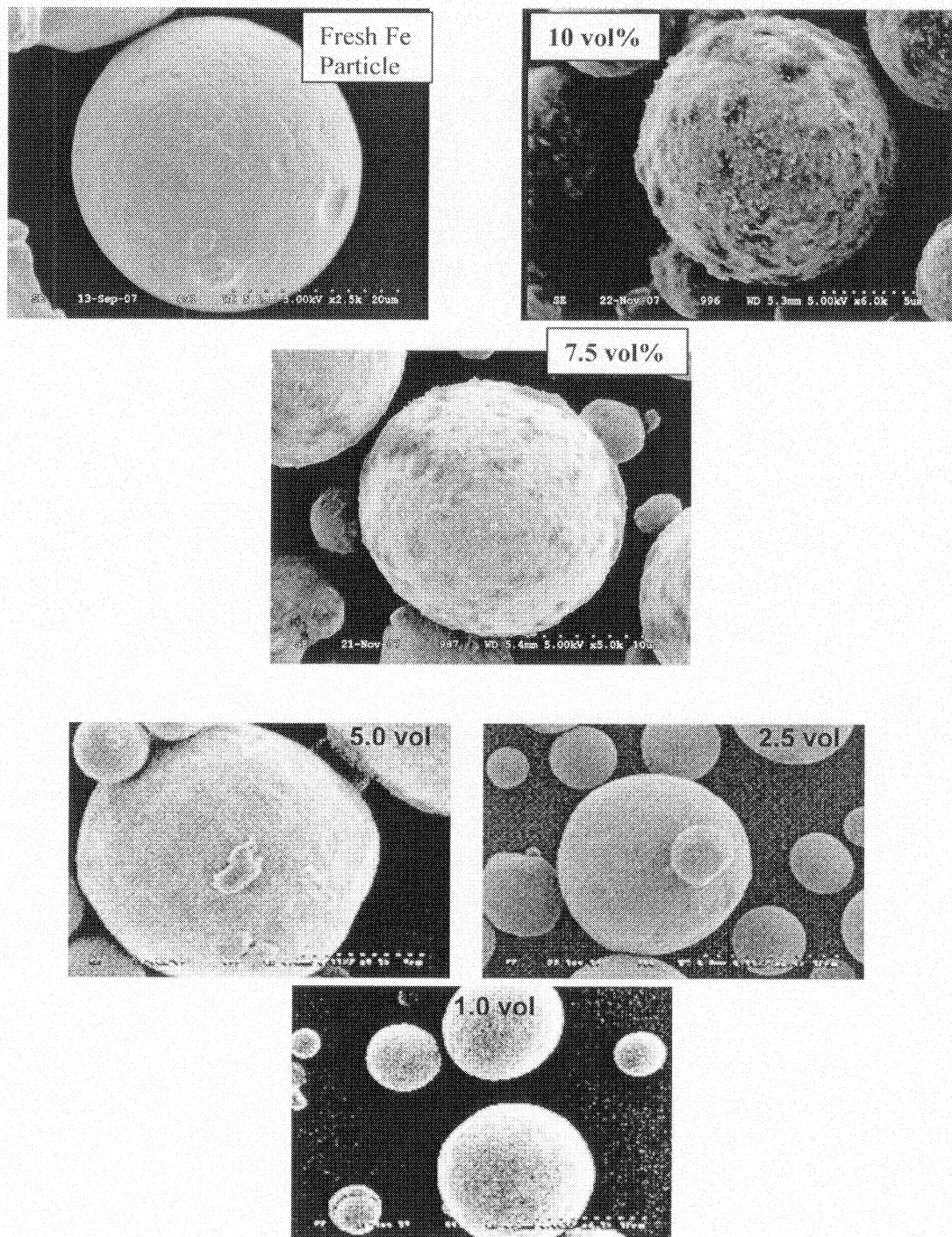
Figure 4: SEM images of fresh Fe particle and Fe particle with varying concentrations of polymer

With further increment of PTFE concentration (3.0 wt%) into the Fe powder system, it is more easier to identify the PTFE layer onto the spherical Fe particles (Figure 5).
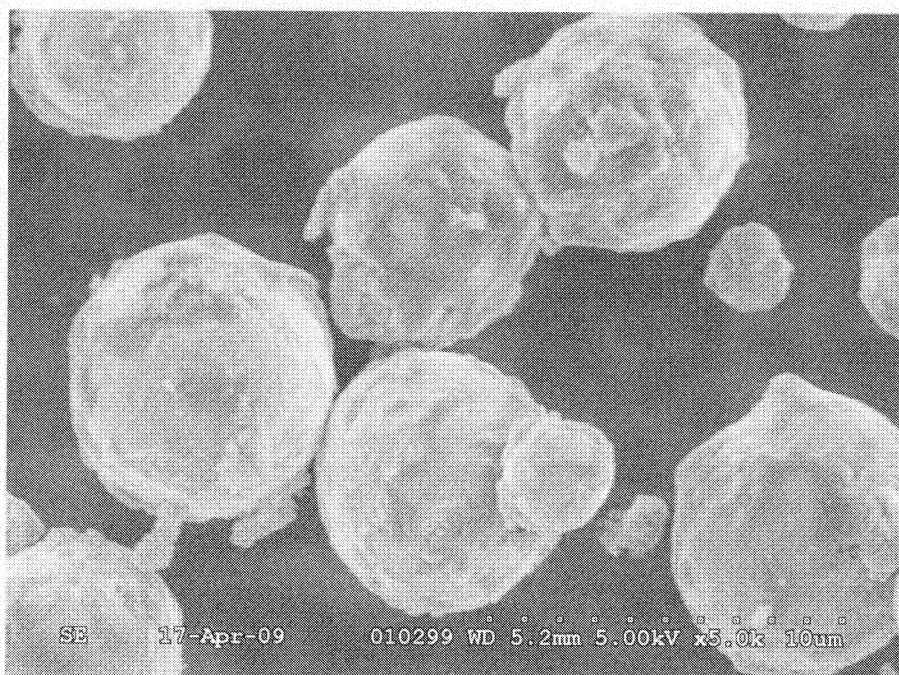
Figure 5: SEM image of Fe-3 wt.% PTFE

Flow characterization of the powder system:

Powder characterization results are summarized in table 1 to table 4.

Table 1. AOR and densities of pure Fe and Fe-polymer system

Materials	AOR(°)	Aerated Density (g/cc)	Packed Density (g/cc)
Fe	51.5	3.65	4.96
Polymer		0.391	0.583
Fe-Polymer (5 wt%)	51.3	2.58	3.96
Fe-Polymer (2.5 wt%)	51.2	2.13	4.17

Table 2. AOR of Fe-Polymer mixtures:

Polymer Conc. (vol%)	AOR (1st run)	AOR (2nd run)
0	50.3	51.3
33	50.5	51.5
19.4	51.9	51.2
5	52.3	52.5
2.5	50.4	50.0
1	50.4	49.0

To increase the flowability of the powder system, small amount (0.5%) of flow additive is added with Fe-polymer mixtures. Effect of the addition of flow additive reflects in AOR. AOR have been gradually reduced in the Fe-PTFE-flow additive mixtures when the concentration of PTFE decreases keeping the flow additive concentration same.

Table 3. AOR of Fe-Polymer-flow additive mixtures:

PTFE Conc. (vol%)	AOR (1st run)	AOR (2nd run)
5	47.2	46
2.5	47.1	46.5
1	45	44.3

After further processing of Fe-polymer-flow additive mixtures drastically decrease the AOR making the powder system as much flowable as rapid steel.

Table 4. AOR and densities of Fe-Polymer-flow additive mixtures: *After further processing*

Polymer Conc. (vol%)	AOR (°)			Aerated Density (g/cc)	Packed Density (g/cc)
	1st run	2nd run	3rd run		
5.0	39.7	38.0	38.7	3.63	4.575
2.5	38.0	36.7	38.3	3.65	4.623
1.0	37.0	37.0	36.7	3.694	

After characterizing the powder blends, 2.5 vol% polymer blends are used in SLS

equipment located at NRC. Low concentration polymer mixture is chosen to run in SLS

machine from the fact that the lower the concentration of polymer the lower would be the

chance of part shrinkage and the greater would be the dimensional accuracy. A number of

parameters of SLS process such as, laser power, laser scan speed, outline laser scan

speed, part bed temperature etc. have been changed to successfully sinter the polymer to

build a part. However, although the temperature has reached to 300° C while laser scans

the bed, no part has been built due to very low concentration of polymer used in the

blends.

When 2.5 vol% polymer-metal mixture fails, 5, 7.5 and 10 vol% polymer-Fe blends are

tested in the lab scale furnace to observe which polymer concentration works better to

make a solid part of certain strength. After the furnace test, 7.5 vol% shows some

strength; however the solid shape breaks upon applying minimum force. Then 10 vol%

mixture is tested in the furnace and solid shape is observed to be strong enough that is

stable under certain force. However, increment of flow additive above 0.5% decreases the

strength of the solid part. From the furnace tests, it is anticipated that 10 vol% polymer-

Fe mixture would be promising to build successful part in SLS machine. However, in

actual SLS process, even the 10 vol% PTFE-Fe mixture has not resulted in stronger parts;

only fragile parts are made out of this high concentration polymer mixture. The reason

behind the low strength of the parts is that PTFE has a very high melting point ($\sim 330^{\circ}$C).

Due to their high melting point, they could not bind or sinter the steel particle well in the

existing working environment of the SLS equipment; particularly the temperature at

which the part bed is heated is not high enough to promote sintering of PTFE-Fe

mixtures.

Conclusions

High melting point thermoplastic such as PTFE is not the ideal choice as the binder to the

steel particles to be used in the SLS process. However, due to vigorous mixing of PTFE-

Fe mixtures and the introduction of nano-sized flow additive, the flowability of the

powder system is improved in terms of lowering the angle of repose. The improved

flowability enables powders to flow well with the dispensing roller.

References

1. Wohlers, T., Wohlers Report 2003: Rapid Prototyping, Tooling & Manufacturing State of the Industry Annual Worldwide Progress Report. *Wohlers Associates, Inc.*, Fort Collins, US, **2003.**

2. Pham, D.T.; Dimov, S.S., Rapid Manufacturing: the Technologies and Applications of Rapid Prototyping and Rapid Tooling. *Springer-Verlag London Limited,* **2001.**

3. Subramanian, K.; Vail, N.; Barlow, J.; Marcus H.L., Selective Laser Sintering of Alumina with Polymer Binders. *Rapid Prototyping Journal* **1995,** 1 (2), 24-35.

4. Ippolito R.; Iuliano, L., Benchmarking of Rapid Prototyping Techniques in Terms of Dimensional Accuracy and Surface Finish. *CIRP Annals, Manufacturing Technology* **1995,** 24, 157-160.

5. Ramos, J.A.; Bourell, D.L.; Beaman, J.J., Surface Characterization of Laser Polished Indirect-SLS Parts. *Solid Freeform Fabrication Symposium Proceedings,* **2002,** 554-562.

6. Sirram, V.; Wood, K.; Bourell, D.; Beaman, J.J., Selective Laser Sintering of DuraformTM Polyamide with Small-scale Features. *Solid Freeform Fabrication Symposium Proceedings* **2003,** 585-595.

7. Bourell, D.L.; Boivie, K., SLS Application of the Fe-Cu-C System for Liquid Phase Sintering. *Solid Freeform Fabrication Symposium Proceedings* **2001,** 141-149.

8. Rahbari, M., *M.E.Sc. Thesis,* The University of Western Ontario, **2005.**

9. Geldart, D., Types of gas fluidization. *Powder Technology* **1973,** 7 (5), 285-297.

10. Zhu J.; Zhang H., Fluidization Additives to Fine Powders, *US Patent 6,833,185.* **2004.**

11. Zhu, J.; Zhang, H., Ultrafine powder coatings: An innovation. *Powder Coat.,* **2005,** 16 (7): 39-47.

12. McGeary, R.K., Mechanical Packing of Spherical Particles. *Journal of American Ceramic Society* **1961**, 44, 513-522.

13. German R.M., Powder Metallurgy Science. *Metal Powder Industries Federation: Conference Proceedings* **1994**.

Appendix B1
Copyright Permissions from JADA

April 22, 2010
A.S. Mohammad Sayem Mozumder
Graduate Student
The University of Western Ontario
1151 Richmond Street
London, Ontario, N6A 5B9
Canada

RE: Request for Permission to Reproduce Tables, Photos, Figures, Illustrations, etc. in Print and Electronic Media

Dear Mr. Mozumder:

Thank you for your recent inquiry regarding permission to reproduce the copyrighted material listed below that was published in our journal, The Journal of the American Dental Association ("JADA").

  1. Orchardson R, Gillam DG. Managing dentin hypersensitivity. JADA 2006;137(7):Figure 1, page 991.

Subject to the terms and conditions contained in this letter and in the attached document titled "Copyright Permission Terms and Conditions," permission is granted for a limited, non-exclusive, one-time-use only to reproduce the figure listed above (hereinafter, the "Item") in the doctoral thesis listed below:

Presenter(s):   A.S. Mohammad Sayem Mozumder, Jesse Zhu, Hui Zhang, Stephen Ferrier
Title of thesis: Applications of ultrafine powder coatings: Dentinal tubule occlusion to treat dentine hypersensitivity
Presented to: The University of Western Ontario
Year of Presentation: 2010

The Item may be reproduced solely in the following types of media: (1) solely as a contribution to a "collective work," as defined in 17 U.S.C. sec. 101; (2) a printed publication; and (3) electronic, DVD and CD-Rom format.

You must run the following credit line in a visible position for each Item of material requested:

Orchardson R, Gillam DG. Managing dentin hypersensitivity. JADA 2006;137(7):990-98. Copyright © 2006 American Dental Association. All rights reserved. Reproduced by permission.

Please note that we do not allow any full text reproduction of any articles on any Internet Web site other than the American Dental Association's own Web site, located at URL: www.ADA.org. You may not store, republish, reproduce or distribute the material

requested on the Internet or in any other media or format, including without limitation in any digital or electronic format. Also, we do not allow translation of JADA articles into another language.

Please be advised that the full text and graphics of JADA, from 1995 to the present, are available via the Internet on the ADA's Web site at **http://jada.ada.org**. Access to articles posted in the previous 12 months is restricted to ADA members and JADA subscribers. Articles that have been online for more than 12 months are open to all visitors at no charge. Permission is granted to download, print and retain one copy of each article solely for personal use. Any other copying, distribution, retransmission, or modification of information or materials on this site, whether in electronic or hard copy form, without the express prior written permission of the American Dental Association is strictly prohibited.

To view all of our publications, go to the Publishing Division's Home Page at **http://www.ada.org/prof/resources/pubs/about.asp**.

Your interest and support in our publication is very much appreciated. If you have any questions or need further information, please do not hesitate to contact me at (312) 440-2787.

Sincerely,

Karen London
Permissions Editor
Publishing Division

enclosure

American Dental Association

Copyright Permission Terms and Conditions

1. This permission applies only to copyrighted material that the American Dental Association owns, and not to any copyrighted materials or illustrations owned by third parties, that may be incorporated into the material requested.

2. The permission granted is nonexclusive and is limited to the specific use, format(s) and edition specified in this letter.

3. Permission is granted for a one-time-use only or life-of-an-edition basis. Unless otherwise specified herein, no permission is granted for making use of the material requested in any future reproductions, editions, revisions, ancillary products, translations, or other derivative works.

4. Unless otherwise specified in this letter, no adaptations of content are permitted, including the removal of legends or explanatory material from figures and tables, changes to the layout or graphics, or the removal of abstracts from full text articles.

5. Unless otherwise specified in this letter, you may not store, reproduce, republish, distribute, publicly perform or display, adapt or create derivative works of, any copyrighted material owned by the ADA in any digital or electronic format (including without limitation in CD-ROMs, floppy disks, PDF or HTML files, wide or local area networks, databases, or online or proprietary computer services), or on the Internet (including via e-mail or the World Wide Web).

6. All material reproduced by you or your organization from copyrighted material owned by the American Dental Association ("ADA") remains the full and exclusive property of ADA. ADA reserves all rights to grant permission to third parties.

7. You may not use any trademarks, service marks, logos or symbols owned by American Dental Association, including the names, covers and logos of ADA's publications, without written permission. No copyrighted material owned by ADA may be used in any manner implying endorsement or promotion by the ADA, or one of its publications, of any third party product or service. Authors' names may not be used on promotional materials without the author's written permission.

8. Unless otherwise specified in this letter, you may not translate the material requested into another language.

9. This permission is contingent upon payment to ADA Publishing of all applicable permission fees within thirty (30) days of receipt of this letter.

Appendix B2
Copyright Permissions from RSC

Dear Mr Mozumder

The Royal Society of Chemistry hereby grants permission for the use of the material specified below in the work described and in all subsequent editions of the work for distribution throughout the world, in all media including electronic and microfilm. You may use the material in conjunction with computer-based electronic and information retrieval systems, grant permissions for photocopying, reproductions and reprints, translate the material and to publish the translation, and authorize document delivery and abstracting and indexing services. The Royal Society of Chemistry is a signatory to the STM Guidelines on Permissions (available on request).

Please note that if the material specified below or any part of it appears with credit or acknowledgement to a third party then you must also sec ure permission from that third party before reproducing that material.

Please ensure that the published article carries a credit to The Royal Society of Chemistry in the following format:

[Original citation] – Reproduced by permission of The Royal Society of Chemistry

and that any electronic version of the work includes a hyperlink to the article on the Royal Society of Chemistry website. The recommended form for the hyperlink is http://dx.doi.org/10.1039/*DOI suffix*, for example in the link http://dx.doi.org/10.1039/b110420a the DOI suffix is 'b110420a'. To find the relevant DOI suffix for the RSC paper in question, go to the Journals section of the website and locate your paper in the list of papers for the volume and issue of your specific journal. You will find the DOI suffix quoted there.

Regards

Gill Cockhead

Contracts & Copyright Executive

Gill Cockhead (Mrs), Contracts & Copyright Executive

Royal Society of Chemistry, Thomas Graham House

Science Park , Milton Road, Cambridge CB4 0WF , UK

Tel +44 (0) 1223 432134, Fax +44 (0) 1223 423623

http://www.rsc.org

-----Original Message-----
From:
Sent: 22 April 2010 14:32
To: CONTRACTS-COPYRIGHT (shared)
Subject: Permission Request Form: A. S. Mohammad Sayem Mozumder

```
Name      : A. S. Mohammad Sayem Mozumder
Address :

Canada


I am preparing the following work for publication:

Article/Chapter Title  : Development of Superhydrophobic Coatings
Journal/Book Title      : Applications of Ultrafine Powder Coatings
Editor/Author(s)          : A. S. Mohammad Sayem Mozumder, Jesse Zhu, Hui
Zhang
Publisher               : The University of Western Ontario

I would very much appreciate your permission to use the following
material:



Journal/Book Title      : Journal of Materials Chemistry
Editor/Author(s)        : Yuyang Liu, Jing Tang, Ronghua Wang, Haifeng
Lu, Li Li, Yeeyee Kong, Kaihong Qi and J. H. Xin
Volume Number           : 17
Year of Publication     : 2007
Description of Material : Artificial lotus leaf structures from
assembling carbon nanotubes and their
Page(s)                 : 1071-1078


Any Additional Comments         :

Figure 1(a, b, c) will be used in my PhD thesis if you permit. I need
your permission by April 23, 2010, if not possible by April 26, 2010.
```

DISCLAIMER:

This communication (including any attachments) is intended for the use of the addressee only and may contain confidential, privileged or copyright material. It may not be relied upon or disclosed to any other person without the consent of the RSC. If you have received it in error, please contact us immediately. Any advice given by the RSC has been carefully formulated but is necessarily based on the information available, and the RSC cannot be held responsible for accuracy or completeness. In this respect, the RSC owes no duty of care and shall not be liable for any resulting damage or loss. The RSC acknowledges that a disclaimer cannot restrict liability at law for personal injury or death arising through a finding of negligence. The RSC does not warrant that its emails or attachments are Virus-free: Please rely on your own screening.

Appendix B3
Copyright Permission from SAGE Publication Ltd.

Journal of Biomaterials Applications — track SCHOLAR Manuscripts

JOURNAL CONTRIBUTOR'S PUBLISHING AGREEMENT

TITLE OF CONTRIBUTION: Nano-TiO2 Enriched Polymeric Powder Coatings Support Human Mesenchymal Cell Attachment and Growth
INTENDED FOR PUBLICATION IN: Journal of Biomaterials Applications
AUTHOR NAME(S): Mozumder, Mohammad Sayem; Zhu, Jesse; Perinpanayagam, Hiran
CORRESPONDING AUTHOR NAME: Dr. Hiran Perinpanayagam
ADDRESS: Dental Sciences Building 0079 London, Ontario N6A 5C1 Canada

SOLE AND EXCLUSIVE LICENSE TO PUBLISH
I represent that the Contribution is owned by me unless the following applies:
Work made for hire for employer/Work done in the course of employment - The Contribution was prepared by me at the request of my employer and within the scope of my employment and copyright in the Contribution is owned by my employer. (Both the Contributor and an authorized representative of the Contributor's employer must sign this Agreement.)
U. S. Government work I am an employee of the United States Government and prepared the Contribution as part of my official duties.
(If the Contribution was not prepared as part of the Contributor's official duties, it is not a U.S. Government work. If the Contribution was jointly authored, all the co-authors must have been U.S. Government employees at the time they prepared the Contribution in order for it to be a U.S. Government work; if any co-author was not a United States Government employee, then the Contribution is not a U.S. Government work. If the Contribution was prepared under a U.S. Government contract or grant, it is not a U.S. Government work - in such case, copyright is usually owned by the contractor or grantee.)
If either of the above appies to your Contribution, please download a print copy of this form to enable additional signature by an authorized representative of your employer. Return the print signed copy via mail, fax or email. By email - a scanned copy of the Agreement with signatures or a digital original copy with electronic signature are equally acceptable.
In consideration for publication in the above Journal, of the above Contribution, I hereby grant to SAGE Publications Ltd ('SAGE') the sole and exclusive right and licence to produce, publish and make available the Contribution and the abstract prepared by me to

accompany the Contribution for the full legal term of copyright and any renewals thereof throughout the world in all languages and in all formats, and through any medium of communication now known or later conceived or developed.

By signing this Contributor Agreement I agree both to the above provisions and to the terms of the agreement outlined below.

If you are opting to make your paper freely available online under the SAGE Open publishing option please click here to request a SAGE

Open License Agreement. For more information on SAGE Open options please visit

TERMS OF THE AGREEMENT
Copyright
While copyright remains mine as the author, I hereby authorise SAGE to act on my behalf to defend my copyright should it be infringed and to retain half of any damages awarded, after deducting costs.

http://mc.manuscriptcentral.com/jba?URL_MASK=ZwJtkMyKCM6Bj... 1/21/2010
Warranties
I warrant to SAGE that the Contribution is my original work, that I have the full power and authority to enter into this Agreement and to convey the rights granted herein to SAGE and to submit the work for first publication in the Journal and that it is not being considered for publication elsewhere and has not already been published elsewhere, either in printed or electronic form, that I have obtained and enclose all necessary permissions for the reproduction of any copyright works (including artistic works, e.g. illustrations, photographs, charts, maps, other visual material, etc.) contained in the Contribution and not owned by me and that I have acknowledged all the source(s), that the Contribution contains no violation of any existing copyright, other third party rights or any libellous or untrue statements and does not infringe any rights of others, and I agree to indemnify SAGE against any claims in respect of the above warranties. I further agree to be bound by the Conditions of Publication provided herein as part of this Agreement which outline the circumstances under which work may be reused.

Declaration of Conflicting Interests
I certify that:

1. All forms of financial support, including pharmaceutical company support, are acknowledged in the Contribution

2. Any commercial or financial involvements that might present an appearance of a conflict of interest related to the Contribution are disclosed in the covering letter accompanying the Contribution and all such potential conflicts of interest will be discussed with the Editor as to whether disclosure of this information with the published Contribution is to be made in the Journal.

3. I have not signed an agreement with any sponsor of the research reported in the Contribution that prevents me from publishing both positive and negative results or that forbids me from publishing this research without the prior approval of the sponsor.

4. I have checked in the manuscript submission guidelines whether this Journal requires a Declaration of Conflicting Interests and complied with the requirements specified where such a policy exists.

It is not expected that the details of financial arrangements should be disclosed. If the Journal does require a Declaration of Conflicting Interests and no conflicts of interest are declared, the following will be printed with your article: 'None Declared'.

Termination

SAGE, in its sole, absolute discretion, may determine that the Contribution should not be published in the Journal. If in the rare circumstance the decision is made not to publish the Contribution after accepting it for publication, then all rights in the Contribution granted to SAGE, shall revert to you and this Agreement shall be of no further force and effect, and neither you nor nor SAGE will have any obligation to the other with respect to the Contribution.

Counterparts; Facsimile

This Agreement may be executed in counterparts each of which shall be deemed the original, all of which together shall constitute one and the same Agreement. A faxed copy or other electronic copy shall be deemed as an original.

Electronic Signature Authorization

This transaction may be conducted by electronic means and the parties authorize that their electronic signatures act as their legal signatures of this Agreement. This Agreement will be considered signed by a party when his/her/its electronic signature is transmitted. Such signature shall be treated in all respects as having the same effect as an original handwritten signature. (You are not required to conduct this transaction by electronic means or use an electronic signature, but if you do so, then you hereby give your authorization pursuant to this paragraph.)

Modification; Entire Agreement; Severability

No amendment or modification of any provision of this Agreement shall be valid or binding unless made in writing and signed by all parties. This Agreement constitutes the entire agreement between the parties with respect to its subject matter, and supersedes all prior and contemporaneous agreements, understandings and representations. The invalidity or unenforceability of any particular provision of this Agreement shall not affect the other provisions, and this Agreement shall be construed in all respects as if any invalid or unenforceable provision were omitted.

Governing Law; Arbitration

This Agreement shall be deemed to be a contract made in England and shall be construed and applied in all respects in accordance with English law and the parties submit and agree to the jurisdiction of the English courts.

If any difference shall arise between you and SAGE touching the meaning of this Agreement or the rights and liabilities of the parties thereto, the same shall be referred to the arbitration of two persons (one to be named by each party) or their mutually agreed umpire, in accordance with the provision of the England Arbitration Act 1996 or any amending or substituted statute for the time being in force.

http://mc.manuscriptcentral.com/jba?URL_MASK=ZwJtkMyKCM6Bj... 1/21/2010

Contributor

AUTHOR NAME(S): Mozumder, Mohammad Sayem; Zhu, Jesse; Perinpanayagam, Hiran

CORRESPONDING AUTHOR NAME: Dr. Hiran Perinpanayagam

By checking the "I accept" box below I warrant I am the above named corresponding author and I am authorized to sign on behalf of myself and, in the case of a multi-authored contribution, on behalf of all other authors of the Contribution.

Please check the box below.

I accept

Once checked and submitted this represents your electronic signature.

If you are required to submit an addendum by your employer or research funding body, please continue to accept and submit the form and make your request via email indicating the name of the Journal and the title of your paper.

For any other queries relating to copyright policies or permissions at SAGE, please visit our Journal Author Gateway.

http://mc.manuscriptcentral.com/jba?URL_MASK=ZwJtkMyKCM6Bj... 1/21/2010

ScholarOne ManuscriptsTM v4.2.1 (patent #7,257,767 and #7,263,655). © ScholarOne, Inc., 2009. All Rights Reserved.

ScholarOne Manuscripts is a trademark of ScholarOne, Inc. ScholarOne is a registered trademark of ScholarOne, Inc.

Terms and Conditions of Use - ScholarOne Privacy Policy -
http://mc.manuscriptcentral.com/jba?URL_MASK=ZwJtkMyKCM6Bj... 1/21/2010

Curriculum Vitae

Name: A. S. Mohammad Sayem Mozumder

Education: University of Western Ontario (UWO)
Doctor of Philosophy, April 2010

King Fahd University of Petroleum & Minerals (KFUPM)
Master of Science in Chemical Engineering, May 2004

Bangladesh University of Eng. & Tech. (BUET)
Bachelor of Engineering (Chemical), June 2000

Work Experiences: Research & Teaching Assistant, UWO, 2005-2010.

Teaching Assistant, UWO, 2005-2009

Research & Teaching Assistant, KFUPM, 2002-2004

Patents: Jesse Zhu, **A.S. Mohammad Sayem Mozumder**, Hiran Perinpanayagam and Hui Zhang, "Development of Powder Coatings for Tissue Cell Attachment and Growth", **A Provisional US Patent**, Filed on January 22, 2010.

A.S. Mohammad Sayem Mozumder and others, "Novel application of ion-leachable glass ionomer powders to occlude dentinal tubules". (A Report Of Invention (**ROI**) has been submitted to WorlDiscoveries™).

Publications: **Mozumder, Mohammad Sayem**, Zhu, Jesse and Perinpanayagam, Hiran. "Nano-TiO2 enriched Polymeric Powder Coatings Support Human Mesenchymal Cell Attachment and Growth", *Journal of Biomaterials Applications*, In Press.

Alnaizy, R., **Mozumder, M. Sayem**, and Abu-Sharkh, B. F., *Journal of Water Supply: Research and Technology*, Vol 57 (5) (2008): 329-336.

Ibnelwaleed A. Hussein, **M. Sayem Mozumder**, Basel F. Abu Sharkh, Sk. Asrof Ali, Raafat Al-Naizy, *European Polymer Journal*, Vol 41 (2005): 2472-2482.

M. Sayem Mozumder, R.S. Alnaizy, Y. Umar, Sk. Asrof Ali, B.F. Abu-Sharkh, *European Polymer Journal*, Vol 41 (2005): 2224-2231.